Combinatorial Problems in Energy Networks
Graph-theoretic Models and Algorithms

zur Erlangung des akademischen Grades eines

Doktors der Naturwissenschaften

von der KIT-Fakultät für Informatik
des Karlsruher Instituts für Technologie (KIT)

genehmigte

Dissertation

von

Franziska Wegner

aus Potsdam

Tag der mündlichen Prüfung:	12. Dezember 2019
Erste Gutachterin:	Prof. Dr. Dorothea Wagner
Zweite Gutachterin:	Prof. Dr. Sylvie Thiébaux

„Nach Wahrheit forschen, Schönheit lieben, Gutes wollen, das Beste thun, das ist die Bestimmung des Menschen.“ Moses Mendelssohn (1729–1786)

I dedicate this work to my beloved parents and my beloved deceased brother Nico.

Acknowledgements

This thesis would not have been possible without the help of different people. I would like to thank Dorothea Wagner for giving me the opportunity to work in her group and to take care of the funding. During that time I was part in different projects such as the Helmholtz Program Storage and Cross-linked Infrastructure (SCI), Energy System Integration (ESI), and as an associate in the GRK Energy Status Data, where I learned a lot. In addition, I would like to thank my reviewers Sylvie Thiébaux and Dorothea Wagner for their comments and their advises.

Working on such a complex topic alone would have been impossible and thus, I would like to thank my coauthors Alban Grastien, Sebastian Lehmann, Thomas Leibfried, Tamara Mchedlidze, Nico Meyer-Hübner, Martin Nöllenburg, Ignaz Rutter, Peter Sanders, Dorothea Wagner, and Matthias Wolf for their discussions and collaboration. I owe a big thanks to Andreas Gemsa, Sascha Gritzbach, Matthias Wolf, and Philipp Bohnenstengel who proofread parts of my thesis. A special thanks goes to Philipp, who read the whole thesis and fixed my "-ly", and "analysis" problems, and found the "conjured complex" to be a bit magical.

To get a broader knowledge, I was lucky to work on other topics, collaborate with other groups, and learn from different colleagues. A special thanks here goes to Moritz Baum from whom I learned how to collaborate on a paper and who gave me very good advises. In addition, I would like to thank for the numerous colleagues Moritz Baum, Thomas Bläsius, Johannes Garttner, Andreas Gemsa, Sascha Gritzbach, Sören Hohmann, Heiko Maaß, Carina Mieth, Martin Pfeifer, Ignaz Rutter, Philipp Staudt, Torsten Ueckerdt, Dorothea Wagner, Christof Weinhardt, and Matthias Wolf with whom I was allowed to work together on different papers in external projects.

Research is one thing, but we have also the responsibility to communicate our knowledge in a better and more understandable way. I was very lucky to work with Anna Caroline Hein on an article that describes our work in a more accessible way. She taught me how to write an article for non-specialists and what are common tools to spread our knowledge.

I thank the colleagues at NICTA for the very good working atmosphere. I learned a lot from the team about electrical flows and optimization. Major parts of the switching paper were developed during that time and afterwards with Matthias Wolf, from whom I learned theoretical techniques and who is a kind reviewer of my writings. Furthermore, I thank also my colleagues at the institute from whom I learned a lot in algorithmics and theoretical computer science. Especially, I would like to thank Spyros Kontogiannis, who was my first temporary office mate in the "exile" office, and

my office mates Benjamin Niedermann and Matthias Wolf with whom I enjoyed the daily vending machine trips and “apple walks” a lot. In addition, I recall the times with most of my coworkers when we spent long nights at the institute, the Dibbelt ghost and its hectic squeak of shoe soles, the weekends at work with the Italian course at the Pizzahaus and the pizza “Quattro Fromage”, the Saboteur counterpart, the members of the Escorial committee, the Obstfreunde meetings, the soccer games after work, the legendary “Frauenwasserballweltmeisterschaft” in Gernsbach, and the illegal office chair race. I would like to thank especially these colleagues that made long or bad days enjoyable.

There are people in the background that help out with all the administration and technical belongings, which helped me to focus on my main work. This part was perfectly done by Lilian Becker, Isabelle Junge, Ralf Kölmel, Laurette Lauffer, and Tanja Wehrmann, whom I would particularly like to thank.

Starting a thesis template from scratch would take a lot of time. I inherited the template and improvements from Thomas Bläsius and Moritz Baum, respectively. I would like to thank both, since it was super easy to add additional fixes and ideas to the template.

In the end, I would like to thank my friends, my family, dedicated teachers (especially Eva Pudewell and Jana Schreiber), inspiring research staff such as Ingo Boersch that invested time for students from school, and all people who brought me back on track and supported me over all this years. A special thanks goes to Katja and Marius Rothe, Philipp Bohnenstengel, Moritz Baum, Anna Caroline Hein, Andreas Gemsa, Thomas Bläsius, Benjamin Niedermann, and Cliff Mändl, who supported me mentally and emotionally very much.

Abstract

In this thesis, we study combinatorial problems in energy networks with the focus on power grids. At present we see a paradigm shift in power grids towards renewable energy, while making use of the traditional power grid. This shift changes the production pattern from a centralized way towards a distributed production, leading to bottlenecks and other problems. We try to efficiently exploit the existing infrastructure by analyzing the structure of and developing algorithms for electrical flows, placement problems, and layout problems to improve the existing power grid. We remark that the results of this work might be applicable to other energy networks as well [Gro+19] and certain phenomena such as the Braess's Paradox (i. e., for road network it means that adding a road to the traffic network can cause longer travel times) indicate that the provided techniques in this thesis could be used for traffic networks, too.

One main task of this work was the identification of problem statements in energy networks. We first translate the problems to graph-theoretical models such that we are able to analyze the problems, study their complexity, develop algorithms, and evaluate them using either existing data sets or generated data if there are no publicly available suitable data sets. We develop algorithms that provide in most cases quality guarantees on certain graph classes that can be then used as good heuristics on general graphs. At first we focus on the modeling of power grids and the behavior of electrical flows in power grids using a linearized model that makes use of some simplifications. These simplifications are based on realistic assumptions for high-voltage power grids on which we lay our focus.

This thesis has four main content chapters. The first part focuses on algorithms to compute electrical flows. We describe the mathematical structure and focus on some major properties of electrical flows. Note that apart from solving a system of linear equations or an exponential time algorithm there are no known algorithms to compute electrical flows. One way to tackle this problem are electrical preserving transformations. Electrical preserving transformations are common techniques in the electrical flow analysis. Based on these transformations, we will present a first algorithm for electrical flows on s-t-planar biconnected graphs. In addition to that, we discuss different representations and formulations of electrical flows that increase the understanding of the electrical flow's behavior. We make use of these representations to describe the balancing property by separating the quadratic relationship of voltage and current. This leads us to the duality of the two Kirchhoff laws and another algorithmic approach.

The second and third part of this thesis focus on the increasing of the efficiency of the electrical network. We exploit the Braess' Paradox by switching lines (i. e., temporarily removal of a line or cable) or by using an edge weight scaling (i. e., susceptance scaling). We design novel algorithms that improve the throughput of the power grid or decrease the overall operating costs. These algorithms are the first that provide some quality guarantees or bounds. Each of these parts includes simulations to evaluate the algorithms on a realistic data set.

The last part of this thesis is about transmission network expansion planning on a greenfield motivated by the wind farm cabling problem. Algorithmically, it represents a layout problem. Within this part, we present a first proper model formulation for this particular problem, give a benchmark generator, and design a meta-heuristic approach to tackle the wind farm cabling problem that is then evaluated on a generated data set.

Contents

1 Introduction **1**
- 1.1 Main Contributions . . . 4
- 1.2 Thesis Outline . . . 7

2 Literature Overview **11**
- 2.1 Graph-theoretical Flows and Electrical Flows . . . 12
- 2.2 Reduction Rules for the Analysis of Power Grids . . . 13
- 2.3 Braess's Paradox – Effects that Influence the Power Grid Efficiency and Stability . . . 17
  - 2.3.1 Switching – A Discrete Manipulation of the Power Grid Topology 18
  - 2.3.2 FACTS – A Continuous Manipulation of the Power Grid Topology 19
- 2.4 The Wind Farm Cabling Problem . . . 21

3 Fundamentals **25**
- 3.1 Fundamental Graph-theoretic Terminology . . . 25
- 3.2 Fundamentals in Graph-theoretic Flows . . . 29
- 3.3 The Power Flow Feasibility Problem . . . 31
  - 3.3.1 Alternating Current Power Flow Model . . . 32
  - 3.3.2 Linearized Alternating Current Power Flow Model . . . 49
  - 3.3.3 The Voltage Normalized Lossless Real Power Flow Model – A Model between AC and DC Model . . . 52
  - 3.3.4 Alternating vs. Direct Current Model . . . 54

4 The Direct Current Feasibility Problem
An Algorithmic Approach to Computing Electrical Flows **57**
- 4.1 A Mathematical Model for the Feasibility Problem of Electrical Flows 58
  - 4.1.1 Properties of Electrical Flows . . . 67
  - 4.1.2 Scalability of Electrical Flows . . . 71
  - 4.1.3 Integral Electrical Flows . . . 73
  - 4.1.4 Planar Graphs . . . 74
  - 4.1.5 Matroids and Independence Systems . . . 75
- 4.2 Electrical Preserving Transformations . . . 76
- 4.3 Representations and Formulations of Electrical Flows . . . 85
  - 4.3.1 The Duality Concept for Graphs . . . 85
  - 4.3.2 Simultaneous Flow Representation . . . 86

4.3.3 Rectangular Representation . . . 89
4.4 The Balancing Property . . . 90
4.5 An Algorithm for Electrical Flows on s-t Planar Graphs . . . 94
4.5.1 Bipolar Orientation . . . 95
4.5.2 Planar Embedding and Dual Graph Construction . . . 96
4.5.3 KCL Conflict Resolution . . . 97
4.6 Conclusion . . . 100

5 Discrete Control Units
Switching – A Temporary Removal of Links and Cables **103**
5.1 A Mathematical Model for the Placement of Discrete Control Units . 104
5.2 Complexity Considerations of using Discrete Control Units . . . 111
5.2.1 Literature Overview . . . 113
5.2.2 NP-hardness of Source-Sink-MTSF on Series-Parallel-Graphs 113
5.3 Network Modeling . . . 116
5.4 MTSF on Source-Sink-Networks . . . 119
5.4.1 The Dominating Theta Path (DTP) . . . 120
5.4.2 DTP without Merging the Labels . . . 124
5.4.3 Reachability Test . . . 125
5.4.4 Analyses of the DTP . . . 127
5.5 Computing one DTP in Polynomial Time . . . 130
5.6 Approximation Algorithm on Cacti . . . 132
5.7 Simulations . . . 134
5.8 Conclusion . . . 137

6 Continuous Control Units
Ideal FACTS Placement – A Susceptance Scaling Approach **139**
6.1 Preliminaries . . . 143
6.2 A Hybrid Mathematical Model for the Placement of Continuous Control Units . . . 146
6.2.1 The Objective Function . . . 146
6.2.2 Power Flow Models . . . 147
6.2.3 Flow Control Units on Vertices . . . 148
6.2.4 Flow Control Units on Edges . . . 149
6.2.5 Reduction to MinCostFlow . . . 150
6.3 Complexity . . . 152
6.4 Planar Problem Reinterpretation . . . 157
6.5 Placing Flow Control Buses . . . 158
6.5.1 Experiments . . . 158
6.5.2 Structure of Optimal Solutions . . . 160
6.6 Grid Operation Under Increasing Loads . . . 164

6.7 Evaluation of Placing Flow Control Edges . . . 166
6.8 Effect of FCEs in Comparision to FCVs . . . 167
6.9 Conclusion . . . 169

7 Transmission Network Expansion Planning
The Wind Farm Cabling Problem – A Greenfield Approach **171**
7.1 A Mathematical Model for the Wind Farm Cabling Problem . . . 174
7.2 Simulated Annealing-based Approach . . . 178
7.3 Benchmark Generation . . . 181
7.4 Simulations . . . 182
7.5 Conclusion . . . 184

8 Conclusion **187**
8.1 Summary . . . 187
8.2 Outlook . . . 188

Bibliography **191**

List of Figures **225**

List of Tables **227**

Glossary **229**

A Problem Definitions **241**
A.1 Flow Feasibility Problems . . . 241
A.2 Flow Optimization Problems . . . 242
A.3 Discrete Placement Problems . . . 243
A.4 Continuous Placement Problems . . . 244
A.5 Others . . . 246

B Fundamentals **249**
B.1 Instantaneous Curves . . . 249
B.2 Complex Power Injection . . . 250
B.3 Complex Power Flow . . . 251
B.4 Complex Current Flow . . . 252
B.5 Formulations . . . 253
B.5.1 Polar PQV Formulation . . . 253
B.5.2 Rectangular PQV Formulation . . . 254
B.5.3 Polar IV Formulation . . . 255
B.5.4 Rectangular IV Formulation . . . 256
B.5.5 DC Assumption 3 . . . 257

C Discrete Changes to the Power Grid **259**

D Continuous Changes in the Power Grid **263**

E Curriculum Vitæ **267**

F List of Publications **271**

G Deutsche Zusammenfassung **273**

1 Introduction

The power grid represents one of the major backbones of the human civilization. It determines our supply chain, which includes important infrastructures such as water supply and heating. Elsberg [Els17] gives an impression—although fictional—of how essential the power grid is and which parts of our daily life are actually affected by a blackout. However, to sustain the basic human needs we have to change towards a more sustainable and environmentally friendly behavior in general and in power grids in particular. Thus, the future power grid has to become more efficient to handle the increasing demand for energy as well as the planned increasing number of generators that transform renewable energies [Jus14], e. g., wind into electrical energy. We call these generators *renewable energy producers*. Renewable energy producers such as wind turbines are independent power producers (IPP) that have a volatile power production pattern—meaning that the amount of production is influenced by many uncertainties such as the weather—that is totally different from *conventional power generators* (e. g., nuclear and coal power plants), where the production is stable.

The power grid has evolved historically and the traditional structure interconnects few central conventional power generators with many consumers (Figure 1.1 left side) in such a way that the demand of the consumers is always satisfied. Similar to the road network, where we distinguish roads by their speed limits and size into rural roads, highways, and motorways, we are able to distinguish the lines in the power grid depending on the amount of power they are able to transfer. The power grid's hierarchical structure in Germany consists of high (110 kV, 220 kV, and 380 kV), medium (1 to 50 kV), and low voltage layers (230 V and 400 V; see Figure 1.1) representing transmission and distribution power grids, respectively. In a conventional power grid the power producers are connected to the high voltage layer directly and the consumers are either connected to the medium voltage layer (e. g., industries), or low voltage layer (e. g., households and small industries). Within this hierarchical structure the power grid consists of edges that are represented by power lines or cables that interconnect producers with consumers. These edges are often denoted as elements (or branches) as they could also represent power electronics such as transformers, resistors, and conductors.

Renewable energy producers are often added to the medium and low voltage layer (Figure 1.1 right side). This eventually causes a bidirectional power flow which the conventional power grid was not designed for. This change in the power grid usage might cause instabilities and new critical lines. Critical lines represent lines, which removal might cause a blackout. The idea of the latter problem is exemplary shown

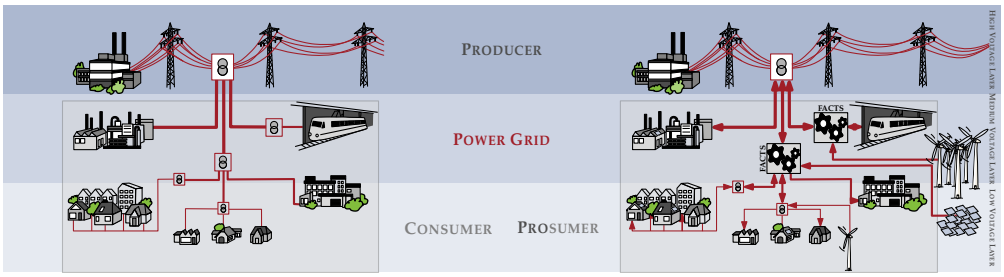

Figure 1.1: Two exemplary power grids showing the conventional power grid (left) and the current development of the power grid (right). Both power grids consists of three voltage layers. On the high voltage layer there are the conventional power plants (e. g., coal and nuclear power plants) as well as bigger collections of wind farms and virtual power plants located. The industrial consumers are usually located on the medium voltage layer that mainly presents a distribution layer. In the low voltage layer, we have the households and small industrial consumers. Note that on the right side, participants of the last two layer might have photovoltaics and wind turbines and are thus denoted by the term *prosumers* (i. e., acting as producer and consumer simultaneously).

in [Wit+16]. Offshore wind farms in the North and Baltic Sea (see Figure 1.2) provide another example for such producers. In this particular case, the suitability of a location for such farms highly depends on the wind profile and available space. Thus, the location for wind farms is not as flexible as for conventional power plants. These offshore wind farms produce—similar to conventional power plants—a high amount of electrical energy that is not used on-site. However, it is largely required in areas such as the Ruhr region, and southern regions of Germany [ent18, ent19a, ent19b, ent19c], since a large number of industrial consumers are located there. Sending such an amount of energy through the power grid causes new bottlenecks or is simply impossible. Switching these wind farms off to sustain the grid safety is not a desirable solution. Thus, to cope with these new challenges the transmission system operator (TSO) can follow at least two possible strategies.

(S1) The expansion of the power grid by adding new transmission lines and

(S2) the installation of advanced control units such as Flexible AC Transmission Systems (FACTS) and switches for a better utilization of the existing power grid.

The mentioned power grid structure and strategies lead to the *dynamic* and *static transmission design problem* [BPG01a]. Binato et al. [BPG01a] consider Strategy 1 as dynamic transmission design problems [BPG01a, Cho+06, GMM92] under which long-term power grid configuration such as Transmission Network Expansion Planning (TNEP) is encountered. TNEP [HHK13] is the design problem of adding new transmission lines or circuits under different objectives such as the cost minimization of

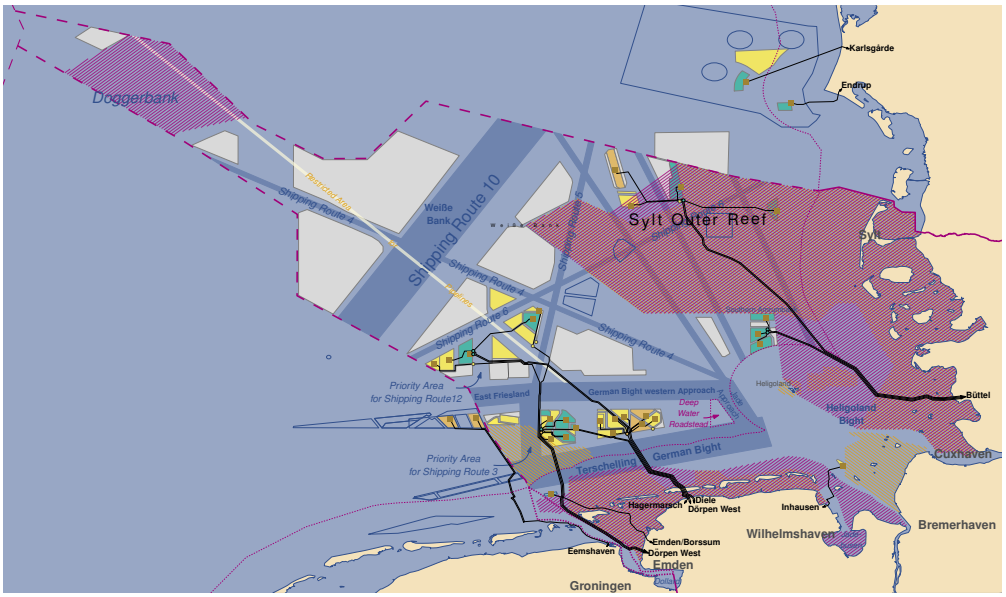

Figure 1.2: The German offshore wind farms in the North Sea, where the green, orange, yellow, and gray areas represent wind farms that are operating, under construction, approved, and planned, respectively. There are many restricted zones that are prohibited for wind farm planning such as shipping routes, areas reserved for gas pipelines, biota (violet hatched area), and bird sanctuaries (orange hatched area). A substation represents roughly speaking a collection point that collects the produced energy of wind turbines and forwards it. The connections from the last on-water substation to the first substation on the land-side (e. g., Dörpen West, Diele and Büttel have substations) are usually implemented by high-voltage direct current (HVDC). Note that this figure is a modification of [Dör17].

the new added transmission lines or maximization of the throughput of the power grid. Adding new transmission lines decreases the total power grid resistance [Cof+14], which results in less energy losses. However, adding lines can also decrease the operation limit—meaning the throughput—of the power grid, which becomes more clear in Chapter 5.

Long-term power grid configuration has the major disadvantage that the planning horizon is often in terms of decades [ent18], which is counterproductive for the desired plan to change the power grid quickly in the next few years [Jus14]. In addition, each expansion planning is done for a certain topological scenario meaning a fixed power grid, generation, and demand configuration. Different scenarios already occur with different productions and consumptions. Thus, another strategy that covers different scenarios and different topology changes is the placement of advanced control units (Strategy 2). This is known as static design problem, which is a subproblem of the

dynamic design problem. The latter is less cost intensive and represents a short-term configuration.

For Strategy 2 devices such as circuit breakers (known as *switches*) and Flexible AC Transmission Systems (FACTS) are able to manipulate the power flow by opening a circuit (switching a transmission line off) or rerouting a certain fraction of power by changing the susceptance of a transmission line in a device-specified interval, respectively. Both switches and FACTS are able to reduce the generation cost while increasing the power grid operation limit and satisfying the $N-1$ criterion [Li+13]. The $N-1$ criterion is a security and reliability criterion to ensure a stable operation while one element is removed or has a failure. Fisher ET AL. [FOF08] mentioned that switching is already used by TSOs in certain cases of emergency to decouple parts of the grid, avoid abnormal voltage situations, or improve voltage profiles. However, it is currently not used to extend the operability of the grid or reduce costs and losses, since the TSOs wish to interfere as little as possible in the power grid to avoid instabilities.

Since power grids are one of the major backbones, their reliability is crucial. A common and natural belief is that only TNEP has the ability to maintain and improve the reliability and operability of the power grid. However, placing switches and FACTS is another way—though counterintuitive—to improve the efficiency and reliability of the power grid. This counterintuitive behavior is known as Braess's Paradox [BNW05, Bra68] that is a common phenomenon in many physical networks (see Section 2.3). Furthermore, Schnyder and Glavitsch [SG90] mentioned that both switches and FACTS have the possibility to control over- and under-voltage situations, and line overloads. Other papers confirm loss and cost reductions [SG90], system security improvements [SG88], and combinations of all [HOO11a].

In this work, we mainly focus on Strategy 2 by placing elements such as switches or FACTS in such a way that we increase the operability of the power grid and thus, the power grid's capacity. Note that increasing the power grid capacity makes the power grid more reliable. Both electrical elements can increase the maximum load. Switching provides a possibility to remove a transmission line from the power grid temporarily. To the contrary, FACTS are control units that are able to influence the power flow in a certain range. However, FACTS are also more expensive and complex. We will look on Strategy 1 from the perspective of a plane grid with generators and consumers, but no preinstalled interconnection. We motivate this scenario by a wind farm planning problem denoted by wind farm cabling problem.

1.1 Main Contributions

The contributions of this thesis are mainly covered by four parts. The first part is about algorithms and structural results on electrical flows (also known by the term *power flows*) and is called the DIRECT CURRENT FEASIBILITY PROBLEM. The following two

parts cover an overview of the results that concern the efficient utilization of the existing power grid by placing switches (i. e., discrete changes to the power grid) and Flexible AC Transmission Systems (FACTS; i. e., continuous changes to the power grid), respectively. In the fourth part of this work, the wind farm cabling results are outlined that cover Strategy 1.

The Direct Current Feasibility Problem. One main tool that we use in this thesis are electrical flows commonly known under the term power flows. In this part, we will focus on the Direct Current Feasibility Problem (DC FEAS) that is an approximation of the Alternating Current Feasibility Problem (AC FEAS) (see Section 3.3). An algorithmic approach to computing electrical flows will be our first contribution in this thesis and our most fundamental result. We first give a mathematical description and structural overview of the problem structure. This description is used to develop algorithms for the electrical flow. One result shows that electrical flows do not constitute totally unimodular (TUM) bases. However, we show a possible way to solve the integer DC FEAS.

The first algorithm for DC FEAS is based on commonly known reduction rules that will give us an algorithm that runs in $O(|V|^3)$ time for an s-t planar power grid (i. e., a power grid with one generator and one consumer). We give another algorithmic idea for planar graphs that separates the quadratic relationship of voltage and current by using two graphs and a mapping of their edges. In addition to that, we are able to use a geometric interpretation of the problem to improve the understanding for discrete and continuous changes. Note that for linear systems the superposition principle holds in the physics and thus, calculating DC FEAS for all generator and consumer pairs results in an electrical flow for the whole power grid.

Discrete Changes in Power Grids. The placement of switches represents a discrete change in the power grid and is the first placement contribution we will focus on in this work. Note that a discrete change represents a topology change. In particular, we address a subproblem of the static design problem called Maximum Transmission Switching Flow Problem (MTSFP), which we model based on the DC electrical flow (see Section 5.1). The problem's combinatorial nature makes it hard to solve [LGH14] and the current ways to tackle the problem are exact but slow methods such as Mixed-integer Linear Program (MILP) [FOF08] or even more complex models [Hag15, KGD13], or heuristics without provable quality guarantees. In contrast, we focus on structural properties and algorithms with provable performance guarantees for the MTSFP. While it was known that MTSFP is NP-hard in general [LGH14], we show that it is also NP-hard if the network contains only one generator and one consumer (s-t-networks). The latter is a generalization of another NP-hardness proof given

by Kocuk ET AL. [Koc+16][1]. For s-t-networks on restricted graph classes (including cacti) we present an exact algorithm based on DOMINATING THETA PATHS (DTPs; see Section 5.4.1). These paths can be computed on general graphs and form the basis for a new centrality measure resulting in a new algorithm that works well in practice. To the best of our knowledge, we are the first to provide an approximation and an exact algorithm for MTSFP on special graph classes. Simulations on the NICTA Energy System Test Case Archive (NESTA) benchmark set show that these algorithms produce near-optimal results on most of the practical instances and thus, much better solutions compared to the proven guarantee.

Continuous Changes in Power Grids. Another way to use the grid more efficiently is by placing FACTS. Contrary to switches that allow discrete changes, FACTS represent a control unit that change the electrical flow by scaling the susceptance. This represents another static design problem and makes use of the existing power grid, too. We assume that a flow control unit is an *ideal* FACTS [GAG96] controlling the electrical flow on its branch without any restrictions. In the first work, we placed FACTS on buses and in the follow-up, we considered ideal FACTS as elements that can be only placed on branches. In general, the FACTS placement was shown to be NP-hard [LGH16]. Thus, most of the literature uses exact methods such as Quadratic Programming (QP) for the general formulation and for ideal FACTS we will use an MILP.

Using the well-known IEEE power systems test cases [Alb+79, AS74, Bil70, Cro15, Dem+77, GJ03, Gri+99, Jos+16, LB10, Les+11, Mat13, Uni14, WWS13, ZMT11], we performed simulation experiments related to two key questions, which take into account that the FACTS needed for implementing our flow control vertices in the real power grid constitute a significant and expensive investment and hence their number should be as small as possible. We investigate the following two research questions.

(Q1) How many ideal FACTS are required and where do they have to be placed in order to obtain a lower bound for the operating costs?

(Q2) If the number of available ideal FACTS is given, do we still see a positive effect on the operating costs and on the operability of the grid during peak periods of the grid?

In our simulations we determine the minimum number of flow control units necessary to achieve the same solution quality as in a power grid in which each element is controllable and which clearly admits a best bound on what can be achieved with the network topology. Interestingly, it turns out that a relatively small number of ideal FACTS are sufficient for this. In fact, we can prove a theorem stating a structural

[1] We thank Thomas William Brown for mentioning the paper of Kocuk ET AL. [Koc+16] to us after the conference talk of our paper [Gra+18], since this work was not known to us.

graph-theoretic property, which, if met by the placement of flow control units, implies the optimality of the power flow and serves as a theoretical explanation of the observed behavior. Research Question 1 becomes increasingly relevant as the consumption of electrical energy grows faster than the grid capacities. The Optimal Power Flow (OPF) minimizes the total generation costs of the power grid while maintaining a feasible electrical flow. Our experiments indicate that installing few ideal FACTS in a power grid is sufficient not only to achieve lower costs compared to an OPF solution, but also allows to operate the grid at capacities for which no feasible OPF solution exists any more.

Transmission Network Expansion Planning on the Green Field. Wind farms are an important and powerful possibility to convert wind into electricity. There are different challenges that come with the planning of wind farms such as the placement of turbines, the configuration/profile of turbines and substations, and the cabling of turbines. The configuration of the whole farm is computationally too expensive and even the cabling with multiple cable types is in general NP-hard (see Section 2.4). To solve this NP-hard problem, we use a heuristic approach called Simulated Annealing (see Section 7.2). We structure the problem into multiple layers that decrease the overall complexity of the problem. The problem is decomposed into circuits, substation problem, and full wind farm cabling problem. We created a first openly available wind farm benchmark set that is generated randomly and therefore is less structured than the standard wind farm.

1.2 Thesis Outline

We give a brief overview of the organization of this thesis. In particular, we would like to emphasize that parts of this thesis appeared in previously published proceedings, and reports [Gra+18, Leh+17, Lei+15a, Lei+15b, Mch+15].

Chapter 2 To understand the state of the art, we give a literature overview that is related to our research and differentiate our work to the known literature. In the beginning, we give a short summary on results concerning (electrical) flows and the development of digital techniques to compute such flows. A synergy of techniques known from graph-theoretical and power grid analysis is given in Section 2.2 that will provide us with techniques to understand and analyze power grids. Since our focus is on combinatorial problems in power grids, we describe the paradox (see Section 2.3) that makes switching a possible way to extend the operability of the power grid. Note that a similar effect is observed with FACTS. We show that there are works describing the Braess's Paradox not only for power grids and present known theoretical results. As already mentioned, switching increases the operability of the power grid. In Section 2.3.1,

we give an overview of known techniques to tackle the switching problem and show how we classify our work in the current literature. We analyze similar things for the FACTS placement in Section 2.3.2 and for the wind farm cabling problem in Section 2.4.

Chapter 3 In this chapter, we introduce basic terms and notions that will be used in this thesis with regards to graph theory (see Section 3.1), graph-theoretical flows (see Section 3.2), and electrical flows (see Section 3.3). For the two latter sections, we define the feasibility problems and show the relationships between the different models. In Section 3.3, we do not only define the feasibility problems, but give a broad overview of the models, describe the assumptions, advantages and disadvantages of certain model assumptions as well as common problems and the complexity of the power flow analysis.

Chapter 4 To analyze networks, we describe that the electrical flow (see Section 3.3) is a subproblem of many problems that optimize and analyze power grids. In the literature overview, we commonly see the usage of the mathematical formulation that is solved using a solver such as Gurobi [Gur16]. However, in this chapter, we analyze the mathematical structure of the Direct Current Feasibility Problem. We develop some algorithms for the DC electrical flow using the developed structural knowledge of the problem and show that the matrices are separately totally unimodular (TUM). The whole system is not TUM. The first algorithm is based on contraction rules with worse runtime than solving the system of linear equations of the mathematical formulation. Using a reformulation of the electrical flow, we are able to design another algorithmic approach that is much simpler.

Chapter 5 This chapter is published in [Gra+18]. Switching is one of the problems that show the existence of Braess's Paradox. We classified our work already in Section 2.3.1. A fundamental problem definition of Optimal Transmission Switching Problem (OTSP) and Maximum Transmission Switching Flow Problem (MTSFP) is given in Section 5.1 describing the relationships between different problems. Several transformations of the network model are introduced in Section 5.3. In Section 5.4, we describe algorithms and structural properties of switching on s-t-networks as well as showing when it becomes NP-hard. A 2-approximation on special graph structures is provided in Section 5.6. In Section 5.7, we evaluate our algorithms with methodical extensions. We conclude our work in Section 5.8 by summarizing the obtained results and outline future work including open problems.

Chapter 6 This chapter is published in [Lei+15a, Lei+15b, Mch+15]. Whereas switching represents a discrete change in the power grid, FACTS allow a change of

the electrical flow within an interval by scaling parameters such as the susceptance. Thus, it represents another possibility to "rebalance" the electrical flow by changing line parameters that have temporary influence on the topology of the power grid. In this chapter, we show that FACTS as well as switches are able to increase the operability of the power grid, while decreasing the overall generation costs. In addition, we give theoretical evidence that certain graph structures provide an optimal electrical flow that is equivalent to the min-cost flow.

Chapter 7 This chapter is published in [Leh+17]. A fundamental problem definition for the wind farm cabling problem is given in Section 7.1, where we introduce a first formal hierarchical structure definition of the wind farm problem; we further differentiate the full farm problem into the substation and circuit problem. The basic simulated annealing algorithm is introduced in Section 7.2 and we give our methodical extensions to this algorithm for the wind farm cabling problem. In Section 7.4, we evaluate our algorithm by using generated graphs as benchmark set. These benchmark sets are often harder than the current real world wind farms. We conclude our work in Section 7.5 by summarizing the obtained results and outline future work.

Chapter 8 This chapter summarizes the work we have done on the previously introduced placement problems in power grids that can influence the effect of the Braess's Paradox and thus, are able to improve the efficiency of power grids. However, this work is just a start to look at these problems from an algorithmic point of view and a lot of further investigations are necessary to improve existing algorithms and to understand these problems in more detail. Some ideas for possible future investigations are outlined in this chapter.

2 Literature Overview

In this chapter, we give a literature overview of the state of the art that is relevant for this thesis. We start with a brief literature summary with regards to (electrical) flows. Note that we will discuss (electrical) flows formally in more detail in Chapter 3. For now it suffices that an electrical flow represents some physical flow that differs from a graph-theoretical flow in the sense that it has some (roughly speaking) balancing properties that makes it inefficient in most cases with regards to optimization criteria that we focus on (e. g., maximizing the throughput). However, it reduces the overall energy loss (see Equation 4.26) making it more energy efficient. In addition, there are different approximation levels for electrical flows that are used for certain scenarios, which we discuss in more detail in Chapter 3. A common way to calculate electrical flows is by using solvers that search for a feasible solution. However, this gives us very little structural insights in how electrical flows work and thus, we give an overview of common reduction and transformation rules from the literature in Section 2.2 that make use of the superposition principle for linear systems. Note that we use the term network analysis in the context of calculating an electrical flow by using techniques that give more insights into the problem structure. There is currently not much known about structural insights to solve electrical flows using algorithms. We only found reduction and transformation rules that are not much investigated for a more complex power grid analysis. The only problem specific algorithm known is an exponential time algorithm [Sha87, SR61].

A major contribution of this work are placement problems. Placement problems exploit the structure in the sense that they modify the electrical flow such that some objective is optimized such as the throughput. This optimization is possible since the electrical flow has the property of balancing itself and thus, does not represent the best possible flow for a given topology. A literature overview on the behavior of electrical flows and the placement problems we focus on is given in Section 2.3. For the placement problems, we distinguish between discrete (see Section 2.3.1) and continuous placement problems (see Section 2.3.2), on which we give literature overviews by considering the placement of switches and Flexible AC Transmission Systems (FACTS), respectively. For transmission network expansion planning, we will focus on literature for the wind farm planning with the focus on wind farm cabling in Section 2.4. In this literature overview, we will see that there is little known about the problem with regards to structural results. Since there are not a lot of structural results, there are not a lot of algorithms to tackle electrical flows and because of that to tackle the aforementioned placement problems using algorithms.

2.1 Graph-theoretical Flows and Electrical Flows

The graph-theoretical flow complies with the conservation of flow meaning that the incoming flow is equal to the outgoing flow. This is similar to the principle of conservation of energy. If maximized it is called Maximum Flow Problem (MFP; Section 3.2). If each edge has a cost function, the problem of minimizing the total cost is called Minimum Cost Flow Problem (MCFP; Section 3.2). Both optimization variants are well known problems with efficient algorithms for both MFP [GT14] and MCFP [EK72, GT89, GT90, Kle67, Orl97]. The graph-theoretical flow complies with the conservation of flow (i. e., incoming is equivalent to the outgoing flow at each vertex) and the capacity constraints at each edge. However, electrical flows that we also call *power flows* have to obey some physical laws. The physical relationship between current, voltage, and resistance was first formalized by Kirchhoff [Kir47] in Kirchhoff's Voltage Law (KVL) and Kirchhoff's Current Law (KCL). The latter is equivalent to the flow conservation of graph-theoretical flows. The KVL represents a conservation of flow on cycles and not on vertices. The latter law states that the flows in a cycle (also known as mesh) sum up to zero. A base is a maximum independent set. Kirchhoff introduces for the KVL the concept of cycle bases, which we will discuss in more detail in Chapter 4. He shows which equations form a cycle base (i. e., a number of equations that suffice to compute the KVL), and he reformulates the voltage law in terms of a cycle base. This basically means that the number of equations for the KVL is reduced from potentially exponentially many equations to polynomially many equations while assuming simple graphs. Later, Maxwell [Max65] describes the electrical charge, electrical current, electrical field and magnetic field in more detail. These works formalize the operation of power grids and thus, build the foundation that is used in the power flow literature.

(Optimal) Electrical Flow Solution Techniques. In the aforementioned paragraph, we described that an electrical flow complies with the KCL and KVL. These laws constrain the electrical flow. A usual question in power grids is if the demand can be fulfilled with the currently available generation. This problem is called Feasibility Problem (FEAS). If we constraint the flow with the KCL and KVL law, we call it the electrical flow feasibility problem. We will see in Section 3.3 that there are different approximations for electrical flow and thus, different feasibility problems. In the following, we will give a brief overview of existing solution techniques for electrical flow feasibility problems in general. We will also mention the Optimal Power Flow Problem (OPFP) that is an optimization problem that minimizes the generation costs while complying with an electrical flow (here called power flow).

There are different techniques to solve electrical flow feasibility problems. One of the first surveys outlines digital techniques to solve the electrical flow [SJ67]. Another survey of electrical flow and optimal electrical flow solution techniques is

given by Huneault and Galiana [HG91] outlining the first automated digital solution technique by Ward and Hale [WH56], and the Gauss-Seidel method introduced by Carpentier [Car62, Car79], that is later replaced by the Newton-Raphson method [dMP99, Pes+68].

The problem of generating the required amount of power while obtaining minimum operation cost is called *Economic Dispatch Problem* (EDP). To cope with the EDP while incorporating an electrical flow feasibility problem is called the Optimal Power Flow Problem (OPFP) that was introduced by Carpentier [Car62]. The development of solution techniques on OPFP is summarized by Frank et al. [FSR12a, FSR12b].

Stott [Sto74] reduces the memory consumption and running time for electrical flow feasibility problems by introducing sparsity techniques for the admittance matrix and compares it to other methods. The idea behind the approach of Stott is that the power grid has a very sparse network structure [COC12, p.17] and thus, techniques that exploit the sparsity improve the running time and memory consumption. A comparison of different power formulations (see Section 3.3.1) is given by da Costa and Rosa [dR08]. Molzahn and Hiskens [MH19] give a survey of relaxations and approximations of the electrical flow equations. In Section 2.2, we outline some literature that mention possible ways to analyze power grids. Note that as far as we know there is no "purely" algorithmical approach to solve the power flow problem apart from an exponential time algorithm [Sha87, SR61]. For linear systems there are reduction and transformation rules known, which are not used so far to create an algorithm for electrical flows. A literature overview including known applications of these rules is given in the following.

2.2 Reduction Rules for the Analysis of Power Grids

In this work, we focus on a linear approximation of the electrical flow. Thus, all equations, constraints, and objectives are linear functions. The goal of the network analysis is to design algorithms that exploit the structure of the problem such that these algorithms run in polynomial time in the input size. There are different possibilities to analyze power grids. The common way to compute electrical flows is to solve a set of linear equations using solvers such as the Gurobi Optimizer [GUR13, Gur16]. However, the input size has often a big influence on the running time to solve a problem. A possibility to reduce the input size is to use reduction rules. However, reduction rules in power grids include contraction and transformation rules. Contraction rules are series (see Figure 2.1a) and parallel contractions (see Figure 2.1b) and transformation rules are Δ-Y- (delta-wye) and Y-Δ- (wye-delta) transformations (see Figure 2.1c). The latter rule transforms a triangle to a star by adding one vertex into the center and adding edges from the center to the already existing vertices, while removing the original edges, and vice versa for the inverse transformation, respectively. The generalization of the Δ-Y-

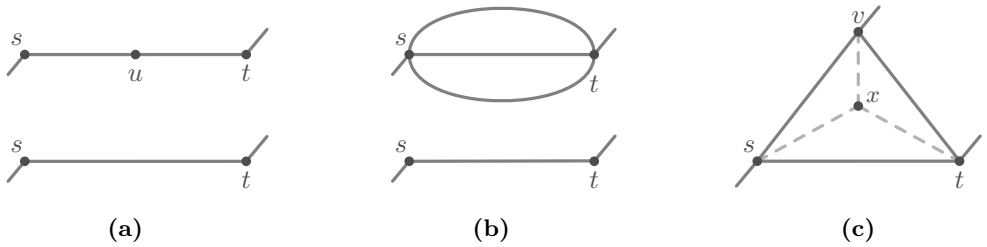

Figure 2.1: Three different subgraphs that lead to different transformation rules each. These common transformation rules provide possibilities to reduce the network size. (a) In a series contraction a path with vertices of degree two can be contracted to a single edge. (b) In a parallel contraction multiple parallel edges can be contracted to a single edge. (c) The Δ-Y-transformation (delta-wye; respectively Y-Δ-transformation known as wye-delta) represent a possibility to increase (respectively decrease) the number of vertices and reduce (respectively increase) the number of triangles by one.

and Y-Δ-transformations are the star-mesh- (or star-polygon-) transformations [Bed61, LO73]. Other common rules are self-loop and degree-1 removals.

These reduction rules are applied on different problems in different fields of research such as in statistical physics involving the evolution of crystal lattice energy [Bax16], network reliability [Leh63, ST93, Tra02], knot theory [Rei83, Tra02], and graph theory [Ake60, CE17]. We start with some initial algorithmic results on the transformation rules in the following.

Reducibility of Graphs and Complexity of Reduction Algorithms. The first more general structural observations concerning reduction rules are by Akers [Ake60] and Lehman [Leh63]. Both independently introduce the conjecture that by using a combination of Y-Δ- and Δ-Y-transformations, as well as series and parallel contractions the connected, two-terminal, undirected, planar graph can be reduced to a single edge connecting the given terminals [Leh63, pp.795ff.]. The latter conjecture is then independently proven by Grünbaum and Kaibel [GK03] using a graph without terminals, and a complicated and non-constructive proof by Epifanov [Epi66]. Using Δ-Y- and Y-Δ-transformations Epifanov proves that any polyhedral graph (i. e., an undirected graph that is a representation of a convex polyhedron) can be reduced to a K_4 (i. e., complete graph with four vertices). The proofs of the conjecture is simplified by Truemper [Tru89] using a constructive proof incorporating graph minors. One major property used in Truemper's proof is that planar graphs can be embedded as grid graphs. Truemper provides a much simpler polynomial time algorithm for planar graphs than the one by Feo [Feo85]. Truemper's [Tru89] algorithm requires $O(|V|^2)$ space, but he did not mentioned the running time of the algorithm. However, Feo [Feo85] designed a more complex algorithm that runs in $O(|V|^2)$ time and needs $O(|V|)$

space. Valdes ET AL. [VTL79] showed that the series, parallel, loop, and single degree reductions for series-parallel-graphs can be done in $O(|V|)$ time. In addition, Politof [Pol83] showed that every Y-Δ graph (i. e., a graph that can be reduced to a vertex by the aforementioned reduction rules) is planar. The term C_i (also known as i-cyclic graph) represents a closed walk of length $i \in \mathbb{N}$ with i being the number of vertices. A planar graph is a Y-Δ graph if and only if it is a $(C_5 + 2K_1, K_2 \times C_4)$-free graph [Pol83] or $(K_5, K_{2,2,2}, C_8(1,4), K_2 \times C_5)$-free graph [APC90, ST90], respectively. To the extent of our knowledge, it is unknown whether these algorithms are applicable to power grids or not. Some application to graph-theoretical problems are given in the next paragraph.

Preservation of Optimization Properties. Regardless of the structural point of view, these transformations are used when solving algorithmic problems. Dependent on the problem, it is necessary to show that the transformation and contraction rules preserve a solution space. This is roughly done by Akers [Ake60] for the MAXIMUM FLOW PROBLEM (MFP) and SHORTEST PATH PROBLEM (SPP). He used the transformations to simplify the network such that algorithmic problems become easier to solve. Akers [Ake60] applied the transformations to solve SPP and MFP on undirected 2- and 3-terminal graphs while preserving the optimal length or flow value. Interestingly, the transformations shown in Akers [Ake60] also behave dually meaning that, e. g., the calculation of the capacities of the series reduction is the calculation of the parallel reduction in the dual problem. The duality of the transformations is shown for example in Akers [Ake60]. Another work by Chang and Erickson [CE17] uses these reduction rules to untangle planar curves meaning to simplify a planar graph with a certain number of self-crossings. In the next paragraph, we show the usage of the reduction rules with regards to network reliability. Within network reliability there is a lot of literature available that gives structural results on the hardness of the problem and uses methodology to tackle NP-hard problems, which we will use for some placement problems.

Preservation of Network Reliability. In network reliability these reductions rules are used extensively. Network reliability studies the probability that at least one path connecting two terminals operates successfully. The edges in such a network have success probabilities. The problem of computing the all-terminal reliability for arbitrary networks is known to be NP-hard [PB83, Val79]. The hardness remains even for planar graphs [Ver05]. Lehman [Leh63] showed that series, parallel, degree-1, and loop reductions preserve reliability in the two-terminal and undirected network case. The Δ-Y- and Y-Δ-transformations for boolean functions (also known as switching-functions) are introduced by Lehman [Leh63, Section 4]. However, he shows that these transformations do not calculate the exact probability, but an approximation

to it. Since the problem is in general NP-hard, Satyanarayana and Tindell [ST93] developed efficient algorithms for special graph classes, which run in $O(|V|\log|V|)$ time. The latter work [ST93] uses the technique of forbidden minors (i. e., a minor H is a graph that can be extracted from a graph G by applying vertex and edge deletions and edge contractions) to develop efficient algorithms for reliability analysis on graph subclasses. Satyanarayana and Tindell not only focused on the two terminal case, but on the K-terminal reliability that focuses on the probability that there is a path between every pair of terminals. Where Lehman [Leh63] showed that not all transformations are reliability preserving reductions, Satyanarayana and Tindell [ST93] focused on reliability preserving reductions and introduced a trisubgraph-Y-reduction. They focused on block-cut-trees, 3-connected graphs, and series-parallel graphs. For the latter graph structure they observed that it depends on the distribution of the terminals whether the graph is reducible or irreducible and thus, reliability preserving using the standard reduction rules or not. The K-terminal reliability on series-parallel-reducible networks can be computed in $O(|E|)$ time using series, parallel, degree-1, and -2 contractions [SW85, pp.827ff.]. However, for series-parallel-irreducible graphs these reduction rules are not sufficient and thus, Satyanarayana and Wood [SW85] designed a linear time algorithm using the *polygon-to-chain reduction* that reduces two parallel paths $\pi_1(s,t)$ and $\pi_2(s,t)$ with inner vertices of degree-2 to one path having a length of $\max\{|\pi_1(s,t)|, |\pi_2(s,t)|\}$. For basically series-parallel directed graphs (i. e., graphs where the underlying graph is a series-parallel graph) Agrawal and Satyanarayana [AS84, AS85] provide an $O(|E|)$ time algorithm to compute source-to-K-terminal reliability. Politof and Satyanarayana [PS86, PS90] show that for $K_2 \times C_4$-free graphs the reliability can be computed in linear time and Politof ET AL. [PST92] show that the all-terminal reliability of a $(K_5, K_{2,2,2})$-free graph can be computed in $O(|V|\log|V|)$ time. Satyanarayana and Tindell [ST93, p.13, Proposition 2] show that a Y-Δ graph allows a trisubgraph-Y reduction resulting in a Y-Δ graph.

Further Results. There are results on reducibility for planar graphs, non-planar graphs, and special graphs that we outline here. Gitler [Git91] proofs for reducibility for graphs with no K_5 minor and graphs with no $K_{3,3}$ minor. The reducibility for projective-planar graphs (i. e., a projective plane is an extension of the euclidean space, where parallel edges intersect in a point and thus, all edges intersect in some point) and graphs with crossing number one was shown by Archdeacon ET AL. [Arc+00]. For 4-terminal reducibility of planar graphs, Demasi and Mohar [DM15] show that a sufficiently connected cubic graph (i. e., a graph, where all vertices have a degree of three) are reducible if and only if it does not contain a Petersen graph as minor. Later Wagner [Wag15] presents a reducibility for almost-planar graphs with the condition that all graphs in the reduction sequence remain almost-planar. Other works define the reducibility with a set of forbidden minors [Yu04, Yu06] and design algorithm for

3-terminals, special cases of 4-terminal planar graphs, k-cofacial terminals in planar graphs [Git91, GS].

2.3 Braess's Paradox – Effects that Influence the Power Grid Efficiency and Stability

The main focus of this thesis is on placement problems with additional physical properties. In the introduction (see Chapter 1), we discuss two strategies to improve the power grid efficiency. In contrast to our intuition, not only the expansion of the power grid (TNEP; Strategy 1 in Chapter 1), but also switching can be used to improve the efficiency of the power grid. This implies that adding a new line to the power grid can also decrease the throughput of the power grid or increase the overall generation costs.

A similar phenomenon exists for road networks and is called Braess's paradox [BNW05, Bra68]. Introducing a new road to the traffic network might cause longer travel times [YGJ08]. The main reason is that every participant wants to independently minimize its own travel time, while ignoring the decision's effect on other travelers [PP97]. In addition, Pas and Principio [PP97] show that the occurrence of the Braess's paradox highly depends on the instance parameters, i. e., demand and congestion functions. Thus, the paradox usually occurs within some bounds that make it possible that the network might "grow in" and "grow out" of the paradoxical situation with increasing (traffic) demand.

Cohen and Horowitz [CH91] describe the existence of the paradox in mechanical [PV12] and electrical networks (for both see [PP03]). Other works show that the paradox also appears in oscillator networks [WT12], where adding a line can cause instabilities and even power outages, which confirms once more the existence of the Braess's paradox in real power grids [WT12, p.11]. Another example for this exists in quantum physics [Pal+12].

Cohen and Horowitz [CH91] also emphasize the non-intuitive behavior of the Nash equilibrium that arises in most physical networks. We know from Dubey [Dub86, p.4, Section 3] that Nash Equilibria "tend to be inefficient in the Pareto sense". We will give an explanation of that in Chapter 4. The Nash Equilibrium is a known fix point in Game Theory and represents a state, where no player wants to change its choice. In contrast, the Pareto optimum means that there is no possible better choice of one player that does not decrease the payoff of another player. Thus, it is the optimum with regards to a cost function. The Pareto front represents the set of Pareto optima. However, the Pareto optimization plays a crucial role in the multi-criteria optimization. We show an example for a Pareto front in Figure 6.7a. An easy example that shows Pareto optima and Nash Equilibriums is given in Dubey [Dub86, p.5, Figures 2–4].

Another theoretical insight given by Valiant and Roughgarden [VR06] explaining that the Braess's paradox occurs very often in random graphs. Note that many of the networks in the real world have properties similar to random graphs [Hof19, p.xiii]. Thus, in Chapter 5, we exploit the Braess's paradox to improve the efficiency of the power grid, whereas in the TNEP problem, we have to add lines in a way that the efficiency of the power grid increases and thus, the effect of the Braess's paradox does not appear. The effect that the Braess's Paradox highly depends on the instance parameters [PP97] is shown in Chapters 5 and 6, where we use switches and FACTS to influence these parameters.

2.3.1 Switching – A Discrete Manipulation of the Power Grid Topology

Recall that switching is the process of temporarily removing a transmission line from the power grid by using devices such as circuit breakers. Kirchhoff model this behavior by changing the resistance to infinity [Kir47, p.501]. Switching was first analyzed as a negative effect in the power grid [Gla85] responsible for overloads, voltage drops, and the loss of network stability. Koglin and Müller [KM80] introduce transmission switching as a corrective control action to reduce transmission line overloads. Later other positive switching effects were recognized such as improving currents, decreasing loads and angles, creating voltage drops, and changing the short-circuit power [Gla85, HOO11a, RM99].

O'Neill et al. [ONe+05] and Fisher et al. [FOF08] introduce the Optimal Transmission Switching Problem (OTSP) and its formulation based on the Direct Current Optimal Power Flow (DCOPF) [Cho+06], respectively. The OTSP using DC-constraints is called DCOTS. Fisher et al. [FOF08] observe that switching may improve the economic efficiency of the Economic Dispatch Problem (EDP). However, they could not find any general trend in the physical characteristics of the switched lines. Many models were presented that are more complex [Bai+15, SF14] or minimize either the overload [MTB89, MWH86, Wru+96], voltage problems [BM87, RIM95], losses [BG88], or generation costs [FOF08, ONe+10]. Others enhance the security [BDD89, SG90], reliability [DK15, ZS17, ZW14], economic seasonal [JWV15], or Transmission Network Expansion Planning (TNEP) costs [KSK10, VP12].

DCOTS is known to be NP-hard [LGH14, LGH15] and solving it by running an Integer Linear Programming (ILP) has impracticable running times [FOF08]. The complexity is reduced by limiting the solution set, i. e., number of switches [Hed+08, Hed+09, SV05]. Often a small number of switches is sufficient to reach the optimum. This is a central property in most heuristics [CW14, FRC12, Hed+11] that use a ranking of the transmission lines based on different criteria. Pourahmadi et al. [PJH16] show that switching lines with high congestion costs is a reasonable criterion to reduce the overall cost. Other pre-screening techniques rank the lines on their dual prices

for each bus [LWO12]. Other approaches are Evolutionary Algorithms [AF09, DV01], branch-and-bound [TC14b], and partitioning [Bai+17, Li+13, Mäk+14]. Yang ET AL. [YZX14] use a soft rounding heuristic [Jün+10, p.629] not fixing all variables to a value but obtaining this by changing the objective function coefficient of the binary variables.

However, there is not a lot known with regards to structural exploits of the power grid topology. Ostrowski ET AL. [OWL12, OWL14] exploited the symmetry of transmission lines for the switching problem by removing identical parallel transmission lines. Different network parameters lead to a different system performance and are connected in some sense to switching [Ari+09, BNX09, HB08]. Barrows ET AL. [BB11, BB12, BBB13] use topological and electrical parameters as a heuristic. In addition, they investigate parameters concerning OTS such as resistance, reactance, susceptance, vertex degree, thermal limits, and edge-betweenness centrality [HB08] (number of shortest paths through an edge) but find no statistically significant relationship. Recall that Pas and Principio [PP97] show that the Braess's Paradox highly depends on the instance parameters and that a single parameter evaluation lacks in this particular case as it is influenced by multiple parameters such as topology, susceptance, and capacity. In addition, there exist also screening and ranking systems based on network flows [MWH86, Wru+96].

Most of the work so far tries to adapt OTS to other problems, reformulates the model, or analyzes it for different power grids. However, the majority of the papers have problems to solve their models to optimality even on small instances. Thus, most heuristics try to decrease the search space, a few concentrate on structural aspects of power grids, while others try to find correlations between power grid parameters and switching. A common observation is that the effects of transmission switching are relatively localized [BB11, BB12, Gla85]. This observation is debatable as it is made without solving the problem to optimality and using test cases such as the *reliability test system 1996* RTS-96 test case that is three copies of the 24-bus power system linked together. However, in general there is no network property found to distinguish the switched lines [BB11]. Thus, current techniques do not provide a deeper understanding of the problem structure. The latter will be our contribution to the community for certain graph structures, which we give in Chapter 5.

2.3.2 FACTS – A Continuous Manipulation of the Power Grid Topology

Recall that the graph-theoretical flow is a flow mainly controlled by the KCL and capacity constraints, whereas the electrical flow has to obey physical laws. The graph-theoretical flow and the electrical flow give us, while maximized (respectively when the generation cost is minimized), the upper and lower bounds (respectively lower and upper bounds), respectively (more on that in Chapter 4). In addition, Pas and Principio

[PP97] show that different instance parameters influence the effect of the Braess's Paradox. Thus, changing the parameter helps to change the effect the Braess's Paradox has on the network. With FACTS the idea is to exploit the network structure such that the flow behaves more like a graph-theoretical flow and thus, closer to the best bound. Recall that a similar approach is done by switching.

With the increasing availability and technological advancement of FACTS researchers began to study the possible benefits of their installation in power grids from different perspectives to approach the Research Questions 1–2 (see Section 1.1 on Page 6).

From an economic perspective, it is of interest to support investment decisions in power grid expansion planning by considering alternative investment strategies that either focus on new transmission lines or allow mixed approaches including FACTS placement. Blanco ET AL. [Bla+11] present a least-squares Monte-Carlo method for evaluating investment strategies and argue that FACTS allow for a more flexible, mixed strategy that fares better under uncertainty. Tee and Ilić present an optimal decision-making framework for comparing investment decisions, including FACTS [TI12].

From the perspective of operating a power grid, the main question is how many ideal FACTS are required and where do they have to be placed in order to optimize a certain criterion. Cai ET AL. [CES04] propose and experimentally evaluate a genetic algorithm for allocating different types of FACTS in a power grid in order to optimally support a deregulated energy market. Gerbex ET AL. [GCG01] and Ongsakul and Jirapong [OJ05] study the placement of FACTS with the goal of increasing the amount of energy that can be transferred. Gerbex ET AL. [GCG01] present a genetic algorithm that simultaneously optimizes the energy generation costs, transmission losses, line overload, and the acquisition costs for FACTS. Ongsakul and Jirapong [OJ05] use evolutionary programming to place FACTS such that the total amount of energy that can be transferred from producers to consumers is maximized. In contrast to our setting, they may also increase the demands of consumers arbitrarily. Contrary to these heuristic approaches Melo Lima ET AL. [Mel+03] use mixed-integer linear programming to optimally increase the loadability of a system by placing FACTS subject to limits on their number or cost. Similar to our approach, they do not distinguish different types of FACTS but rather assume "ideal" FACTS that can control all transmission parameters of a branch. However, they focus only on loadability and do not consider generation costs and line losses. The latter two objectives will be considered in our work.

All related work mentioned so far considers the DC model for electrical networks as an approximation to the AC model (more on that in Section 3.3) and aims at providing a preliminary step in an actual planning process, where this approximation is sufficient. There are also a few attempts to solve the placement problem for FACTS in the more realistic but also more complicated AC models [MEA99]. These models can be categorized as follows:

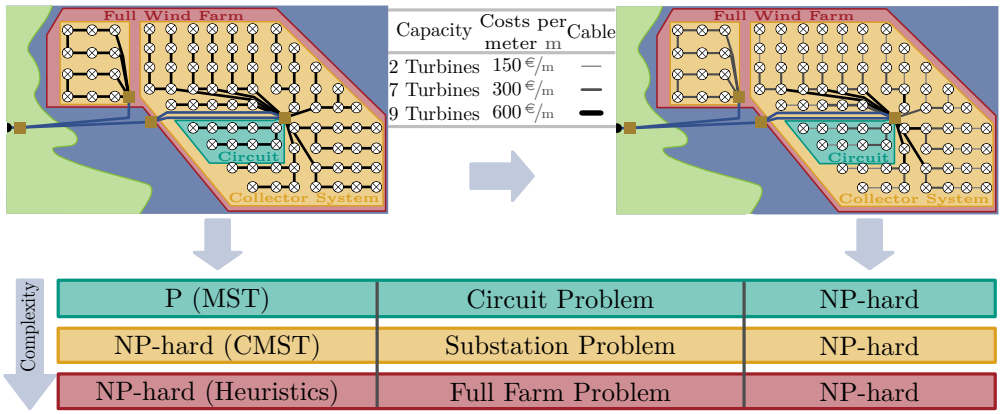

Figure 2.2: The wind farm topology consists typically of turbines ⊗ and substations ■. The complexity of cabling a wind farm differs depending on the cost function. If we assume unit costs—meaning we have only one cable type ━ available—then the problem is slightly easier to solve (see left side) than when allowing multiple cable types ☰ (see right side). The different cable types are shown in the table. The complexity of the problem also increases dependent on the problem layers. The easiest layer is the Circuit Problem (CP), followed by the Substation Problem (SP) and Full Farm Problem (FFP).

- AC models with sinusoidal loads (non-convex and non-linear formulation),
- AC quadratic approximations (non-convex and quadratic formulation),
- AC piece-wise-linearization (non-convex and integer linear programming formulation), and
- AC linearization (convex and linear formulation).

Sharma et al. [SGV03] develop an evaluation whether transmission lines are critical and propose to place FACTS at critical lines in order to improve voltage stability in the grid. Ippolito and Siano [IS04] present a genetic algorithm for FACTS placement in AC networks and experimentally evaluate it in a case study. In contrast to these heuristic approaches, Farivar and Low [FL13] observe exact OPF evaluation in a relaxed AC-model. In this context, they place phase shifters to exploit structural characteristics that are similar to our approach.

2.4 The Wind Farm Cabling Problem

The amount of renewable energy producers started to increase significantly a few years ago. However, there is not a lot of research done in the field of wind farm planning. From an algorithmic point of view and using just a single cable type,

the Circuit Problem (CP) can be solved using a Minimum Spanning Tree (MST) algorithm [Gab+86, HK71], whereas the Substation Problem (SP) can be solved using Capacitated Minimum Spanning Tree (CMST) [Voß09]. However, CMST is already NP-hard, but approximation algorithms and heuristics exist for this type of problem [EW66, Mar67, Voß09]. This is visualized in Figure 2.2. We are interested in the layout problem using multiple cable types with different capacities and costs per meter, which is already NP-hard for two cable types in the Circuit Problem. Using brute force for $|K|$ different cable types and $|E|$ possible interconnections would mean that there are $|K|^{|E|}$ possible combinations to compute. However, to compute cabling layouts with multiple cable types some work is done in the area of cluster-based, MST-based and genetic algorithms. Dutta and Overbye [DO11] used the Quality Threshold (QT) Clustering algorithm to group the turbines into collector systems or even groups within a collector system. They evaluate—based on reliability, power losses and cabling costs—three different layouts namely the radial, cluster-based, and mixed layout.

If the wind farm planning does not consider the cabling of turbines, but the connection of entire offshore wind farms among themselves and to the mainland, then the clustering approach based on k-mean [Kan+02] from Svendsen [Sve13] tries to model and propose an algorithm for that kind of problem by taking investment costs and operational costs with different stakeholders into account.

A more general attempt—not using clustering, but a MST-based approach—was given by Berzan et al. [Ber+]. It solves the circuit problem for multiple cable types.

In contrast, evolutionary algorithms present a very promising approach to solve complex, multi-variable and multi-objective optimization problems with many design variables (see Chapter 7). Within evolutionary algorithms, a genetic algorithm (GA) is usually applied to problems with huge solution space and discrete variables. There are GA approaches introducing different encodings and solution methods for electrical systems integrating different electrical components to be optimized such as type of turbine and substation [Gon+12, LYX09, ZCB04, ZCB09, ZCH06].

A different modeling approach was proposed by Hertz et al. [Her+12] including unsplittable electrical flows into the Mixed-integer Linear Program (MILP) for the wind farm design problem, which forbids to split the incoming power from one cable.

In general, the cabling problem has a lot in common with transportation of goods, where the cost of laying a cable does not necessarily depend on the actual amount of power it transports. If the maximum power exceeds the capacity (thermal limit) of a cable, a different and more expensive cable is deployed. This raises the costs in a non-convex manner and makes it NP-hard [YK12]. In transportation of goods, trucks and goods are an analogous example of cables and power, respectively. Heuristical approaches to solve the problem in logistics are Tabu Search [GL99], Ant Colony Optimization [Dor01] and simulated annealing (SA) [OL96]. Yaghini and Kazemzadeh

solved the Multicommodity Capacitated Network Design (MCND) Problem in the field of logistics with a SA approach. This algorithm serves as basis for our algorithm and is improved for the wind farm cabling problem.

In contrast to the GA approaches, we are not interested in solving the configuration, but the physical layout. Furthermore, the choice of the GA's cost function is debatable, since integrating the throughput of a farm might be also important. Our model omits unsplittable flows, since it increases the complexity of the problem without bringing an additional benefit and distorts the electrical reality.

Most of the papers evaluate their algorithms on a small instance or on a small set of benchmark data. Especially for evolutionary algorithms, this can lead to a falsification of the results, since the configuration of the algorithm is improved with regards to one specific data set, but might perform poorly on others. Thus, we generate a test data benchmark set on which we perform our simulations to avoid such effects and give a more general statement.

3 Fundamentals

In this chapter, we introduce fundamental terms concerning graph theory (Section 3.1) and graph-theoretical flows (Section 3.2). For complexity theory, we refer to the common literature [Aus+99, GJ79]. The Feasibility Problem (FEAS) checks whether for a given supply and demand there is a feasible (electrical) flow. We give an overview of the different feasibility problems in power grids in Section 3.3 that form the basis of any problem in the power grid analysis. We start with the Alternating Current Feasibility Problem (AC FEAS) and its different formulations in Section 3.3.1. In the latter section, we define different functions that are used in this thesis and give a short overview of the common transmission line representations that are used in the literature. Furthermore, we give an idea of how we are able to add more complex elements such as transformers and Flexible AC Transmission Systems (FACTS) to the models without changing the models themselves, but a component of the analysis.

AC FEAS is NP-hard [LGH16, Ver10]. Since FEAS is a subproblem of all placement problems, we use an approximation of AC FEAS that is polynomial time solvable to increase the (structural) understanding. In Section 3.3.2, we introduce different assumptions that result in such a (linear) feasibility problem commonly known as Direct Current (DC) FEAS. While the model is derived from an AC model, we will give the analogies to the DC model of the DC network to understand the meaning of the name. A feasibility problem that uses one assumption less than the DC feasibility problem is denoted by the Voltage Normalized Lossless Real Power Flow FEAS (VNLP), which is described in Section 3.3.3. The problem is known to be NP-hard [BV19, Ver10]. Afterwards, we discuss the practicability of the simplifying model assumption in Section 3.3.4.

3.1 Fundamental Graph-theoretic Terminology

The underlying power grid is in our case *reciprocal* (also known as bilateral), i. e., a bidirectional power flow is allowed, and it is common to give each edge an orientation for notational convenience. Thus, the power grid's topological structure can be represented by a *(simple) undirected graph* $G = (V, \overleftrightarrow{E})$ with a set $V(G)$ of *vertices*, representing buses in our case, and a set $\overleftrightarrow{E}(G) \subseteq \binom{V}{2}$ of *edges* that is represented by unordered pairs of vertices $\overleftrightarrow{e} = \{u, v\} \in \overleftrightarrow{E}(G)$ representing electrical elements such as cables or lines. Note that buses represent electrical junction points and that an edge can represent devices such as transformers, circuit breakers, or FACTS; or simpler

elements such as inductors, resistors, or capacitors. Depending on the literature edges are sometimes denoted as branches or circuits. The term *simple* denotes that there is at most one edge per vertex pair allowed.

Even though the underlying power grid is in our case *reciprocal*, it is common to give each edge an orientation for notational convenience. A *directed graph* is a tuple $G = (V, E)$, where each edge in the set $E(G)$ of edges has an orientation that is represented by an ordered pair of vertices $e = (u, v) \in E(G)$. If not ambiguous, for $V(G)$, $\overleftrightarrow{E}(G)$, and $E(G)$ we simply write V, $\overleftrightarrow{E}$, and E, respectively.

In general, power grids can have multiple edges between to vertices. There are multi-graphs $G = (V, E, \mu_{\text{para}})$ with the multiset $E \subseteq V \times V$ of edges. Thus, there is a mapping $\mu_{\text{para}} \colon \overleftrightarrow{E} \to \{\{u, v\} \mid u, v \in V; u \neq v\}$ identifying edges $\overrightarrow{e}_i \colon \{u, v\}^i$ with $1 \leq i \leq k$ being the k parallel edges (i. e., in our case conductors) that belong to the same electricity link $\{u, v\}$. Note that in terms of power grids a multi-graph can be easily simplified to a simple graph (see Section 4.2). Thus, if not mentioned otherwise, we assume that our graphs are simple and for notational simplicity use both the directed graph and the underlying undirected graph that are distinguished by the notation of the edge set.

Vertices that have an edge in common are called *adjacent* and are *neighbors*. The set of neighbors, i. e., the neighborhood, of a vertex v in an undirected graph is denoted by $N(v) = \{u \in V \mid \{u, v\} \in \overleftrightarrow{E}\}$. For a vertex v in a directed graph, we distinguish between incoming edges $(u, v) \in E$ and outgoing edges $(v, w) \in E$ for all $u, w \in V$. The neighborhood created by incoming and outgoing edges is denoted by $N^+(v) := \{u \in V \mid (u, v) \in E\}$ and $N^-(v) := \{u \in V \mid (v, u) \in E\}$, respectively. A vertex that represents an endpoint of an edge is *incident* to that very edge. The *degree* of a vertex v denotes the number of edges it is incident to. We distinguish between degree, in-degree, and out-degree defined by $|N(v)|$, $|N^+(v)|$, and $|N^-(v)|$, respectively.

Cain et al. [COC12, p.13] mention that power grids are planar. A graph is called *planar* if it can be embedded into the plane without any edge crossings, i. e., the edges have no common point, but the two vertices representing the endpoints of an edge. However, note that there is usually more than one embedding for a graph G that is planar. Thus, let us assume a fixed *planar embedding* $\mathcal{E}$ of a graph G into the plane with $G(\mathcal{E}) \cong G$ (i. e., $G(\mathcal{E})$ is isomorphic to G) and an injective function $\mu_{\mathcal{E}} \colon V \to \mathbb{R} \times \mathbb{R}$ meaning there is a correspondence between the vertices V of the graph and the geometrical points $\mathcal{P}$ of the plane embedding. An edge set $E(G)$ of $G(\mathcal{E})$ is a subset of a topological space $\mathcal{T}$, where each edge in $G(\mathcal{E})$ is a Jordan curve in $\mathcal{T}$ and the incidences and adjacencies are defined accordingly [GT01].

An *induced* subgraph $G[V']$ of a graph G is a graph $H = (V' \subseteq V(G), \{(u, v) \in E(G) \mid u, v \in V'\})$ whose vertices V' are a subset of $V(G)$ and that has exactly these edges that have both endpoints in V'. Note that this definition also applies to undirected

graphs with the set of edges $\overleftrightarrow{E}$. Note that a subgraph that is not induced does not necessarily incorporate all edges, where both endpoints are in V'.

A *path* from a vertex s to a vertex t (or s-t-path) is a sequence of edges $\pi(s,t) \coloneqq \big((s,v_1),(v_1,v_2),\ldots,(v_{k-1},v_k),(v_k,t)\big)$, where two successive edges have an endpoint in common. We call a path *simple* if no vertex is visited twice and thus, all vertices $s, v_1, v_2, \ldots, v_k, t$ are distinct. In general, there is more than one path from s to t. We denote the *set of simple paths* from s to t by $\Pi(s,t)$. A *cycle* c is a path $\pi(s,t)$, where the first and the last vertex are identical meaning $s = t$. A cycle is called *simple* if all vertices are distinct with the exception of s and t. A graph with no cycles is called *acyclic*.

A *connected component* is a subgraph, where there is a path between each pair of vertices. Furthermore, we call a graph G *connected* if it has one connected component. A *tree* is a connected graph $T = (V, \overleftrightarrow{E})$ that has no simple cycles. A tree T that connects all vertices of a connected graph $G = (V, \overleftrightarrow{E})$ is called a *spanning tree* with $V(T) = V(G)$ and $\overleftrightarrow{E}(T) \subseteq \overleftrightarrow{E}(G)$ with $|\overleftrightarrow{E}(T)| = |V| - 1$ being the number of edges. If graph G is not connected and has k connected components then we construct a spanning tree for each connected component. The set of spanning trees is called spanning forest $\mathcal{T}$ and thus, the number of edges in a spanning forest is $|V| - k$. Let $\mathcal{T}$ be some fixed spanning forest in G. Edges of graph G that are not branches of that spanning forest $\mathcal{T}$ are given by $\overleftrightarrow{E}(G) \setminus \overleftrightarrow{E}(\mathcal{T})$ and are called *chords* with respect to $\mathcal{T}$. The number of chords is given by $|\overleftrightarrow{E}| - |V| + k$, where k is the number of connected components.

An *edge cut-set* $K \subsetneq \overleftrightarrow{E}$ is a set of edges with $\overleftrightarrow{E} \setminus K$ that decomposes the graph G into at least two new components. In terms of Whitney [Whi32] or Seshu and Reed [SR61, p.27] this means that the rank $\mathrm{rk}(G)$ of the graph G reduces by at least one. The *rank* of a graph is defined by $|V| - k$, where k is the number of connected components. Note that cycles and cut-sets are closely related to each other as shown in Chapter 4.

A graph can be represented in different ways as a matrix. Note that we represent a *matrix* with bold capital letters and *vectors* with an overhead arrow. The *oriented adjacency matrix* $\mathbf{A} \in \{-1,0,1\}^{|V|\times|V|}$ represents the connections of a graph by vertex adjacencies meaning an entry in row u and column v is 1 (respectively -1) if there is an edge $(u,v) \in E(G)$ (respectively $(v,u) \in E(G)$). The entry is 0, if there is no such edge in the graph. The *oriented incidence matrix* $\mathbf{I} \in \{-1,0,1\}^{|V|\times|E|}$ is another matrix that represents connections of a graph. An entry in row u and column e of the oriented incidence matrix $\mathbf{I}$ is 1 (respectively -1) if e is an incoming edge (respectively outgoing edge) at vertex u, and 0 otherwise (see for example Figure 4.6 on Page 69). The following properties of the incidence matrix illustrate the importance of spanning forests.

(**I**–P1) The rank $\mathrm{rk}(\mathbf{I})$ of the incidence matrix $\mathbf{I}$ is $|V| - k$, where k is the number of connected components [SR61, p.62, Theorem 4-3], and

(**I**–P2) a square submatrix of the incidence matrix $\mathbf{I}$ of size $\mathrm{rk}(\mathbf{I}) \times \mathrm{rk}(\mathbf{I})$ is nonsingular (i. e., the determinant is either 1 or -1) if and only if the submatrix's columns

constitute a spanning forest $\mathcal{T}$, otherwise the determinant is 0 [SR61, p.69, Theorem 4-10].

An example for incidence property **I**–P2 is given in Figure 4.6 on Page 69. Within this example adding a cycle edge (e. g., edge g) and removing a spanning tree edge (e. g., edge d) would destroy the consecutive one diagonal in the upper left partition and thus, the determinant becomes 0. Note that the subgraph with the latter configuration is disconnected.

Another possibility to represent the graph G is the *oriented circuit matrix* $\mathbf{B} \in \{-1, 0, 1\}^{|C|\times|E|}$, where C is the set of simple cycles. Assume we define a direction for each cycle. The matrix has a 1-entry if the edge is in the cycle and aligned with the cycle direction, -1 if it is opposite to the defined direction, and 0 otherwise (see for example Figure 4.6 on Page 69). The properties of the circuit matrix give a hint of the duality of the incidence and circuit matrix that we describe in more detail in Section 4.1.

(**B**–P1) The rank $\operatorname{rk}(\mathbf{B})$ of a circuit matrix $\mathbf{B}$ is $|E| - |V| + k$, where k is the number of connected components, and

(**B**–P2) a square submatrix of $\mathbf{B}$ of size $\operatorname{rk}(\mathbf{B}) \times \operatorname{rk}(\mathbf{B})$ is nonsingular if the submatrices columns constitute a set of chords that belong to a spanning forest $\mathcal{T}$.

Note that the circuit matrix property **B**–P2 becomes clear from Figure 4.6 on Page 69. Swapping a chord with a spanning tree edge destroys the consecutive one diagonal of the bottom right section.

The *oriented cut-set matrix* $\mathbf{Q} \in \{-1, 0, 1\}^{|\mathcal{K}|\times|E|}$, where $\mathcal{K}$ is the set of cut-sets. The entry is 1 (respectively -1) if the edge is in the cut-set and oriented in the arbitrarily predefined direction (respectively in the opposite direction), otherwise it is 0. The *oriented cut-set matrix* $\mathbf{Q}$ has rank $\operatorname{rk}(\mathbf{Q}) = |V| - 1$ for any connected graph.

Note that all previously shown matrices exist also in a nonoriented fashion that represent undirected graphs with entries $\{0, 1\}$ representing if an element is in the graph, i. e., 1, or if it is not an element, i. e., 0, of the graph G.

The unnormalized Kirchhoff matrix—better known as Laplacian matrix—is defined by $\mathbf{L} \coloneqq \mathbf{I}\,\mathbf{I}^\intercal = \mathbf{D} - \mathbf{A}$, where $\mathbf{D}$ is the diagonal matrix with the vertices' degrees. The relationship $\mathbf{I}\,\mathbf{I}^\intercal = \mathbf{D} - \mathbf{A}$ comes from the matrix multiplication, where the diagonal entries are the scalar product of the row vector $\mathbf{a}_i$ with its transposed $\mathbf{a}_i^\intercal$, where $i \in V$. The latter means the scalar product $\mathbf{a}_i \cdot \mathbf{a}_i^\intercal$, which is equivalent to entry $\mathbf{D}_i$. Otherwise, the entries are -1 if two vertices have an edge in common, since we take the scalar product of a row $\mathbf{a}_u$ of $u \in V$ with another transposed row $\mathbf{a}_w^\intercal$ of $w \in V$. The entries of both rows have a 1 or -1 entry if they are incident to an edge. Thus, if both vertices are incident to the same edge the scalar product is -1. The latter is represented by the subtraction of the adjacency matrix $\mathbf{A}$.

3.2 Fundamentals in Graph-theoretic Flows

Problems in different domains are modeled with graph-theoretic flows. We usually distinguish between the *Maximum Flow Problem* (MFP), and the *Minimum Cost Flow Problem* (MCFP).

Assume a graph G as mentioned in the previous section with additional properties of the edges and certain vertices that influence a flow. Thus, they become part of the graph's description. The edge property is the *capacity* that are functions $\text{cap}\colon \overleftrightarrow{E} \to \mathbb{R}_{\geq 0}$ associating each edge with a capacity. In terms of power grids, the capacity represents a thermal line limit. In addition, we introduce two special vertices to the topology of a graph that are denoted by *source* s and *sink* t with $s, t \in V$. These vertices are usually called *terminals*. Often such a graph is denoted as *capacitated source-sink-graph* that is a tuple $G = (V, E, \text{cap}, s, t)$. We prefer to distinguish between the pure topology that is given by the tuple $G = (V, E)$ and the properties that have influence on the topology by introducing the tuple $\mathcal{N} = (G = (V, E), s, t, \text{cap}, \underline{p_g}, \overline{p_g}, \underline{p_d}, \overline{p_d})$ with minimum and maximum generation $\underline{p_g}, \overline{p_g}\colon \{s\} \to \mathbb{R}_{\geq 0} \cup \{\infty\}$, and minimum and maximum demand $\underline{p_d}, \overline{p_d}\colon \{t\} \to \mathbb{R}_{\geq 0} \cup \{\infty\}$. Note that the p will later stand for real power, but this is of no importance in this section. We call such a tuple a *flow network*.

With these terms it is possible to describe flows. A *flow* is a function $f\colon E \to \mathbb{R}$ that maps each edge to a value representing its flow. Recall that we give each edge an orientation and thus, the graph is directed. In general, we allow a bidirectional flow on each edge. The flow f satisfies the *skew-symmetry* property $f(u, v) = -f(v, u)$ for all $(u, v) \in E$. The *net flow* $f_{\text{net}}(u)$ describes the behavior of a flow at a vertex u and is defined by $f_{\text{net}}(u) := \sum_{\{u,v\} \in \overleftrightarrow{E}} f(u, v)$ for all $u \in V$. It basically defines the difference of incoming and outgoing flow. We distinguish between the net flow at the source s (Equation 3.2), sink t (Equation 3.3), and all other vertices $v \in V \setminus \{s, t\}$ (Equation 3.1).

$$f_{\text{net}}(u) = 0 \qquad \forall u \in V \setminus \{s, t\}, \tag{3.1}$$

$$\underline{p_g}(s) \leq f_{\text{net}}(s) \leq \overline{p_g}(s), \tag{3.2}$$

$$-\overline{p_d}(t) \leq f_{\text{net}}(t) \leq -\underline{p_d}(t). \tag{3.3}$$

The Equations 3.1–3.3 that describe the behavior at each vertex are known as *conservation of flow*. In the electrical engineering community these constraints are more commonly known under the name Kirchhoff's Current Law (KCL) as we will see later in this chapter.

The capacity $\text{cap}\colon \overleftrightarrow{E} \to \mathbb{R}_{\geq 0}$ is a function that represents a property of each edge that restricts the flow on each edge (see Equation 3.4).

$$|f(u, v)| \leq \text{cap}(u, v) \qquad \forall (u, v) \in E. \tag{3.4}$$

Note that we allow negative flows and the skew symmetry describes the interpretation of such flows meaning $f(u, w) = -f(w, u)$. We call a flow complying with Equa-

tions 3.1–3.4 a *feasible flow*. If the generation and demand bounds permit zero generation and consumption, respectively, then a possible feasible flow f can be the trivial solution with $f \equiv 0$. The decision problem is defined in the following problem box.

Flow Feasibility Problem FEAS($\mathcal{N}$)	
Instance:	A flow network $\mathcal{N} = (G, s, t, \text{cap}, \underline{p_g}, \overline{p_g}, \underline{p_d}, \overline{p_d})$.
Question:	Is there a feasible flow f complying with the constraints in Equations 3.1–3.4?

We will see that the flow feasibility problem is a subproblem of all power flow feasibility problems. A *one terminal-pair graph* is a graph with one source s and one sink t that are directly connected by an edge, which is often used for circulation problems. The latter simulates a flow circulation that simplifies the constraints in Equations 3.1–3.3 to one constraint of the form shown in Equation 3.1 for all vertices.

The Maximum Flow Problem. As mentioned above, the flow feasibility problem is a subproblem of many problems that exist in ecology, economics, and information theory (see for example Ahuja et al. [AMO93]). The flow FEAS is a decision problem and the Maximum Flow Problem (MFP) is an optimization problem that maximizes the throughput of the network. Note that we are always able to transform an optimization problem into a decision problem. To formalize the problem, we introduce the *flow value* $F(\mathcal{N}, f)$ of a flow f and a flow network $\mathcal{N}$ that is defined by $f_{\text{net}}(s)$. A feasible flow f that maximizes $f_{\text{net}}(s)$ is called a maximum flow and its value is given by $\text{OPT}_{\text{MFP}}(\mathcal{N})$. We define the optimization problem as follows.

Maximum Flow Problem MFP($\mathcal{N}$)	
Instance:	A flow network $\mathcal{N} = (G, s, t, \text{cap}, \underline{p_g}, \overline{p_g}, \underline{p_d}, \overline{p_d})$.
Objective:	Is there a feasible flow f that maximizes the flow value $F(\mathcal{N}, f)$.

The MFP is a well known problem [GTT89, pp.19ff.]. The dual problem is the Minimum Cut Problem (MCP) that asks for an edge cut-set with minimum capacity. The max-flow min-cut theorem is proved by Dantzig and Fulkerson [DF57] and shows the duality of both problems.

The Minimum Cost Flow Problem. Another problem that incorporates the feasibility problem is the Minimum Cost Flow Problem (MCFP), where we introduce for the flow on an edge $e \in E$ a cost function $\gamma_e : \mathbb{R} \to \mathbb{R}_{\geq 0}$ representing the cost for a flow of $f(e)$, where γ_e is an even function, i. e., $\gamma_e(x) = \gamma_e(-x)$. We require that the generations or the demands have a positive lower bound meaning $\underline{p_g}(s) > 0$ or $\underline{p_d}(t) > 0$. The optimization problem is defined as follows.

Minimum Cost Flow Problem MCFP($\mathcal{N}$)	
Instance:	A flow network $\mathcal{N} = (G, s, t, \text{cap}, \underline{p_g}, \overline{p_g}, \underline{p_d}, \overline{p_d})$ and a cost function γ_e.
Objective:	Find a feasible flow f such that the sum of the cost over all edges $\sum_{e \in E} \gamma_e(f(e))$ is minimized.

The MCFP has the same constraints as the MFP, but a different objective. The problem has two special cases in which it transforms to another problem while fixing some of the constraints. If the capacities are set to infinity $\text{cap}(u, v) = \infty$ for all $(u, v) \in E$, then the problem becomes a Shortest Path Problem (SPP). However, if we would set the cost to zero $\gamma_{(u,v)}(x) = 0$ for all $x \in \mathbb{R}$ and all edges $(u, v) \in E$ the problem is equivalent to FEAS.

There are different algorithms to tackle the MCFP. Since the MCFP constitutes an LP, the simplex algorithm can be used. There is a special network simplex algorithm [OPT93, Orl97, Tar97] that can be used in this case. Others are the cycle canceling [Kle67][GTT89, p.6, p.10, p.50], minimum mean cycle canceling [GT89, p.875], and cost scaling [GT90][GTT89, Chapter 3], successive shortest path and capacity scaling [EK72][GTT89, Chapter 5], and the out-of-kilter algorithm [DK67, Ful61, SW73].

Note that a graph-theoretical flow is not necessarily a valid power flow, since it neglects physical constraints. However, it represents a subproblem in the power flow feasibility problem, which we see in the next section.

3.3 The Power Flow Feasibility Problem

A power grid operates correctly if the total generation in the power grid is equal to the total power consumption (also called demand). The problem—checking whether the demand and generation sum up to zero under model specific constraints—is called the Feasibility Problem (FEAS; see Figure 3.1). In this section, we show different models with their assumptions and constraints.

The Feasibility Problem represents one of the most fundamental problems the transmission system operator (TSO) has to tackle in the power grid. While operating the power grid, the feasibility check can be done online using the grid frequency (Figure 3.1b). The European grid frequency f (nominal frequency) is 50 Hz. Note that there are countries such as Japan that run two frequencies, i. e. 50 Hz and 60 Hz [Gor19]. Regions with different frequencies are connected via high-voltage direct current (HVDC) lines. For the following example [Jas19], we assume a nominal grid frequency of 50 Hz. The normal grid frequency operation is in the range of [49.8 Hz; 50.2 Hz]. Exceeding this interval on the upper end means that there is more production than demand. A usual reaction after 50.2 Hz is to shut down generators that make use of renewable energies (i. e., solar panels) or reduce their power injection; after 51.5 Hz all solar panels

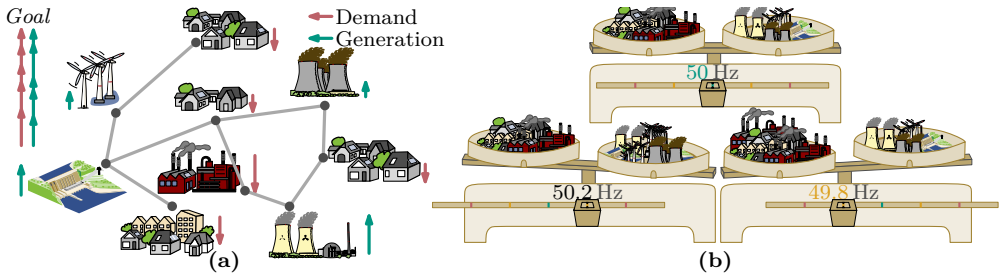

Figure 3.1: The aim of the feasibility problem is to check whether the generation and demand are equivalent. This idea is shown by the two schematic sketches in (a) and (b). (a) gives a rough idea of the feasibility problem in terms of the power grid's generation and demand, (b) represents the same idea in the context of the (nominal) frequency of 50 Hz (top scale). The latter shows that any imbalance leads to a frequency that deviates from the nominal frequency in either way. If the generation is to high the frequency increases (bottom left scale). However, if the consumption is to high the frequency drops (bottom right scale).

are shut down, before reaching the critical value of 52.5 Hz, other renewable generators and power plants are reduced or removed from the grid. On the other end, the TSO activates power reserves at 49.8 Hz, in the range of (48.7 Hz; 49.0 Hz] load shedding (i. e., a TSO-planed shutdown of parts of the power grid for grid security reasons) of 10 − 15%, in the range of (48.4 Hz; 48.7 Hz] load shedding of 20 − 30%, in the range of (48.1 Hz; 48.4 Hz] load shedding of 35 − 50%, and in the range of (47.5 Hz; 48.1 Hz] load shedding of 50 − 70% is done [Jas19]. After that the TSO separates the power plants from the power grid with resulting blackouts. The latter is done to secure the grid equipment. So the total operating frequency range is (47.5 Hz, 52.5 Hz). After a blackout the power grid has to be reconstructed. Thus, the TSO is confronted with the problem in which order the power grid elements have to be added to the power grid without risking another blackout or risking any damage to power grid equipment. The latter problem is denoted by Restoration Order Problem (ROP) that contains the Feasibility Problem (FEAS), too.

Recall that the subproblem of any power grid analysis and thus, every placement problem, is FEAS, i. e., whether there is a feasible power flow for a given generation and demand. This problem is solved to check the reliability of the power grid, to do short- and long-term planning (i. e., placement problems; see Chapters 5 and 6) and to solve other power grid related problems. In this section, we will give an overview of the different basic models, complexities, and relaxations.

3.3.1 Alternating Current Power Flow Model

The Alternating Current (AC) power flow models are the standard models for the power flow analyses. Models are a description of the real-world that make certain

assumptions such that we have to explain why the models that we use are reasonable for the problems that we tackle in this thesis. In this section, we briefly introduce and describe AC FEAS that describes the power flow in an AC power grid. We start with the dynamic AC model that is a very precise model, but also a very complex model. Note that most placement problems in power grids are long-term decisions. For long-term scenarios, it is reasonable—since the power grid converges towards a stable state—to make an assumption such that the AC model becomes time-independent (see Equation 3.7). The time-independent model is called *static* AC model. Using different transformations, we derive different formulations for AC FEAS shifting the non-convex and non-linear formulas in different parts of the system of equations (see Table 3.2). For problems that are long-term decisions these models are good approximations. However, AC FEAS is already NP-hard on star-shaped networks [LGH16]. In this work, we focus on high-voltage power grids only, so we can make some assumption that lead to a linearization of AC models. The linearization is called DC FEAS, which will be described in the next section (Section 3.3.2).

Typically, the theoretical structure of an AC model represents a subproblem of different power grid problems that have to be solved within different time ranges depending on the purpose. For instance, for power grid planning (i. e., Transmission Network Expansion Planning; in short TNEP) the model has to be solved every year [COC12], whereas for day-ahead markets the particular model has to be solved every day [COC12]. For the AC model there are no known fast and robust solution techniques [COC12], which is due to the solver technologies not being able to guarantee global optimality since they get stuck in local optima [Fou96, p.391, Chapter 18].

Dynamic AC Model. The AC power flow in general consists of functions representing complex current injection $i\colon V \times \mathbb{R} \to \mathbb{C}$ and complex voltages injection $v\colon V \times \mathbb{R} \to \mathbb{C}$ at a vertex $u \in V$ and timestamp $t \in \mathbb{R}$ that are sinusoid functions with amplitude $|i|$ and $|v|$, respectively, angular frequency $\omega := {}^{d\theta}/_{dt}$ (i. e., f being the frequency; e. g., 50 Hz or 60 Hz), initial phases for voltage and current $\theta^v\colon V \to \mathbb{R}$ and $\theta^i\colon V \to \mathbb{R}$, respectively, and complex coefficients.

The electrical power is defined by complex current i and complex voltage v such that the complex power $s(u,t)$ is defined by Equation 3.5.

$$s(u,t) := v(u,t) \cdot i(u,t)^\star \qquad \forall u \in V, t \in \mathbb{R}, \tag{3.5}$$

where $i(u,t)^\star$ is the complex conjugate of the current. Since we use the complex conjugate of the current, we get the relationship between voltage and current (see also Figure 3.2) that is the difference between the voltage angle θ^v and the current angle θ^i meaning $\theta^v - \theta^i$ (see Equation 3.7). The latter difference is also called *power angle*. Thus, the function that represents the complex power injection is defined by $s\colon V \times \mathbb{R} \to \mathbb{C}$. The real and imaginary part of a complex number $z \in \mathbb{C}$ is

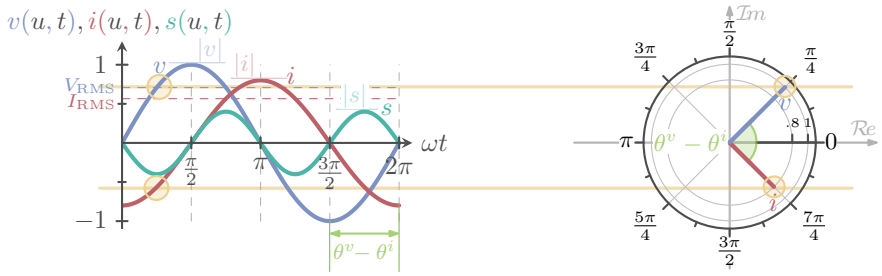

Figure 3.2: The left side of the figure presents voltage $v(u,t)$, current $i(u,t)$, and total instantaneous electric power $s(u,t)$ in terms of trigonometric function for timestamp $t \in \mathbb{R}$ and vertex $u \in V$. The Argand diagram is shown on the right side of the figure, where voltage $v(u,t)$ and current $i(u,t)$ are described by polar coordinates. The current $i(u,t)$ is shifted by $\pi/2$ to the right of voltage $v(u,t)$ (i. e., voltage acts as reference point). The shift between voltage $v(u,t)$ and current $i(u,t)$ by $\theta^v - \theta^i$ is also called power angle. In the right diagram at timestamp $t = 0$ the voltage vector $v(u,t)$ completes a full cycle (i. e., a time period), whereas the current vector $i(u,t)$ is on the negative imaginary axis and thus, lags behind the voltage vector $v(u,t)$ by $\pi/2$. An inductive load could be a cause of that particular shift, since the voltage $v(u,t)$ leads the current $i(u,t)$. The product of voltage $v(u,t)$ and current $i(u,t)$ is equivalent to the total instantaneous electric power $s(u,t)$. Note that the magnitude of the total instantaneous electric power corresponds to the product of the root-mean-squared (RMS) of the voltage magnitude $|v(u)|$ denoted by $V_{\text{RMS}}(u)$ and the current magnitude $|i(u)|$ denoted by $I_{\text{RMS}}(u)$. The derivation of this figure can be found in Appendix B.1.

denoted by $\mathcal{R}e(z)$ and $\mathcal{I}m(z)$, respectively. The voltage magnitude $|v(u)|$ (Equation 3.6) represents the wave crest (see left side of Figure 3.2) at vertex $u \in V$.

$$|v(u)| = \sqrt{\mathcal{R}e(v(u,t))^2 + \mathcal{I}m(v(u,t))^2}. \tag{3.6}$$

The current magnitude $|i(u)|$ is defined accordingly to Equation 3.6. The voltage and current magnitude are time independent, since Equation 3.6 can be written using trigonometric function $|v(u)| \cdot \sqrt{\cos^2(\theta^v(u) + \omega t) + \sin^2(\theta^v(u) + \omega t)}$, where the Pythagorean identity $\sqrt{\cos^2(\theta^v(u) + \omega t) + \sin^2(\theta^v(u) + \omega t)} = 1$ follows from the complex plane representation.

The idea behind this is that the assumption of time-invariance results in an unchanging (i. e., constant) wave crest over time. If we assume that all functions are *time-invariant*—having the same behavior for the same input at any timestamp, i. e., the angular frequency $d\theta/dt = 2\pi f$ is constant—then we call them current and voltage phasors. This allows us to use the phasor transform of Charles Proteus Steinmetz [RM12, YL08] such that we can use simple algebraic equations on the phasors instead of differential equations of the sinusoid signals. Note that the assumption of time-invariance might be acceptable for some power flow analyses and planning problems. However, for smaller periods of time such as the influence of switching processes on the grid

stability this assumption might not be suitable anymore. However, then we get into the range of dynamic analyses [Roh+12, Str18, TC14a, Tim18].

We get the trigonometric relationship depicted in Equation 3.7. The derivation can be found in Equation B.2.

$$s(u,t) = v(u,t) \cdot i(u,t)^\star \tag{3.7a}$$

$$\begin{aligned} &= \underbrace{\mathcal{R}e(v(u,t)) \cdot \mathcal{R}e(i(u,t)) + \mathcal{I}m(v(u,t)) \cdot \mathcal{I}m(i(u,t))}_{=:p(u)} \\ &\quad - \mathbf{j} \cdot \underbrace{\big(\mathcal{R}e(v(u,t)) \cdot \mathcal{I}m(i(u,t)) - \mathcal{I}m(v(u,t)) \cdot \mathcal{R}e(i(u,t))\big)}_{=:q(u)} \end{aligned} \tag{3.7b}$$

$$= |v(u)||i(u)|\Big(\cos\big(\theta^v(u) + \omega t - \theta^i(u) - \omega t\big) + \mathbf{j} \cdot \sin\big(\theta^v(u) + \omega t - \theta^i(u) - \omega t\big)\Big) \tag{3.7c}$$

$$= \underbrace{|v(u)||i(u)| \cos\big(\theta^v(u) - \theta^i(u)\big)}_{=p(u)} + \mathbf{j} \cdot \underbrace{|v(u)||i(u)| \sin\big(\theta^v(u) - \theta^i(u)\big)}_{=q(u)} \tag{3.7d}$$

Note that we have to use the root-mean-squared (RMS) values in Equation 3.7c, since $|v(u)||i(u)|$ would lead in a magnitude that is twice as high as of $v(u,t) \cdot i(u,t)^\star$, which is graphically illustrated in Figure 3.2. To illustrate the time-varying power in Figure 3.2, we use the concept of instantaneous electric power (see Appendix B.1), since the complex power becomes time-independent in Equation 3.7 and thus, constant. To illustrate the signals of the complex power a common way is to use the real part of a signal (in our case the real part of the current i and voltage v, see Appendix B.1 for more details).

The penultimate step in Equation 3.7 follows from the trigonometric addition and product formulas. In the last step, the complex power equation becomes independent from time t and angle frequency ω. The intuition behind this is that in an ideal AC network we start with the initial phase angles θ^v and θ^i, but the angular frequency stays constant meaning $\omega := {}^{d\theta}/_{dt} = 2\pi\mathrm{f}$. Thus, the rotation velocity is the same for both current and voltage. This simplifies the system such that it only depends on the initial phases (see Figure 3.2) and leads to a static analysis by using the resulting time-independent models that are also called static models.

Static AC Models. For general cases a common way to analyze power grids is to use a constant angular frequency and analyze steady-state power grids that have one fixed timestamp per analysis. This will be our main focus in this work. However, the idealization of the angular frequency to a constant is not suitable for certain scenarios, as mentioned above. For this work it means that all previous functions f become time-independent $\mathrm{f}\colon \mathbb{S} \to \mathbb{F}$, where $\mathbb{F}$ is a field and $\mathbb{S}$ is the set we do the mapping from such that for example the voltage function becomes $v\colon V \to \mathbb{R}$.

Equation 3.7c can be rewritten to $s(u) := |v(u)||i(u)|e^{\mathbf{j}\cdot(\theta^v(u)-\theta^i(u))}$ using Euler's formula. The functions $p\colon V \to \mathbb{R}$ and $q\colon V \to \mathbb{R}$ represent the *real* and the *reactive*

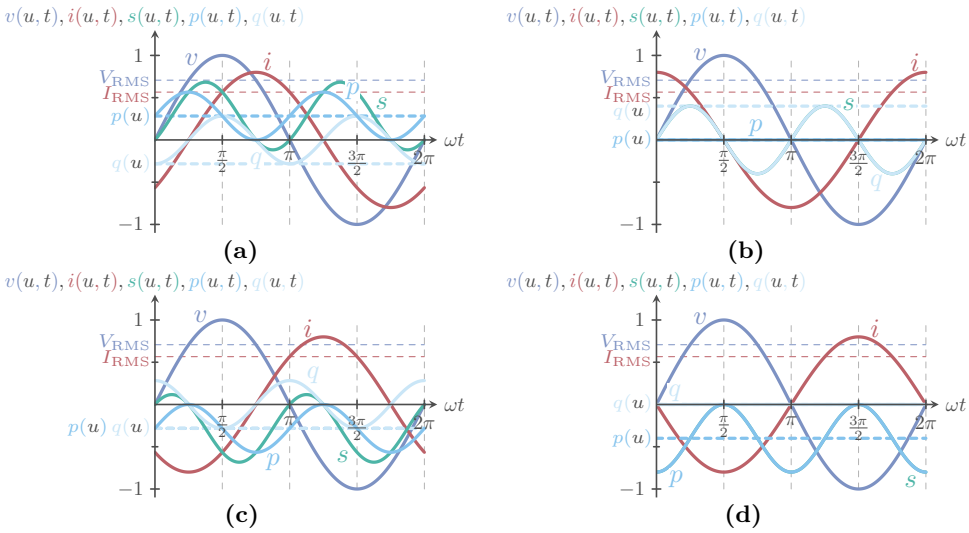

Figure 3.3: The time varying sinusoid curves of voltage $v(u,t)$ with magnitude $|v(u)| = 1$ and effective value $V_{\text{RMS}}(u) = 1/\sqrt{2}$, current $i(u,t)$ with magnitude $|i(u)| = 0.8$ and effective value $I_{\text{RMS}}(u) = 0.8/\sqrt{2}$, total instantaneous electric power $s(u,t)$, its real part $p(u,t)$, and its imaginary part $q(u,t)$ are given for different voltage angle differences $\Delta\theta^v$. The voltage angle differences are (a) $\Delta\theta^v = \pi/4$, (b) $\Delta\theta^v = -\pi/2$, (c) $\Delta\theta^v = 3\pi/4$, and (d) $\Delta\theta^v = \pi$. The total instantaneous electric power $s(u,t)$ is the sum of the real part $p(u,t)$ and the imaginary part $q(u,t)$ of the power. The same behavior is shown for the complex power $s(u)$ and its real power $p(u)$ and reactive power $q(u)$. (a) A stable case is represented that is an operation of current i and voltage v within an angle shift of $[-\pi/2; \pi/2]$. (b) One of the stability borders is $-\pi/2$, where the real part of the total instantaneous electric power $s(u,t)$ is zero over time t. (c) With a voltage angle difference of $3\pi/4$ the power is within the instable section. All power curves are in the negative part. (d) The current $i(u,t)$ and voltage $v(u,t)$ waves are in a state, where the waves cancel each other out. The reactive part of the total instantaneous electric power curve is zero and the real power part is negative. The derivation of this figure can be found in Appendix B.1.

power, respectively. This equation shows very clearly the current angle θ^i and voltage angle θ^v that describe the real and reactive power on each edge. Figure 3.2 shows the relationship of current i and voltage v. The difference between voltage and current is the phase angle difference. The more we increase the phase angle difference (e. g., see Figure 3.3 on Page 36) between current and voltage the smaller the real power gets until a certain point (see Figure 3.3b), where the real power becomes zero. The case, where the wave crests of voltage and current cancel each other out is shown in Figure 3.3d. Note that the reactive power (also known as phantom power) increases while the real power decreases, since current and voltage amplitudes do not decrease. The latter basically describes the *principle of conservation of energy*. The described

relationship between voltage, current, and power can be used to maintain the voltage stability by changing real power demands. A decrease in real power demand can be maintained by an increase in reactive power by changing the phase angle difference between voltage and current. This mechanism helps to maintain voltage on a certain level.

The complex power injection can be written in terms of real and reactive power injection that represent decoupled parts (see Equation 3.8 and its derivation in Equation 3.7).

$$s(u) = \mathcal{R}e(s(u)) + \mathbf{j} \cdot \mathcal{I}m(s(u)) = p(u) + \mathbf{j} \cdot q(u) \qquad \forall u \in V. \tag{3.8}$$

This relationship is shown in Figure 3.3, where the total instantaneous power $s(u,t)$ (respectively complex power $s(u)$) is the sum of the real part $p(u,t)$ and imaginary part $q(u,t)$ of the power (respectively real power $p(u)$ and reactive power $q(u)$). The total instantaneous power curve $s(u,t)$ (respectively complex power $s(u)$) has the same magnitude independent of the power angle. The latter emphasize the principle of conservation of energy.

The real power p is the power that is actually doing work such as heating. However, reactive power is seldom consumed by consumers. Exceptions are motors, generators and transformers that use a magnetic field (inductive components) of industrial consumers that need reactive power. In general reactive power is used to maintain the voltage stability. Increasing the amount of reactive power increases the voltage that has to be kept in a certain range. So reactive power is necessary for the power grid to have a more efficient real power flow. The stability of the power grid is maintained by a balance between real and reactive power and the latter depends highly on the consumed real power.

We usually do a vertex-based analysis meaning that flows are usually modeled by disturbance and injection at a vertex. We introduced for each vertex eight variables denoted by $p_g(u)$, $q_g(u)$, $p_d(u)$, $q_d(u)$, $v(u)$, $i(u)$, $\theta^v(u)$, and $\theta^i(u)$ for all $u \in V$. However, we can always reformulate current i and current angles θ^i in terms of voltage v and voltage angle θ^v using Ohm's law and thus, we have just six variables. We will see later that depending on the vertex type (see Table 3.1) or on the problem some variables are given and thus, fixed to a certain value.

Up to now, we just looked at the power *injections* and not the power *flows*. However, the complex, real, and reactive power flow, as well as the complex current flow are defined by the functions $s\colon E \to \mathbb{C}$ (in Volt Ampere; short VA), $p\colon E \to \mathbb{R}$ (in W), $q\colon E \to \mathbb{R}$ (in Volt Ampere Reactive; short VAr), and $i\colon E \to \mathbb{C}$ (in Ampere; short A), respectively. We distinguish between the injection at the source and sink vertex of each edge, since there are power losses at each electrical element.

Network Parameters. The AC network $\mathcal{N} = (G = (V,E), V_G, V_D, \text{cap}, r, x, b, g, \underline{\Delta\theta^v}, \overline{\Delta\theta^v}, \underline{v}, \overline{v}, \underline{p_g}, \overline{p_g}, \underline{q_g}, \overline{q_g}, \underline{p_d}, \overline{p_d}, \underline{q_d}, \overline{q_d})$ is defined by the topological structure

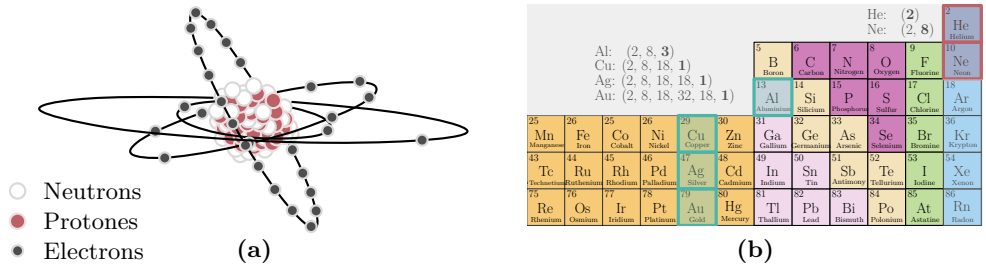

Figure 3.4: Both (a) and (b) represent the atomic structure of one element and of multiple elements, respectively. The conductivity is dependent on the outermost shell denoted by valence shell. (a) The copper-29 isotope that has fully filled electron shells, but the valence shell (outermost shell). The valence shell has just one electron that is highly reactive. (b) Part of the description of the atomic structure of elements. The green marked elements represent common conductors and the red marked elements are strong insulators that are all in the last column.

that is given by the graph $G = (V, E)$, the set $V_G \subseteq V$ of generators, the set $V_D \subseteq V$ of consumers, the resistance function $r\colon \overleftrightarrow{E} \to \mathbb{R}_{\geq 0} \cup \{\infty\}$, the reactance function $x\colon \overleftrightarrow{E} \to \mathbb{R}_{\geq 0} \cup \{\infty\}$, the susceptance function $b\colon \overleftrightarrow{E} \to \mathbb{R}$ (Equation 3.12), the conductance function $g\colon \overleftrightarrow{E} \to \mathbb{R}$ (Equation 3.11), the admittance function $y\colon \overleftrightarrow{E} \to \mathbb{C}$ (Equation 3.9), and the apparent power's thermal line limit function $\mathrm{cap}\colon \overleftrightarrow{E} \to \mathbb{R}$, which can be either $\bar{i}, \bar{s}, \bar{p}$, or $\bar{q}$, and combinations of them. The resistance r and the reactance x are measured in Ohm Ω. The admittance $y(u, v)$ (Equation 3.9) is defined by the conductance $g(u, v)$ (Equation 3.11) and the susceptance $b(u, v)$ (Equation 3.12) that defines how easy the current is able to flow through an element such as a transmission line $\{u, v\} \in \overleftrightarrow{E}$. Note that all three are measured in Siemens S. The conductivity of an electrical element is mainly influenced by the conductance of the material, length, and wire gauge. The conductance of the material is mainly influenced by the atomic structure (see Figure 3.4). Elements that have just one electron on the valence shell (i. e., outermost shell) have a high conductivity such as copper, gold, and silver (Column 11 of the periodic system; see Figure 3.4b green markers). However, elements that have a full valence shell are very good insulators since the conductivity is very low, e. g., helium (last column of the periodic system; see Figure 3.4 red markers). The admittance y,

impedance z, conductance g, and susceptance b are defined in Equations 3.9–3.12.

$$y(u,w) \coloneqq \frac{1}{z(u,w)} = g(u,w) + \mathbf{j} \cdot b(u,w) \qquad \forall \{u,w\} \in \overleftrightarrow{E}, \tag{3.9}$$

$$z(u,w) = \frac{1}{y(u,w)} = r(u,w) + \mathbf{j} \cdot x(u,w) \qquad \forall \{u,w\} \in \overleftrightarrow{E}, \tag{3.10}$$

$$g(u,w) \coloneqq \frac{r(u,w)}{r(u,w)^2 + x(u,w)^2} \qquad \forall \{u,w\} \in \overleftrightarrow{E}, \tag{3.11}$$

$$b(u,w) \coloneqq -\frac{x(u,w)}{r(u,w)^2 + x(u,w)^2} \qquad \forall \{u,w\} \in \overleftrightarrow{E}. \tag{3.12}$$

Note that the admittance matrix $\mathbf{Y}$ is defined by the self-admittances representing the diagonal entries $y(u,u) = y(u,0) - \sum_{\{u,w\} \in \overleftrightarrow{E}} y(u,w)$, where $y(u,0)$ is the admittance to ground, and the entries of Equation 3.9 that represent the entries for the incident edge.

Power Grid Bounds. There are lower and upper bounds restricting the voltage angle differences $\underline{\Delta\theta^v}$ and $\overline{\Delta\theta^v}$, the voltages $\underline{v}$ and $\overline{v}$, the real power generation $\underline{p_g}$, $\overline{p_g}$, the reactive power generation $\underline{q_g}$, $\overline{q_g}$, the real power demand $\underline{p_d}$, $\overline{p_d}$, and the reactive power demand $\underline{q_d}$, $\overline{q_d}$, respectively. The constraint of the voltage angle difference (Equation 3.13) restricts the power flow on each edge (Equation 3.7).

$$\underline{\Delta\theta^v}(u,w) \leq \theta^v(u) - \theta^v(w) \leq \overline{\Delta\theta^v}(u,w), \tag{3.13a}$$

$$\underline{\Delta\theta^v}(u,w) \leq \arctan\left(\frac{\mathcal{I}m(v(u))}{\mathcal{R}e(v(u))}\right) - \arctan\left(\frac{\mathcal{I}m(v(w))}{\mathcal{R}e(v(w))}\right) \leq \overline{\Delta\theta^v}(u,w), \tag{3.13b}$$

for all $\{u,w\} \in \overleftrightarrow{E}$. In Equation 3.13b, we use the trigonometric relationship of the real part $\mathcal{R}e(v(u))$ and imaginary part $\mathcal{I}m(v(u))$ that is defined by $\tan\left(\theta^v(u)\right) = {}^{\text{adjacent}}/_{\text{opposite}} = {}^{\mathcal{I}m(v(u))}/_{\mathcal{R}e(v(u))} = {}^{\sin\left(\theta^v(u)\right)}/_{\cos\left(\theta^v(u)\right)}$. The voltage angle difference is often restricted to the interval of $[-\pi/2; \pi/2]$ for stability reasons (see Figure 3.3 for different voltage angle differences). If the balance between real power generation and demand cannot be maintained (i. e., is not zero), then there is an issue in the angle stability, i. e., the voltage angle difference cannot be maintained within the stability interval. This in particular means the smaller the angle difference the more balance between real power generation and demand exists. This is due to the fact that the reactive power is used to compensate the lack of real power generation and demand by shifting voltage and current using devices such as capacitor banks. Figure 3.3 explains why exceeding the $\pi/2$ would lead to instabilities in the power grid. Note that mainly generators are able to influence the voltage, power curves, and the power angle (see Table 3.1). Thus, the network stability is mainly driven by generators (including devices such as capacitor banks). If the power angle exceeds the stability

range the power curves shift into the negative quadrant and the effective power values are negative, too (see Figure 3.3b–d). However, a power grid has a predefined flow direction and a negative real power can be interpreted as a "backward power movement" (see Figure 3.3a). A rough idea of the latter is given by a simple DC circuit with a preinstalled diode. Note that a diode has a predefined direction making the network nonreciprocal. The predefined direction defines the anode and cathode for the battery connection. Connecting the battery in the wrong sense would lead to a diode that does not flash.

In addition, the smaller the shift the less losses and the more stable the power grid works. In Section 3.3.4, we will see that the differences are often smaller than $\pi/6$. However, the voltage angle difference $\Delta\theta^v$ also correlates with the real power that flows from one vertex to another over the power grid. The relationship becomes much clearer if we look at the linearization of the AC model in Section 3.3.2.

In some literature there is a constraint restricting the voltage angles $\theta^v(u)$ for all $u \in V$ themselves (see Equation 3.14).

$$\underline{\theta^v}(u) \leq \theta^v(u) \leq \overline{\theta^v}(u) \qquad \forall u \in V. \tag{3.14}$$

The latter restricts the solution space and might exclude feasible solutions, but does not represent a physical constraint. However, it improves the running times to solve the feasibility problem and to fulfill assumptions such as the stability range or later the Assumption 2 in Section 3.3.2.

The voltage magnitude is bounded by either Equation 3.15a, or by Equation 3.15b and Equation 3.15c depending on the formulation that is either polar or rectangular, respectively.

$$|\underline{v}(u)| \leq |v(u)| \leq |\overline{v}(u)| \,, \tag{3.15a}$$

$$\underline{v}(u)^2 \leq \mathcal{R}e(v(u))^2 + \mathcal{I}m(v(u))^2 \,, \tag{3.15b}$$

$$\mathcal{R}e(v(u))^2 + \mathcal{I}m(v(u))^2 \leq \overline{v}(u)^2, \tag{3.15c}$$

for all vertices $u \in V$. This is mainly motivated by the power grid elements that work within a certain voltage range. Most elements perform poorly on the lower voltage end—e. g., inductive motors overheat—and on the upper end the elements can get destroyed. The thermal line limits can be represented in different ways that mainly depend on the formulation. If the formulation uses current and voltage, Equations 3.16a and 3.16b are used. Otherwise, if it uses real power, reactive power, and voltage angles, Equations 3.16c and 3.16d are used.

$$\{i(u,w) \in \mathbb{C} \mid \mathcal{R}e(i(u,w))^2 + \mathcal{I}m(i(u,w))^2 \leq \bar{i}(u,w)^2\}, \tag{3.16a}$$

$$|i(u,w)| \leq \bar{i}(u,w), \tag{3.16b}$$

$$\{s(u,w) \in \mathbb{C} \mid \mathcal{R}e(s(u,w))^2 + \mathcal{I}m(s(u,w))^2 \leq \bar{s}(u,w)^2\}, \tag{3.16c}$$

$$|s(u,w)| \leq \bar{s}(u,w), \tag{3.16d}$$

for all $(u, w) \in E$. Note that these constraints are convex and quadratic as the geometric figure of its boundary is a closed disk. In addition, the reactive power might increase the voltage stability, but it also consumes bandwidth of the transmission line capacity. Thus, to maximize the throughput of real power in the power grid the reactive power has to be minimized such that the voltage stays in its range. Note that increasing the real power decreases the losses.

The power injection constraints basically constrain the injection (Equations 3.17a and 3.17b) or demand (Equations 3.17c and 3.17d) of a vertex depending on it being a generator or demand, respectively.

$$\underline{p_g}(u) \leq p_g(u) \leq \overline{p_g}(u) \qquad \forall u \in V_G, \tag{3.17a}$$

$$\underline{q_g}(u) \leq q_g(u) \leq \overline{q_g}(u) \qquad \forall u \in V_G, \tag{3.17b}$$

$$\underline{p_d}(u) \leq p_d(u) \leq \overline{p_d}(u) \qquad \forall u \in V_D, \tag{3.17c}$$

$$\underline{q_d}(u) \leq q_d(u) \leq \overline{q_d}(u) \qquad \forall u \in V_D. \tag{3.17d}$$

The losses heavily depend on the voltage level (Figure 1.1) and the amount of real power that flow through an element.

Real power p and voltage angles θ^v strongly depend on each other, as well as reactive power q and voltage magnitudes $|v|$ (see Section 3.3.2 Assumption 3 with Equation 3.31). The P-θ^v and Q-V problems are weakly dependent on each other. Thus, the AC power flow is usually solved in a decoupled way (see for example [Gao+18]). This is reasonable if we follow the assumption that phase angle differences $\Delta\theta^v(u, v)$ are small and high-voltage transmission lines are mainly reactive meaning $r(u, v) \ll x(u, v)$ for all $\{u, v\} \in \overleftrightarrow{E}$ (note that the latter relationship is used in Assumption 1 in Section 3.3.2). The approach separates both subproblems and iterates between them. The decoupled version decouples the AC power flow into two separate problems. However, the full AC power flow includes both problems without these assumptions.

Assuming that the demands are fixed, then out of the six variables $\Delta\theta^v, v, p_g, q_g, p_d$, and q_d only four remain. Each vertex specifies a certain type that is denoted by *vertex type* that actually defines which variables are fixed. The common vertex types are shown in Table 3.1. In Chapter 4, we describe the mathematical structure and relationship of the linearized AC model. Within that structure it becomes obvious why we chose exactly one vertex per connected component as slack vertex. The basic idea is that a slack vertex represents a reference for the voltage angles of the system and thus, choosing a voltage angle for that vertex defines the voltage angles for all others. In Table 3.1 there are exactly two types that are able to work as slack vertex that are denoted by *slack*, or *slack demand*. The PQ vertices are vertices without generation and thus are, pure demand vertices. The PV is separated into two classes that are both able to control voltage by adjusting the reactive power within certain limits by either controlling the reactive power generation or demand. A source of reactive

Table 3.1: This table is adopted from [WW96, p.70, Figure 4.4] and specifies the different vertex types in a power grid. The known variables at a vertex $u \in V$ are marked by ✓ and the unknowns by ✗. Note that this table is for the *PQV* formulation of an AC model.

Vertex Type	Variables				Comments	Code
	$p(u)$	$q(u)$	$v(u)$	$\theta^v(u)$		
Load	✓	✓	✗	✗	Usual load representation	PQ
Voltage Controlled	✓	✗	✓	✗	$\lvert v(u)\rvert$ is held constant	CV
Generator or Synchronous Condenser	✓	✗	✓, when $\underline{q_g}(u) < q_g(u) < \overline{q_g}(u)$	✗	Generator or synchronous condenser ($p(u) = 0$) has VAr limits; $\lvert v(u)\rvert$ is held as long as $q_g(u)$ and $q_d(u)$ are within limit	PV
	✓	✓, when $-\overline{q_d}(u) < q_d(u) < -\underline{q_d}(u)$	✗	✗		
Fixed Z to Ground	✗	✗	✗	✗	Only Z is given	
Reference, Slack	✗	✗	✓	✓	*Swing bus* must adjust net power to hold voltage constant (essential for solution)	Vθ^v
Slack demand or tie	✗	✓	✗	✓	The *tie* has no generation and demand attached	Qθ^v

power uses a capacitor such as a capacitor bank resulting in a leading current flow by $\pi/2$ to voltage, whereas a sink of reactive power uses an inductive device such as a coil resulting in a lacking current flow by $\pi/2$. An example for the latter is given in Figure 3.2 and Figure 3.3. Note that reactive power cannot be transmitted over long distances as the losses are too high. However, the real and reactive power production is restricted by the generators operation limits. If these limits are not sufficient to reach the voltage stability additional equipment for reactive power is required. Another vertex that is able to control voltage is the CV vertex that is either a special transformer that is able to control its tap ratio or a FACTS.

The network parameters show the dependencies of the model and how complex it is to maintain network stability in such networks. We already saw different formulations of the complex AC model using either complex numbers or real numbers with sinusoid functions. These non-linearities and the dependencies of certain variables make the AC model hard to solve. In the following, we describe the differences of these formulations.

Polar and Rectangular Formulations. In the previous part, we could see the different formulations of the voltage angle differences and the power grid bounds. Depending on which formulation we choose, we shift the complexity of the AC model to different parts as shown in Table 3.2. We distinguish between the *rectangular* and the *polar* formulation of the complex terms.

The polar formulation is given by the magnitude (i. e., length of the vector) and the angle of its vector. We represented the complex power in its polar form in Equation 3.7d, where $|v(u)|$ is the voltage magnitude (also known as voltage amplitude) and $\theta^v(u)$ represents the corresponding voltage angle. Contrary to that, the rectangular form of a complex number is given by the real $\mathcal{Re}(\cdot)$ and imaginary part $\mathcal{Im}(\cdot)$ of the complex number representing the horizontal (x-axes) and vertical (y-axis) components in the Argand diagram (i. e., geometric interpretation of a complex number; see Equation 3.7b and Figure 3.2 right side). In addition to that we are able to reformulate the power flow to calculate it in terms of real power p, reactive power q, and voltage v. This formulation is often denoted as PQV model (see Equations B.5 and B.6). Another alternative is the IV model that formulates the AC model in terms of current i and voltage v (see Equations B.7 and B.8). We already saw parameter-dependent formulations in the power grid bounds part.

Note that the literature standard is the polar PQV model [WW96, ZM11] (see Equation B.5).

PQV Formulations. The complex power injection at a vertex was introduced in Equation 3.7d using voltage and current as unknowns, which is denoted as IV formulation. However, the formula can be restated to a complex power flow on an edge by introducing the relationship that the current on an edge is defined by $i(u,w) \coloneqq y(u,w) \cdot \big(v(w) - v(u)\big)$ for all $(u,w) \in E$. Using this relationship we get Equation 3.18 in its rectangular formulation. The derivation can be found in Equation B.3.

$$
\begin{aligned}
s(u,w) &= v(u) \cdot i(u,w)^\star && \text{(3.18a)}\\
&= v(u) \cdot y(u,w)^\star \cdot \big(v(w)^\star - v(u)^\star\big) && \text{(3.18b)}\\
&= \left.\begin{aligned} & g(u,w)\big(\mathcal{Re}(v(u))\,\mathcal{Re}(v(w)) + \mathcal{Im}(v(u))\,\mathcal{Im}(v(w)) - \mathcal{Re}(v(u))^2 - \mathcal{Im}(v(u))^2\big) \\ & +b(u,w)\big(\mathcal{Re}(v(w))\,\mathcal{Im}(v(u)) - \mathcal{Re}(v(u))\,\mathcal{Im}(v(w))\big) \end{aligned}\right\} =: p(u,w)\\
&\quad +\mathbf{j} \cdot \left.\begin{aligned} & \Big(g(u,w)\big(\mathcal{Re}(v(w))\,\mathcal{Im}(v(u)) - \mathcal{Re}(v(u))\,\mathcal{Im}(v(w))\big) \\ & +b(u,w)\big(\mathcal{Re}(v(u))^2 + \mathcal{Im}(v(u))^2 - \mathcal{Re}(v(u))\,\mathcal{Re}(v(w)) - \mathcal{Im}(v(u))\,\mathcal{Im}(v(w))\big)\Big) \end{aligned}\right\} =: q(u,w)\\
& && \text{(3.18c)}
\end{aligned}
$$

for all $(u,w) \in E$. The rectangular Equation 3.18c has only quadratic terms. It is possible to decompose the equation into the real and reactive part of the complex power, which we already saw in Equations 3.7d and 3.8. The real part can be transformed into

the polar form (see Equation 3.19).

$$\begin{aligned} p(u,w) = g(u,w)\Big(&|v(u)||v(w)|\cos\big(\theta^v(u)-\theta^v(w)\big) - |v(u)|^2\Big) \\ &+ b(u,w)|v(u)||v(w)|\sin\big(\theta^v(u)-\theta^v(w)\big) \end{aligned} \tag{3.19a}$$

Similar, the reactive part can be transformed into the polar form (see Equation 3.20).

$$\begin{aligned} q(u,w) = \;& g(u,w)|v(u)||v(w)|\sin\big(\theta^v(u)-\theta^v(w)\big) \\ &- b(u,w)\Big(|v(u)||v(w)|\cos\big(\theta^v(u)-\theta^v(w)\big) - |v(u)|^2\Big) \end{aligned} \tag{3.20a}$$

The disadvantage of the polar formulations of the real and reactive power in Equations 3.19 and 3.20 are the quadratic terms of the voltages and the trigonometric functions of the voltage angle differences.

IV Formulation. The KCL describes the flow of current at a vertex (see Equation 3.21). It states that the net flow of current at each vertex is equal to zero that is similar to the graph-theoretical conservation of flow shown in Equation 3.1.

$$i(u) \coloneqq \sum_{w\colon\, \{u,w\}\in\overrightarrow{E}} i(u,w) \qquad \forall u \in V. \tag{3.21}$$

The complex current can be restated in terms of voltages using Ohm's law. This is shown in Equation 3.22 that is a linear function of complex voltages.

$$i(u) = y(u,0)\cdot v(u) + \sum_{\{w\colon\, \{u,w\}\in\overrightarrow{E}\,|\,u\neq w\}} \Big(\underbrace{y(u,w)(v(w)-v(u))}_{=:i(u,w)}\Big) \qquad \forall u \in V \tag{3.22}$$

The current injection $i(u)$ at a vertex $u \in V$ is described by the voltage to ground—using admittance to ground $y(u,0)$—and the current-based net flow. Note that the voltage to ground represents disturbances at the vertex. The complex current flow can be rewritten into two decoupled parts representing the real and imaginary part of the complex current flow of an edge $(u,w) \in E$ (see Equation 3.23). The derivation can be found in Equation B.4.

$$\begin{aligned} i(u,w) &= \big(g(u,w)+\mathbf{j}\cdot b(u,w)\big)\big(v(w)-v(u)\big) \\ &= \Big(g(u,w)+\mathbf{j}\cdot b(u,w)\Big)\Big(\mathcal{R}e(v(w)) + \mathbf{j}\cdot\mathcal{I}m(v(w)) - \mathcal{R}e(v(u)) - \mathbf{j}\cdot\mathcal{I}m(v(u))\Big) \\ &= \underbrace{g(u,w)\big(\mathcal{R}e(v(w))-\mathcal{R}e(v(u))\big) - b(u,w)\big(\mathcal{I}m(v(w))-\mathcal{I}m(v(u))\big)}_{=:\mathcal{R}e(i(u,w))} + \\ &\quad \mathbf{j}\cdot\Big(\underbrace{g(u,w)\big(\mathcal{I}m(v(w))-\mathcal{I}m(v(u))\big) + b(u,w)\big(\mathcal{R}e(v(w))-\mathcal{R}e(v(u))\big)}_{=:\mathcal{I}m(i(u,w))}\Big) \end{aligned} \tag{3.23}$$

More generally, we can write the problem of checking whether generation and consumption agree as AC FEAS, which decision problem depends on the formulation (see Table 3.2) and is defined in the following problem box.

Alternating Current Feasibility Problem AC FEAS($\mathcal{N}$)	
Instance:	An AC network $\mathcal{N} = (\, G = (V, E), V_G, V_D, \text{cap}, r, x, b, g, \underline{\Delta\theta^v}, \overline{\Delta\theta^v}, \underline{v}, \overline{v}, \underline{p_g}, \overline{p_g}, \underline{q_g}, \overline{q_g}, \underline{p_d}, \overline{p_d}, \underline{q_d}, \overline{q_d}\,)$.
Question:	Is there a feasible electrical flow complying with one of these model constraints in Table 3.2?

Summarizing the AC FEAS problem is a non-linear non-convex problem that is under the assumption of time-invariance a model that is a good approximation to a realistic power grid. Furthermore, it represents a subproblem of all problems that have the power grid as an input.

Lehmann et al. [LGH16] discuss that the decoupled AC power flow model is weakly NP-hard on trees (stars). It represents a stronger result in terms of graph classes, but includes real and reactive power as decoupled formulation. An outline of the proof is given by Lavaei and Low [LL12].

Normalization. Note that for the power flow analysis it is common to normalize the system using the per-unit-system (p.u.). The normalization is done for the complex power, real power, reactive power, and voltage using the base units S_{base}, P_{base}, Q_{base}, and V_{base}, respectively. The other units can be normalized by the bases derived from the previous power and voltage base such that $I_{\text{base}} = {}^{S_{\text{base}}}/_{V_{\text{base}}}$, $Z_{\text{base}} = {}^{V_{\text{base}}}/_{I_{\text{base}}}$, and $Y_{\text{base}} = {}^{1}/_{Z_{\text{base}}}$.

Table 3.2: This table is inspired by Cain ET AL. [COC12] from FERC that analyzed AC OPF and compares the different AC models. The columns represent different constraint types that are related with the network flow, voltage angle differences, and vertices. For each formulation, the property describes the complexity of the constraint and the Ref. represents the equation's reference number either in this chapter or for some of the complete models in the appendix.

Constraints	Polar				Rectangular				DC	
	PQV		IV		PQV		IV			
	Property	Ref.	Property	Ref.	Property	Ref.	Property	Ref.	Property	Ref.
Network Flow	Quadratic equation and trigonometric functions	3.19, 3.20.	Quadratic equation and trigonometric functions	based on 3.22, 3.23.	Quadratic equations	3.18c.	Linear constraints	3.21, 3.22, 3.23.	Linear equations	3.37
Voltage Angle Difference $\Delta\theta^v$	Linear constraints	3.13a.	Linear constraints	3.13a.	Non-convex constraints with trigonometric functions	3.13b.	Non-convex constraints with trigonometric functions	3.13b.	Linear constraints	3.38.
Vertices & Edges	Linear constraints	3.15a, 3.17.	Linear constraints	3.15a, 3.16a, 3.16b, 3.7d ineq.	Quadratic inequalities (some non-convex)	3.15b, 3.15c, 3.7b with 3.16a.	Quadratic inequalities (some non-convex)	3.15b, 3.15c, 3.16b.	Linear constraints	3.33–3.36
Models	Equation B.5		Equation B.7		Equation B.6		Equation B.8		Equations 3.33–3.38	

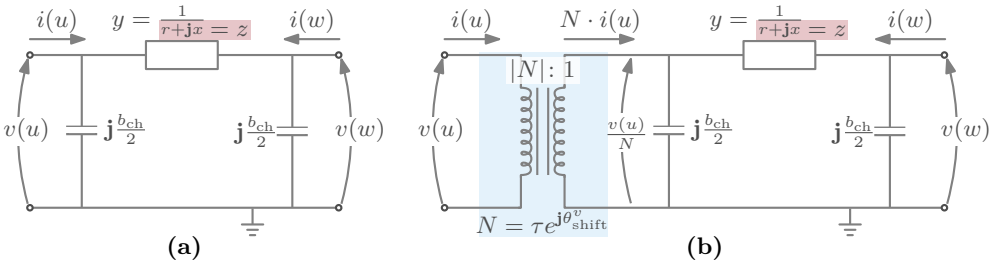

Figure 3.5: The Pi-equivalent circuit represents a model of a transmission line with medium length. Note that this figure is partly adopted from Zimmerman and Murillo-Sanchez [ZM11, p.17, Figure 3-1]. (a)&(b) The two capacitors model the transmission line charging b_{ch}, the impedance z models the resistive behavior of a transmission line (red). (b) If the line represents a phase shift transformer then the transformer is modeled on one of the two end vertices (blue). The transformer (blue) is usually modeled at the vertex with the primary coil with a fix tap ratio τ and in that particular case with a fix phase shift angle θ^v_{shift}. The voltage v and current i change with respect to the number of windings $|N|$ on the side of the secondary coil.

Transmission Line Representation. We use transmission line representations (also known as branch or transmission line models) to simplify the power flow analysis to a purely vertex-based analysis using the admittances between adjacent vertices (see Equations 3.18b and 3.22).

For the model formulation of the previous part of this section, we used a single line model and considered a transmission line model that is denoted by *short transmission line representation* that neglects shunt elements such as the shunt capacitance b_{ch} representing the charging of a line (see Figure 3.5). The short transmission line representation approximates lines that are up to 80 km long by using a similar model as the RLC circuit, meaning resistance, impedance, and capacitance are in series (see also Kirchhoff's 3rd postulate [SR61, p.127]). Note that the assumption for the short transmission line representation is reasonable, since the line charging is negligible. Within the AC model terminology, we often model the *shunt conductance* and *shunt susceptance* as elements connected to the vertices. These elements are purely model-based theoretical elements used to model elements such as transmission lines or synchronous condensers. Depending on which transmission line representation is used, the shunt elements are included or not.

For high voltage power grids it is more common to model the transmission lines using the *medium line approximation* that includes a lumped shunt admittance. There are two different models denoted by *pi representation* (see Figure 3.5(a)) and *T representation*. Wood and Wollenberg [WW96, p.75] and applications such as Matpower [ZM11, pp.16ff.] and Pypower [Lin11] use the pi representation. However, there is much more investigation in this topic as can be seen by Cano ET AL. [Can+17], who introduce different transmission line representations. Note that the standard pi representation

does not include transformers (see the next paragraph on transmission line elements). In Figure 3.5(b), we can see the pi representation with a tap transformer. Note that there are also *long line approximations* that are not considered in this work. However, the pi representation is the standard model for medium length transmission lines that are up to 250 km long, which is a realistic assumption for AC models. Note that most of the transmission lines are up to 100 km long [Nov+12, p.112].

The line charging susceptance $b_{\text{ch}}(u, w)$ is a parameter of a transmission line $\{u, w\} \in \overleftrightarrow{E}$ as medium to long transmission lines tend to have an inherent capacitance. The pi model provides us with the ability to introduce the impedance $z(u, w)$ and line charging susceptance $b_{\text{ch}}(u, w)$ to the admittances $y(u, w)$ for all $\{u, w\} \in \overleftrightarrow{E}$ and use the standard power flow analysis as shown in the previous part of this section. The only difference are the charge elements in the complex power equations (see Equation 3.24).

$$p(u, w) + \mathbf{j} \cdot q(u, w) \tag{3.24a}$$

$$= v(u)\Big(\big(v(u) - v(w)\big)y(u, w)\Big)^{\star} + v(u)\big(v(u)y_{\text{ch}}(u, w)\big)^{\star} \tag{3.24b}$$

$$= \Big(|v(u)|^2 - |v(u)| \cdot |v(w)| \cos\left(\theta^v(u) - \theta^v(w)\right) - \mathbf{j} \cdot |v(u)||v(w)| \sin\left(\theta^v(u) - \theta^v(w)\right)\Big) \cdot y(u, w)^{\star} - |v(u)|^2 y_{\text{ch}}(u, w)^{\star} \tag{3.24c}$$

for all $(u, w) \in E$. However, the admittance changes a bit. Using the pi representation with transformer (see Figure 3.5b), the admittance y changes in the following way. Each transformer has two different windings, one on the primary side and the other one on the secondary side. We denote the ratio by turn ratio (or tap ratio) $\tau(u, w) := {}^{|v(w)|}/_{|v(u)|} = {}^{v(w)}/_{v(u)} = -{}^{i(u,w)}/_{i(w,u)}$ that can be calculated by the voltage ratios of both sides. The self-admittance is defined by $y_{\text{ch}}(u, u) := \left(y(u, w) + \mathbf{j}\frac{b_{\text{ch}}}{2}\right)\frac{1}{\tau^2}$ and the edge admittance is defined by $y_{\text{ch}}(u, w) := -y(u, w)\frac{1}{\tau e^{-\mathbf{j}\theta^v_{\text{shift}}}}$. Note that the transformer *tap ratio* τ only influences the admittance at u, but not at w. However, the admittance for the edge is symmetric apart from the sign of the exponent.

In the latter line model, we added a transformer that changed the admittance entries only. Adding transformers or FACTS on an edge $\{u, w\} \in \overleftrightarrow{E}$ changes the entries of the admittances $y(u, w)$. However, it does not influence the power grid analysis, which we describe in the following.

Transmission Line Elements. One possibility to model transformers or FACTS is by adjusting the entries of the admittance matrix $\mathbf{Y}$ (see Equation 3.25). Thus, it has no effect on the steps of the previously shown vertex-based analysis. From Cain ET AL., we know that the matrix is usually sparse [COC12, p.17]. The lowest density is given by a spanning forest and the highest density by a complete graph. It is very

uncommon for power grids to correspond to the latter graph structure for more than three vertices.

An ideal in-phase transformer usually has two sides denoted by primary and secondary side that we denote by u and w, respectively. Ideal means that there is no resistance in the windings, no leaking flux, and no hysteresis losses [COC12, p.17]. Thus, the phases on both ends are assumed to be equal meaning $\theta^v(u) = \theta^v(w)$. Recall from the previous paragraph that each transformer has two different windings, one on the primary side and the other one on the secondary side and that the turn ratio is defined by $\tau(u,w) := {}^{|v(w)|}/_{|v(u)|} = {}^{v(w)}/_{v(u)} = -{}^{i(u,w)}/_{i(w,u)}$ that can be calculated by the voltage ratios of both sides. However, the voltage angles at the primary and secondary coil change for a phase shift transformer. Thus, we have an additional parameter that is called the phase angle shift θ^v_{shift} that changes the voltage angle difference to $\theta^v(u) - \theta^v(w) - \theta^v_{\text{shift}}(u,w)$. Thus, the ratios are defined by ${}^{|v(w)|}/_{|v(u)|} = \tau(u,w)e^{\mathbf{j}\theta^v_{\text{shift}}(u,w)}$ and ${}^{i(u,w)}/_{i(w,u)} = -\tau(u,w)e^{-\mathbf{j}\theta^v_{\text{shift}}(u,w)}$. In Equation 3.25 the entries of the admittance matrix Y for an edge $(u,w) \in E$ are given for two different transformers and the third setting is when there is no transformer (i. e., standard pi representation).

$$\mathrm{Y} = \begin{cases} y(u,w) & = y'(u,w) & \text{No Transformer} \\ y(u,w)\cdot\tau(u,w)^2 & = y'(u,w) & \text{Ideal Transformer} \\ \left.\begin{array}{ll} \tau(u,w)^2 y(u,u) & = y'(u,u) \\ -\tau(u,w)e^{-\mathbf{j}\theta^v_{\text{shift}}(u,w)}y(u,w) & = y'(u,w) \\ y(w,w) & = y'(w,w) \\ -\tau(u,w)e^{\mathbf{j}\theta^v_{\text{shift}}(u,w)}y(w,u) & = y'(w,u) \end{array}\right\} & \text{Phase Shift Transformer} \end{cases} \tag{3.25}$$

The self-admittances $y(u,u)$ is defined by the admittance-to-ground $y(u,0)$ and the sum of the admittances of all adjacent edges, where $y(u,w)$ is defined as above (see Equation 3.26).

$$y(u,u) = y(u,0) + \sum_{w:\ \{u,w\}\in\overleftrightarrow{E}} y(u,w) \qquad \forall u \in V. \tag{3.26}$$

This shows that the integration of transmission elements such as different line types or transformers can be done by the admittances in the vertex-based analysis.

3.3.2 Linearized Alternating Current Power Flow Model

The Alternating Current power flow models represent the standard models to analyze the networks. However, they are non-linear, complex, and slow to compute. Since the feasibility problem for the AC power flow model is already NP-hard on trees [LGH16], an approximation of that model might be reasonable. We go through the different steps of the approximation until we reach the linearized AC power flow

model that is often denoted as DC power flow model. After reaching the DC power flow model, we will discuss the analogies to the model for DC networks to understand the meaning of the name. The DC assumptions of the power flow model are as follows.

(A1) The series resistance is negligible, i. e., $r(u,w) \ll x(u,w)$ for all $\{u,w\} \in \overleftrightarrow{E}$,

(A2) the voltage angle differences $\theta^{\upsilon}(u) - \theta^{\upsilon}(w)$ are small for all $(u,w) \in E$, and

(A3) the voltage magnitudes are equal among all vertices' voltages, meaning $|\upsilon(u)| = |\upsilon(w)|$ for all $u, w \in V$.

In the DC Assumption 1, we assume that the ratio between resistance $r(u,w)$ and reactance $x(u,w)$ is very small such that we may approximate the resistance to be $r(u,w) \approx 0$ for all edges $\{u,w\} \in \overleftrightarrow{E}$. Zimmerman and Murillo-Sanchez [ZM11, p.20] neglects the resistance r and the line charging capacitance b_{ch} meaning $b_{\text{ch}} \approx 0$. This means that we assume that the network is lossless as has no charging effects. Thus, all models using these assumption are denoted as *lossless* models. If we apply this assumption to the AC model this simplifies in particular the conductance $g(u,w)$ in Equation 3.11 and the susceptance $b(u,w)$ in Equation 3.12 to Equation 3.27 and Equation 3.28 for all edges $\{u,w\} \in \overleftrightarrow{E}$, respectively.

$$g(u,w) := \frac{r(u,w)}{r(u,w)^2 + x(u,w)^2} \overset{r \approx 0}{=} 0 \qquad \forall \{u,w\} \in \overleftrightarrow{E}, \tag{3.27}$$

$$b(u,w) := -\frac{x(u,w)}{r(u,w)^2 + x(u,w)^2} \overset{r \approx 0}{=} -\frac{1}{x(u,w)} \qquad \forall \{u,w\} \in \overleftrightarrow{E}. \tag{3.28}$$

Thus, the conductance $g(u,w)$ is zero and the susceptance $b(u,w)$ is purely reciprocal to the reactance. This simplifies Equations 3.19a and 3.20a to Equation 3.29a and Equation 3.29b, respectively.

$$p(u,w) \overset{(A1)}{=} |\upsilon(u)||\upsilon(w)|\Big(\quad b(u,w) \sin\left(\theta^{\upsilon}(u) - \theta^{\upsilon}(w)\right)\Big) \tag{3.29a}$$

$$q(u,w) \overset{(A1)}{=} -b(u,w)\Big(|\upsilon(u)||\upsilon(w)| \cos\left(\theta^{\upsilon}(u) - \theta^{\upsilon}(w)\right) - |\upsilon(u)|^2\Big) \tag{3.29b}$$

Recall from the transmission line representation (see Section 3.3.1) that in literature the standard representation of a transmission line is the pi representation (see Figure 3.5).

In the DC Assumption 2 , we assume that the voltage angle difference $\theta^{\upsilon}(u) - \theta^{\upsilon}(w)$ is small such that the cosine is approximately 1 (i. e., constant) and we are able to approximate the sine by $\sin(x) \approx x$. The voltage angle difference—when assumed to be small—is at most 30° (i. e., $\pi/6$) that corresponds to 0.52 radian. However, a typical value is 15° or even less [Pur+05]. Applying this assumption to Equation 3.29a and Equation 3.29b yields Equation 3.30a and Equation 3.30b, respectively.

$$p(u,w) \overset{(A2)}{=} |\upsilon(u)||\upsilon(w)|b(u,w)\left(\theta^{\upsilon}(u) - \theta^{\upsilon}(w)\right) \tag{3.30a}$$

$$q(u,w) \overset{(A2)}{=} -|\upsilon(u)||\upsilon(w)|b(u,w) + |\upsilon(u)|^2 b(u,w) \tag{3.30b}$$

In the DC Assumption 3 the voltage magnitudes $|v(u)|$ for all $u \in V$ are assumed to be equal. Thus, we can normalize all voltage magnitudes to 1 p.u.. The idea behind this assumption is that the voltage range should be in a certain bound such that all electrical devices work properly or (at least) are not damaged. The voltages in p.u. typically range in practice between 0.95 p.u. and 1.05 p.u. [Pur+05]. Thus, the maximum voltage magnitude difference is 0.1 p.u..

$$p(u,w) \overset{(A3)}{=} b(u,w)\big(\theta^v(u) - \theta^v(w)\big) \qquad \forall (u,w) \in E \tag{3.31a}$$

Reformulating Equation 3.30b into a vertex-based equation, since we do a vertex-based analysis, the reactive power is given in Equation 3.32 (derivation Equation B.9).

$$q(u) \overset{(A3)}{=} -b(u,u) - \sum_{w:\ \{u,w\} \in \overrightarrow{E}} b(u,w)\,(|v(w)| - |v(u)|) \qquad \forall u \in V \tag{3.32a}$$

A similar transformation can be done for the real power yielding a similar equation including the sum over all adjacent edges, but with the phase angle differences. Note that the real and reactive power both depend on the susceptance, but are either dependent on the voltage angle difference or on the voltage magnitude differences, respectively. From the maximum value of the voltage angle difference and the voltage magnitude difference, we know that $p \gg q$, which implies that we can neglect the reactive power. The net flow at a vertex $u \in V$ is defined by $f_{\text{net}}(u) := \sum_{w:\ \{u,w\} \in \overrightarrow{E}} p(u,w)$.

$$f_{\text{net}}(u) = 0 \qquad \forall u \in V \setminus (V_G \cup V_D) \tag{3.33}$$

$$-\overline{p_d}(u) \leq f_{\text{net}}(u) \leq -\underline{p_d}(u) \qquad \forall u \in V_D \tag{3.34}$$

$$\underline{p_g}(u) \leq f_{\text{net}}(u) \leq \overline{p_g}(u) \qquad \forall u \in V_G \tag{3.35}$$

$$|p(u,w)| \leq \text{cap}(u,w) \qquad \forall (u,w) \in E \tag{3.36}$$

$$b(u,w) \cdot \left(\theta^v(u) - \theta^v(w) - \theta^v_{\text{shift}}\right) = p(u,w) \qquad \forall (u,w) \in E \tag{3.37}$$

$$\underline{\Delta\theta^v}(u,w) \leq \theta^v(u) - \theta^v(w) \leq \overline{\Delta\theta^v}(u,w) \qquad \forall (u,w) \in E \tag{3.38}$$

The above Equations 3.33–3.38 describe a linearization of the AC model. The DC Feasibility Problem is a linear convex model that can be solved in $O(|V|^{2.5})$ time [BC75, Vai89] and its decision problem is defined in the following box.

Direct Current Feasibility Problem DC FEAS($\mathcal{N}$)

Instance: A DC network $\mathcal{N} = (G, V_G, V_D, \text{cap}, b, \underline{p_g}, \overline{p_g}, \underline{p_d}, \overline{p_d})$.

Question: Is there a feasible electrical flow complying with the Equations 3.33–3.38?

Note that the DC FEAS($\mathcal{N}$) constitutes a system of linear equations that can be solved in polynomial-time.

Analogies to the DC Model. The DC model is defined by Ohm's Law (Equation 3.39), which states that voltage and current are directly proportional to each other. The resistance is usually a known value representing the constant of proportionality. The latter can be seen as a property of a conductor that is (usually) fixed.

$$I(u,w) := \frac{V(u,w)}{R(u,w)} \tag{3.39}$$

$$= G(u,w) \cdot V(u,w) \tag{3.40}$$

In the linearized AC model, the real power flow $p(u,w)$ behaves like the current $I(u,w)$ in the DC network (see Equations 3.41 and 3.42). In addition, the susceptance $b(u,w) := -1/x(u,w)$ behaves like the electrical conductance $G(u,w) := 1/R(u,w)$. The voltage angle difference $\Delta\theta^{v}(u,w)$ behaves like the voltage $V(u,w)$ in the DC network.

$$p(u,w) = b(u,w) \cdot \Delta\theta^{v}(u,w) \tag{3.41}$$

$$I(u,w) = G(u,w) \cdot V(u,w) \tag{3.42}$$

In literature it is common to use capital letters, since in an ideal DC model voltage, current and power do not change over time (see Figure 3.6a), neglecting temperature and other influences over time.

3.3.3 The Voltage Normalized Lossless Real Power Flow Model – A Model between AC and DC Model

In Section 3.3.1, we discussed nonlinear power flow models (AC power flow models) that are also non-convex. The nonlinear and non-convex model makes the Feasibility Problem (FEAS) difficult to solve to optimality as most nonlinear solvers provide locally optimal solutions, since they get stuck in a local optima. Thus, a common way is to simplify the model. In Section 3.3.2, we showed how to simplify the AC model by linearizing it to the so called DC model. Though it is not the model for the DC network, we could show the analogies to it that make algorithms for the linearized AC model applicable to DC networks.

Donde et al. [Don+05, pp.60, Equation 1] and Pinar et al. [Pin+10, p.1791, Equation 3.1] introduced another power flow model that is either called *"lossless" model* or *Sin model*. However, we denote it as Voltage Normalized Lossless Real Power Flow (VNLP) model for a clear description and distinction from the other models. It represents a hybrid model between the AC and DC model. This model is not as general as the AC model as it incorporates DC Assumption 1 and DC Assumption 3, but more general than the DC model as it neglects DC Assumption 2. From DC Assumption 1, the model is often denoted by the term "lossless". By introducing DC Assumption 3 (i. e., fixing all—i. e., for all u in V—voltage magnitudes $|v(u)|$ to 1 p.u.), we know from Section 3.3.2 that the reactive power becomes negligible.

As the previous models do, the VNLP model incorporates the conservation of flow (KCL; Equations 3.43a–3.43c), the power flow equation (KVL-like; Equation 3.43d), and the voltage angle difference bounds (Equation 3.43e). The latter constraints model the steady-state stability [Ver10, p.113]. Recall that $f_{\text{net}}(u) \coloneqq \sum_{w\colon \{u,w\} \in \overleftrightarrow{E}} p(u,w)$.

$$f_{\text{net}}(u) = 0 \qquad \forall u \in V \setminus (V_G \cup V_D), \tag{3.43a}$$

$$\underline{p_g}(u) \leq f_{\text{net}}(u) \leq \overline{p_g}(u) \qquad \forall u \in V_G, \tag{3.43b}$$

$$-\overline{p_d}(u) \leq f_{\text{net}}(u) \leq -\underline{p_d}(u) \qquad \forall u \in V_D. \tag{3.43c}$$

$$b(u,w) \cdot \sin\left(\theta^v(u) - \theta^v(w)\right) = f(u,w) \qquad \forall (u,w) \in E \tag{3.43d}$$

$$|\theta^v(u) - \theta^v(w)| \leq \frac{\pi}{2} \qquad \forall (u,w) \in E \tag{3.43e}$$

$$|f(u,w)| \leq \text{cap}(u,w) \qquad \forall (u,w) \in E \tag{3.43f}$$

Recall that we look at the real part $\mathcal{Re}(\cdot)$ of the power flow model and that the angle differences are restricted to $[-\pi/2; \pi/2]$. The Equations 3.43d–3.43f can be reformulated to Equations 3.44 and 3.45, respectively. Note that Equation 3.44 is just a reformulation of Equation 3.43d. Since the sine for $\pm\pi/2$ (voltage angle difference restriction; Equation 3.43e) is ± 1 the voltage angle difference is the minimum of 1 and $x(u,w) \cdot \text{cap}(u,w)$.

$$\theta^v(u) - \theta^v(w) = \arcsin\left(x(u,w) \cdot f(u,w)\right) \qquad (u,w) \in E, \tag{3.44}$$

$$|\theta^v(u) - \theta^v(w)| \leq \arcsin(\min\{1, x(u,w) \cdot \text{cap}(u,w)\}) \qquad (u,w) \in E. \tag{3.45}$$

Equation 3.45 incorporates the voltage angle differences (Equation 3.43e) and the capacity constraint (Equation 3.43f). Verma [Ver10, p.114, Lemma 4.2.1 & Theorem 4.2.2] showed the uniqueness of a feasible power flow in the VNLP-model. Note that in general the power grid has no hard capacities. The thermal line limits for the calculation is usually to maintain the safety of the lines such that they are not overheating. Since the power flows are unique, we can neglect the capacity constraints for the Feasibility Problem. Note that we prove and use the same observation in Chapter 4 in a different way. When neglecting the capacity constraint the right-hand side of Equation 3.45 becomes arcsin(1). The decision problem of the VNLP is defined in the following problem box.

Voltage Normalized Lossless Real Power Flow Feasibility Problem

Instance: A VNLP network $\mathcal{N} = (G, V_G, V_D, \text{cap}, b, \underline{p_g}, \overline{p_g}, \underline{p_d}, \overline{p_d})$.

Question: Is there a feasible electrical flow complying with Equations 3.43a–3.43f?

Note that the model is non-linear and non-convex [Ver10]. On general graphs, Verma [Ver10] shows that the capacitated version of VNLP is NP-complete (see Section 3.3.3).

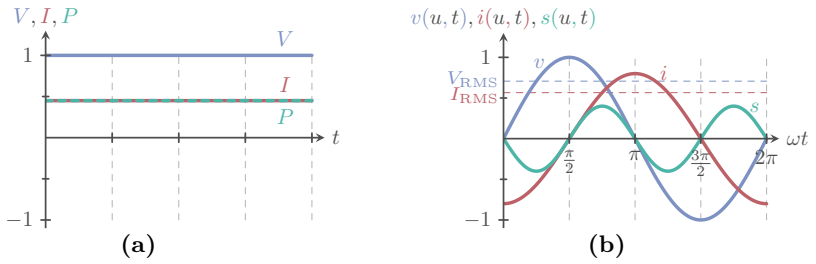

Figure 3.6: The plots for AC and DC models differ in their power, current and voltage curves. (a) The curves of the linearized AC model can be interpreted like the curves of the DC model as constant functions over time. Thus, power P, current I, and voltage V are time-independent functions. (b) The AC model consists of sinusoid functions. The instantaneous power $s(u,t)$, current $i(u,t)$, and voltage $v(u,t)$ are functions over time. The root-mean-squared (RMS) of voltage V_{RMS} and current I_{RMS} are represented by the dashed-colored horizontal lines.

In this work they do a reduction from one-in-three 3-SAT, where each clause has exactly one true literal. Bienstock and Verma [BV19] extended that to strong NP-hardness.

For the VNLP model (Section 3.3.3), the feasibility problem can be solved in polynomial time in the size of the network and $1/\epsilon$ for graphs with bounded tree-width and any given tolerance ϵ.

3.3.4 Alternating vs. Direct Current Model

Historically, the question of whether AC or DC would be used arose in the 1800s. There was a competition between two companies of Thomas Edison and George Westinghouse that developed and spread the use of DC and AC, respectively. This competition is also known as "war of the currents". In the end AC imposed, since the first transformers were invented for AC, allowing a simple change in voltage level and long distance transmission as well as usage of electricity in households. The first long distance transmission of three-phase AC was in 1891. It is impressive that the first pure DC transformer was invented in 1976, since technologies such as semiconductors had been developed. Nowadays, the question arises in terms of distribution systems [Ham07].

However, if we look at the current power grid, we mainly have an AC power grid with a few HVDC lines. So we focus on the question of whether our model assumptions are reasonable and when the errors would become significant. Recall that the DC power flow model introduces three assumptions (DC Assumptions 1–3) that simplify the AC power flow to a DC power flow model. The question of when the DC model is useful, thus, depends on three parameters: resistance of the lines, voltage angle differences, and voltage magnitude deviations. An evaluation that tests the three assumptions is given by Purchala ET AL. [Pur+05].

The TSOs usually say that the resistance of the transmission network is negligible. This statement is basically covered in DC Assumption 1. The transmission network in Germany has voltages of 110 kV, 220 kV, and 380 kV. These voltage layers define the high voltage level. The higher the voltage the lower the current and thus, the lower the influence of the resistance (see Equations 3.18b and 3.39). So our expectation would be that this assumption mainly depends on the voltage level and on the line resistances. Purchala ET AL. [Pur+05, p.4] show that for the Belgian grid with voltage levels of 70 kV, 150 kV, 220 kV, and 380 kV the X/R ratio ranges from 0.8 for the 70 kV voltage level to 12.5 for the 380 kV voltage level. The real power estimation error (that increases with increasing resistance) for these voltage levels is less than 5% and for the 380 kV power grid drops below 2.5%. Both errors are small and thus, the resistance for such X/R ratios in high voltage levels is negligible.

The DC Assumption 2 assumes that the voltage angle difference is small enough such that the sine function is negligible. The system's stability is guaranteed in the range of $[-\pi/2; \pi/2]$. However, 30° or $[-\pi/6; \pi/6]$ is the range where the sine can be approximated by $\sin(x) = x$. Thus, if the difference is within this range, the real power error should be small. Purchala ET AL. [Pur+05, p.2] evaluate for the Belgian power grid with voltages ranging from 70 kV to 380 kV that the highest voltage angle difference was 7° and in 94% of the lines it was less than 2°. One explanation is that the inductive and conductive properties of an edge are quite small. However, the lines inductive property is usually slightly higher, though for long distances the capacitive property increases (see the transmission line representation section in Section 3.3.1 on Page 47).

The last assumption—DC Assumption 3—is about a flat voltage profile, e. g., all voltages are equal to 1 p.u.. If there is a voltage deviation then this would automatically lead to a voltage difference that is simply not modeled in the DC model. The real power error increases with increasing voltage deviation [Pur+05, p.4, Figure 7]. Thus, a flat voltage profile is important but difficult to establish in power grids.

This particularly means that the most critical assumption is the flat voltage profile. The others can be at least established quite well in a high voltage power grid. However, flat voltage profiles are difficult to establish and thus, the results have to be carefully interpreted in terms of an AC power grid. However, this discussion also shows that the more complex Sin-model including the sine function might be a more realistic model, but that the assumption is not critical for the real power error and thus, it might increase the complexity unnecessarily. However, from a theoretical perspective this model is quite interesting as the feasibility problem is already strongly NP-hard Bienstock and Verma [BV19].

Problems. The AC feasibility problem is a subproblem of many optimization problems such as the TRANSMISSION NETWORK EXPANSION PLANNING (TNEP) problem,

the Optimal Transmission Switching Problem (OTSP) and the Maximum Power Flow Problem (MPFP).

The Economic Dispatch Problem (EDP) minimizes the total cost represented by the sum of all generator cost functions γ. It is the simplest problem formulation that checks whether demand and supply match by abstracting from the power grid and incorporates the energy balance equation, and the generator constraints (see Equations 3.17a and 3.17b). After adding the power grid specifics, the problem is called either AC or DC Optimal Power Flow Problem (OPFP). All the problems mentioned so far have continuous variables only. In terms of planning problems, we introduce integer or binary variables. The most commonly known problems for finding an optimal topology are TNEP, OTSP, and MTSFP.

4 The Direct Current Feasibility Problem [1]

An Algorithmic Approach to Computing Electrical Flows

The Alternating Current Feasibility Problem (AC FEAS; see Section 3.3.1) and Direct Current Feasibility Problem (DC FEAS; see Section 3.3.2) are subproblems of most power grid related problems such as switching (see Chapter 5) and ideal FACTS placement (see Chapter 6). In this chapter, we formalize the operation of the power grid in such a way that we are able to develop algorithmic approaches for the electrical flow computation. With the latter formulations, we are able to develop better algorithms for problems that incorporate the electrical flow computation as a subproblem. Recall that one of the first persons who increased the knowledge in DC FEAS was Kirchhoff [Kir47], who formalized the electrical flow and introduced structural properties.

In Section 3.3, we described different models and approximations to analyze the network by calculating the power flow, which we call more generally electrical flow. In this chapter, we focus on the Direct Current Feasibility Problem (DC FEAS; commonly known as Power Flow; in short PF) and the DC Maximum Power Flow Problem (DC MPFP). We describe their mathematical models using different formulations and give some structural insights that will be important to develop algorithms for DC FEAS and DC MPFP (see Section 3.3.2). Note that one of the first algorithms—though with exponential running time—to compute electrical flows uses spanning trees (see Lemma 4.6; [Sha87, SR61]). We describe the latter algorithm [Sha87, SR61] briefly in Section 4.1. This algorithm was used by Felsner [Fel13] to construct a squaring of a rectangle [Fel13, pp.17ff.]. Felsner shows that the flow of a graph that represents such a squaring of a rectangle is equivalent to a solution of an integer DC FEAS, meaning all flows have to be integral. Since this problem uses integral electrical flows (i. e., the flow is a function $f : E \to \mathbb{Z}$), we usually cannot apply an LP from Section 3.3.2, but have to use an ILP. In general solving ILPs is NP-hard [GJ79, p.245, MP1]. However, if the solution space has some properties, it is possible to solve it with other techniques and algorithms in polynomial time. One possibility would be to relax the variables of DC FEAS, which means that a solution of an LP yields an integral solution. However, we show that this technique does not necessarily result in an integral flow. However, if we do not have a fixed generation, a fixed demand, and neglect the capacities, meaning $\text{cap} \equiv \infty$, but ask for a generation and demand such that we get integral electrical flows, we can make use of some properties of the solution space.

[1] I would like to thank especially Matthias Wolf and Torsten Ueckerdt for questions, discussions, and comments. In addition, I would like to thank Marc Timme for some initial conversations, his time, and that he encouraged me (more or less) to write this chapter.

In Section 4.2, we first give an overview over known transformation and contraction rules. In the end of Section 4.2, we give an algorithm for the s-t-DC FEAS and -MPFP on planar biconnected graphs that runs in $O(|V|^3)$ time. Recall that DC FEAS and MPFP can be formulated as a linear system of equations and an LP, respectively, that can be solved in $O(|E|^{2.5})$ time [BC75, Vai89]. Thus, using the contraction and transformation rules in the fashion described in Section 4.2 does not yield an algorithm that has a better running time than the known mathematical methods. However, it gives some structural information.

While restricting our graphs to biconnected planar s-t-graphs, we develop an algorithm that transforms the formulation given in Section 3.3 and Section 4.1 to an equivalent formulation of *simultaneous flows* (Section 4.3.2). For this formulation, we are able to develop an algorithmic approach for s-t- DC FEAS and -MPF algorithm for biconnected graphs (Section 4.5) that can be extended to an algorithm for multiple sources and multiple sinks on planar graphs by using the superposition principle for linear physical systems.

4.1 A Mathematical Model for the Feasibility Problem of Electrical Flows

Cain et al. [COC12, p.13] give the structural hint that power grids are often planar. Note that this might not be true in general. In addition, power grids are quite sparse. The electrical network's topology is described by a bidirected graph $G = (V, E)$, where V is the set of vertices representing the buses (i. e., line junctions), and E is the set of edges representing the lines or cables (the conventional name is branch). Though the underlying graph is undirected [COC12, p.13], we are always able to direct its edges $\{u, w\} \in \overleftrightarrow{E}$ by inserting two edges in opposite direction $(u, w), (w, u) \in E$. Introducing the direction is motivated by the electrical network's direction that is usually defined by the voltage or current source representing the *reference* vertex (also known as *slack* or *datum*; see Table 3.1 on Page 42). The direction is used for notational convenience and for electrical networks that are *nonreciprocal*. Nonreciprocal electrical networks have components on their edge that have a predefined direction such as diodes. However, in our case the electrical network is reciprocal (also known as *bilateral*) and thus, the flow on each edge is allowed to flow in both directions. The underlying graph is undirected, and we define for notational convenience the set $\overleftrightarrow{E}$ of undirected edges by $\overleftrightarrow{E} = \{\overleftrightarrow{e} \mid e \in E\}$, i. e., $\overleftrightarrow{(u, w)} = \overleftrightarrow{(w, u)} = \{u, w\}$.

Each edge has a thermal limit and a susceptance that are represented by the functions $\mathrm{cap}\colon \overleftrightarrow{E} \to \mathbb{R}$ and $b\colon \overleftrightarrow{E} \to \mathbb{R}$, respectively. The set V_G of generators represents the energy sources and the demands are represented by a set V_D of consumers. Without loss of generality, we assume that $V_G \cap V_D = \emptyset$ and $V_G \cup V_D \subseteq V$. An *electrical network* is defined by a tuple $\mathcal{N} = (G, V_G, V_D, \mathrm{cap}, b, \underline{p_g}, \overline{p_g}, \underline{p_d}, \overline{p_d})$ with min-

imum and maximum generation $\underline{p_g}, \overline{p_g} \colon V \to \mathbb{R}_{\geq 0} \cup \{\infty\}$, and minimum and maximum demand $\underline{p_d}, \overline{p_d} \colon V \to \mathbb{R}_{\geq 0} \cup \{\infty\}$, respectively. In general, we distinguish between *bounded* (i. e., $u \in V_G \colon \overline{p_g}(u) < \infty$ and $u \in V_D \colon \overline{p_d}(u) < \infty$), *unbounded* (i. e., $\overline{p_g} \equiv \overline{p_d} \equiv \infty$), and *exact* (i. e., $\underline{p_g} \equiv \overline{p_g}$ and $\underline{p_d} \equiv \overline{p_d}$) networks.

The power is defined by current and voltage functions. These functions over time map an edge and a point in time to voltage and current values (see Section 3.3.1). However, in this work we focus on *steady-state* systems that are invariant and thus, bind the functions to one particular timestamp. The latter means that all functions become time independent. A *flow* is a function $f \colon E \to \mathbb{R}, (u, w) \mapsto f(u, w)$. A flow complies with the skew-symmetry property $f(u, w) = -f(w, u)$ for all $(u, w) \in E$. The *net flow* at a vertex $u \in V$ is defined by $f_{\text{net}}(u) \coloneqq \sum_{\{u,w\} \in \overleftrightarrow{E}} f(u, w)$. We define the *flow value* $F(\mathcal{N}, f)$ to be the sum of all generator excesses $\sum_{u \in V_G} f_{\text{net}}(u)$.

The behavior of voltage and current in the classical physics are described by the Kirchhoff's laws [Kir47][SR61, p.120, Definition 6-1]. Since we are interested in power flows while using a linearization of an AC power flow (known as DC FEAS), we map DC currents i to real power p, which we denote by f and DC voltage v to voltage angle differences $\Delta\theta^v$ (see Section 3.3.2 on Page 52).

Kirchhoff's Current Law (KCL). The first law is called the *Kirchhoff's Current Law* (KCL; Equations 4.1–4.3) and describes that the power entering a vertex $u \in V$ is equal to the power exiting u. This is equivalent to the conservation of flow in graph theory.

$$f_{\text{net}}(u) = 0 \qquad \forall u \in V \setminus (V_G \cup V_D), \tag{4.1}$$

$$\underline{p_g}(u) \leq f_{\text{net}}(u) \leq \overline{p_g}(u) \qquad \forall u \in V_G, \tag{4.2}$$

$$-\overline{p_d}(u) \leq f_{\text{net}}(u) \leq -\underline{p_d}(u) \qquad \forall u \in V_D. \tag{4.3}$$

The Equations 4.1–4.3 constrain the flow on the edges incident to a vertex $u \in V$. We distinguish between intermediate vertices (Equation 4.1), vertices with a generator (Equation 4.2) having an excess of power, and vertices with a consumer (Equation 4.3) having a demand (disturbance) in power. Recall from Section 3.3.2 that the latter equations (Equations 4.1–4.3) are equivalent to Equations 3.33–3.38. Note that as long as we only consider the KCL, we can always connect generator vertices $u \in V_G$ with a super source s using $\overline{p_g}(u)$ as capacity, and demand vertices $u \in V_D$ with a super sink t using $\overline{p_d}(u)$ as capacity. This results in a single-source and single-sink flow that is a notational simplification. Note that we can connect the super source s and super sink t with each other resulting in a circulation problem.

Though, the aforementioned formulation is our standard way to describe the KCL, we need the algebraic formulation of the KCL to get some structural insights. We assume from now on—if not stated otherwise—that we have an exact network. Thus,

Equations 4.2 and 4.3 become Equations 4.5 and 4.6 with $p_g \equiv \underline{p_g} \equiv \overline{p_g}$ and $p_d \equiv \underline{p_d} \equiv \overline{p_d}$, respectively. Recall from Section 3.1 that an oriented incidence matrix (also known as connection matrix) represents the graph's connections in terms of the vertex-edge incidence relations, i. e., an entry in row u and column e is 1 (respectively -1) if edge e is an incoming (respectively outgoing) edge, and 0 otherwise. The properties of such a matrix are given in Section 3.1. The Equations 4.1–4.3 can be restated using the oriented incidence matrix $\mathbf{I} \in \{-1, 0, 1\}^{|V|\times|E|}$ and the vector of flows $\vec{f} \in \mathbb{R}^{|E|}$ with $\vec{f} \coloneqq \big(f(u,w)\big)_{(u,w)\in E}$. The KCL in matrix form is given in Equations 4.4–4.6.

$$\mathbf{I}_{V\setminus(V_G\cup V_D)}\vec{f} = \vec{0}, \tag{4.4}$$

$$\mathbf{I}_{V_G}\vec{f} = \vec{p_g}, \tag{4.5}$$

$$\mathbf{I}_{V_D}\vec{f} = \vec{p_d}, \tag{4.6}$$

where $\vec{0}$ is the zero vector of size $|V \setminus (V_G \cup V_D)|$, $\mathbf{I}_{V\setminus(V_G\cup V_D)}$ is a submatrix of the incidence matrix $\mathbf{I}$ constituted by the vertices that are neither generators nor consumers. Similar notion is used for the submatrix of the generators and consumers in Equation 4.5 and Equation 4.6. Note when $(s,t) \in E$ the flow vector $\vec{f}$ would have a fixed entry with $\vec{f}_{(s,t)} = \sum_{u\in V_G} p_g(u) = \sum_{w\in V_D} p_d(w)$ and Equation 4.4 is sufficient. Equations 4.4–4.6 constitute an incidence matrix $\mathbf{I} \in \mathbb{R}^{|V|\times|E|}$ with $\mathbf{I} \coloneqq (\mathbf{I}_{V\setminus(V_G\cup V_D)}, \mathbf{I}_{V_G}, \mathbf{I}_{V_D})^\intercal$ and right-hand side vector $\vec{p_\mathbf{I}} \in \mathbb{R}^{|V|}$ with $\vec{p_\mathbf{I}} \coloneqq (\vec{0}, \vec{p_g}, \vec{p_d})^\intercal$. The whole system of linear equations is given in Equation 4.7.

$$\mathbf{I} \cdot \vec{f} = \vec{p_\mathbf{I}}. \tag{4.7}$$

The system $\mathbf{I} \cdot \vec{f} = \vec{p_\mathbf{I}}$ represents a translation of the solution set $\mathbf{I} \cdot \vec{f} = \vec{0}$. The latter equation is also called *homogeneous equation* (or homogeneous problem) and has always the trivial solution $\vec{f} = \vec{0}$. If we have a solution $\vec{f}_{\text{nh}}$ for the nonhomogeneous system then the whole solution space can be described by $\vec{f}_{\text{nh}} + \{\vec{f}_{\text{h}} \mid \vec{f}_{\text{h}} \in \mathbb{R}^{|E|}, \mathbf{I} \cdot \vec{f}_{\text{h}} = \vec{0}\}$, where $\vec{f}_{\text{h}}$ is a solution vector of the homogeneous system.

KCL Flow. We call a flow f complying with the KCL as a *KCL flow*. Recall that we can interpret vectors in the euclidean space geometrically as a line segment from the origin with magnitude and direction. Two vectors are orthogonal to each other if the angle α between them is 90° and $\cos(\pi/2) = 0$. Thus, the dot product is zero meaning $\vec{i_u} \cdot \vec{f} = \vec{0}$, since $\vec{i_u}\vec{f} = \left\|\vec{i_u}\right\|_2 \left\|\vec{f}\right\|_2 \cos(\alpha)$ for all vertices $u \in V$. If we have $\mathbf{I} \cdot \vec{f} = \vec{0}$ this implies that every vector $\vec{i_u}$ in the vector space (here a row u in $\mathbf{I}$) is orthogonal to the vector $\vec{f}$.

Properties of the Incidence Matrix. Note that Equation 4.4 means that the incidence matrix $\mathbf{I}$ and the vector $\vec{f}$ are orthogonal to each other—meaning every row

vector of $\mathbf{I}$ is orthogonal to $\vec{f}$. Note that this implies that the vectors are also linear independent, since there is no scalar that makes $\vec{f}$ colinear to one of the vertices in $\mathbf{I}$. The latter is equivalent to $\vec{f} \in \ker(\mathbf{I})$ with $\ker(\mathbf{I}) \coloneqq \{\vec{f} \in \mathbb{R}^{|E|} \mid \mathbf{I} \cdot \vec{f} = \vec{0}\} \subseteq \mathbb{R}^{|E|}$.

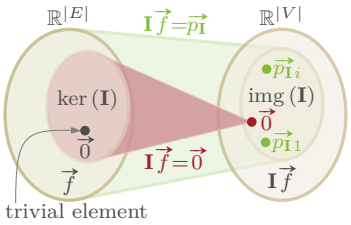

Figure 4.1: The image $\mathrm{img}(\mathbf{I})$ and kernel $\ker(\mathbf{I})$ of the incidence matrix $\mathbf{I}$ for the linear map $\mathbf{I}\colon \mathbb{R}^{|E|} \to \mathbb{R}^{|V|}$.

Note that a *trivial element* of the kernel is the neutral element, i. e., in the vector space this is the zero vector $\vec{0}$ (see Figure 4.1 left side). If the kernel consists of the neutral element only then the linear map is injective. From Seshu and Reed [SR61, p.66, Theorem 4–3], we know that the rank of the matrix $\mathbf{I}$ is $\mathrm{rk}(\mathbf{I}) = |V| - k$ with k being the number of connected components. The idea is that summing up the rows leads to one row of zeros per connected component, since every column of the incidence matrix $\mathbf{I}$—representing an edge—consists of exactly one 1 entry and one -1 entry, which gives us $\mathrm{rk}(\mathbf{I}) \leq |V| - k$ (see Figure 4.6b on Page 69 as example). The aforementioned structure of the incidence matrix $\mathbf{I}$ leads to an upper triangle matrix for each connected component that cannot be reduced further leading to $\mathrm{rk}(\mathbf{I}) \geq |V| - k$ and thus, $\mathrm{rk}(\mathbf{I}) = |V| - k$. Recall that the rank of the incidence matrix $\mathbf{I}$ (i. e., $\mathrm{rk}(\mathbf{I})$) corresponds to the number of edges in a spanning forest. To determine the nullity $n(\mathbf{I}) \coloneqq \dim(\ker(\mathbf{I}))$ of the incidence matrix $\mathbf{I}$, we introduce the *rank-nullity theorem.*

Theorem 4.1 (Rank-nullity Theorem). *For any matrix $\mathbf{A} \in \mathbb{R}^{r \times c}$ with r rows and c columns the rank $\mathrm{rk}(\mathbf{A})$ and nullity $n(\mathbf{A})$ sum up to the number of columns.*

$$\mathrm{rk}(\mathbf{A}) + n(\mathbf{A}) = c.$$

The generalization to linear maps $\mathbf{A}\colon \mathbb{R}^{|C|} \to \mathbb{R}^{|R|}$ is given by

$$\dim(\mathrm{img}(\mathbf{A})) + \dim(\ker(\mathbf{A})) = \dim(\mathbb{R}^{|C|}) = |C|.$$

The incidence matrix $\mathbf{I}$ can be viewed as a linear map $\mathbf{I}\colon \mathbb{R}^{|E|} \to \mathbb{R}^{|V|}$ with $\vec{f} \mapsto \mathbf{I} \cdot \vec{f}$. The kernel $\ker(\mathbf{I})$ and image $\mathrm{img}(\mathbf{I})$ of the incidence matrix $\mathbf{I}$ are given in Equation 4.8.

$$\ker(\mathbf{I}) \coloneqq \{\vec{f} \in \mathbb{R}^{|E|} \mid \mathbf{I} \cdot \vec{f} = \vec{0}\} \subseteq \mathbb{R}^{|E|} \tag{4.8a}$$

$$\mathrm{img}(\mathbf{I}) \coloneqq \{\vec{p_\mathbf{I}} \in \mathbb{R}^{|V|} \mid \exists \vec{f} \in \mathbb{R}^{|E|}\colon \mathbf{I} \cdot \vec{f} = \vec{p_\mathbf{I}}\} \subseteq \mathbb{R}^{|V|} \tag{4.8b}$$

A kernel $\ker(\mathbf{I})$ of the incidence matrix $\mathbf{I}$ is a set $\ker(\mathbf{I})$ of vectors $\vec{f}$ such that the homogeneous system $\mathbf{I} \cdot \vec{f} = \vec{0}$ holds for all vectors in that set (see Figure 4.1 red

area and text). The image img (**I**) of the incidence matrix are all vectors $\vec{p_I}$ for which a solution exist (see Figure 4.1 green area and text).

Using the rank-nullity theorem (see Theorem 4.1) we get the dimension of the kernel (i. e., the nullity when talking about matrices) of $\dim(\ker(\mathbf{I})) = \dim(E) - \dim(\text{img}(\mathbf{I})) = |E| - |V| + k$ that corresponds to the number of chords (i. e., edges not on a spanning forest). A common way to construct the incidence matrix **I** (see Chapter 3 on Page 27) of row size $|V| - k$ is to define one vertex $u \in V_G$ per connected component as slack vertex and remove its row u (see example Figure 4.6 b on Page 69, where we remove vertex 3). From the property of the incidence matrix **I** we know that every square submatrix of **I** has a determinant that is either -1, 0, or 1. Since every square non-singular submatrix of the incidence matrix **I** of size $(|V|-k)\times(|V|-k)$ that is the maximum square submatrix that constitutes a spanning tree is unimodular (i. e., the determinant takes ± 1 values only) and all determinants are either 0, 1, or -1, the incidence matrix **I** is totally unimodular (in short TUM).

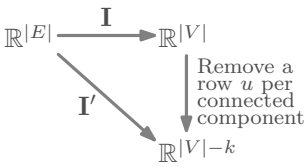

Figure 4.2: Linear maps of the incidence matrix **I** and **I**′, where k is the number of connected components.

If not noted otherwise, if we speak from now on of the incidence matrix **I**, we mean the reduced incidence matrix that has $|V| - k$ rows and thus, is defined by $\mathbf{I} \in \{-1, 0, 1\}^{(|V|-k)\times|E|}$ (see Figure 4.2).

Feasible Flows and Thermal Line Limit. As already mentioned each edge has a natural limit of flow it is able to carry. This is usually modeled by the capacity constraint that basically models the thermal line limit (Equation 4.9).

$$|f(u,w)| \leq \text{cap}(u,w) \qquad \forall (u,w) \in E. \tag{4.9}$$

We denote a flow f complying with the capacity constraints as *feasible flow*. A KCL flow (see KCL flow on Page 60) complying with the capacity constraint is thus called a *feasible KCL flow*.

Kirchhoff's Voltage Law (KVL). Kirchhoff's second law is known as *Kirchhoff's Voltage Law* (KVL) and describes the voltage angles in a *cycle* (also known as *mesh*). A cycle is a path $\pi(s,t) := \big((s,u_1),(u_1,u_2),\ldots,(u_i,t)\big)$, where at least $s = t$, otherwise it would not be closed. Cycles have by definition an even degree. The set C of cycles includes all cycles of a graph G, which can be exponentially many in general. Note that we distinguish between cycles and *circuits*. A circuit has a degree of 2. Thus, circuits are the same as simple cycles. Kirchhoff's Voltage Law states that the voltages in a cycle sum up to zero (Equation 4.10). Recall from Section 3.3.2 that in DC FEAS the voltages are substituted by the voltage angle differences $\Delta\theta^v$ and the resistances r by $1/b$. The KVL-like equation is given by $\sum_{(u,w)\in C} b(u,w)\cdot\Big(\theta^v(w) - \theta^v(u) - \theta^v_{\text{shift}}(u,w)\Big) = 0$.

In this section, we assume that $\theta^{\upsilon}_{\text{shift}}(u, w) = 0$, i. e., we assume that there are no phase transformers or FACTS (see the discussion in Section 3.3.1). In terms of linear algebra, we can rewrite the latter by using the circuit matrix $\mathbf{B}$ and the $\overrightarrow{\Delta\theta^{\upsilon}}$ vector (Equation 4.10). The oriented circuit matrix $\mathbf{B} \in \{-1, 0, 1\}^{|C|\times|E|}$ is a matrix, where each row c represents a cycle $c \in C$ and a column e represents an edge $e \in E$. The entry of $\mathbf{B}$ is either 1 (respectively -1) when an edge e is in cycle c in direction (respectively opposite) with some predefined direction for each cycle $c \in C$, or 0 if the edge is not in the cycle c. The KVL using the circuit matrix is defined in Equation 4.10.

$$\mathbf{B}\overrightarrow{\Delta\theta^{\upsilon}} = \overrightarrow{0}, \tag{4.10}$$

where $\mathbf{B} \in \{-1, 0, 1\}^{|C|\times|E|}$ [SR61, p.91] is the oriented circuit matrix (e. g., see Figure 4.6 a or b on Page 69; bottom partition), and $\overrightarrow{\Delta\theta^{\upsilon}} \in \mathbb{R}^{|E|}$ with $\Delta\theta^{\upsilon} := (\theta^{\upsilon}(w) - \theta^{\upsilon}(u))_{(u,w)\in E}$ is a vector of voltage angle differences at an edge with $\overrightarrow{\Delta\theta^{\upsilon}} \in \ker(\mathbf{B})$, and $\overrightarrow{0}$ is the zero vector of size $|C|$. The formulation in Equation 4.10 represents a homogeneous equation and thus, has always the trivial solution $\overrightarrow{\Delta\theta^{\upsilon}} = \overrightarrow{0}$.

Properties of the Circuit Matrix. Recall that the set C of cycles includes potentially exponentially many cycles. However, it suffices to work with a base of the cycle space [Kir47, pp.498ff.] and thus, the circuit matrix $\mathbf{B}$ will only incorporate a fundamental cycle base in this work.

If we speak of the circuit matrix $\mathbf{B}$ and we did not mention anything else, we speak of the circuit matrix that only has fundamental cycles as row vectors.

Definition 4.2 (Base)**.** *A* base *in a vector space is a maximum independent set of vectors that suffice to span the vector space.*

In general there are multiple bases that span the same vector space, which we will see soon. Note that all bases have the same size [Whi35, p.514, Theorem 6].

Definition 4.3 (Fundamental Cycle Base)**.** *Let $G = (V, E)$ be a graph, let $T = (V, E)$ be a spanning forest, and let $E_{\text{chords}} := E(G) \setminus E(T)$ be a set of chords. A walk from one endpoint u of the chord (u, w) to the other endpoint w using the spanning forest branches $E(T)$ defines a cycle that differs from the other cycles in $\mathbf{B}$ by at least the chord edge (u, w). A* fundamental cycle base *is defined by a spanning forest (by a spanning tree if the graph is connected), and a cycle in that base is defined by a chord (i. e., non-tree edge).*

Note that a spanning forest has $|V| - k$ edges—also denoted as tree branches—and $|E| - |V| + k$ chords, where k is the number of connected components. The rank of the circuit matrix is $\text{rk}(\mathbf{B}) = |E| - |V| + k$ [SR61, p.66, Theorem 4-5] and the nullity is $n(\mathbf{B}) = |V| - k$ [SR61, p.64, Corollary 4-4]. In general, the circuit matrix $\mathbf{B}$ does not have a determinant of ± 1 [Oka55][Kav+09, p.12, Lemma 3.3].

The circuit matrix $\mathbf{B}$ is a linear map $\mathbf{B}\colon \mathbb{R}^{|E|} \to \mathbb{R}^{|C|}$ with $\overrightarrow{\Delta\theta^v} \mapsto \mathbf{B} \cdot \overrightarrow{\Delta\theta^v}$. The kernel $\ker(\mathbf{B})$ and image $\operatorname{img}(\mathbf{B})$ of the circuit matrix $\mathbf{B}$ are defined in Equation 4.11 and illustrated in Figure 4.3 by the red or green area, respectively.

$$\ker(\mathbf{B}) := \{\overrightarrow{\Delta\theta^v} \in \mathbb{R}^{|E|} \mid \mathbf{B} \cdot \overrightarrow{\Delta\theta^v} = \vec{0}\} \subseteq \mathbb{R}^{|E|} \tag{4.11a}$$

$$\operatorname{img}(\mathbf{B}) := \{\overrightarrow{p_\mathbf{B}} \in \mathbb{R}^{|C|} \mid \exists \overrightarrow{\Delta\theta^v} \in \mathbb{R}^{|E|} \colon \mathbf{B} \cdot \overrightarrow{\Delta\theta^v} = \overrightarrow{p_\mathbf{B}}\} \subseteq \mathbb{R}^{|C|} \tag{4.11b}$$

A kernel $\ker(\mathbf{B})$ of the circuit matrix $\mathbf{B}$ is a set $\ker(\mathbf{B})$ of vectors $\overrightarrow{\Delta\theta^v}$ such that the homogeneous system $\mathbf{B} \cdot \overrightarrow{\Delta\theta^v} = \vec{0}$ holds for all vectors in that set (see Figure 4.3 red area and text). The image $\operatorname{img}(\mathbf{B})$ of the circuit matrix are all vectors $\overrightarrow{p_\mathbf{B}}$ for which a solution exist (see Figure 4.3 green area and text).

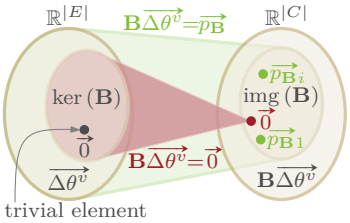

Figure 4.3: The image $\operatorname{img}(\mathbf{B})$ and kernel $\ker(\mathbf{B})$ of the circuit matrix $\mathbf{B}$ for the linear map $\mathbf{B}\colon \mathbb{R}^{|E|} \to \mathbb{R}^{|C|}$.

Using the rank-nullity theorem (see Theorem 4.1) we get the dimension of the kernel (nullity when talking about matrices) of $\dim(\ker(\mathbf{B})) = \dim(E) - \dim(\operatorname{img}(\mathbf{B})) = |E| - |E| + |V| - k = |V| - k$. However, Cederbaum [Ced55] showed that for a fundamental system of circuits—that is used in our case—the determinant can only take values of -1, 0, or 1 for every square submatrix and ± 1 for a set of chords that represents a maximal square matrix (see Figure 4.6a or b bottom right partition). As for the incidence matrix $\mathbf{I}$ above this means that the matrix $\mathbf{B}$ is TUM.

Lemma 4.4 (TUM bases)**.** *The incidence matrix* $\mathbf{I}$ *and the circuit matrix* $\mathbf{B}$ *are TUM bases.*

Relationship between Incidence and Circuit Matrix. We get the relationship between the incidence matrix $\mathbf{I}$ and the circuit matrix $\mathbf{B}$ in Equation 4.12.

$$\mathbf{I}\mathbf{B}^\intercal = \mathbf{0} \quad \text{and} \quad \mathbf{B}\mathbf{I}^\intercal = \mathbf{0}, \tag{4.12}$$

where $\mathbf{0}$ is a matrix with zeros only of dimension $|V| \times |C|$ (respectively $|C| \times |V|$). Thus, the incidence matrix $\mathbf{I}$ is orthogonal to the circuit matrix $\mathbf{B}$. One way to prove that is given by Seshu and Reed [SR61, p.66, Theorem 4-6] that uses the property of circuits that have a degree of $\deg(u) = 2$ at all vertices $u \in V$. Again note that both matrices $\mathbf{I}$ and $\mathbf{B}$ are orthogonal to each other (i. e., every vector of $\mathbf{I}$ is orthogonal to every vector in $\mathbf{B}$). Note that this also means that the vectors are linear independent to each other. By doing a vertex transformation, we are able to describe the voltage angle difference $\Delta\theta^v(u, w)$ vector by voltage angles $\theta^v(u)$ and $\theta^v(w)$ for all edges $(u, w) \in E$. However, this simple transformation is based on the connection

that $\mathbf{B}\overrightarrow{\Delta\theta^v} = \vec{0}$ and based on the relationship shown in Equation 4.12. The connection given in Equation 4.12 allows us to describe $\overrightarrow{\Delta\theta^v}$ by the linear combination of the tree branches $\overrightarrow{\Delta\theta^v} = \mathbf{I}^\intercal\overrightarrow{\theta^v}$ for each connected component (compare also Equations 3.31a and 4.13), where $\overrightarrow{\theta^v} \in \mathbb{R}^{|V|-k}$ with k representing the number of connected components [SR61, Theorem 6-6, p. 123]. This means, we can find $\mathbf{B}\overrightarrow{\Delta\theta^v} = \vec{0}$, which is equivalent of finding a $\mathbf{B}\mathbf{I}^\intercal\overrightarrow{\theta^v} = \vec{0}$. Since we know from Equation 4.12 that $\mathbf{B}\mathbf{I}^\intercal = \mathbf{0}$ this equation holds independent of the voltage angle vector $\overrightarrow{\theta^v}$. In addition, we would like to know when there is a $\overrightarrow{\theta^v} \in \mathbb{R}^{|V|}$ such that $\overrightarrow{\Delta\theta^v} = \mathbf{I}^\intercal\overrightarrow{\theta^v}$. The latter is equivalent to the question of when $\overrightarrow{\Delta\theta^v} \in \operatorname{img}(\mathbf{I}^\intercal)$. We have to show when $\ker(\mathbf{B}) \subseteq \operatorname{img}(\mathbf{I}^\intercal)$. This is the case when we chose the same spanning tree to construct both matrices. Note that it suffices to compute the voltage angle differences along a spanning tree, since the others result from these voltage angles.

KVL Flow. Applying the latter to Ohm's law gives us the typical equation known from literature (Equation 4.13).

$$b(u,w)\cdot\left(\theta^v(w)-\theta^v(u)\right) = f(u,w). \tag{4.13}$$

A flow f complying with Equation 4.13 is called *KVL flow* and if it complies with the capacity constraint it is called *feasible KVL flow*.

Using the aforementioned relationship (Equation 4.13), we can reformulate Equation 4.10 such that we replace voltage angle differences $\overrightarrow{\Delta\theta^v}$ by flows $\vec{f}$. Note that $b(u,w) = 1/x(u,w)$ and that "$\circ$" is the Schur product (or entrywise product).

$$\vec{f} = \vec{b}\circ\overrightarrow{\Delta\theta^v} \Leftrightarrow \quad \overrightarrow{\Delta\theta^v} = \vec{x}\circ\vec{f} \tag{4.14a}$$

$$\mathbf{B}\overrightarrow{\Delta\theta^v} = \vec{0} \quad \Leftrightarrow \underbrace{\left(\mathbf{B}\circ\left(\mathbb{1}^{|E|\times 1}\cdot\vec{x}^\intercal\right)\right)}_{=:\mathbf{B}'}\cdot\vec{f} = \vec{0} \tag{4.14b}$$

Since $\vec{x}$ is a vector of constant values, we just multiply the entries in the circuit matrix $\mathbf{B}$ by $\vec{x}$ resulting in a new circuit matrix $\mathbf{B}'$, which results in Equation 4.15.

$$\mathbf{B}'\cdot\vec{f} = \vec{0} \tag{4.15}$$

Feasible Electrical Flow. In the following, we define feasible electrical flows that represent solutions to DC FEAS.

Definition 4.5 (Feasible Electrical Flow)**.** *A KVL flow that is also a KCL flow is called* electrical flow *and if it complies to the capacity constraint, too, it is called a* feasible electrical flow.

DC FEAS and DC MPFP constitute a system of linear equations and an LP, respectively. In the following, we summarize the problem definitions of DC FEAS and MPFP.

Direct Current Feasibility Problem DC-FEAS($\mathcal{N}$)	
Instance:	An exact bounded network $\mathcal{N} = (G, V_G, V_D, \text{cap}, b, \underline{p_g}, \overline{p_g}, \underline{p_d}, \overline{p_d})$, i. e., $p_g \equiv \underline{p_g} \equiv \overline{p_g}$ and $p_d \equiv \underline{p_d} \equiv \overline{p_d}$.
Question:	Is there a feasible electrical flow f (see Equations 4.7, 4.9 and 4.10)?

A feasible electrical flow that maximizes the flow value $F(\mathcal{N}, f) \coloneqq \sum_{u \in V_G} f_{\text{net}}(u)$ is called MPFP($\mathcal{N}$) and its value is denoted by $\text{OPT}_{\text{MPFP}}(\mathcal{N})$. The optimization problem is stated in the following.

Direct Current Maximum Power Flow Problem DC-MPFP($\mathcal{N}$)	
Instance:	A network $\mathcal{N} = (G, V_G, V_D, \text{cap}, b, \underline{p_g}, \overline{p_g}, \underline{p_d}, \overline{p_d})$.
Objective:	Find a feasible electrical flow f (see Equations 4.7, 4.9 and 4.10) such that the flow value $F(\mathcal{N})$ is maximum among all choices of f.

Algorithms to Solve DC FEAS. Possibilities to get a feasible power flow are to formulate the system of linear equations or LP and run it using a solver such as Gurobi [Gur16], or to apply the following algorithm.

Lemma 4.6 (Shapiro [Sha87, p.36, Lemma 1])**.** *Let every edge of G have a resistance $r \equiv 1$. Let T denote the number of spanning trees and let $T(s, u \to w, t)$ be the number of spanning trees that contain the edge (u, w) in that particular direction meaning the spanning tree has a path from s to t that visits vertex u first and then vertex w by using the edge $(u, w) \in E$. Let $p_g \equiv p_d \equiv 1$ and let $f(u, w) = \left(T(s, u \to w, t) - T(s, w \to u, t)\right)/T$. Then f is a feasible electrical flow in G.*

The generalization—where we have no unit resistances r, but arbitrary ones—given by Shapiro [Sha87, p.38] was already given by Seshu and Reed [SR61, pp.155ff.]. Instead of just using the number of spanning trees, we calculate for each spanning tree the product of the admittances of the branches of that spanning tree and sum over all spanning trees. The proof of the lemma uses the Binet-Cauchy-Theorem [SR61, p.32]. Note that a graph can have exponentially many spanning trees and computing the flow for each edge using this techniques is quite inefficient, but provides an exponential time algorithm to compute the electrical flow of the power grid.

4.1.1 Properties of Electrical Flows

Note that we use a base for the columns of the incidence and circuit matrix denoted by $\mathbf{I}$ and $\mathbf{B}$, respectively, where all equations are linear independent. Since the whole system of equations has full rank the solution to a feasible electrical flow is unique, which we show in the following.

Lemma 4.7 (Uniqueness of DC Electrical Flows)**.** *There is a unique solution to* DC *electrical flows if we have exact bounds.*

Proof. Recall that the incidence matrix $\mathbf{I}$ with $\mathbf{I} \in \mathbb{R}^{(|V|-k)\times|E|}$ and the circuit matrix $\mathbf{B}$ with $\mathbf{B} \in \mathbb{R}^{(|E|-|V|+k)\times|E|}$ are bases. Since both matrices are bases the vectors are linear independent in each matrix (i. e., this is a property of a base shown in Equations 4.4 and 4.10). We now define a matrix $\mathbf{A}$ by $\mathbf{A} \coloneqq \binom{\mathbf{I}}{\mathbf{B}'}$ with $\mathbf{B}'$ from Equation 4.15, where $\mathbf{A} \in \mathbb{R}^{|E|\times|E|}$ can be generalized to a linear map $\mathbf{A}\colon \mathbb{R}^{|E|} \to \mathbb{R}^{|E|}$ with $\vec{f} \mapsto \mathbf{A}\cdot\vec{f}$. Thus, the system of equations is defined by $\mathbf{A}\cdot\vec{f} = \vec{p_\mathbf{A}} \coloneqq \binom{\vec{p_\mathbf{I}}}{\vec{0}}$ with vector $\vec{0}$ of size $|C|$. The kernel $\ker(\mathbf{A})$ and the image $\operatorname{img}(\mathbf{A})$ of matrix $\mathbf{A}$ are defined in Equation 4.16.

$$\ker(\mathbf{A}) \coloneqq \{\vec{f} \in \mathbb{R}^{|E|} \mid \mathbf{A}\cdot\vec{f} = \vec{0}\} \subseteq \mathbb{R}^{|E|} \tag{4.16a}$$

$$\operatorname{img}(\mathbf{A}) \coloneqq \{\vec{p_\mathbf{A}} \in \mathbb{R}^{|E|} \mid \exists\vec{f} \in \mathbb{R}^{|E|}\colon \mathbf{A}\cdot\vec{f} = \vec{p_\mathbf{A}}\} \subseteq \mathbb{R}^{|E|} \tag{4.16b}$$

From Equation 4.12, we know that $\mathbf{I}\mathbf{B}^\intercal = \mathbf{0}$ and $\mathbf{B}\mathbf{I}^\intercal = \mathbf{0}$, which means that the dimension of the image of $\mathbf{A}$ is the sum of the dimension of the images of the incidence matrix $\mathbf{I}$ and circuit matrix $\mathbf{B}$ given by $\dim(\operatorname{img}(\mathbf{A})) = \dim(\operatorname{img}(\mathbf{I})) + \dim(\operatorname{img}(\mathbf{B})) = |V|-k+|E|-|V|+k = |E|$. Using the rank-nullity theorem (see Theorem 4.1), we know that the dimension of the kernel is $\dim(\ker(\mathbf{A})) = 0$. Thus, $\mathbf{A}$ as linear map is injective. The dimension of the image of $\mathbf{A}$ is $|E|$, which means that the matrix has full rank. We conclude that the system has a unique non-trivial solution (see Figure 4.4). □

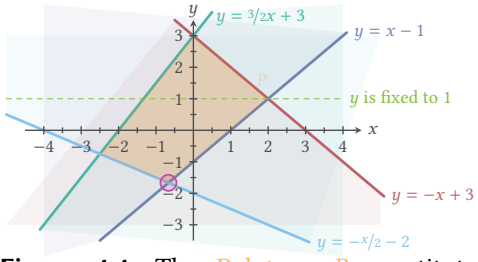

Figure 4.4: The Polytope P constituted by $y \leq 3/2x + 3$, $y \geq x - 1$, $y \leq -x + 3$, and $y \geq -x/2 - 2$. If $y = 1$, we reduce the solution space to $x \in [-4/3, 2]$. However, if $y = -5/3$ the solution is unique $x = -2/3$. So a unique solution corresponds to one point ○.

Note that the system has no non-trivial solution if the generations and demands are exact and the capacities are chosen in such a way that these generations and demands cannot be fulfilled. In the following, we extend the system by capacity constraints discussed in Equation 4.9.

The capacity constraint can be reformulated in a matrix writing by $\mathbb{1}^{|E|\times|E|}\cdot\vec{f} \leq \overrightarrow{\text{cap}}$, where $\mathbb{1}^{|E|\times|E|}$ is the identity matrix of size $|E| \times |E|$ and the vector of capacities is $\overrightarrow{\text{cap}} \in \mathbb{R}^{|E|}$. With the

capacity constraint we get a matrix $\mathbf{A}' = (\mathbf{I}, \mathbf{B}', \mathbb{1}^{|E|\times|E|})^\top$ of size $\mathbf{A}' \in \mathbb{R}^{(2|E|)\times|E|}$ with $\mathbf{B}'$ from Equation 4.15. Note that the additional submatrix has no influence on the dimension of the image meaning $\dim(\text{img}(\mathbf{A}')) = |E|$, i. e., using the rank-nullity-theorem (Theorem 4.1), we get the dimension of the kernel $\dim(\ker(\mathbf{A})) = 0$. The matrix remains to have a full rank, but we have inequality constraints. With exact supplies (i. e., $p_g \equiv \underline{p_g} \equiv \overline{p_g}$) and exact demands (i. e., $p_d \equiv \underline{p_d} \equiv \overline{p_d}$) the capacity constraints have only influence on the feasibility of a solution, since $\mathbf{A} \cdot \vec{f} = \vec{p_\mathrm{A}}$ gives us a unique solution the inequality $\mathbb{1}^{|E|\times|E|} \cdot \vec{f} \leq \vec{\text{cap}}$ might lead to a polytope that does not include that solution.

If we apply upper bounds $\overrightarrow{p_{\mathrm{A}\uparrow}}$ with $\overline{p_g}, \overline{p_d} \in \mathbb{R}_{\geq 0}$, and lower bounds $\overrightarrow{p_{\mathrm{A}\downarrow}}$ with $\underline{p_g}, \underline{p_d} \in \mathbb{R}_{\geq 0}$ for the generations and demands, we get the following system of inequalities.

$$\mathbf{A} \cdot \vec{f} \leq \overrightarrow{p_{\mathrm{A}\uparrow}} \tag{4.17a}$$

$$-\mathbf{A} \cdot \vec{f} \leq -\overrightarrow{p_{\mathrm{A}\downarrow}} \tag{4.17b}$$

Without capacities, if we set the bound for each $\vec{p_\mathrm{A}}$ between $\overrightarrow{p_{\mathrm{A}\uparrow}}$ and $\overrightarrow{p_{\mathrm{A}\downarrow}}$ (see Equation 4.17) to exact, we would get a unique solution. Otherwise, this set of solution can be represented by a polytope that is no longer just a point, but defined by the faces H_i that build a convex hull. However, while maximized, we can simply use the upper bound vector $\overrightarrow{p_{\mathrm{A}\uparrow}}$. Thus, the solution for the MPFP is still unique. Note that this is no longer true when we add capacity constraints.

Lemma 4.8 (Uniqueness of MPFP)**.** *There is a unique solution to (feasible)* DC *electrical flows, when maximized as long as there are no capacity constraints.*

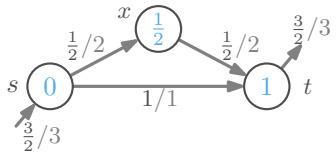

Figure 4.5: A TUM counter example with three vertices with voltage angles θ^v that are written in the vertices, flows f and capacities cap are written on the edges f/cap. This example shows that flows are not necessarily integral, since the edges $(s, x), (x, t) \in E$ have each a flow of $1/2$.

Another application, where the rank of the matrix can be used is to check whether a network with a given set of sensors is observable (i. e., all other variables can be calculated by the measured ones). Kalman [Kal59, p.487, (47)] uses the property that if a set of vectors is linear independent then the system becomes observable. Note that another way to prove the uniqueness was given by Verma [Ver10, p.114, Lemma 4.2.1] and Rockafellar [Roc84, p.361].
A system of linear inequalities represents a convex polytope $P = \{\vec{f} \in \mathbb{R}^{|E|} \mid \mathbf{A}\vec{f} \leq \vec{p_\mathrm{A}}\}$. Let H_i be a hyperplane defined by $H_i := \{\vec{f} \in \mathbb{R}^{|E|} \mid \mathbf{A}_i \cdot \vec{f} = \vec{p_{\mathrm{A}i}}\}$ that represents the i^{th} row with $1 \leq i \leq |E|$. The cuts of a convex polytope P with each hyperplane H_i is given by $\{P \cap H_i \mid 1 \leq i \leq |E|\}$ and represents the set of faces that form a *convex hull*.

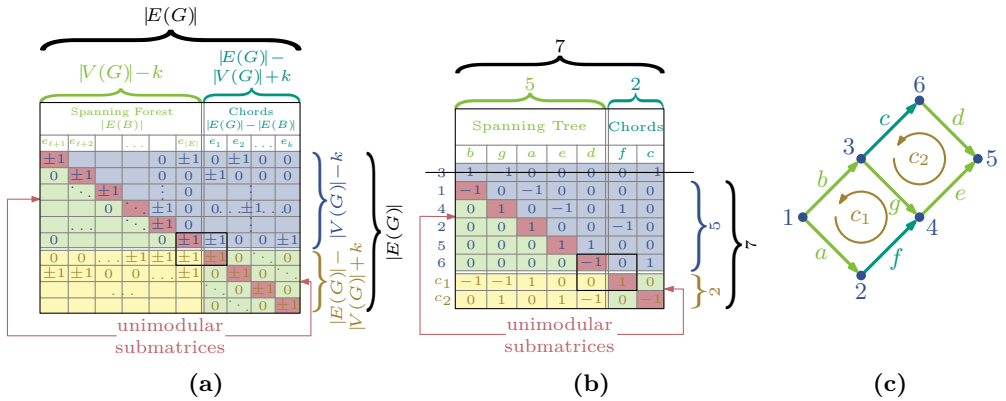

Figure 4.6: The structure of the matrix $\mathbf{A} \coloneqq \binom{\mathbf{I}}{\mathbf{B}}$ that is a construction of the incidence matrix $\mathbf{I}$ (top partition) and circuit matrix $\mathbf{B}$ (bottom partition). The left partition of size $|V| - k$, with k being the number of connected components (for (b) and (c) with one connected component $k = 1$), represents some spanning forest (for $k = 1$ a spanning tree) of the graph G. The right partition represents the edges that are not in the spanning forest of the left partition (also called chords). The latter partition has a size of $|E| - |V| + k$. The green areas have entries that are all zero and the main diagonal with entries all ± 1 is marked in red. The general structure is given in (a) and a small example is given in (b) with the corresponding graph in (c).

Consider any objective then an optimal solution of a convex polytope P is on the vertices of P. Thus, if the vertices of a convex polytope P lie on integral coordinates than P is called an *integral polytope*. If all square submatrices of $\mathbf{A}$ have a determinant of -1, 0, or 1 then $\mathbf{A}$ is TUM. This in particular means that the polytope of such a TUM matrix is integral independent on the vector $\overrightarrow{p_{\mathbf{A}}}$.

Recall that we know that the incidence matrix $\mathbf{I}$ and circuit matrix $\mathbf{B}$ are each TUM by itself (see Lemma 4.4). In the following, we prove that the whole system $\mathbf{A} \coloneqq \binom{\mathbf{I}}{\mathbf{B}}$ is not TUM and thus, the convex polytope is not necessarily integral.

Lemma 4.9. *The bases of the incidence matrix* $\mathbf{I}$ *and the circuit matrix* $\mathbf{B}$ *are each TUM. However, the whole system of linear equations* $\mathbf{A} \coloneqq \binom{\mathbf{I}}{\mathbf{B}}$ *to compute a feasible electrical flow using the KCL (Equation 4.7) and KVL (Equation 4.10) is not TUM.*

Proof. A counter example is shown in Figure 4.5 that basically describes why a feasible electrical flow f is not integral for every right hand-side vector $\overrightarrow{p_{\mathbf{A}}}$. □

The KCL (see Equation 4.7) and the KVL (see Equation 4.10) do not incorporate network elements in any sense—i. e., these equations are purely topological [SR61, p.127, Section 6-3]—the vector of voltage angle differences $\overrightarrow{\Delta\theta^v}$ can be replaced by the flow vector $\overrightarrow{f}$.

Let T be a spanning tree in G. The matrix $\mathbf{A} \coloneqq \begin{pmatrix} \mathbf{I}_{E(T)} & \mathbf{I}_{E(G)\setminus E(T)} \\ \mathbf{B}_{E(T)} & \mathbf{B}_{E(G)\setminus E(T)} \end{pmatrix}$ can be decomposed into two parts column-wise represented by the partitions that are the set $E(T)$ of spanning tree edges (see Figure 4.6a left top and bottom partition) and the set $E(G)\setminus E(T)$ of chords (see Figure 4.6a right top and bottom partitions) for some arbitrary but fixed spanning tree T. The partition of the rows into two parts is given by construction $\mathbf{A} = \binom{\mathbf{I}}{\mathbf{B}}$. Recall that all maximum square non-singular submatrices (i. e., matrices that have a nonzero determinant) of the incidence matrices $\mathbf{I}$ of size $(|V|-1)\times(|V|-1)$ are formed by some spanning tree $T \in \mathcal{T}$ and submatrices of the circuit matrix $\mathbf{B}$ of size $(|E|-|V|+1)\times(|E|-|V|+1)$ that are formed by a set of chords, are unimodular (i. e., the determinant is ± 1; see Figure 4.6 top left and bottom right partition, respectively). The structure allows us to permute the entries such that the main diagonal has only ± 1 entries (see Figure 4.6a and b for example). We describe in the following how we permute the matrix $\mathbf{A}$.

We can order the rows and columns of the incidence matrix $\mathbf{I}$ that are in the spanning tree partition (see Figure 4.6a and b top left partition) such that entries below the diagonal are all zero in that partition. This particular form of a matrix is denoted by the term *upper triangular matrix*. A property of the incidence matrix $\mathbf{I}$ is that it has at most two non-zero entries per column. In addition, the number of leaves $\mathcal{L} \coloneqq \{u \in V \mid \deg(u) = 1\}$ in a spanning tree depend on the degree of the vertices meaning $|\mathcal{L}| \geq \max_{u\in V} \deg(u)$, which means that there is always enough space to the right of the diagonal. To construct an upper triangular matrix in $\mathbf{A}$ (see Figure 4.6a), we perform a breadth-first search (BFS). The BFS processes the inner vertices of the spanning tree first and at the end all leaves. Using the aforementioned observation of the number of leaves, we know that there is always enough space to the right of the main diagonal. For the chord partition of the circuit matrix $\mathbf{B}$, we are always able to adjust the entries such that the lower and upper triangle of the matrix have zero entries only (Figure 4.6a and b; bottom right partition). We describe the BFS in the following.

Let T be an arbitrary but fixed spanning tree and let $\mathbf{B}$ be the base of the columns of the circuit matrix constructed from spanning tree T. We start at some vertex $u \in V(G)$ (see Figure 4.6c vertex 3) and process its incident edges $\{u, v\} \in \overleftrightarrow{E}(T)$. We add the columns of the incident edges to an empty matrix $\mathbf{A}'$ and the adjacent vertices $v \in V(G)$ as row. We proceed the aforementioned procedure with the next row's vertex v. Afterwards, we add the cycles $c \in C$ that are in the circuit matrix base $\mathbf{B}$. Since each cycle in the base contributes one nonzero chord entry, we add for each cycle the corresponding chord column $\overleftrightarrow{e} \in \overleftrightarrow{E}(G) \setminus \overleftrightarrow{E}(T)$. The resulting matrix is of the form $\mathbf{A}' \coloneqq \begin{pmatrix} \mathbf{I}_{E(T)} & \mathbf{I}_{E(G)\setminus E(T)} \\ \mathbf{B}_{E(T)} & \mathbf{B}_{E(G)\setminus E(T)} \end{pmatrix}$. We can conclude this discussion with the following lemma.

Lemma 4.10. *Let* $\mathbf{A} = \binom{\mathbf{I}}{\mathbf{B}}$ *be the matrix formed by the incidence matrix* **I** *and circuit matrix* **B**. *The matrix's columns and rows can be permuted such that we get the form shown in Figure 4.6a.*

To investigate the TUM property, we take a look at the intersections of the matrix **A** that are represented by all four partitions (see Figure 4.6a). Thus, we distinguish between the following three main cases.

Case 1**:** The intersection between the chord and spanning tree partition of
  (a) the incidence matrix **I** (Figure 4.6a & b; top left and top right partition),
  (b) the circuit matrix **B** (Figure 4.6a & b; bottom left and bottom right partition).

Case 2**:** The intersection between the incidence matrix **I** and the circuit matrix **B** of
  (a) the spanning tree partition (Figure 4.6a & b; top left and bottom left partition),
  (b) the chord partition (Figure 4.6a & b; top right and bottom right partition).

Case 3**:** The intersection of all four partitions.

Since each matrix is TUM by itself Case 1 is unproblematic (see Lemma 4.4). In Case 2, we are already able to find a square submatrix with determinant unequal ± 1 or 0 (see Figure 4.6b row 5 columns e and d). In Case 3 it is also possible to construct a graph such that there is a submatrix, where the determinant is 2 (see the example in Figure 4.6a and b). Inverting the direction of all cycles or edges has no influences on the determinant. Same holds for Case 2. Note that inverting the direction of the edges does not help, since the direction changes in the incidence and circuit matrix and thus, it only changes the sign of the determinant.

Assume that a flow is a function $f : E \to \mathbb{Z}$ that is an integral flow, we get a system of integral equations (IE). Such integral systems of equations or ILPs are usually a hint that the underlying problem is NP-hard [GJ79, p.245, MP1]. A relaxation of the function f (i. e., mapping to $\mathbb{R}$ instead of $\mathbb{Z}$) does not necessarily yield an integral solution, since the polytope vertices do not lie on integral coordinates (see Lemma 4.9).

Thus, with this technique we are not able to solve the problem by Felsner [Fel13, pp.17ff., Theorem 4.1] in polynomial time. However, in Section 4.1.2 we see a technique that leads to an integral electrical flow. Another possibility would be to restrict the algorithm in Section 4.5 to integral flows only.

4.1.2 Scalability of Electrical Flows

As already mentioned by Goldberg and Tarjan [GT89, p.114] a lot of flow algorithms use scaling techniques. Whether it is the scaling of the capacity—introduced by Edmonds and Karp [EK72]—or the scaling of the excess that was introduced by Ahuja and Orlin [AO89]. For electrical flows, we will use scaling, too. The following scaling lemma follows directly from Equations 4.1–4.3 and 4.13.

Lemma 4.11 (Scaling). *Every non-zero electrical flow $f' \colon E \to \mathbb{R}_{>0}$ can be rescaled to a feasible electrical flow f by applying a scaling factor χ, where*

$$\underline{\chi} := \max\left(\max_{u \in V_D} \frac{\underline{p_d}(u)}{p_d(u)}, \max_{u \in V_G} \frac{\underline{p_g}(u)}{p_g(u)}, \right) \leq \chi \leq \min\left(\min_{e' \in E} \frac{\mathrm{cap}(e')}{f'(e')}, \min_{u \in V_D} \frac{\overline{p_d}(u)}{p_d(u)}, \min_{u \in V_G} \frac{\overline{p_g}(u)}{p_g(u)}\right) =: \overline{\chi}$$

to $f(e) = f'(e) \cdot \chi$ for all $e \in E$.

Proof. Assume $\vec{f}'$ is an electrical flow complying Equations 4.7 and 4.10 or alternatively Equations 4.1–4.3 and 4.13. Multiplying $\vec{f}'$ by a scalar χ yields in a flow $\chi \cdot \vec{f}' = \vec{f}$ that is still an electrical flow, since it is only a scaling of an unrestricted vector. The latter means that multiplying Equations 4.7 and 4.10 (assuming $\Delta\theta^v \equiv f$) by a scalar (standard operation on a field) yields in a magnitude increase of all vectors including $\vec{f}$. However, to scale an electrical flow to a feasible electrical flow the flow has to comply with the capacity constraints (Equation 4.9).

For $\chi \leq \overline{\chi}$ we have

$$\begin{aligned} f(e) &= \chi \cdot f'(e) \\ &\leq \overline{\chi} \cdot f'(e) \\ &= \min_{e' \in E} \frac{\mathrm{cap}(e')}{f'(e')} \cdot f'(e) \\ &\leq \frac{\mathrm{cap}(e)}{f'(e)} \cdot f'(e) \\ &= \mathrm{cap}(e). \end{aligned}$$

Note that we included the maximum generation and demand $p_g = \chi \cdot {p_g}'(u) \leq \overline{\chi} \cdot {p_g}'(u) = \min_{u \in V_G} {}^{\overline{p_g}(u)}/_{{p_g}'(u)} \cdot {p_g}'(u) = \overline{p_g}(u)$. □

Note that the last lemma would be much simpler if we make the bounded network to an unbounded network. For this we will use Lemma 5.3 on Page 118 (see also Figure 5.5).

Lemma 4.12 (Scaling Restatement). *Let $\mathcal{N} = (G, V_G, V_D, \mathrm{cap}, b, \underline{p_g}, \overline{p_g}, \underline{p_d}, \overline{p_d})$ be a power grid with minimum and maximum generations and demands. We model the upper and lower bounds of the generations and demands in the same fashion as in Lemma 5.3 (Figure 5.5 on page 117) as lower and upper capacities. The edge capacities are $\underline{\mathrm{cap}} \equiv 0$ and $\overline{\mathrm{cap}} \equiv \mathrm{cap}$. Every non-zero electrical flow $f' \colon E \to \mathbb{R}_{>0}$ can be rescaled to a feasible electrical flow f by applying a scaling factor χ, where*

$$\underline{\chi} := \max_{e' \in \overleftarrow{E}} \frac{\underline{\mathrm{cap}}(e')}{f'(e')} \leq \chi \leq \min_{e' \in \overrightarrow{E}} \frac{\overline{\mathrm{cap}}(e')}{f'(e')} =: \overline{\chi}$$

to $f(e) = f'(e) \cdot \chi$ for all $e \in E$.

We can use the latter two results to up scale or down scale electrical flows. An s-t-network is a network with one generator $\{s\} =: V_G$ (i. e., $|V_G| = 1$) and one consumer $\{t\} =: V_D$ (i. e., $|V_D| = 1$). Since there is a unique solution to a feasible electrical flow f (see Lemma 4.7) and we can rescale every electrical flow by a factor χ (Lemma 4.12), we chose an edge with the maximum violation of the capacity constraint, compute the factor $\overline{\chi}$, and scale the flow on all edges in the network down according to $\overline{\chi}$. The next lemma follows directly from Lemma 4.12, since $\overline{\chi}$ is the largest possible scaling such that $\vec{f}$ yields a feasible electrical flow. This flow represents the maximum possible feasible electrical flow for an s-t-network that is equivalent to a DC maximum power flow (DC MPF). Note that for s-t-networks there is only one controllable generator that means the MPF is unique, too.

Lemma 4.13. *For an s-t-network $\mathcal{N}$ any non-zero electrical flow $f' : E \to \mathbb{R}_{>0}$ can be rescaled to an* MPF *by using a scaling factor of $\overline{\chi}$ (see Lemma 4.12).*

Note that for multiple generators the MPF is not necessarily unique, since different real power generations p_g can lead to the same optimal value $\mathrm{OPT}_{\mathsf{MPFP}}(\mathcal{N})$.

4.1.3 Integral Electrical Flows

In general, we can assume that the parameters of a DC power grid $\mathcal{N}$, such as the susceptance b, are rational $\mathbb{Q}$ and thus, the equations constitute a rational polytope, since the cuts of the hyperplanes can only constitute rational numbers (see Definition 4.14).

Definition 4.14 (Rational Polytope; Schrijver [Sch03, p.61])**.** *A system of linear inequalities of the form $\{\vec{f} \in \mathbb{R}^m \mid \mathbf{A}\vec{f} \leq \vec{p_{\mathrm{A}}}\}$, where $\mathbf{A} \in \mathbb{Q}^{n \times m}$ and $\vec{p_{\mathrm{A}}} \in \mathbb{Q}^n$, is called a* rational system of linear inequalities. *A rational system of linear inequalities constitutes a rational polytope. The latter means that all vertices of the polytope lie on rational coordinates. Such a rational polytope represents the convex hull of a finite set of rational vectors.*

Naturally, feasible electrical flows are not integral (see Lemma 4.9), which means that feasible electrical flows are not integral for every right-hand side vector $\vec{p_{\mathrm{A}}}$. Let f be a feasible electrical flow. If we neglect the capacity constraints (see Equation 4.9; or equivalently define cap $\equiv \infty$) and relax the generation and demand constraints. Assuming that the flow $f \in \mathbb{Q}$ then we can rescale the flow to an integral flow using the least common multiplier (LCM) and the technique presented in Lemma 4.12.

Theorem 4.15 (Integral Electrical Flow)**.** *If there is a (nonzero) solution to an electrical flow f with $f \in \mathbb{Q}$ then there is a nonzero integral electrical flow that can be reached by scaling.*

Unfortunately, the scaling to integral electrical flows (Theorem 4.15) does not answer the question of the worst case size of integral electrical flows. This highly depends on the right-hand side vector.

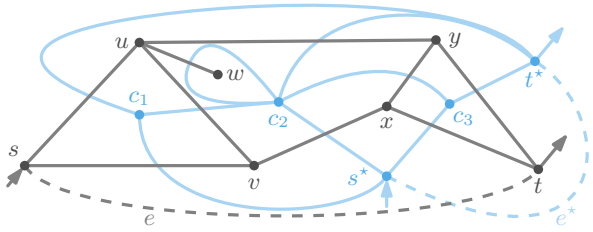

Figure 4.7: A plane single-source s and single-sink t graph G (dark gray vertices ● and edges) and its combinatorial dual graph $G^\star$ (cyan blue vertices ● and edges). Adding the edge e (dark gray dashed line) divides the outer face into two faces representing the faces that include the dual source $s^\star$ and dual sink $t^\star$ of the dual graph. Note that since we have a one-to-one correspondence of the edges, adding the edge e in G is symmetrical to adding the edge $e^\star$ in $G^\star$.

4.1.4 Planar Graphs

We will focus on planar graph in this chapter, which we will introduce in this section. Cain ET AL. [COC12, p.13] mention that power grids are planar. A graph is called *planar* if it can be embedded into the plane without any edge crossings, i. e., the edges have no common point, but the two vertices representing the endpoints of an edge. However, note that there is usually more than one embedding for a graph G that is planar. Thus, let us assume a fixed *planar embedding* $\mathcal{E}$ of a graph G into the plane with $G(\mathcal{E}) \cong G$ (i. e., $G(\mathcal{E})$ is isomorphic to G) and an injective function $\mu_\mathcal{E} : V \to \mathbb{R}\times\mathbb{R}$ meaning there is a correspondence between the vertices V of the graph and the geometrical points $\mathcal{P}$ of the plane embedding. An edge set $E(G)$ of $G(\mathcal{E})$ is a subset of a topological space $\mathcal{T}$, where each edge in $G(\mathcal{E})$ is a Jordan curve in $\mathcal{T}$ and the incidences and adjacencies are defined accordingly [GT01].

For power grids such an embedding is usually given by the geographical location of the network components, where $\mathcal{P}$ represents the locations of the buses in terms of latitude and longitude. In addition, we assume a network $\mathcal{N} = (G, V_G, V_D, \text{cap}, b, \underline{p_g}, \overline{p_g}, \underline{p_d}, \overline{p_d})$ with $|V_G| = 1$ and $|V_D| = 1$. The vertices that represent the single generator and single demand are denoted by source s and sink t, respectively.

For plane graphs, we have the concept of duality, which we will link with the results of duality given in Section 4.1.5. The geometric dual of a plane *primal graph* G is called the *dual graph* $G^\star$. An example is given in Figure 4.7. To construct a dual graph, we introduce the concept of a *face*. We denote faces by c. An *inner face* is a region that is bounded by edges and vertices in graph G. We say that these edges are incident to the face. The *outer face* is the unbounded region (see Figure 4.7 face c_t). The dual graph $G^\star$ is constructed by introducing a vertex for each face and connecting two vertices if the faces have an edge in common. Note that we introduce an edge in the

dual graph $G^\star$ for each edge in the primal graph G. Note that a face might represent more than just a cycle, e. g., if vertex w in Figure 4.7 is a graph itself.

4.1.5 Matroids and Independence Systems

A lot of model transformations, properties, and relationships that we use in the following with regard to matroids (see the postulates of Whitney [Whi35, p.510, Theorem 1]) are based on the discussion by Seshu and Reed [SR61] and Whitney [Whi31, Whi35]. A matroid [Whi35] represents a generalization of a graph [Whi31]. A *matroid* is an abstraction of the independence term that is used in different fields such as graph theory and geometry. Though different matroids are considered in different fields, the consensus stays the same. We recall the definition of a *matroid* by Korte and Vygen [KV00, pp.279] (first version was given by Whitney [Whi35, p.510]). A *matroid* is an ordered pair $(U, \mathcal{I})$, where U is the universe and $\mathcal{I} \subseteq \mathcal{P}(U)$ is an *independence system*, which satisfies the following three axioms.

Axiom 1. $\emptyset \in \mathcal{I}$ (neutral element).

Axiom 2. If $I \in \mathcal{I}$ and $I' \subseteq I$ then $I' \in \mathcal{I}$ (monotonicity).

Axiom 3. If $I_1, I_2 \in \mathcal{I}$ with $|I_1| < |I_2|$ then there is an $e \in (I_2 \setminus I_1)$ such that $I_1 \cup \{e\} \in \mathcal{I}$ (augmentation).

Note that the Axiom 1 and Axiom 2 represent axioms that also hold for any independence system. However, the Axiom 3 makes it a matroid that is a generalization of the term linear independence. Whitney [Whi35] defines a *base* as a maximal independent submatroid and a *cycle* as a minimal dependent submatroid.

Definition 4.16 (Whitney [Whi35, p.509])**.** *A subgraph of a graph is independent if it contains no cycles.*

In this work, we use an important mathematical principle called *duality*. In different research areas it has different meanings. However, for us it basically means that if there is a bijection between the edges (i. e., columns) in $\mathbf{I}$ and the edges in $\mathbf{B}$ and for a submatroid $\mathbf{I}'$ of $\mathbf{I}$ and the corresponding dual $\mathbf{B}'$ in $\mathbf{B}$, we have the relationship $\operatorname{rk}(\mathbf{B}') = \operatorname{rk}(\mathbf{B}) - n(\mathbf{I}')$, then $\mathbf{I}$ is a dual of $\mathbf{B}$ and $\mathbf{B}$ is a dual of $\mathbf{I}$ [Whi35, pp.521ff.]. The latter is called *involution* implying that the dual of the dual of $\mathbf{I}$ is $\mathbf{I}$ itself. Though "every matroid has a dual" [Whi35, p.522, Theorem 22] the concept applies from a graph-theoretical perspective to plane graphs only. Only plane graphs have a dual graph.

The following theorems state very central results that are used in this work.

Theorem 4.17 (Whitney [Whi35, p.527, Theorem 31])**.** *For any graph G the matroids corresponding to its incidence matrix $\mathbf{I}$ and its circuit matrix $\mathbf{B}$ are duals.*

For graphs we restricted the duality to plane graphs, since there is only a dual graph if the primal graph is planar. For matroids this restriction does not hold and thus, if we do not restrict ourself to the plane (i. e., sphere with genus 0) but other surfaces with genus greater 0, we can still embed a non-planar graph on a more complex surface without any crossing by making use of the holes. An example is the embedding of the K_5 on a torus (i. e., surface of genus 1). Note that we focus on planar graph and genus 0.

The aforementioned duality (see Theorem 4.17) applies to the matroids $\mathbf{I}$ and $\mathbf{B}$. The next theorem follows from Axiom 2 and the aforementioned discussion of the incidence matrix.

Theorem 4.18 (Whitney [Whi35, p.510, Theorem 1])**.** *A set $\mathbf{I}' \subseteq \mathbf{I}$ is independent if and only if it is contained in a base, or, if and only if it contains no cycles.*

The next lemma follows from Theorem 4.17 and is illustrated in Figure 4.7.

Lemma 4.19 (Seshu and Reed [SR61, p.85, Corollary 4-24])**.** *If G_1 and G_2 are dual graphs, the incidence matrix of either graph is a circuit matrix of the other (with the proper rank, and each row representing a cycle); that is*

$$\mathbf{I}_1 = \mathbf{B}_2 \text{ and } \mathbf{I}_2 = \mathbf{B}_1.$$

The lemma concludes the duality and is extensively used in this chapter (see Sections 4.3.2 and 4.5).

4.2 Electrical Preserving Transformations

In this section, we introduce some standard reduction rules used in literature that lead in the end to an algorithm to solve the DC FEAS. Most transformations make use of the superposition principle for linear power grids, e. g., the Δ-Y- and Y-Δ-transformations. The superposition principle holds (i. e., used for the superposition of, e. g., forces), since the constraint matrix $\mathbf{A}$ is a linear map and thus, superposition becomes a simple addition of linear equations (i. e., standard operation in a field $\mathbb{F}$). Though we give rules to compute the capacity cap, these formulas can be dependent on the actual flow (see Reduction Rule 4.26). Computing any electrical flow becomes trivial if we contract the graph to one edge since on trees the electrical flow is equivalent to a graph-theoretical flow [Lei+15a][LGH15, p.9, Lemma 4].

Recall that we have a unique electrical flow in s-t-graphs (see Lemma 4.7), we can scale it to a multiple such that it complies with the capacity constrains (Equation 4.9). Thus, we are able to neglect the capacity constraints and rescale the electrical flow

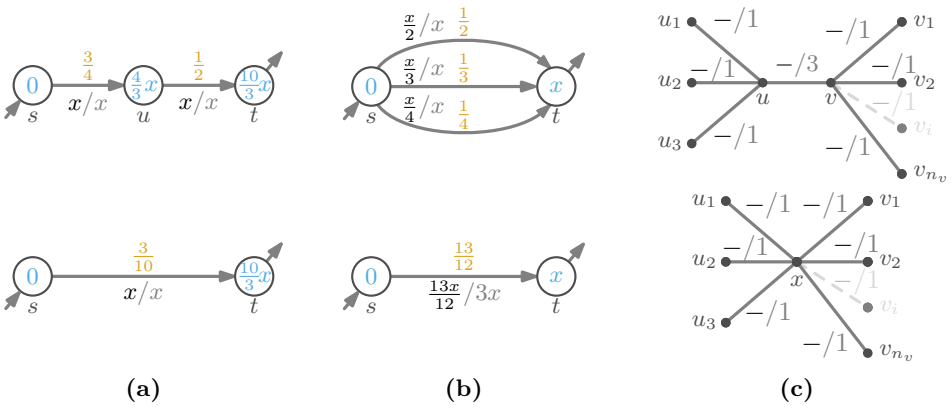

Figure 4.8: Three example graphs in which we label each vertex $u \in V$ that is represented by a cycle ○ with a voltage angle $\theta^v(u)$. If the voltage angles are not important, we just use standard bullets ●. On the edges, we write the flow f and the edge's capacity cap in the form f/cap. If the susceptance b is important for the transformation, we write it on the edge. The series-parallel-contraction and contraction of superfluous edges in energy networks simplifies the graph structure. (a) In a series-contraction a path is contracted to a single edge. (b) In a parallel-contraction multiple parallel edges (multi-edges) are contracted to one edge. (c) A scenario where shortening of superfluous edges (Reduction Rule 4.25) is reasonable. This figure is adapted from [Ake60, p.313, Figure 4]. The upper figure is an example, where the capacity of edge $\text{cap}(u,v) \geq \min\left(\sum_{\{u_i,u\}\in E} \text{cap}(u_i,u), \sum_{\{v_i,v\}\in E} \text{cap}(v_i,v)\right)$. In the bottom figure the resulting graph after contracting the superfluous edge $\{u,v\}$ to a vertex x is shown.

afterwards such that the capacity constraints are fulfilled using Lemma 4.13. From the Equations 4.1–4.3 and 4.13, we have only one component that has a crucial influence on the electrical flow and that is the susceptance b. The susceptance represents a ratio that can be interpreted as how many electrons go through a path. Thus, the notion of electrical preserving is purely susceptance based.

Definition 4.20 (Electrical Preserving Transformation)**.** *Let f be a given flow and let $\theta^v(u)$ be the voltage angles before the transformation for all $u \in V(G)$ with regard to f. An electrical preserving transformation $\mathcal{T}$ on $\mathcal{N}$ is a function $\mathcal{T}\colon \mathcal{M}(\mathcal{N}) \to \mathcal{M}(\mathcal{N})$ with $(G = (V, \overleftrightarrow{E}), b) \mapsto (G' = (V', \overleftrightarrow{E}'), b')$ and new voltage angle assignments $\theta^v{}'(u)$ for all $u \in V'$ such that the susceptances are transformed in such a way that for the flow f we have $\theta^v{}'(u) = \theta^v(u)$ for all vertices $u \in (V \cap V')$.*

Transformation rules are useful to simplify the network and compute network parameter more efficiently. Examples are the effective values, e. g., effective resistance, conductance/susceptance, the "effect of earth admittances on the balance of a Wheatstone bridge and earth capacity effects in AC" [But21, Ros24], and the effective unbalanced capacity [Ros24, p.916].

For edges that operate in series—meaning they represent a path—where there is no generator or demand vertex in between, we know that the flow f on each edge along the path is the same. Lets assume a path with two edges $\{u,v\},\{v,w\} \in \overleftrightarrow{E}$. Since all mappings are linear and we work on a field $\mathbb{F}$ (i. e., here it is $\mathbb{R}$), we get the following relationship $\left(\Delta\theta^v{}_1(u,v)+\Delta\theta^v{}_2(v,w)\right)/f = 1/b_1(u,v) + 1/b_2(v,w) = 1/b(u,w)$ with $f(u,v) = f(v,w) = f$, which we will generalize in the following rule.

Reduction Rule 4.21 (Series Contraction)**.** *Let $\pi(u,w)$ be a simple terminal-free path (i. e., for internal vertices of the path holds that $v \in V \setminus (\{u,w\} \cup V_G \cup V_D)$) whose internal vertices $v \in \pi(u,w)$ with $v \neq u,w$ have degree $\deg(v) = 2$. Then, such a path $\pi(s,t) \coloneqq ((s,u_1),(u_1,u_2),\dots,(u_i,t))$ is equivalent to one edge (s,t) (see Figure 4.8a) with the susceptance, voltage angle difference, and capacity being*

$$b(u,w) = \left(\sum_{e\in\pi(u,w)} b(e)^{-1}\right)^{-1}, \tag{4.18a}$$

$$\Delta\theta^v(u,w) = \frac{\min_{e\in\pi(u,w)} \operatorname{cap}(e)}{b(u,w)}, \tag{4.18b}$$

$$\operatorname{cap}(u,w) = b(u,w)\cdot\Delta\theta^v(u,w), \tag{4.18c}$$

respectively.

For multiple parallel edges between two vertices $u,v \in V(G)$, we can make the observation that the voltage angles $\theta^v(u)$ and $\theta^v(v)$ are the same for each edge. Thus, the voltage angle difference $\Delta\theta^v(u,v)$ is the same. Since we work on a field $\mathbb{F}$ and have linear maps only, we do a simple addition operation on a field such that we get $\left(f(\{u,v\}^1)+f(\{u,v\}^2)\right)/\Delta\theta^v(u,v) = b(\{u,v\}^1) + b(\{u,v\}^2) = b(u,v)$ for two parallel edges $\{u,v\}^1,\{u,v\}^2 \in \overleftrightarrow{E}$. We generalize this to multiple edges in the following rule.

Reduction Rule 4.22 (Parallel Contraction)**.** *Let $p\colon \overleftrightarrow{E} \to \{\{u,v\} \mid u,v \in V; u \neq v\}$ with $\{u,v\}^i \mapsto \{u,v\}$ with $1 \leq i \leq k$ being k parallel edges. Let the parallel edges be $e_i\colon \{u,v\}^i \in \overleftrightarrow{E}$ with $1 \leq i \leq k$, i. e., $p(e_i) = p(e_{i+1})$ for all $1 \leq i \leq k-1$. These parallel edges are equivalent to one edge (see Figure 4.8b) with the susceptance b, voltage angle difference $\Delta\theta^v$, and capacity* cap *being*

$$b(u,v) = \sum_{\{u,v\}^i\in\overleftrightarrow{E}} b\left(\{u,v\}^i\right), \tag{4.19a}$$

$$\Delta\theta^v(u,v) = \min_{\{u,v\}^i\in\overleftrightarrow{E}} \left(\Delta\theta^v\left(\{u,v\}^i\right)\right), \tag{4.19b}$$

$$\operatorname{cap}(u,v) = b(u,v)\cdot\Delta\theta^v(u,v), \tag{4.19c}$$

respectively.

Every vertex $v \in V$ has a voltage angle $\theta^v(v)$ that can be interpreted as a potential. For a self-loop the voltage angles at both ends are the same and thus, the flow f on the self-loop is zero (see Equation 4.13).

Reduction Rule 4.23 (Self-loop Contraction)**.** *Let $p\colon \overleftrightarrow{E} \to \{\{u,v\} \mid u,v \in V\}$ be a function with $\{u,u\} \mapsto \{u\}$, where $p(e) = \{u\}$ with $e \in \overleftrightarrow{E}$ is a self-loop with both ends of edge e ending in u. Then the edge e can be removed without any electrical effect, but with one edge less (see Equation 4.13 with the additional note that both voltage angles are the same and thus, the difference is zero).*

Reduction Rule 4.24 (Degree-1 Contraction)**.** *Let $u \in V \setminus (V_G \cup V_D)$ be a vertex with degree $\deg(u) = 1$ with its only edge (u,v). Then u can be removed.*

The next reduction rule can be used for shortest paths and graph-theoretical flows. However, in general it is not applicable for electrical networks. We remark that in the next section we only work with shortest paths and graph-theoretical flows.

Reduction Rule 4.25 (Shortening of Superfluous Edges [Ake60, p. 313, Rule 3])**.** *Let $u \in V$ and let $\{u,w\} \in \overleftrightarrow{E}$ be an incident edge with capacity*

$$\operatorname{cap}(u,w) \geq \min\left(\sum_{\{u,v\} \in \overrightarrow{E} \setminus \{\{u,w\}\}} \operatorname{cap}(u,v), \sum_{\{w,v\} \in \overrightarrow{E} \setminus \{\{u,w\}\}} \operatorname{cap}(w,v) \right)$$

(see Figure 4.8c top) then we can contract vertices u and v to a new vertex x (see Figure 4.8c bottom).

A more general example of the latter transformation is applied on [Ake60, p. 316, Figure 7] in the third transformation.

The next graph transformations are more complex and were first introduced by Kennelly [Ken99]. The Δ-Y-Transformation (also known as Delta-Wye- or Triangle-Star-Transformation) and Y-Δ-Transformation are inversions to each other.

Reduction Rule 4.26 (Δ-Y-Transformation)**.** *Let u, v, and w form a complete graph with the edge set $\overleftrightarrow{E}_\Delta \subseteq \overleftrightarrow{E}$ (see Figure 4.9a). This delta Δ can be transformed to a wye Y by adding a new vertex c representing the center of the wye Y to V and new edges to the triangle's vertices $\overleftrightarrow{E} \cup \left\{\{c,u\} \mid \{u,v\} \in \overleftrightarrow{E}_\Delta\right\} \setminus \overleftrightarrow{E}_\Delta$ (see Figure 4.9b).*

$$b(u,c) = \frac{b(u,v) \cdot b(u,w) + b(u,v) \cdot b(v,w) + b(u,w) \cdot b(v,w)}{b(v,w)} \tag{4.20a}$$

$$\operatorname{cap}(u,c) = \operatorname{cap}(u,v) + \operatorname{cap}(u,w) - \big(f(v,c) - f(w,c)\big) \tag{4.20b}$$

The inverse rule of the Δ-Y-transformation is denoted by Y-Δ-Transformation.

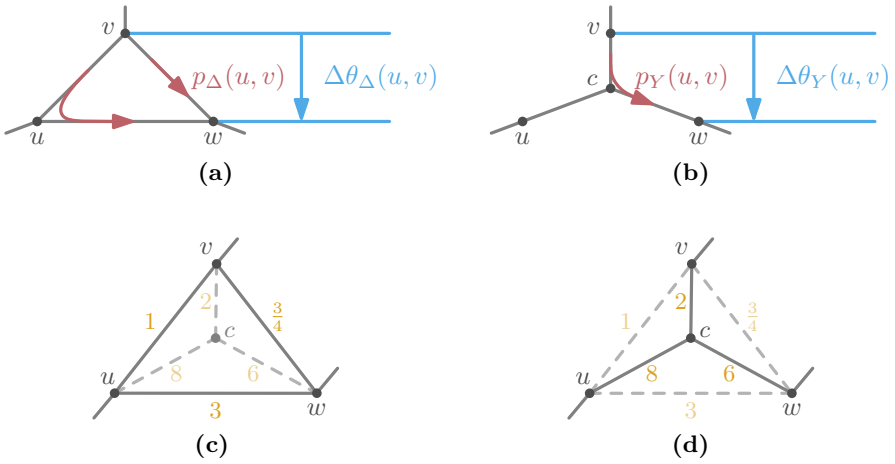

Figure 4.9: The delta-wye- (Reduction Rule 4.26) and wye-delta-transformations (Reduction Rule 4.27) represent possible transformation rules in electrical networks. In this example, we have a graph with three (respectively four) vertices ●. If we explicitly compute the susceptances we write the susceptance b on each edge. (a) The triangle Δ can be transformed to a star Y. Recall that we have only linear maps and work on a field $\mathbb{F}$ (here $\mathbb{R}$). Thus, we can superpose the paths that is a simple addition operation, e. g., (v, w) is equal to the series circuit of (v, u) and (u, w), which is parallel to (v, w) meaning $\big((v, u), (u, w)\big)||(v, w)$. This electrical addition can be done for the susceptances b and electrical (e. g., power) flows p. The voltage angle (potential) difference stays the same $\Delta\theta^v$. (b) This star Y can be transformed to a triangle Δ and can use similar properties as described in (a). (c) The Δ-Y-transformation increases the number of vertices by one and decreases the number of cycles by one. (d) The Y-Δ-transformation increases the number of cycles by one and decreases the number of vertices by one.

Reduction Rule 4.27 (Y-Δ-Transformation)**.** *Let $c \in V \setminus (V_G \cup V_D)$ be a vertex with a degree of* $\deg(c) = 3$ *(see Figure 4.9b and d). Thus, vertex c forms the center of a wye Y with neighbors u, v, and w. The transformation of the wye Y results in a equivalent network that is a delta Δ by $\overleftrightarrow{E}'' \cup \big\{\{u, v\} \mid \{c, u\} \in \overleftrightarrow{E}, \{c, v\} \in \overleftrightarrow{E} \text{ with } u \neq v\big\} \setminus \big\{\{c, u\} \in \overleftrightarrow{E}\big\}$ and $V \setminus \{c\}$ (see Figure 4.9a and c) with the susceptances*

$$b(u, v) = \frac{b(u, c) \cdot b(v, c)}{b(u, c) + b(v, c) + b(w, c)}. \tag{4.21}$$

The basic idea of the latter transformation is that we remove a vertex c that is the center of a wye Y and connect all its neighbors by an edge. Note that the previous transformation removes a vertex from the graph, which reduces the size of the network. The next transformation is a generalization of Reduction Rule 4.27.

Note that a star of arbitrary degree $\deg(c)$, where c is the center of a star, is a more general notation for wye and in this case a *polygon* is a complete graph $K_{\deg(c)}$ representing a generalization of a triangle (i. e., K_3).

Reduction Rule 4.28 (Star-Polygon-Transformation [Ros24, p.916]). *Let $c \in V \setminus (V_G \cup V_D)$ be a vertex with a degree of* $\deg(c)$. *Thus, vertex c forms the center of a star with neighbors $N(c)$. Transforming a star into a polygon by $E' = E \cup \big\{\{u,v\} \mid u \in N(c), v \in N(c) \text{ with } u \neq v\big\} \setminus \big\{\{c,u\} \in E \mid u \in N(c)\big\}$ and $V' = V \setminus \{c\}$, we get the susceptances*

$$b(u,v) = \frac{b(u,c) \cdot b(v,c)}{\sum_{\{u,c\} \in E} b(u,c)} \qquad \forall u, v \in N(c). \tag{4.22}$$

One of the first applications is given by Butterworth [But21] on the earth capacity effects. Rosen [Ros24, p.917, Figure 3] calculates the effective conductance between two terminals using the next transformation. Rosen [Ros24, p.917, Figure 4] calculates the effect on the balance of Wheatstone bridges by the earth admittance between two terminals using the latter transformation.

Note that if there is already an edge $\{u,v\} \in \overleftrightarrow{E}$, we can apply in addition to Reduction Rule 4.28 a parallel contraction in form of Reduction Rule 4.22. We now reference two other reduction rules for the sake of completeness.

Reduction Rule 4.29 (Polygon-to-Chain-Reduction [SW85]). *See Satyanarayana and Wood [SW85] for more information.*

Reduction Rule 4.30 (Trisubgraph-Y-Reduction [ST93]). *See Satyanarayana and Tindell [ST93] for more information.*

We denote a graph G to be *k-edge reducible* if there is a series of application of reduction rules (Reduction Rules 4.21, 4.22, 4.26 and 4.27) such that the resulting graph has only k remaining edges.

Theorem 4.31 (Epifanov [Epi66]). *Every biconnected plane s-t-graph with an (s,t)-edge is 1-edge reducible.*

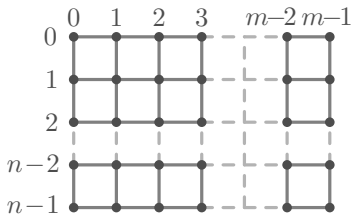

Figure 4.10: A grid graph G of size $n \times m$ with $n, m \geq 2$.

To understand the next result, we define grid graphs and minors. A (square) *grid graph* $G_{\text{grid}} = (V_{\text{grid}}, E_{\text{grid}})$ (also known as lattice graph) is a plane graph, where each edge has unit length and is drawn either by a horizontal or a vertical straight curve. The grid points are crossings represented by vertices (Figure 4.10). A *minor* is a graph that can be obtained from a graph G by contracting edges and by deleting vertices and edges.

We use the following results to provide a first algorithm for DC FEAS and MPFP on plane s-t-graphs G.

Algorithm 1: *s-t* Planar DC FEAS($\mathcal{N}$) & *s-t* Planar MPFP($\mathcal{N}$)

```
Data: A network N = ( G, V_G, V_D, cap, b, p_g, p̄_g, p_d, p̄_d ) with |V_G| = 1 (i. e.,
      {s} = V_G), |V_D| = 1 (i. e., {t} = V_D), p_g = p̲_g = p̄_g, and p_d = p̲_d = p̄_d.
Result: Flow f(u, w) for all (u, w) ∈ E, flow value F(f, N), and voltage angles θ^v(u)
        with u ∈ V.
1 E     = planarEmbeddingOf(G) ;                          ▷ PQ-Tree; see Section 4.5.2
2 E_grid = gridEmbeddingOf(G(E)) ;                        ▷ see Lemma 4.34
3 (N = N_0, ..., N_k = (({s, t}, {e'}), {s}, {t}, cap', b', p_g, p_d)))
      = contractGridGraphToEdge(N(E_grid)) ;              ▷ see Lemma 4.35
4 f(e') = p_g = p_d ;
5 f     = decontractEdgeToGridGraph((N_0, ..., N_k), f(e')) ;
6 f     = rescalePowerFlow(N, f);                         ▷ see Lemma 4.12
7 return f;
```

Lemma 4.32 ([Tru89, p.144, Lemma 6])**.** *Every plane graph is a minor of some grid graph.*

Let a grid graph $G_{\text{grid}} = (V_{\text{grid}}, E_{\text{grid}})$ be a graph that is numbered column-wise from left to right with $1, \ldots, m$ and row-wise from top to bottom with $1, \ldots, n$ (see Figure 4.10). Similar to Truemper [Tru89], we define an *extended grid graph* G^{ℓ}_{ex} as a graph on a grid with $\ell \geq 2$, where $\ell \in \mathbb{N}$ represents the number of columns and rows with $0 \leq i \leq \ell - 1$. Since the grid is quadratic, we have ℓ^2 vertices, and edges connecting a vertex $v_{i,0}$ on the left border at row i column 0 of the grid to a vertex $v_{\ell-1,i}$ on the bottom border (see Figure 4.11) such that either the source s or the sink t is located on the inner face (in Figure 4.11 the source s is on the inner face). We illustrated such a graph G^{ℓ}_{ex} in Figure 4.11.

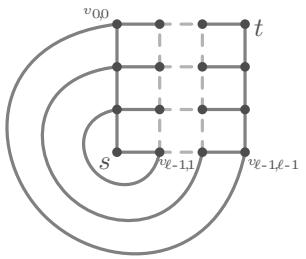

Figure 4.11: An extended grid graph G^{ℓ}_{ex} with a grid of dimension $\ell \times \ell$ and ℓ^2 vertices.

Lemma 4.33 ([Tru89, p.145, Lemma 13])**.** *Any plane graph G with $(s, t) \in E$ and with one of the two terminals (i. e., source s or sink t) on the outer face, is a minor of some extended grid graph G^{ℓ}_{ex} with $\ell \geq 2$.*

Note that it is always possible to use the inverse of all reduction rules but Reduction Rule 4.28. In the following, we try to embed the graph G such that the embedding has the form of an extended grid graph. We need the concept of a face in the following (Section 4.1.4). For a plane graph G a face c is a region that is bounded by the edges and vertices of G. Two faces are incident if they share at least one edge.

Lemma 4.34. *Any plane s-t-electrical-network $\mathcal{N}$ with at least one terminal on the outer face can be embedded into a grid in $O(|V|)$ time.*

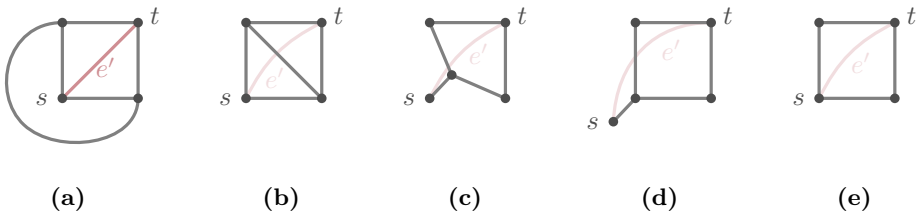

Figure 4.12: A graph with four vertices, five edges, and one additional edge $e' = (s, t) \in E$. The shown steps represent the reduction of the smallest possible extended grid graph G^{ℓ}_{ex} with $\ell = 2$. The steps are given in Truemper [Tru89] for graphs in general. From (a) to (b) we just swap the outer edge to the inner face. From (b) to (c), we do a triangle to star transformation (see Reduction Rule 4.26) of the lower left triangle. In the last step from (d) to (e), we do a series contraction (see Reduction Rule 4.21) and contract the edge in the bottom left with e'. To contract the remaining graph to one edge $e' = \{s, t\}$, we do two series contractions and one parallel contraction.

Proof. Note that the maximum degree of a grid graph $G_{\text{grid}} = (V_{\text{grid}}, E_{\text{grid}})$ is at most 4. Thus, we split all vertices $v \in V(G)$ with degree of at least $\deg(v) \geq 5$. With $\deg(v) \leq 2n_v + 2$, we split them into $n_v = \lceil {}^{\deg(v)-2}/_{2} \rceil = \lceil {}^{\deg(v)}/_{2} \rceil - 1$ vertices v_i with $1 \leq i \leq n_v$ with $V_v := \{v_i \mid 1 \leq i \leq n_v, v \in V\colon \deg(v) \geq 5\}$ such that $V_{\text{grid}} = \bigcup_{\{v \in V \mid \deg(v) \geq 5\}} V_v \cup (V(G) \setminus \{v\})$ and $E_{\text{grid}} = E(G) \cup \big\{\{v_i, v_{i+1}\} \mid v_i, v_{i+1} \in V_v, \forall v \in V_{\text{grid}} \setminus V(G)\big\}$ with susceptance $b(e) = \infty$ with $e \in E_{\text{grid}} \setminus E(G)$. We set the susceptance to infinity such that $\Delta\theta^v(v_i, v_{i+1}) = {}^{f(v_i, v_{i+1})}/_{b(v_i, v_{i+1})} = {}^{f(v_i, v_{i+1})}/_{\infty} \approx 0$ meaning that the voltage angles $\theta^v(v_i)$ are the same for all $v_i \in V_v$ with $1 \leq i \leq n_v$. Since the average degree of a finite plane graph is strictly less than 6, we get 2 new vertices per vertex on average and thus, we have $O(|V|)$ vertices.

Assume an arbitrary planar embedding of G_{grid}. Thus, we choose an inner face c_{s_1} that is incident to the vertex s and choose a cut in the dual graph $S \subseteq E$ between c_{s_1} and the outer face c_o. Let $G'_{\text{grid}} = (V'_{\text{grid}}, E'_{\text{grid}})$ be a new graph with vertex set $V' = V \cup \{s'\}$ and edge set $E(G') = E(G) \cup \big\{\{s, s'\}\big\} \setminus S$ with $b(s, s') = \infty$. This graph can be embedded in $O(|V|)$ time into a grid of size at most $|V| \times |V|$ using, e. g., the algorithm of Biedl and Kant [BK98]. Thus, we need $O(|V|^2)$ space. This takes $O(|V|)$ time. □

We note that the outer edges that make the grid graph into an extended grid graph can be added by applying the following steps: We add the remaining edges in S. We place s' on the bottom left corner. Each time we add an edge $\{u, v\} \in \overleftrightarrow{E}$ we check if $u_{i_u,0} = v_{\ell-1,i_v}$. If neither is true then we add $i_v - i_u$ new rows if $i_u < i_v$ or new columns if $i_v < i_u$.

Every plane electrical network can be embedded into a grid by using the aforementioned algorithm. Thus, we make use of the following lemma.

Lemma 4.35 ([Tru89, pp.142ff., Theorem 2 & Lemma 14])**.** *Every (extended) grid graph with one source and one sink is 1-edge reducible.*

So far we explained the different parts of the algorithm. Note that we assume a plane s-t-graph G for the algorithm. The algorithm (see Algorithm 1) works as follows. From Lemmas 4.34 and 4.35, we know that any plane graph can be embedded into a grid (see Algorithm 1 Line 2) and that every grid graph can be contracted to a single edge e' (see Algorithm 1 Line 3 and Figure 4.12). In each Δ-Y-reduction, we compute the susceptances by the aforementioned rules (see Reduction Rules 4.26 and 4.27). In the decontraction step (see Algorithm 1 Line 5), we compute based on the given susceptances on the different contraction levels the voltage angles $\theta^v(u)$ with $u \in V_i$ and the flow for each contraction level i. We start with $\mathcal{N}_k$ consisting of a single edge e', over $\mathcal{N}_{k-1}$, and in the end we compute the voltage angles and the flow for the original network $\mathcal{N}_0$. For each level transition, we apply the reverse of the applied transformation rules given in Reduction Rules 4.21–4.24, 4.26 and 4.27. Note from Lemma 4.12 on Page 72 that the capacities can be neglected, since we are always able to rescale a nontrivial electrical flow. This rescaling is not necessary for DC FEAS, since a capacity violation would imply a non-existing feasible electrical flow. However, assume that we apply an arbitrary flow on e' (see Algorithm 1 Line 4) resulting in an electrical flow that is not necessarily feasible, since the capacity constraint might be violated. To fix the violation, we use Lemma 4.13 on Page 73 on the decontracted graph G with flow f to rescale the flow to a feasible, e. g. MPF (see Algorithm 1 Line 6). From Truemper [Tru89], we get the following running time.

Lemma 4.36. *The algorithm runs in $O(|V|^3)$ time.*

The contraction step of the algorithm Algorithm 1 Line 3 is illustrated in Figures 4.12 and 4.13 for an extended grid graph.

Lemma 4.37. *A planar s-t-graph G can always be contracted to one edge by a series of reduction rules (see [Tru89]).*

For the reverse operation, we remark that the voltage angles in a parallel and series contraction do not change. For the series contraction, we have to compute the voltage angles for the inner vertices using Equation 4.13. For the Δ-Y- and Y-Δ-transformation, the voltage angles at the three outer vertices do not change. For the center of the star, we have to compute the voltage angle using Equation 4.13. The reconstruction steps can be done during the recursive return. If the capacities are violated, we rescale the flow f using Lemma 4.12. From the previous discussion follows the next theorem.

Theorem 4.38. *The algorithm computes a feasible electrical flow for a planar s-t-graph G.*

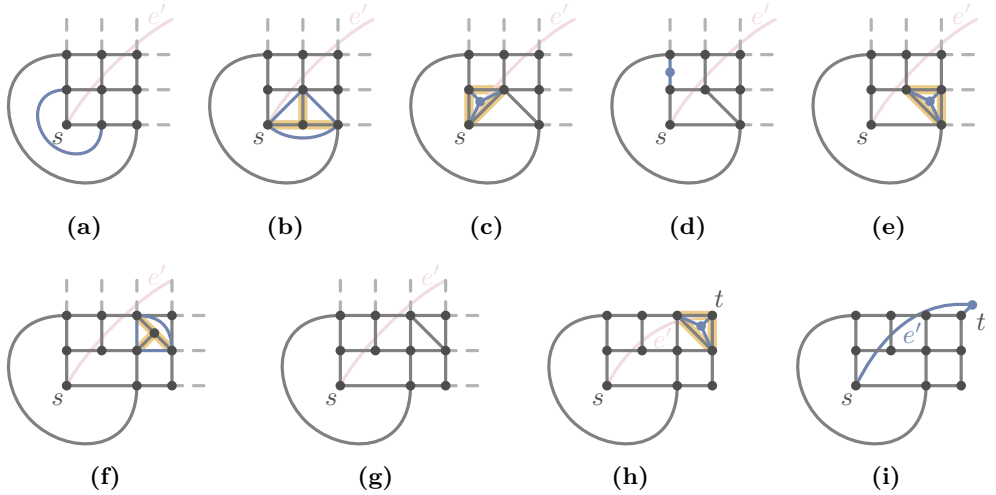

Figure 4.13: A general extended grid graph G^{ℓ}_{ex} with ℓ^2 vertices. Blue edges and blue vertices represent the edges and vertices of the transformation and replace the orange marked edges. The steps are basically given by Truemper [Tru89] for graphs in general. From (a) to (b) we use the steps already shown in Figure 4.12.

4.3 Representations and Formulations of Electrical Flows

Cain ET AL. [COC12, p.13] mention that power grids are planar (see Section 4.1.4) and undirected. Recall from Section 3.1 that we can transform any undirected graph to a directed graph, which we do for notational conveniences. The planarity of graph G is a crucial property of the network $\mathcal{N}$ for this section. In addition, we assume that the graph G is biconnected.

4.3.1 The Duality Concept for Graphs

Using the duality of the incidence matrix $\mathbf{I}$ and circuit matrix $\mathbf{B}$ that was shown in Section 4.1.5, we translate the algebraic duality of the two matrices into a graph theoretical duality (Section 4.1.4). Recall that a base of a matroid (see Definition 4.2) is a maximum independent set. The complement of a base in the primal graph G is the base in the dual graph $G^{\star}$ (see Lemma 4.19).

Theorem 4.39 ([Whi35, p.522, Theorem 23])**.** *Let $\mathcal{E}$ be a planar embedding of a graph G. The graphs G and $G^{\star}$ are duals if and only if there is a bijection $\mu_{\text{dual}} \colon E(G) \to E(G^{\star})$ between their edges such that bases in one correspond to base complements in the other.*

The construction in Section 4.1.4 implies a bijection of edges in the primal graph G to edges in its dual graph $G^{\star}$. It is called a combinatorial dual in terms of the Whitney

duality (bijection of edges; and a set of edges forming a cut corresponds to a cycle in the combinatorial dual). Note that the dual of a dual graph $G^\star$ is isomorphic to the primal graph G as long as G is connected.

From Equations 4.1–4.3, we know that a feasible KCL flow on the primal graph G is equivalent to a graph theoretical flow in the primal graph G. It follows from Lemma 4.19 that a feasible KVL flow corresponds to a graph theoretical flow in the dual graph. Thus, we get the following lemma.

Lemma 4.40. *A feasible KVL flow f_G in the primal graph G is equivalent to a feasible KCL flow $f_{G^\star}$ in the corresponding dual graph $G^\star$.*

Note that we can apply any flow f on a self-loop $e = (u, u)$, since it is redundant. Thus, we get the following observation.

Observation 4.41. *Let the primal graph G be a tree. Thus, there is only one face that is equivalent to the outer-face c_t. The dual graph consists of self-loops only. Let f be any feasible flow on G. Then, flow f is also a feasible electrical flow.*

Recall from Section 4.2 that every self-loop can be removed (see Reduction Rule 4.23). The aforementioned observation is a geometrical explanation for planar graphs of the results of Lehmann ET AL. [LGH15, p.9, Lemma 4] and Leibfried ET AL. [Lei+15a] that on trees any graph-theoretical flow is also electrical feasible.

We note that a series contraction (see Reduction Rule 4.21) in G is an equivalent transformation to the parallel contraction (see Reduction Rule 4.22) in the dual graph $G^\star$. We highlight that by the following structural observation.

Observation 4.42. *The series contraction in the primal graph G is equivalent to the parallel contraction in its dual $G^\star$ and vice versa.*

Observation 4.43. *The Δ-Y-transformation in the primal graph G is equivalent to the Y-Δ-transformation in the dual graph $G^\star$ and vice versa.*

In the following section, we will make use of the duality by reformulating the problem.

4.3.2 Simultaneous Flow Representation

We use the aforementioned duality and structure of the problem to reformulate DC FEAS in terms of the *Simultaneous Flow Problem* (SFP). For SFP the graphs are not necessarily duals, but share some edges.

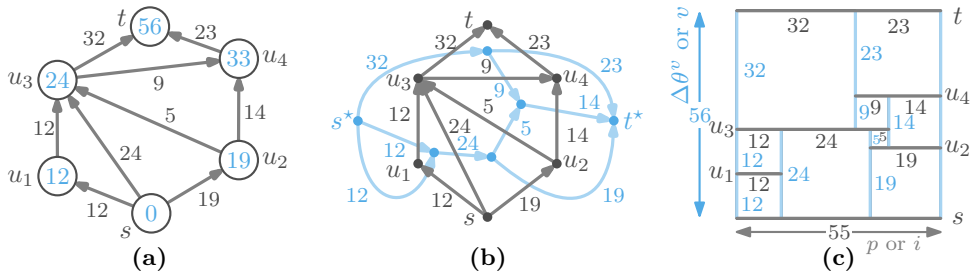

Figure 4.14: We use the example graph of Felsner [Fel13, p.18]. The susceptances are $b \equiv 1$, the feasible electrical flow $f(e)$ is written on each edge $e \in E$, and we neglect the capacities meaning $\text{cap} \equiv \infty$. (a) The example graph's feasible electrical flow is in this case the minimum integer feasible electrical flow f and the corresponding voltage angles θ^v. (b) The flow f and the voltage angle differences $\Delta\theta^v$ can be separated into two graphs, which are the primal graph G and its dual graph $G^\star$, respectively. (c) Since the susceptances are $b \equiv 1$ a similar representation is a squaring of a 55×56 rectangle, where the width and the height of each square is represented by the flow in the primal and dual graph, respectively. Each vertex in the primal and dual graph represents a horizontal or vertical segment, respectively. For clarity we labeled the vertices for the primal graph only, since otherwise this figure seems overloaded. An edge represents a side of a square.

Simultaneous Flow Problem [2] SFP($\mathcal{N}$)

Instance: Two graphs G_1 and G_2, subsets $E_1 \subseteq E(G_1)$ and $E_2 \subseteq E(G_2)$, and a bijection $\mu_{\text{SFP}} \colon E_1 \to E_2$.

Question: Are there nonzero KCL-feasible flows f_{G_1} and f_{G_2} in G_1 and G_2 such that for every edge $e \in E_1$ we have $f_{G_1}(e) = f_{G_2}(\mu_{\text{SFP}}(e))$?

The reformulation of DC FEAS separates the constraints—meaning KCL and KVL—by the usage of two graphs, which we define in the following. Recall that our graph is planar and biconnected, and that we denote by $\mu_{\text{dual}} \colon E(G(\mathcal{E})) \to E(G^\star)$ the bijection of the edges with $e_i \mapsto \mu_{\text{dual}}(e_i) = e_i^\star$. An edge $(u, w) = e_i \in G$ corresponds to an edge $(c_1, c_2) = e_i^\star \in G^\star$ and vice versa if and only if e_i is incident to both faces c_1 and c_2, and $e_i^\star$ is incident to the faces u and w. Since there is no unique embedding of a biconnected planar graph the mapping is not unique. This means that the bijection is always related to some planar embedding of graph G.

Without loss of generality, we assume that flow f is a function $f \colon E \to \mathbb{Z}$. Recall that we can always rescale f to a feasible electrical flow that is non-integral (meaning $f \colon E \to \mathbb{R}$) by using the scaling from Lemma 4.12.

From Theorem 4.17, we know that a graph's base of the incidence matrix and the corresponding base of the circuit matrix are duals. Given a graph and its dual, we

[2] After showing our results to Guido Brückner, he mentioned the SFP generalization to us. We would like to thank him for that generalization of the biconnected planar s-t-DC FEAS-problem.

know from Lemma 4.19 that the incidence matrix of either graphs is equivalent to the circuit matrix of the other, whereby equivalent means here that an edge-cut at a vertex in one graph represents a simple cycle in the other graph and vice versa. The latter means that for a spanning tree T in graph G the set $E' = E(G) \setminus E(T)$ of chords in one graph corresponds to a set $E'' = \{\mu_{\text{dual}}(e) \mid e \in E'\}$ of edges in the dual graph, where E'' constitutes a tree. Now, Theorem 4.39 and Lemma 4.40 can be used to transform DC FEAS in terms of simultaneous flows. An edge cut H at vertex $u \in V(G^\star)$ with $H(u) = \{e \in \overleftrightarrow{E}(G^\star) \mid u \in e\}$ is a cycle c in the biconnected planar graph G. A conservation of flow at u means that the incoming flow is equivalent to the outgoing flow. For the corresponding cycle c this means that flows along the cycle sum up to zero. Note that a flow direction in G corresponds to a flow direction in $G^\star$ and vice versa.

The following problem is equivalent to DC FEAS on s-t plane graphs.

s-t Planar DC FEAS($\mathcal{N}$)	
Instance:	A plane s-t-graph G, its dual graph $G^\star$, and the corresponding bijection $\mu_{\text{dual}} \colon E(G) \longrightarrow E(G^\star)$.
Question:	Are there simultaneous flows on G and $G^\star$ such that $f_G(e) = f_{G^\star}\left(\mu_{\text{dual}}(e)\right) \cdot b(e)$ for all $e \in E(G)$?

In the objective of the reformulated s-t planar DC FEAS and DC MPFP, we can easily see that this is a restatement of Equation 4.13 by replacing the phase angle difference $\Delta\theta^v(u,w) \coloneqq \theta^v(w) - \theta^v(u)$ with the flow in the dual graph $f_{G^\star}(\mu_{\text{dual}}(e))$ with $e = (u,w) \in E$. An example for the reformulation is given in Figure 4.14b. In Figure 4.14a and b an electrical flow with its unique voltage angle assignment and its translation to simultaneous flows is shown, respectively. Using simultaneous flows Equation 4.13 becomes Equation 4.23.

$$f_G(e) = f_{G^\star}\left(\mu_{\text{dual}}(e)\right) \cdot b(e) \qquad \forall e \in E \tag{4.23}$$

Roughly speaking, the susceptance b represents a gear ratio between the primal graph's flow f_G and the dual graph's flow $f_{G^\star}$.

Theorem 4.44. *A flow f in G is an electrical flow if and only if the primal flow $f_G \equiv f$ and the flow $f_{G^\star}$ in the dual graph $G^\star$ comply the flow conservation (KCL) and if for every edge $e \in E$ the flow complies $f_G(e) = f_{G^\star}\left(\mu_{\text{dual}}(e)\right) \cdot b(e)$.*

Proof. The left-hand side of Equation 4.24a and Equation 4.24b comes from Equation 4.7 and Equation 4.10, respectively. Recall that we can reformulate Equation 4.10 with $\mathbf{B}(G) \cdot \overrightarrow{\Delta\theta^v} = \overrightarrow{0}$ in terms of flows using Equation 4.14 with $\mathbf{B}'(G) \cdot \overrightarrow{f} = \overrightarrow{0}$. From Lemma 4.19, we know that the incidence matrix $\mathbf{I}$ and the circuit matrix $\mathbf{B}$ are

duals meaning $\mathbf{I}(G) = \mathbf{B}'(G^\star)$ and $\mathbf{B}'(G) = \mathbf{I}(G^\star)$. Using the duality, we get for Equation 4.7 and Equation 4.10 the following.

$$\mathbf{I}(G) \cdot \overrightarrow{f_G} = \vec{0} \quad \Leftrightarrow \quad \mathbf{B}(G^\star) \cdot \overrightarrow{\Delta\theta^v{}_{G^\star}} = \vec{0} \tag{4.24a}$$

$$\mathbf{B}(G) \cdot \overrightarrow{\Delta\theta^v{}_G} = \vec{0} \quad \Leftrightarrow \quad \mathbf{I}(G^\star) \cdot \overrightarrow{f_{G^\star}} = \vec{0} \tag{4.24b}$$

From Equation 4.13 and Equation 4.24b we get Equation 4.25.

$$f_G(e) = b(e) \cdot \Delta\theta^v{}_G(e) \tag{4.25a}$$

$$f_G(e) = b(e) \cdot f_{G^\star}(\mu_{\text{dual}}(e)) \tag{4.25b}$$

The illustration of the relationship is given in Figure 4.15. □

Another equivalent representation is given in Figure 4.14c, which we describe in the following.

4.3.3 Rectangular Representation

Another representation of simultaneous flows was given by Felsner [Fel13, p.18] and is shown in Figure 4.14c. We note that this is basically an adopted idea of Rosenstiehl and Tarjan [RT86] that use a similar construction for rectilinear planar layouts but do not use it for a squaring of an outer rectangle. This representation is in general denoted by *rectangular dissection* $\mathcal{R}$. Within this representation a vertex is either a horizontal or vertical line segment dependent on whether the vertex is in the primal graph G or dual graph $G^\star$. In Figure 4.14c, a horizontal segment corresponds to a vertex in the primal graph G and a vertical segment corresponds to a vertex in the dual graph $G^\star$. We illustrate the latter in Figure 4.14c for the primal graph by labeling the segments with the corresponding vertices $s, u_1, u_2, u_3, u_4, t \in V$. An edge represents a side of a square. Dependent on the graph a flow on that edge affects either the horizontal or vertical side ratio (i. e., the width or height of a rectangle).

Felsner shows that a special case of simultaneous flow can be represented by squaring of an outer rectangle. The case in Figure 4.14c shows such a special case, where all inner partitions of an outer rectangle are squares. The reason for that is that the susceptance b is $b \equiv 1$ and thus, Equation 4.23 becomes $f_G(e) = f_{G^\star}\big(\mu_{\text{dual}}(e)\big)$ for all $e \in E$.

However, a more general definition that is closer to power grids would be to allow arbitrary susceptances $b(\overleftrightarrow{e})$ with $\overleftrightarrow{e} \in \overleftrightarrow{E}$. Than the representation is not a *squaring* of an outer rectangle. Meaning that the inner partitions are not necessary squares, but can be rectangles with differing aspect ratio dependent on the susceptance b. An example is given in Figure 4.15.

Note that from Lemma 4.40 we know that a feasible flow in the primal graph G models the actual (power) flow that is equivalent to a current flow i (see Section 3.3.2

on Page 52) and that a feasible flow in the dual graph $G^\star$ models the voltage angle differences $\Delta\theta^v$ that is equivalent to the voltage drops v (see Section 3.3.2 on Page 52). Recall that a flow f_G in the primal graph G represents one side of the rectangle (in Figure 4.15c this would be the width) and the $f_{G^\star}$ in the dual graph $G^\star$ represents the other side of the rectangle (in Figure 4.15c this would be the height). Thus, the surface of a rectangle represents the power p, which explains the quadratic relationship (see Lemma 4.45).

Lemma 4.45. *The primal graph G and the dual graph $G^\star$ model the quadratic relationship between voltage v and current i meaning $p = v \cdot i$ (see Equation 3.5).*

Felsner [Fel13, p.8] restricted $\mathcal{R}$ to the case, where there is no point where four rectangles meet each other. However, in Figure 4.15c we can see that this is possible and does not cause any problem. Such a representation can be also seen as a segment contact representation. We refer for the latter representation to Felsner [Fel13].

For a given graph the drawing of a squaring of rectangles is unique, which follows from Lemma 4.7. In Section 4.5.1, we will see that a bipolar orientation exists if the graph is biconnected. The embedding of biconnected planar graph is not unique, since we can switch for example the order of parallel paths. However, from Lemma 4.7 we know that the flows are unique.

Lemma 4.46 (Unique Partition of a Rectangular Representation)**.** *The rectangles of a rectangular representation have unique minimum integral sizes. The embedding of these rectangles can vary.*

This concludes a very important property of simultaneous flows and a rectangular representation. These representations separates the quadratic relationship and help to understand important properties of electrical flows, which we will see in the next section. In the following, we will discuss the balancing property that will be used as a criteria for termination and basically describes the conflict resolution in each graph.

4.4 The Balancing Property

Electrical flows have a property of balancing meaning the flows do not congest certain edges but spread the load over multiple paths from s to t. Note that this is the main difference to graph-theoretical flows that try—while maximized—to congest all edges as much as possible. The balancing property of electrical flows is equivalent to flows that minimize the total losses (Equation 4.26).

$$\min \sum_{e \in \overrightarrow{E}} f(e)^2 / b(e), \tag{4.26}$$

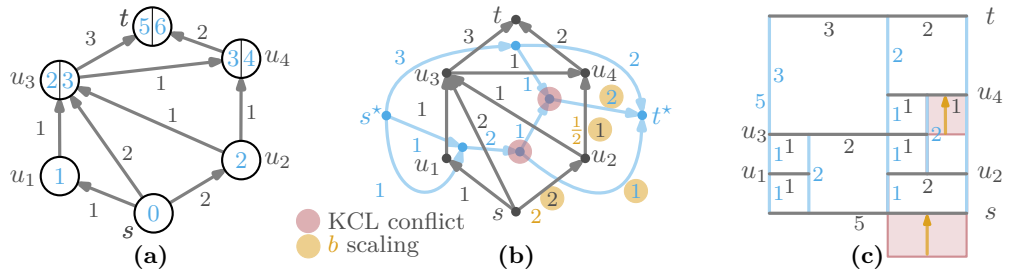

Figure 4.15: We use the example graph of Felsner [Fel13, p.18] that is also used in Figure 4.14. The susceptances are $b \equiv 1$ and we neglect the capacities meaning $\text{cap} \equiv \infty$. We write the flows f on the edges or on the rectangle's side. (a) We apply some feasible flow f (i. e., complying the KCL and capacity constraints only) on graph G. The feasible flow f is not a feasible electrical flow, since the voltage angles (distance labels)) θ^v at the vertices ○ are not unique. The latter can be seen in the double assignments at $u_3, u_4, t \in V$. Thus, the KVL is violated. (b) It is always possible to transform a feasible flow f into a feasible electrical flow f' by scaling the susceptances b at certain edges such that the ratio $f/\Delta\theta^v \equiv f_G/f_{G^\star} \equiv b$ changes the flow $f_{G^\star}$ in such a way that it becomes feasible (i. e., complying KCL and thus, KVL) as long as the susceptance b is not restricted meaning $b \in [0, \infty]$. (c) In the geometric setting a susceptance scaling represents an aspect ratio scaling (indicated by the arrows ↑). The bottom right box would exceed the outer rectangle by one unit without the susceptance scaling of 2. Without the susceptance scaling of $1/2$ there would be a gap of one unit in the right center.

which is a quadratic function [Chr+11, p.275, Section 2.2, Energy Equation]. In this section, we describe this property in terms of simultaneous flows using algorithmic properties that exploit the aforementioned structure (see Lemma 4.45)

Ford and Fulkerson [FF56, p.404, Section 3] introduced the duality between maximum flows and shortest paths in which a minimum cut in G corresponds to a shortest path in the dual graph $G^\star$. To use shortest paths, we first introduce a distance metric for power grids. The distance between two vertices is usually the length of an edge or time to pass that edge. The distance in an electrical network, is given by the potential difference $\theta^v(w) - \theta^v(u)$ that is the voltage angle difference $\Delta\theta^v(u, w)$.

For a given flow f the voltage angle difference on any u-w-path $\pi(u, w)$ is given in Equation 4.27 and is derived from Equation 4.13. We now give a generalization of the voltage angle difference $\Delta\theta^v$ that is original defined on edges to the voltage angle difference on paths that is a distance function $\Delta\theta^v : \Pi \to \mathbb{F}$, where $\mathbb{F}$ is a field (e. g., $\mathbb{R}$) and Π is a set of paths. Note that the equations that are build from Equation 4.27 constitute a matrix and the generalization is a simple sum of the rows that result in Equation 4.13.

$$\Delta\theta^v(\pi(u, w)) \coloneqq \sum_{(i,j)\in\pi(u,w)} \frac{f(i, j)}{b(i, j)}, \tag{4.27}$$

for a path $\pi(u,w) \in \Pi$ with $u, w \in V$. For electrical flows the metric is $f(e)/b(e)$ deduced from Equation 4.27. The Shortest Path Problem (SPP) computes a path with minimum length $\pi_{\mathsf{SP}}(s,t) \coloneqq \min_{\pi(s,t)\in\Pi} \sum_{e\in\pi(s,t)} f(e)/b(e)$. Contrary, the Longest Path Problem (LPP) computes a path that has the longest distance between two vertex pairs $\pi_{\mathsf{LP}}(s,t) \coloneqq \max_{\pi(s,t)\in\Pi} \sum_{e\in\pi(s,t)} f(e)/b(e)$.

From the previous section (see especially Equations 4.10 and 4.13) we know that the voltage angle assignments are unique and thus, we get the following observation that is illustrated in Figure 4.16.

The distance between to vertices $u, w \in V$ with $(u,w) \in E$ is given by the voltage angle difference $\Delta\theta^v(u,w) \coloneqq \theta^v(w) - \theta^v(u)$ with voltage angles θ^v that can be interpreted as distance labels. The voltage angle difference (i. e., the electrical distance) for a path $\pi(s,t)$ is given by $\Delta\theta^v(\pi(s,t)) = \sum_{(u,w)\in\pi(s,t)} \Delta\theta^v(u,w) = \sum_{(u,w)\in\pi(s,t)} f(u,w)/b(u,w)$.

Lemma 4.47 (Balancing Flow Property)**.** *Given a primal graph G and its dual graph $G^\star$, for which the shortest path $\pi_{\mathsf{SP}}(s,t) \in \Pi(G)$ in G (respectively longest path $\pi_{\mathsf{LP}}(s,t) \in \Pi(G)$) can differ to the shortest path $\pi_{\mathsf{SP}}(s,t) \in \Pi(G^\star)$ in $G^\star$ (respectively longest path $\pi_{\mathsf{LP}}(s,t) \in \Pi(G^\star)$). A flow f is an electrical flow if and only if the longest and shortest path have the same length $\Delta\theta^v(\pi_{\mathsf{SP}}(s,t)) = \Delta\theta^v(\pi_{\mathsf{LP}}(s,t))$ in G with $s,t \in V(G)$ and $\Delta\theta^v(\pi_{\mathsf{SP}}(s^\star,t^\star)) = \Delta\theta^v(\pi_{\mathsf{LP}}(s^\star,t^\star))$ in $G^\star$ with $s^\star, t^\star \in V(G^\star)$ (with respect to the distance metric f/b).*

Proof. $\Rightarrow$: First we show the one direction, where f is a feasible electrical flow, which implies that the length of all paths is equivalent $\Delta\theta^v(\pi_{\mathsf{SP}}(s,t)) = \Delta\theta^v(\pi_{\mathsf{LP}}(s,t))$.

Let f be a feasible electrical flow. If $\Delta\theta^v(\pi_{\mathsf{SP}}(s,t)) \neq \Delta\theta^v(\pi_{\mathsf{LP}}(s,t))$ in G with $s,t \in V(G)$ then there is no unique voltage angle assignment $\theta^v(u)$ for all $u \in V(G)$. This implies that f does not comply with the KVL (see Equation 4.13). If $\Delta\theta^v(\pi_{\mathsf{SP}}(s^\star,t^\star)) \neq \Delta\theta^v(\pi_{\mathsf{LP}}(s^\star,t^\star))$ in $G^\star$ with $s^\star, t^\star \in V(G^\star)$ then there is no unique voltage angle assignment in $G^\star$ (see Equation 4.24), which means that f does not comply with the KCL (see Equations 4.4–4.6). Any one of the two cases would be a contradiction to f being a feasible electrical flow (see Definition 4.5).

$\Leftarrow$: With the other direction, we show that if $\Delta\theta^v(\pi_{\mathsf{SP}}(s,t)) = \Delta\theta^v(\pi_{\mathsf{LP}}(s,t))$ then this implies that f is a feasible electrical flow. Given two paths from s to t denoted by $\pi_1(s,t), \pi_2(s,t) \in \Pi$ that merge at vertex x, meaning $\pi_1(x,t) = \pi_2(x,t) =: \pi$. In addition, we have given the distance metric $f(u,w)/b(u,w)$ then from $\Delta\theta^v\big(\pi_1(s,t)\big) = \Delta\theta^v\big(\pi_2(s,t)\big)$ using the distance metric follows

$$\sum_{(u,w)\in\pi_1(s,t)} \frac{f(u,w)}{b(u,w)} = \sum_{(u,w)\in\pi_2(s,t)} \frac{f(u,w)}{b(u,w)}.$$

We define the voltage angles on the source s and sink t to be $\theta^v(s) \coloneqq 0$, and $\theta^v(t) \coloneqq \Delta\theta^v\big(\pi_1(s,t)\big) = \Delta\theta^v\big(\pi_2(s,t)\big)$.

$$\theta^v(s) + \sum_{(u,w)\in\pi_1(s,x)} \frac{f(u,w)}{b(u,w)} + \pi = \theta^v(t)$$
$$\theta^v(s) + \sum_{(u,w)\in\pi_2(s,x)} \frac{f(u,w)}{b(u,w)} + \pi = \theta^v(t)$$

Since $\pi = \pi_1(x,t) = \pi_2(x,t)$, $\theta^v(s) = 0$, and the voltage angle $\theta^v(t) = \Delta\theta^v\big(\pi_1(s,t)\big) = \Delta\theta^v\big(\pi_2(s,t)\big)$. It follows that

$$\sum_{(u,w)\in\pi_1(s,x)} \frac{f(u,w)}{b(u,w)} = \sum_{(u,w)\in\pi_2(s,x)} \frac{f(u,w)}{b(u,w)} \qquad = \theta^v(t) - \theta^v(s) - \pi.$$

Thus, the distances from the source s to the vertex x are the same meaning $\Delta\theta^v\big(\pi_1(s,x)\big) = \Delta\theta^v\big(\pi_2(s,x)\big) =: \theta^v(x)$. We can recursively proceed, which gives us the following equality.

$$\sum_{(u,w)\in\pi_1(s,x)} \Delta\theta^v(u,w) = \sum_{(u,w)\in\pi_2(s,x)} \Delta\theta^v(u,w)$$

This relationship is known from Equation 4.13 and restated by $\Delta\theta^v(u,w) := \big(\theta^v(w) - \theta^v(u)\big) = \frac{f(u,w)}{b(u,w)}$. The phase angles on each side cancel each other out, but the source s and the sink t.

$$\begin{aligned}\big(\theta^v(u_1) - \theta^v(s)\big) + \big(\theta^v(u_2) - \theta^v(u_1)\big) \quad &+\big(\theta^v(u_3) - \theta^v(u_2)\big) + \dots \\ \dots + \big(\theta^v(u_n) - \theta^v(u_{n-1})\big) \quad &+\big(\theta^v(u_t) - \theta^v(u_n)\big) = \big(\theta^v(t) - \theta^v(s)\big)\end{aligned}$$

Since the source s and the sink t are for both paths $\pi_1(s,t), \pi_2(s,t) \in \Pi$ the same and both paths have the same distance $\Delta\theta^v\big(\pi_1(s,t)\big) = \Delta\theta^v\big(\pi_2(s,t)\big)$ the voltage angle assignments are unique. We get $\big(\theta^v(t) - \theta^v(s)\big) = \sum_{(u,w)\in\pi_1(s,t)} \frac{f(u,w)}{b(u,w)} = \sum_{(u,w)\in\pi_2(s,t)} \frac{f(u,w)}{b(u,w)} = \frac{f(s,t)}{b(s,t)}$.

□

The intuition that electricity follows the path of the least resistance and tries to balance itself leads us to a *balanced flow*, where all paths have the same length from any vertex to any other vertex. First, we introduce shortest paths for power grids that represent one part of the intuition namely the path with the least resistance. Note that vertex label differences always sum up to zero and thus, these labels, too. Recall that this is exactly the same behavior as in Equation 4.13 for the voltage angles. A vertex v that violates Equations 4.4–4.6 has an excess $f_{\text{net}}(v) \neq 0$. The excess represents the amount of flow that has to be reduced or increased in v's incoming or outgoing flow, respectively. From the duality of the Maximum Flow Problem and Shortest Path Problem [FF56, p.404, Section 3] and the aforementioned discussion on the duality of the KCL and KVL constraints, we get the following observation.

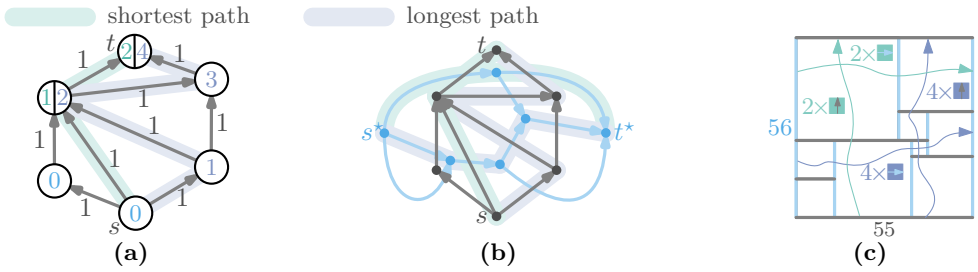

Figure 4.16: We use the example graph of Felsner [Fel13, p.18]. The susceptances are $b \equiv 1$ and we neglect the capacities meaning cap $\equiv \infty$. (a) Assuming unit distances the shortest path $\pi_{\mathsf{SP}}(s,t)$ and longest path $\pi_{\mathsf{LP}}(s,t)$ in the original graph with the corresponding distance labels at the vertices have length 2 and 4, respectively. (b) The shortest and longest path in the primal graph G and dual graph $G^\star$ have the same length. However, adding an edge from s to t describes that this is not always the case. (c) The shortest path $\pi_{\mathsf{SP}}(s,t)$ and longest path $\pi_{\mathsf{LP}}(s,t)$ describe the minimum and maximum number of rectangles (here squares) that are stacked in either directions.

Observation 4.48. *A feasible KVL flow can be computed by a shortest path in the primal graph G.*

Note that a feasible KVL flow is not restricted to shortest paths as long as the voltage angle assignment is unique. Contrary a feasible KCL flow can be computed by a shortest path in the dual graph $G^\star$. This provides us a deeper understanding of why shortest paths work in some cases quite well [Gra+18]. In addition, the maximum flow values of the primal graph $F(G)$ and dual graph $F(G^\star)$ represent upper bounds for the maximum feasible electrical flow.

Lemma 4.49. *A maximum flow (*MF*) in graph G and its dual graph $G^\star$ represent two upper bounds for the* Maximum Power Flow Problem *(*MPFP*).*

However, the electrical flow does not always reach a MF. We discuss this in more detail in Chapters 5 and 6. We use the balancing property in the next section to tackle KCL conflicts.

4.5 An Algorithm for Electrical Flows on s-t Planar Graphs

In this section, we discuss an algorithm for s-t planar graphs for DC FEAS and MPFP. For the algorithm, we mainly use the duality concepts of the aforementioned sections and the reformulation of DC FEAS using simultaneous flow on G and $G^\star$ (Section 4.3.2).

The basic idea of the algorithm is that we switch between the primal graph G and the dual graph $G^\star$ and fix each time the KCL property of the flow that might lead

Algorithm 2: *s-t* Planar DC FEAS($\mathcal{N}$) & *s-t* Planar MPFP($\mathcal{N}$)

```
Data: A network N = ( G, V_G, V_D, cap, b, p_g, p̄_g, p_d, p̄_d ) with |V_G| = 1 (i. e.,
      {s} = V_G), |V_D| = 1 (i. e., {t} = V_D), cap ≡ 0, and cap̄ ≡ ∞.
Result: Flow f(u, w) for all (u, w) ∈ E, flow value F(f, N), and voltage angles θ^v(u)
        with u ∈ V.
1  G = bipolarSubgraphOf(G, s, t);                          ▷ see Section 4.5.1
2  E = planarEmbeddingOf(G);                                ▷ PQ-Tree; see Section 4.5.2
3  (G*, b*, μ_dual : E(G) → E(G*)) = constructDualGraphOf(G(E), b);   ▷ Section 4.5.2
   ▷ Augment flow along an incident edge at source s
4  f ≡ 0; f(s, u) = 1 for some edge (s, u) ∈ E(G);
5  (H, b, s, t) = (G, b, s, t);
6  X = {u ∈ V(H) | f_net(u) ≠ 0};
7  while X ≠ ∅ do                                           ▷ Check KCL property in H
8      f_H = resolveKclConflict(H, X, b, s, t, f_H);
9      (H*, b*, s*, t*) = (H, b, s, t); (H, b, s, t) = dualGraphOf(H*, b*, s*, t*);
10     f_H(e) = f_H*(μ_dual(e)) · b(e);
11     X = {u ∈ V(H) | f_net(u) ≠ 0};                       ▷ New KCL conflicts in the dual graph
12 end
```

to KCL conflict in its dual graph. The property of balancing (see Section 4.4) is used to describe how we fix KCL conflicts and that the algorithm terminates. In Algorithm 2, we show the algorithm to compute an electrical flow in an *s-t* biconnected planar graph. In the following, we will describe each part of the algorithm in more detail.

4.5.1 Bipolar Orientation

In this section, we focus on the function `bipolarSubgraphOf`(G, s, t) in Line 1 of Algorithm 2. Each simultaneous flow has a specific direction, which is naturally given by an electrical flow that is in general a directed acyclic graph (DAG). Another interpretation can be given from the rectangular representation that has a DAG as a visibility graph [Fel13, pp.12f.]. The latter means that there is an edge between two vertices if there is a segment between them. See for example Figure 4.14c, where the horizontal segments u_3 and t are visible to each other, since there is a vertical segment that connects both segments directly. The visibility graph is given in Figure 4.14b, where we represent the visibility of u_3 and t by an edge (u_3, t). So if we define a visibility direction, e. g., from bottom to top (horizontal segment visibility) and from left to right (vertical segment visibility), we get two directed acyclic visibility graphs as shown in Figure 4.14b. Note that the directed acyclic graphs (DAGs) are either called bipolar orientation [FMR95] or *s-t*-numbering [ET76]. Such a numbering gives each

vertex $u \in V$ a number within the range of $[s = 1, \ldots, |V| = t]$, which represents a topological order of the vertices.

Observation 4.50 (Bipolar Duals [Fel13, p.13]). *A bipolar orientation in the primal graph G implies a bipolar orientation in the dual graph $G^\star$.*

To see the latter, observation let us assume a directed edge $(u_1, u_2) \in E(G)$. This edge is incident to two faces $c_1, c_2 \in V(G^\star)$. Looking in the direction of the edge (u_1, u_2), meaning that we look from u_1 to u_2 then the face c_1 is to the left of that edge and c_2 is to the right of that edge. Since we have a bijection of the edges there is an edge $\{c_1, c_2\} \in \overleftrightarrow{E}(G^\star)$. We define that a direction from u_1 to u_2 implies a direction from c_1 to c_2 and thus, a direction from left to right. Thus, if there is a bipolar orientation for graph G this implies a bipolar orientation for its dual graph $G^\star$ by definition. An illustration is given in Figures 4.14 and 4.15 b.

Observation 4.51 (Biconnectivity Assumption [Fel13, p.13]). *If graph G has a bipolar orientation then it is biconnected.*

Calculating a bipolar orientation takes $O(|V|)$ time [Fel13]. An overview of the graph classes that fulfill the latter property are given by Battista ET AL. [Bat+98, p.212, Theorem 6.19]. The most interesting classes to us are planar s-t-graphs, series-parallel digraphs, and planar bipartite digraphs.

4.5.2 Planar Embedding and Dual Graph Construction

Recall that we assume that graph G is planar. To compute a planar embedding $\mathcal{E}$, we use in `planarEmbeddingOf`(G) (Algorithm 2 in Line 2) a linear-time planarity testing algorithm [HT74][RT86, p.345]. These algorithms construct circular lists in $O(|V|)$ that represent for each vertex an ordered list of its incident edges in clock-wise order. The latter represents a set of rotations, which we will use to construct the dual graph $G^\star$. This can be done by selecting any edge $\{u, w\} \in \overleftrightarrow{E}$ and traverse it in one direction such as from u to w. Then select the next edge clockwise at $w \in V$. We proceed this method until we reach u. The walk represents a traversal of a face, where (u, w) represents one boundary edge. We traverse the edge in the other direction meaning (w, u) that gives us the boundary edges of the other face that is incident to edge $\{u, w\} \in \overleftrightarrow{E}$. We proceed with an edge that was not traversed in both direction and apply the aforementioned method. This extracts for each edge the left face c_ℓ and right face c_r with $c_\ell, c_r \in V(G^\star)$ and within that, we construct implicitly the edge $\{c_\ell, c_r\} \in \overleftrightarrow{E}(G^\star)$. The dual graph $G^\star$ of a graph G can be constructed in $O(|V|)$.

Since we use the same construction as Rosenstiehl and Tarjan [RT86, pp.344ff., Section 2], we assume that the graph is biconnected for the aforementioned construction. Otherwise, we add—similar to Rosenstiehl and Tarjan [RT86, p.345]—dummy edges such that G stays planar and becomes biconnected, which is possible in $O(|V|)$.

After the construction of the layout, we will remove the dummy edges, otherwise we would get an electrical flow for another graph than the input graph. In addition, to simplify the translation from one graph into the other one, we define the susceptance $b(e)$ for $e \in \overleftrightarrow{E}(G)$ for the dual graph $G^\star$ by $b^\star(\mu_{\text{dual}}(e)) \coloneqq 1/b(e)$. This is necessary for Line 10 in Algorithm 2.

4.5.3 KCL Conflict Resolution

Recall that an *s-t* electrical flow on planar graphs is a simultaneous flow on G and $G^\star$ with a weighting $b(e)$ for all $e \in E$ that represents the susceptance of an edge (see Equation 4.24). For now, we assume that the source s and the sink t lie on the outer face. From the previous step we have given a plane graph G (i. e., a planar graph with a planar embedding) and its dual graph $G^\star$. We assume that the given bipolar direction represents the direction of an electrical flow. W. l. o. g. we neglect the mapping step by assuming that $f_G \equiv b \cdot f_{G^\star} \equiv f$ meaning a change in f_G represents a direct change in $f_{G^\star}$ without applying an explicit mapping step.

Let the initial flow be $f \equiv 0$. The distance labeling is a function $\theta^v \colon V \to \mathbb{R}_{\geq 0}$ such that the initial labels are $\theta^v \equiv 0$. To find an electrical flow—meaning a feasible electrical flow with capacities $\text{cap} \equiv \infty$—in a plane graph we use the duality between the incidence matrix $\mathbf{I}$ and circuit matrix $\mathbf{B}$ described in the aforementioned section (Lemma 4.19). Initially, we apply one unit of flow to an s incident edge $(s, u) \in E$. Recall that the net flow is defined by $f_{\text{net}}(u) \coloneqq \sum_{\{u,w\} \in \overleftrightarrow{E}} f(u, w)$ for all $u \in V$. Applying a unit flow yields either in an excess at u or if not, we switch the graphs (Algorithm 2 in Line 9). If there is an excess at a vertex $u \in V \setminus \{s, t\}$ then $f_{\text{net}}(u) \neq 0$. Thus, a conflict can be expressed by the net flow (see Definition 4.52).

Definition 4.52 (KCL & KVL Conflict)**.** *A KCL or a KVL conflict at a vertex $u \in V$ is defined by a net flow with an excess unequal zero $f_{\text{net}}(u) \neq 0$ in the primal graph G or dual graph $G^\star$, respectively. We distinguish between the following cases dependent on the net flow $f_{\text{net}}(u)$.*

(CC–1) $f_{\text{net}}(u) > 0$*: Vertex u is defined as temporary source $u_s \in T_s$, and*

(CC–2) $f_{\text{net}}(u) < 0$*: Vertex u is defined as temporary sink $u_t \in T_t$.*

From the previous discussion we know that a conflict resolution in graph G creates a conflict in its dual graph $G^\star$ and vice versa until the flow f corresponds to an electrical flow.

One naïve implementation to solve the KCL conflict would be to define the excess vertices as local source or local sink and run an ordinary flow algorithm. However, using this naïve implementation would skip a feasible solution. The latter approach can lead to an algorithm that does not terminate at all. We made the following observation, which is illustrated in Figure 4.17.

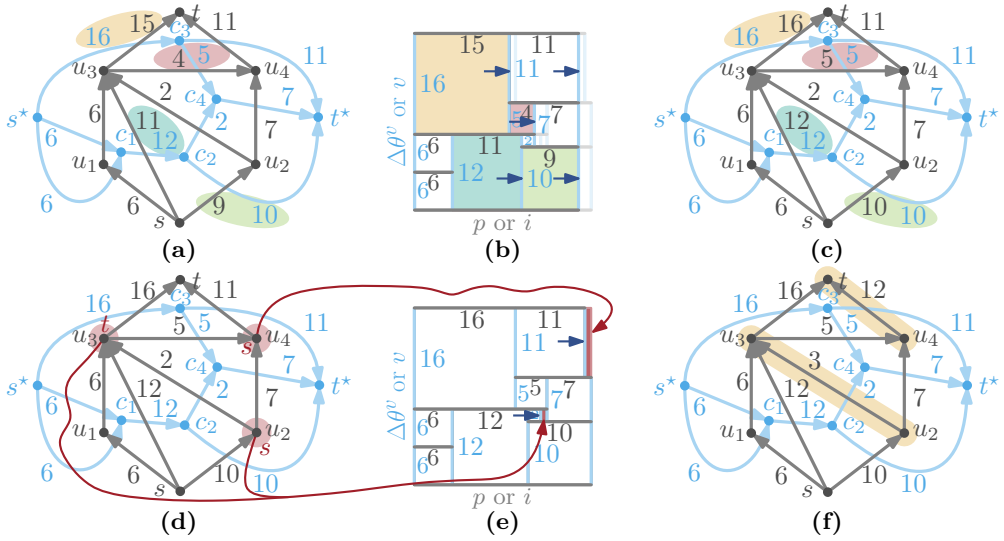

Figure 4.17: A primal graph G and its dual graph $G^\star$ that have each six vertices, nine edges, one source and one sink are shown in (a), (c), (d), and (f). A geometrical representation of both graphs is given in (b) and (e). Each edge in either graphs represents a line segment in the appropriate color and the flow on an edge defines the aspect ratio of a rectangle, e. g., the edges $(c_3, t^\star)$ and (u_4, t) describe the height and width of the upper right rectangle, respectively. (a) A change in flow in the dual graph causes a mapping, which effect is shown in (b) and (c). (b) The mapping causes a rescaling of some rectangles sides, i. e., in this case the width of four rectangles are changed. The outer hull changes from a rectangle to a non-rectangle (shown in the background). (c) After the mapping step the one-to-one-correspondence is retained. (d) In this case the mapping result in a KCL conflict (red) in the primal graph G. (e) Resizing the two rectangles resolves the conflict. (f) The flow on the edges $(u_2, u_3), (u_4, t) \in E(G)$ resolves the conflict.

Observation 4.53 (Resolve KCL Conflicts). *In each* `resolveConflict` *step, we have to minimize the total resizing of the outer rectangle, since a too large increase might skip a valid solution.*

This observation leads us to the definition of a minimum conflict resolution. Recall that a KCL resolution means a KVL resolution in the dual graph. Resolving a KVL conflict leads to an alignment of the length of the longest path $\pi_{\mathsf{LP}}(s,t)$ and the shortest path $\pi_{\mathsf{SP}}(s,t)$ in the dual graph.

Definition 4.54 (Minimal Conflict Resolution). *The shortest path π_{SP} and the longest path π_{LP} are defined by $\pi_{\mathsf{SP}}(s,t) \coloneqq \arg\min_{\pi(s,t)\in\Pi} \sum_{e\in\pi(s,t)} f(e)/b(e)$ with a length of $\Delta\theta^v(\pi_{\mathsf{SP}}(s,t))$ and $\pi_{\mathsf{LP}}(s,t) \coloneqq \arg\max_{\pi(s,t)\in\Pi} \sum_{e\in\pi(s,t)} f(e)/b(e)$ with a length of $\Delta\theta^v(\pi_{\mathsf{LP}}(s,t))$, respectively. A conflict resolution in one graph causes a flow change in either graphs and thus, the minimum conflict resolution is defined in G and $G^\star$ by:*

(CR–1) *Let $\pi_{\mathsf{SP}}(s^\star, t^\star), \pi_{\mathsf{LP}}(s^\star, t^\star) \in \Pi(G^\star)$ then a conflict resolution in $G^\star$ is of minimum size if and only if $\Delta\theta^v(\pi_{\mathsf{SP}}(s^\star, t^\star)) = \Delta\theta^v(\pi_{\mathsf{LP}}(s^\star, t^\star))$.*

(CR–2) *Let $\pi_{\mathsf{LP}}(s,t) \in \Pi(G)$, and let $\Delta\theta^{v\prime}(\pi_{\mathsf{LP}}(s,t))$ and $\Delta\theta^v(\pi_{\mathsf{LP}}(s,t))$ be the longest path before and after the change. Then a conflict resolution in G is minimum if and only if the change of the longest path $\Delta_{\mathsf{LP}}(s,t) \coloneqq \Delta\theta^{v\prime}(\pi_{\mathsf{LP}}(s,t)) - \Delta\theta^v(\pi_{\mathsf{LP}}(s,t))$ is minimized* $\min \Delta_{\mathsf{LP}}(s,t)$.

We call a conflict resolution minimum if and only if CR–1 and CR–2 holds.

The conflict resolution CR–1 does not change the length of the longest path, but adjusts the length of the shortest path to the longest path resulting in a KVL feasible flow. The only conflict resolution that changes the length of the longest path is CR–2. However, this represents the smallest possible change, since we chose the smallest change of the longest path among all choices of changes.

This can be formulated as an LP, where CR–2 is an objective and CR–1 is a constraint. CR–1 is illustrated in Figure 4.17d–f, where the width of the outer rectangle does not change, which is equivalent to not changing longest path. CR–2 is shown in Figure 4.17a–c, where we solved a conflict in the dual graph $G^\star$, which leads in the mapping step to a change of the width (i. e., change in the longest path of the primal graph G). We now use the aforementioned definition (see Definition 4.54) for a minimum conflict resolution to formulate an algorithm for the conflict resolution step `resolveKclConflict`(H, X, s, t, f_H). The set of KCL conflicts is given by $X \coloneqq \{u \in V(H) \mid f_{\text{net}}(u) \neq 0\}$, where H is either G or $G^\star$. The conflict resolution CR–1 implies that the edges for the conflict resolution should lie on path $\pi(s^\star, t^\star)$ with $\pi(s^\star, t^\star) < \pi_{\mathsf{LP}}(s^\star, t^\star)$ of $H^\star =$ `dualGraphOf`(H, s, t). Thus, a possibility is to compute the shortest path graph in $H^\star$. We save all edges in a set of candidate edges E'. We define excesses accordingly by $s, u_s \in T_s$ and $t, u_t \in T_t$.

The conflict resolution CR–2 corresponds to a minimum change of the longest path in H. We have to evenly distribute the flow excess at each vertex $u \in X \subseteq V$ along all paths. Since we wish to minimize $\Delta_{\mathsf{LP}}(s,t) \coloneqq \Delta\theta^v(\pi'_{\mathsf{LP}}(s,t)) - \Delta\theta^v(\pi_{\mathsf{LP}}(s,t))$, we increase the flow only at edges on the shortest paths $\pi_{\mathsf{SP}}(s', t')$ in the dual graph until either s' or t' are saturated.

We augment iteratively one unit of flow along the shortest s-t-path from $s' \in T_s \setminus s$ to $t' \in T_t \setminus t$ using the metric f/b until all $s' \in T_s, t' \in T_t$ have $f_{\text{net}}(u) = 0$ with $u \in (T_s \cup T_t) \setminus \{s, t\}$.

Conjecture 4.55. *Algorithm 2 computes a correct s-t electrical flow of minimum integral size.*

We give an idea how we think the proof could work. Let $f(e)$ be a minimal integral electrical flow. Let $f'(e)$ be some flow with $f'(e) \leq f(e)$ for all $e \in E$ and the flow f' fulfills the KVL. We claim that there is a $f''(e) = f(e)$ for all $e \in E$. Assume that there is an edge $f''(u,t) = f'(u,t) + 1 > f(u,t)$ meaning the flow would skip a

minimal integral solution. This would mean that there is another path from u to t with f'''. Since $\min_{\pi(u,t)\in\Pi} \sum_{(u,v)\in\pi(u,t)} \frac{f(u,v)}{b(u,v)} = \min_{\pi(u,t)\in\Pi} \sum_{(u,v)\in\pi(u,t)} \Delta\theta^v(u,t)$ this represents a contradiction.

We assume that the conjecture is correct for any s-t plane graph G as long as G constitutes an electrical flow. Assuming a graph with $|\overleftrightarrow{E}| = 1$ then applying a flow of $f(s,t) = 1$ along an edge incident to s (which is here the only edge (s,t)) results in a feasible flow f_G in G and in a feasible flow $f_{G^\star}$ in $G^\star$ accordingly.

Now, we assume an arbitrary s-t plane graph G. The construction of the graph is correct (see Section 4.5.2). Since we resolve each conflict optimal meaning using the minimum number of changes in each conflict resolution (see Definition 4.54) and we push only flow in the predefined direction, we get an order of increasing flows and using the minimum conflict resolution does not skip a solution. Since we know that G has an electrical flow the algorithm terminates.

4.6 Conclusion

This chapter provides a thorough analysis of electrical flows. In the beginning, we showed different properties of electrical flows as well as methods that are essential in the first place to design an electrical flow algorithm for planar graphs and matroids. We give a first algorithm for s-t electrical flows that uses electrical preserving transformations and has a running time of $O(|V|^3)$. This is better than the known exponential time algorithm mentioned in Lemma 4.6. Even though both algorithms are constructive and exploit some structure, there is a comparable computation of electrical flows that needs polynomial time for arbitrary networks. To give electrical flows more structure, we present different graph-theoretic representations. These representations help us to separate the quadratic relationship and lead to the balancing property, which will be used in an algorithmic approach that computes s-t electrical flows by using two graphs that are dual (see Section 4.5).

There are still some open conjectures and research questions that we would like to investigate. One of the first questions, we try to investigate is the running time and correctness of Algorithm 2 that depends on the unknown minimum integral generation and demand vector. For arbitrary susceptances b the resolution can have exponential size. However, if we restrict the resolution to some ratio, we might be able to restrict the vector and the running time.

Recall that one assumption on our graphs is that they are planar. On general graphs that cannot be embedded planar on a plane surface (i. e., surface with genus 0), we do not have the concept of faces. However, if we chose a surface with higher genus that allows a plane embedding of the graph, we can make use of the aforementioned algorithms. Thus, we raise the following conjecture.

Conjecture 4.56. [3] *Algorithm 2 or the algorithm from Theorem 4.38 are FPT in the genus.*

We note that computing all s-t electrical flows, adding them, and scaling them leads to a multi-source multi-sink electrical flow algorithm that is not very efficient. Though it might be in general inefficient, it is worth investing these algorithms for dynamic power grids that make use of the s-t-decompositions while starting with some initial electrical flow.

[3] We thank Peter Sanders for the discussion on that topic. In addition, we like to thank Thomas William Brown for mentioning and describing Cohomology to us.

5 Discrete Control Units[1]

Switching – A Temporary Removal of Links and Cables

Future power grids will change towards efficient and environmentally friendly energy operation while handling increasing demands and renewable energy sources [ALH01]. Renewable energy sources are often added to the medium and low voltage layer, leading to a bidirectional power flow which the power grid was not originally designed for. The bidirectional flow dynamically causes new critical lines and instabilities in the power grid and this effect is amplified by the increasing demand. Thus, the network operators have to adapt their power grid to the new challenges by either expanding it (i. e., adding lines) or operating it more efficiently and flexibly by adding control units.

This leads to the *dynamic* and *static transmission design problem* [BPG01a]. Dynamic transmission design [BPG01a, Cho+06, GMM92] is a long-term power grid configuration denoted by Transmission Network Expansion Planning (TNEP) that adds new transmission lines and circuits to the existing power grid. Although adding lines to the power grid decreases the aggregated grid resistance [Cof+14, PH12], it may decrease the operational limit (i. e., a state of power grid congestion is reached earlier). However, it is hard to determine the best power grid topology over a long time horizon for different scenarios. Thus, a subproblem of the dynamic design problem—though less expensive—is the static design problem, which considers the placement of new electrical devices and represents a short-term solution.

For the latter, devices such as circuit breakers (known as *switches*) or FACTS (Flexible AC Transmission Systems) are able to manipulate the power flow by opening a circuit (switching a line off) or routing a certain fraction of power by changing the susceptance at a transmission line, respectively. Switches and FACTS do not intrinsically cause security and reliability problems [Li+13]. However, they are able to reduce the generation costs, while still satisfying the $N-1$ criterion (i. e., power grid elements remain in operation while one element is removed or has a failure) and extending the operability [BPG01b, Lei+15a, Li+13]. While transmission system operators (TSOs) already use switching in certain cases of emergency to decouple parts of the grid, avoid abnormal voltage conditions or improve voltage profiles [FOF08], it is not used to extend the operability of the grid or reduce costs and losses, since TSOs wish to interfere as little as possible with the power grid [2]. However, these interventions are mainly done by rules of thumb, experience or ad-hoc reactions. Our approach tries to structure and improve these interventions.

[1] This chapter is partly published in [Gra+18].

[2] From a conversation with the TSO TransnetBW.

Note that the reliability of the power grid is very important and one would intuitively assume that only TNEP can maintain the power grid's reliability and efficiency. However, both switches and FACTS provide possible control methods for over- and under-voltage situations, line overloads [Gra+06], loss and cost reductions [SG90], improving system security [SG88], and combinations of all [HOO11a]. In addition, in Chapter 6 we show that placing *ideal* FACTS such that the remaining graph is a cactus or tree gives us a cost-equivalent power flow to the minimum cost flow representing a global optimum. Furthermore, the results in Chapter 6 show that placing ideal FACTS in the power grid often increases the operability while lowering the costs. Similar observations were made for switching [HOO11b]. Note that ideal FACTS are more powerful than a combination of FACTS and switches as they can control the power flow without limitations.

In contrast to FACTS and TNEP, transmission switching is a cost-effective way to implement controllability [Xia+16] while using the existing power grid. Most efficiency gains arise while switching branches during peak periods [BB12] though efficiency is not part of the objective. Focusing on increasing the operability during peak periods leads towards the Maximum Flow Problem (MFP) and in terms of power grids towards the Maximum Power Flow Problem (MPFP). Note that the gap between the maximum power flow (MPF) and maximum flow (MF) can be large as Kirchhoff's Voltage Law (KVL) restricts the flow on cycles. Adding switches decreases the gap and leads to the Maximum Transmission Switching Flow Problem (MTSFP). MTSFP tries to use switches to maximize the possible network capacity. Networks with more available capacity are more reliable [HOO10]. Note that AC-feasibility (i. e., deciding whether there is a generator dispatch such that the demand can be satisfied) is already NP-hard on trees [LGH16]. Thus, we use a linearization of the AC power flow, denoted by DC power flow (see Section 3.3.2), where the feasibility is easy to decide. However, MTSFP using DC is already NP-hard (see Section 5.2).

5.1 A Mathematical Model for the Placement of Discrete Control Units

The general feasibility models were introduced in Chapter 3 and a deeper discussion of the DC feasibility problem was given in Chapter 4. The problem we introduce in this section is a Combinatorial Optimization Problem. Note that an optimal solution for switching problems is a subset of the edges E, where the set E of edges represents the set of transmission lines, transformers, phase shifters, and other line-based electrical equipment in a power grid. Every undirected graph can be represented by a directed graph by replacing an undirected edge by two directed edges in either direction. The latter is called a *bidirected graph*. Let $G = (V, E)$ be a bidirected graph with a set of vertices V (also called buses) representing generator vertices $V_G \subseteq V$, consumer

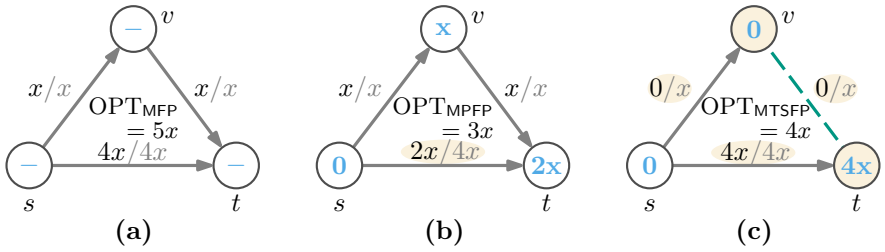

Figure 5.1: A network $\mathcal{N}$ with three vertices and edges, capacities $\mathrm{cap}(u,v)$ (gray), one generator $V_G = \{s\}$, one consumer $V_D = \{t\}$, susceptance $b \equiv 1$ for all $(u,v) \in E$, and voltage angles θ^v (blue) for electrically feasible flows. The successive differences are marked (orange). (a) The MFP($\mathcal{N}$) is the problem that tries to congest all edges and has a value of $\mathrm{OPT}_{\mathsf{MFP}} = 5x$. (b) The MPFP($\mathcal{N}$) with $\mathrm{OPT}_{\mathsf{MPFP}} = 3x$ is restricted by the path with the lowest capacity. (c) Removing an edge with the lowest capacity (dashed line) helps to approach the MF. However, the value of $\mathrm{OPT}_{\mathsf{MTSFP}}$ is $4x$.

vertices $V_D \subseteq V$, and intermediate vertices $V \setminus (V_G \cup V_D)$ such that $V_G \cap V_D = \emptyset$. For simplicity, we use $\overleftrightarrow{E}$ to denote the underlying undirected edge set, and for $e \in E$ we denote by $\overleftrightarrow{e} \in \overleftrightarrow{E}$ the underlying undirected edge, i. e., $\overleftrightarrow{(u,v)} = \overleftrightarrow{(v,u)}$. The power grid is modeled as a network $\mathcal{N} = (G, V_G, V_D, \mathrm{cap}, b, \underline{p_d})$ with a capacity function $\mathrm{cap}\colon E \to \mathbb{R}_{\geq 0}$ representing the thermal line limit of an edge, the susceptance $b\colon E \to \mathbb{R}_{\geq 0}$, and the demands' lower bounds $\underline{p_d}\colon V_D \to \mathbb{R}_{\geq 0}$.

A flow is a function $f\colon E \to \mathbb{R}$ that satisfies the skew-symmetry property $f(u,v) = -f(v,u)$ for all $(u,v) \in E$. Moreover, it has to satisfy the following flow conservation property (Equations 5.1–5.3). For a vertex $u \in V$ the *net flow* is denoted by $f_{\mathrm{net}}(u) \coloneqq \sum_{\{u,v\} \in \overleftrightarrow{E}} f(u,v)$. Similar to Kirchhoff's Current Law (KCL, see Equation 5.1) the conservation of flow describes the flow at each vertex including the consumption or outflow to other network layers, which is bounded by $\underline{p_d} \geq 0$ and often denoted as demand (Equation 5.2), and the generation limits (Equation 5.3).

$$f_{\mathrm{net}}(u) = 0 \qquad \forall u \in V \setminus (V_G \cup V_D), \tag{5.1}$$

$$-\infty \leq f_{\mathrm{net}}(u) \leq -\underline{p_d}(u) \qquad \forall u \in V_D, \tag{5.2}$$

$$0 \leq f_{\mathrm{net}}(u) \leq \infty \qquad \forall u \in V_G. \tag{5.3}$$

A flow f is *feasible* if it obeys the thermal limits given by the capacity constraints (Equation 5.4).

$$|f(u,v)| \leq \mathrm{cap}(u,v) \qquad \forall (u,v) \in E. \tag{5.4}$$

The *flow value* $F(\mathcal{N}, f)$ of a flow f on $\mathcal{N}$ is defined by $\sum_{u \in V_G} f_{\mathrm{net}}(u)$. A feasible flow f on $\mathcal{N}$ maximizing $F(\mathcal{N}, f)$ is called a maximum flow (MF) and the problem of

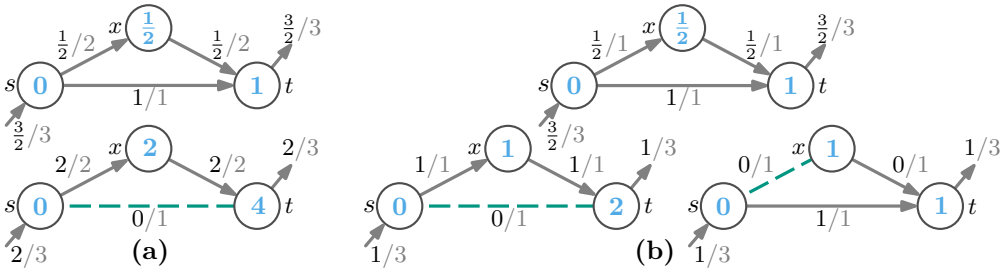

Figure 5.2: The Braess's Paradox highly depends on the network's parameter. A general observation on that was already given by Pas and Principio [PP97]. This example network consists of three vertices, three edges, one generator, one load, susceptances $b \equiv 1$, and different capacity $\mathrm{cap}(e)$ settings (gray) for all $e \in E$. (a) The capacities are chosen in such a way that switching is beneficial in that particular network $\mathcal{N}$. The MPFP has a value of $\mathrm{OPT}_{\mathrm{MPFP}}(\mathcal{N}) = 3/2$, whereas the MTSFP has a value of $\mathrm{OPT}_{\mathrm{MTSFP}}(\mathcal{N}) = 2$. (b) The capacities of the edges (s, x) and (x, t) are set to 1. This small reconfiguration makes switching not beneficial anymore, since the MPFP has a value of $\mathrm{OPT}_{\mathrm{MPFP}} = 3/2 = \mathrm{OPT}_{\mathrm{MTSFP}}$ and any switching has a value of 1.

finding such a flow is denoted by $\mathrm{MFP}(\mathcal{N})$. Its value is denoted by $\mathrm{OPT}_{\mathrm{MFP}}(\mathcal{N}) := \max_f F(\mathcal{N}, f)$ (see Figure 5.1a).

However, a feasible flow neglects some physical constraints of a power flow denoted as Kirchhoff's Voltage Law (KVL, Equation 5.5).

$$b(u,v) \cdot (\theta^v(u) - \theta^v(v) - \theta^v_{\mathrm{shift}}(u,v)) = f(u,v) \qquad \forall (u,v) \in E, \tag{5.5}$$

$$\underline{\theta^v}(u) \leq \theta^v(u) \leq \overline{\theta^v}(u) \qquad \forall u \in V, \tag{5.6}$$

where the voltage angle is a function $\theta^v \colon V \to \mathbb{R}$ describing the potential at each vertex. In general, absolute voltage angles are used, i. e., the angle of one vertex—often the slack—is set to zero and the others are determined from it [see Bol98, p. 40]. A deeper discussion of the latter is available in Section 4.1. The voltage angle $\theta^v(u)$ of a vertex $u \in V$ is often limited to $|\theta^v(u)| \leq 0.6$ radians (see Equation 5.6) to improve the running time [BBB12, FOF08], but this may result in non-optimal solutions or no solution at all. Note that the voltage angle differences are already covered by the capacity constraint (Equation 5.4) and thus, the constraint is not mentioned here. In addition, in most IEEE examples and related works $\theta^v_{\mathrm{shift}} \equiv 0$ representing the transformer (phase shifter) final angle. The latter means that we assume to have neither FACTS nor phase shift transformers on the lines. Thus, we neglect them in the following.

We call a feasible flow complying with Equations 5.5 and 5.6 a *feasible electrical flow*. A feasible electrical flow f on $\mathcal{N}$ that maximizes $F(\mathcal{N}, f)$ is called a maximum power flow (MPF). The corresponding problem is called the Maximum Power Flow

Problem (MPFP) and is denoted by MPFP($\mathcal{N}$). The value of MPFP($\mathcal{N}$) is denoted by $\mathrm{OPT}_{\mathrm{MPFP}}(\mathcal{N})$ and is defined by $\max_f F(\mathcal{N}, f)$ (see Figure 5.1b).

For a subset $S \subseteq \overleftrightarrow{E}$ we consider the graph $G-S$ and the corresponding network $\mathcal{N}-S$ where the functions cap and b are restricted to $E \setminus S$. We call S the set of switched edges (i. e., the switch is in OFF-state for these edges). Typically not all possible switchings are feasible. Feasibility in this context means that there is an electrically feasible flow in $\mathcal{N} - S$. The problem of maximizing the flow value in $\mathcal{N}$ while allowing edges to be switched is called Maximum Transmission Switching Flow Problem (MTSFP) and its value is denoted by $\mathrm{OPT}_{\mathrm{MTSFP}}(\mathcal{N}) := \max_{S \subseteq \overleftrightarrow{E}} \mathrm{OPT}_{\mathrm{MPFP}}(\mathcal{N} - S)$ (see Figure 5.1c). Such a flow obeys Equations 5.1–5.3 and 5.8–5.10. Note that switching is not always beneficial as shown in Figure 5.2b.

Maximum Transmission Switching Flow Problem MTSFP($\mathcal{N}$)

Instance: A network $\mathcal{N}$.

Objective: Find a set $S \subseteq \overleftrightarrow{E}$ of switched edges such that $\mathrm{OPT}_{\mathrm{MPFP}}(\mathcal{N} - S)$ is maximum among all choices of switched edges S.

To model switching an edge we introduce a function $z\colon E \to \{0, 1\}$, which is 0 if an edge is switched and 1 otherwise. To enforce the switching, the flow must be zero on the switched edges. We therefore replace Equation 5.4 with Equation 5.8. This change is not yet sufficient, since the KVL (Equation 5.5) shall only apply to the non-switched edges. Hence, we modify this equation to Equation 5.7.

$$b(u,v) \cdot z(u,v) \cdot (\theta^v(u) - \theta^v(v)) = f(u,v) \qquad \forall (u,v) \in E, \tag{5.7}$$

$$|f(u,v)| \leq z(u,v) \cdot \mathrm{cap}(u,v) \qquad \forall (u,v) \in E. \tag{5.8}$$

Equation 5.7 can be linearized by either adding two big-M constraints (Equations 5.9 and 5.10) or one indicator constraints (Equation 5.11), where M is a suitably large constant.

$$b(u,v) \cdot (\theta^v(u) - \theta^v(v)) + (1 - z(u,v))M \geq f(u,v) \quad \forall (u,v) \in E, \tag{5.9}$$

$$b(u,v) \cdot (\theta^v(u) - \theta^v(v)) - (1 - z(u,v))M \leq f(u,v) \quad \forall (u,v) \in E, \tag{5.10}$$

$$z(u,v) = 1 \Rightarrow b(u,v) \cdot (\theta^v(v) - \theta^v(u)) = f(u,v) \quad \forall (u,v) \in E. \tag{5.11}$$

The parameter M must be reasonably large to not impose any implicit voltage angle difference limit at the edge $(u,v) \in E$. In general, one can choose M for each edge $(u,v) \in E$ by $M(u,v)$ equal to $\max\left\{\sum_{e \in \pi(u,v)} b(e)^{-1}\mathrm{cap}(e)\right\}$, where the maximum ranges over all simple paths $\pi(u,v)$ from u to v. It then suffices to set $M = \max_{(u,v)\in E} M(u,v)$ [BPG01a]. However, it is NP-hard to calculate the longest path [KMR97]. It is simpler to set $M(u,v) = b(u,v) \cdot \sum_{e \in E} \mathrm{cap}(e)/b(e)$. If we restrict the voltage angle θ^v to 0.6 radians in Equation 5.6, which is common [BBB12, Hed+10],

we can use $M(u,v) = 1.2 \cdot |b(u,v)|$. Note that this decreases the solution space and possibly removes feasible and optimal solutions. Thus, this restriction can improve the running time, but might lead to other results and is thus debatable, from a physical point of view. In general, we have lower and upper bounds for generators $\underline{p_g}, \overline{p_g} \colon V_G \to \mathbb{R}_{\geq 0} \cup \{\infty\}$, and demands $\underline{p_d}, \overline{p_d} \colon V_D \to \mathbb{R}_{\geq 0} \cup \{\infty\}$ for $u \in V_D$ such that Equations 5.2 and 5.3 become Equations 5.12 and 5.13, respectively, and the network is defined by $\mathcal{N} = (G, V_G, V_D, \text{cap}, b, \underline{p_g}, \overline{p_g}, \underline{p_d}, \overline{p_d})$. A network with these additional bounds is called *bounded*.

$$-\overline{p_d}(u) \leq f_{\text{net}}(u) \leq -\underline{p_d}(u) \qquad \forall u \in V_D \tag{5.12}$$

$$\underline{p_g}(u) \leq f_{\text{net}}(u) \leq \overline{p_g}(u) \qquad \forall u \in V_G \tag{5.13}$$

A MTSF obeying the latter constraints is a *bounded* MTSF. Note that fixing the demands $\underline{p_d}(u) = \overline{p_d}(u) = p_d(u)$ and generations $\underline{p_g}(u) = \overline{p_g}(u) = p_g(u)$ leads to a Direct Current Feasibility Problem (DC FEAS) also known as Power Flow (PF) that is the search for a feasible electrical flow by given demands and generations. We discussed the latter problem in more detail in Chapter 4.

Suppose every generator $u \in V_G$ has its own generation cost function $\gamma_u \colon \mathbb{R} \to \mathbb{R}_{\geq 0}$ representing the cost for generating the power $f_{\text{net}}(u)$. The problem of minimizing the generation costs of all generators $u \in V_G$ while maintaining a feasible electrical flow in a bounded network with $\underline{p_d}(u) = \overline{p_d}(u) = p_d(u)$ (i. e., Equations 5.1, 5.4–5.6, 5.12 and 5.13) is called Optimal Power Flow Problem OPFP($\mathcal{N}$). The value of OPFP($\mathcal{N}$) is denoted by $\text{OPT}_{\text{OPFP}}(\mathcal{N}) = \min \sum_{u \in V_G} \gamma_u(f_{\text{net}}(u))$. The problem of finding a flow with value $\text{OPT}_{\text{OPFP}}(\mathcal{N})$ by allowing edges to be switched (i. e., Equations 5.1, 5.6, 5.8–5.9, 5.12 and 5.13) is called Optimal Transmission Switching Problem OTSP($\mathcal{N}$) with value $\text{OPT}_{\text{OTSP}}(\mathcal{N}) = \min_{S \subseteq \overleftrightarrow{E}} \text{OPT}_{\text{OPFP}}(\mathcal{N}-S)$ with S being the set of switched edges.

Optimal Transmission Switching Problem OTSP($\mathcal{N}$)

Instance: A network $\mathcal{N}$.

Objective: Find a set $S \subseteq E$ and an electrically feasible flow f in $\mathcal{N} - S$ such that the sum of the generation costs $\sum_{u \in V_G} \gamma_u\left(f_{\text{net}}(u)\right)$ is minimized.

Note that neither the MTSFP nor the OTSP minimize the number of switches. This would result in a min-max-problem that is harder to solve than the presented basic variants (see Section 5.2 on Page 111). From Lehmann et al. [LGH15, Lemma 4] it further follows that the MTSFP and the Maximum FACTS Flow Problem (MFFP) are polynomial-time solvable on trees. Thus, for trees we get the following relationship.

$$\text{OPT}_{\text{MPFP}}(\mathcal{N}) = \text{OPT}_{\text{MTSFP}}(\mathcal{N}) = \text{OPT}_{\text{MFFP}}(\mathcal{N}) = \text{OPT}_{\text{MFP}}(\mathcal{N}).$$

If it is clear, which network is being referred to, we may omit the explicit reference $\mathcal{N}$ and write $\mathcal{P}$ and $\mathrm{OPT}_{\mathcal{P}}$ instead of $\mathcal{P}(\mathcal{N})$ and $\mathrm{OPT}_{\mathcal{P}}(\mathcal{N})$, where $\mathcal{P}$ is a particular problem (e. g., MTSFP). The common constraints of MTSFP and OTSP are the base constraints for the Restoration Order Problem (ROP) [CH15, HCB11] and TNEP [HHK13].

Table 5.1: Overview of known results on the complexity of the MTSFP and OTSP. The complexity increases from top to bottom as shown in the hardness column. Note that the major aspects that influence the complexity of the problem are the graph structure of G, the number of generators V_G, the number of consumers V_D, the susceptance b, and the capacity cap. If there are multiple results or if the results differ for MTSFP and OTSP, we colored the relating entries in green.

	Problem	Network Properties						Complexity		Algorithms		
		Graph Structure	Example	$\lvert V_G\rvert$	$\lvert V_D\rvert$	b	cap	Hardness	Reference	Name	b	cap
1	MTSFP and OTSP	tree graphs	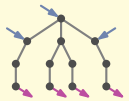	∞	∞	–	–	polynomial-time solvable	Lemma 4.9, Theorem 6.5, Section 3.2 p. 30	MF	∞	∞
2	MTSFP and OTSP	penrose-minor-free graphs		1	1	–	–	polynomial-time solvable	Sections 5.4 and 5.5	DTP	∞	∞
3	MTSFP and OTSP	series-parallel graphs	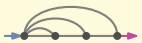	1	1	∞ ∞	∞ 1	NP-hard	[Koc+16] Section 5.2	–	–	–
4	MTSFP and OTSP	cacti with maximum degree of 3		∞	∞	1	∞	NP-hard	[LGH14]	MaxST (see Section 5.6)	–	–
5	MTSFP and OTSP	2-level trees	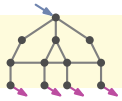	1	∞	∞	∞	NP-hard	[LGH14]	–	–	–
6	MTSFP and OTSP	planar graph with max degree of 3	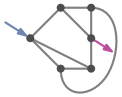	1	1	∞	1	strongly NP-hard	[LGH14]	–	–	–
7	MTSFP OTSP	arbitrary graphs	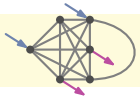	2 1	2 ∞	∞	∞	non-APX	[LGH14] [LGH14]	–	–	–

5.2 Complexity Considerations of using Discrete Control Units

In Section 5.1, we showed that switching introduces a quadratic constraint (see Equation 5.7). Note that models with quadratic constraints and linear objectives are in general NP-hard [Sah74, page 278]. The proof uses a reduction from the Subset Sum Problem (SSP; see Garey and Johnson [GJ79, p.245, MP2] and Ausiello et al. [Aus+99, p.447, MP5] for more information). However, the quadratic constraint can be replace by a big-M constraint (see Equations 5.9 and 5.10) or an indicator constraint (see Equation 5.11). Thus, we lose the bilinearity and the constraint becomes linear.

Problem Definitions. In Section 5.1, we already defined the optimization problems MTSFP and OTSP. However, in this section we give a finer granularity of the problem definitions concerning switching to increase the understanding of the different problems that can be tackled. The first problem considers switching with a fixed number of preinstalled switches—meaning $S \subseteq \overleftrightarrow{E}$ is already given—and is called $\mathrm{MTSFP}(\mathcal{N}, S)$ and its value is defined by $\mathrm{OPT}_{\mathrm{MTSFP}}(\mathcal{N}, S) := \max_{\{z(e)\in\{0,1\}\mid e\in S\}} \mathrm{OPT}_{\mathrm{MPFP}}(\mathcal{N} - \bigcup\{e \mid e \in S \wedge z(e) = 0\})$. The problem is defined in the following.

MTSF Problem with Fixed Switches $\mathrm{MTSFP}(\mathcal{N}, S)$

Instance: A network $\mathcal{N}$ and a set $S \subseteq \overleftrightarrow{E}$.

Objective: Find a switching $z(e) \in \{0, 1\}$ for all $e \in S$ such that $\mathrm{OPT}_{\mathrm{MPFP}}(\mathcal{N} - \{e \mid e \in S \wedge z(e) = 0\})$ is maximum among all choices of z.

The next problem definition will be the first placement problem that relaxes the definition in the sense that only the number of switches is fixed by $k \in \mathbb{N}$ with $|S| = k$, but the placement of the switches—meaning the set $S \subseteq \overleftrightarrow{E}$—is unknown. Thus, we are interested in a maximum possible flow for a network $\mathcal{N}$ and a fixed number of switches $|S| = k$. The problem is called $\mathrm{MTSFP}(\mathcal{N}, k)$ and its value is defined by $\mathrm{OPT}_{\mathrm{MTSFP}}(\mathcal{N}, k) := \max_{S\subseteq\overleftrightarrow{E}} \mathrm{OPT}_{\mathrm{MPFP}}(\mathcal{N} - S)$ with $|S| = k$.

MTSF Problem with k-Switches $\mathrm{MTSFP}(\mathcal{N}, k)$

Instance: A network $\mathcal{N}$ and a parameter $k \in \mathbb{N}$.

Objective: Find a set $S \subseteq \overleftrightarrow{E}$ of switches with $|S| = k$ such that $\mathrm{OPT}_{\mathrm{MPFP}}(\mathcal{N} - S)$ is maximum among all choices of S.

Assume that we have no limitation on the number of switches—meaning the number of switches can be $|S| = |\overleftrightarrow{E}| = k$. Thus, the problem to find a maximum power flow in network $\mathcal{N}$ by allowing as many switches as possible (i. e., some $k \in \mathbb{N}$) is called $\mathrm{MTSFP}(\mathcal{N})$ with value $\mathrm{OPT}_{\mathrm{MTSFP}}(\mathcal{N}) := \max_k \mathrm{OPT}_{\mathrm{MTSFP}}(\mathcal{N}, k)$.

Maximum Transmission Switching Flow Problem MTSFP($\mathcal{N}$)	
Instance:	A network $\mathcal{N}$.
Objective:	Find a set $S \subseteq \overleftrightarrow{E}$ of switched edges such that $\mathrm{OPT}_{\mathrm{MPFP}}(\mathcal{N} - S)$ is maximum among all choices of switched edges S.

The latter problem allows as many switches as necessary to obtain a best possible power flow. However, when there is only one generator and one demand the maximum number of switches $|S|$ is restricted by $|V| - 1$ that represents a tree. Removing more edges would lead—independent on the generation limits—to an infeasible solution, since some demands are cut-off from any generator. If we have multiple generators and demands the maximum number would be restricted by a forest $|V| - k$, where k represents the number of connected components. Note that the number of connected components can be still $k = 1$.

In general an desirable investigation is the minimum number of switches—meaning the smallest k—such that we get the same value as $\mathrm{OPT}_{\mathrm{MTSFP}}(\mathcal{N})$. This problem is called $\mathrm{OPT}_{\mathrm{MNSP}}(\mathcal{N}) := \min_{\mathrm{OPT}_{\mathrm{MTSFP}}(\mathcal{N},k)=\mathrm{OPT}_{\mathrm{MTSFP}}(\mathcal{N})} k$ with the value $\mathrm{OPT}_{\mathrm{MTSFP}}(\mathcal{N})$.

Minimum Number of Switches Problem under MTSF MNSP($\mathcal{N}, k$)	
Instance:	A network $\mathcal{N}$ and $k \in \mathbb{N}$.
Question:	Is it possible to remove a set of edges $S \subseteq E$ such that $k = \lvert S \rvert$ is minimum among all choices of $\mathrm{OPT}_{\mathrm{MTSFP}}(\mathcal{N})$?

Note that similar definitions can be made for the OTSP. An overview of the switching related problems is given in Appendix A.3.

Decision Problems. MTSFP is an optimization problem that involves searching for the best solution from some large set of solutions. Any optimization problem can be transformed into a decision problem by asking whether the optimum value is at least or at most k for some $k \in \mathbb{R}$. We denote the corresponding decision problem for MTSFP($\mathcal{N}$) by k-MTSFP.

k-Maximum Transmission Switching Flow Problem k-MTSFP($\mathcal{N}, k$)	
Instance:	A network $\mathcal{N}$ and $k \in \mathbb{Q}_{\geq 0}$.
Question:	Is it possible to remove a set of edges S such that there is an electrically feasible flow f in $\mathcal{N} - S$ with flow value $F(\mathcal{N} - S, f) \geq k$?

Note that decision problems are often used to show that a particular problem is NP-hard. We will use this problem in Section 5.2.2 to show that MTSFP($\mathcal{N}$) is NP-hard. An overview of the switching decision problems can be found in Appendix A.3.

5.2.1 Literature Overview

We will see in Definition 5.14 (see also Section 5.4.4 and Figure 5.11) that for single-source single-sink penrose-minor-free graphs (see Table 6.1–1) the MTSFP($\mathcal{N}$) is polynomial-time solvable. We will look at this structure in Section 5.4.1. However, Kocuk ET AL. [Koc+16] showed that for arbitrary susceptance b and capacity cap this problem is already NP-hard[3]. In Section 5.2.2, we will provide a different reduction that is also a generalization of the proof of Kocuk ET AL. [Koc+16]. Contrary to series-parallel graphs, cactus graphs have the special property that the cycles in a cactus do not share an edge. Thus, the dependencies on the voltage angles of a vertex decrease. Though, for single-source single-sink this problem is polynomial-time solvable, it becomes already NP-hard for an arbitrary number of generators and consumers (see Table 6.1–3). Lehmann ET AL. [LGH14, pp.8ff., Section 5] motivated another non-standard graph structure from the disaster management. The idea is that after a blackout a TSO will try to recover the power grid by establishing a tree-like structure. The graph structure is denoted by N-level tree (see Table 6.1–4), which has a generator at the root and consumers at the leaves. For each level there is a total order of the vertices that also defines the intra-level neighbors of a vertex. The tree allows intra-level connections to direct neighbors. Note that these intra-level connections cause cycles that share edges with other cycles. Thus, this structure is more complex than a cactus. The next graph structure that is more complex are planar graphs (see Table 6.1–5) for which Lehmann ET AL. [LGH14, p.13, Section 7] show that the problem is strongly NP-hard for planar graphs with maximum degree of 3, one generator, one consumer, and having unit capacities. Naturally this problems stays NP-hard for arbitrary graphs, but it is not possible for any $\epsilon > 0$ to find an approximation algorithm within a factor of $2^{O((\log n)^{1-\epsilon})}$ [LGH14, pp.10ff.] [KMR97, pp.95ff.].

5.2.2 NP-hardness of Source-Sink-MTSF on Series-Parallel-Graphs

First we prove that MTSFP is in NP by providing a polynomial time algorithm that is denoted by $\texttt{valid}(\mathcal{N}, S)$. The polynomial algorithm specifies whether the set of switched edges S is a valid solution for an instance $\mathcal{N}$. It is not hard to determine that an instance $\mathcal{N}$ and a solution S are properly defined (Section 5.1). Checking whether a switching S provides an electrically feasible flow that is at least k can be done by LINEAR PROGRAMMING (LP) in polynomial time (see Section 5.1).

To show that k-MTSFP is also NP-hard we reduce the SUBSET SUM PROBLEM to k-MTSFP.

[3] We found out about that proof after the publication of the later proof in [Gra+18] thanks to Thomas William Brown.

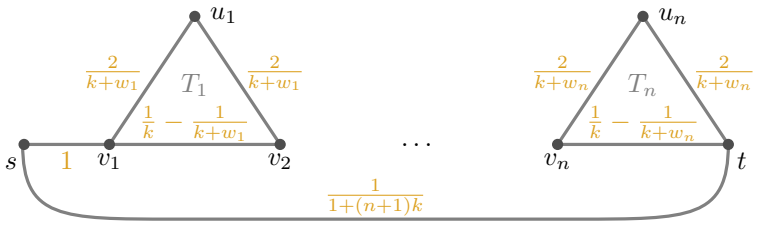

Figure 5.3: A network $\mathcal{N}$ constructed from an instance of SSP having one source $s \in V_G$ (i. e., $|V_G| \equiv 1$) and one sink $t \in V_D$ (i. e., $|V_D| \equiv 1$). All edges $(u, v) \in E$ have a capacity of cap $\equiv 1$ and the susceptances b are shown next to the edges.

Subset Sum Problem SSP(W, k)	
Instance:	A finite set of numbers $W = \{w_1, w_2, \ldots, w_n\}$ with $w_i \in \mathbb{N}$ and a $k \in \mathbb{N}$.
Question:	Is there a set of elements $x_1, \ldots, x_n \in \{0, 1\}$ such that $\sum_{j=1}^{n} w_j x_j = k$?

Lemma 5.1. *k-MTSFP is NP-complete even if there is only one source and one sink in the network and all edge capacities are* 1.

Proof. We show the NP-hardness by reducing SSP to this restricted MTSFP-variant in polynomial time. Since SSP is weakly NP-complete [GJ79], MTSFP is NP-hard, too. Given an SSP-instance (W, k) we construct an instance of MTSFP that allows a flow of 2 if and only if there is a solution of the SSP-instance. We may assume without loss of generality that no element of W is larger than k as these elements are never part of any solution. In the constructed network $\mathcal{N}$ there is one source $\{s\} =: V_G$ (i. e., $|V_G| \equiv 1$) and one sink $\{t\} =: V_D$ (i. e., $|V_D| \equiv 1$; see Figure 5.3). All edges $e \in E$ have capacity cap $\equiv 1$. There is one edge from s to t with susceptance $1/(1+(n+1)k)$, where $n = |W|$. For each element $w_i \in W$ we build a triangle with vertices v_i, u_i, and v_{i+1}. We set $b(v_i, u_i) := b(u_i, v_{i+1}) := 2/(k+w_i)$ and $b(v_i, v_{i+1}) := 1/k - 1/(k+w_i)$. Note that the triangles for w_i and w_{i+1} have the vertex v_{i+1} in common. We set $v_{n+1} = t$ and add the edge (s, v_1) with susceptance $b(s, v_1) = 1$. Note that the edge (s, v_1) is necessary when we do not switch any triangle, since this would exceed the flow of one in the upper part.

To achieve a flow of 2 in the network both edges incident to s must be saturated. In particular, the flow through the chain of triangles is 1 and $\Delta\theta^v(s, t) = 1 + (n + 1)k$. Consider the triangle T_i for the element $w_i \in W$. In this triangle v_i acts as a source and v_{i+1} as a sink. There are two paths from v_i to v_{i+1} in T_i: The direct path consisting only of the edge (v_i, v_{i+1}) and the path via u_i. In any solution to $\mathcal{N}$ at most one of these

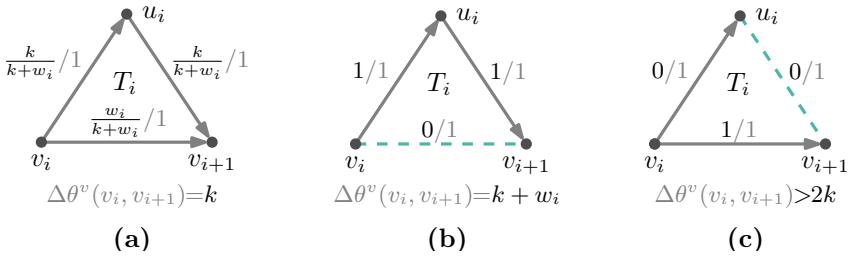

Figure 5.4: Possible ways to switch the triangles T_i in a network $\mathcal{N}$ with corresponding angle differences and flows. (a) If no edges are switched the angle difference is k. (b) If the edge (v_i, v_{i+1}) is switched, the angle difference is $k + w_i$. (c) If an edge incident to u_i is switched, the angle difference is larger than $2k$.

paths may be switched as otherwise the total flow in $\mathcal{N}$ is at most 1. If no edge in T_i is switched (Figure 5.4a), we obtain $\Delta\theta^v(v_i, v_{i+1}) \equiv k$ for one unit flowing through T_i. If the edge (v_i, v_{i+1}) is switched (Figure 5.4b), we have $\Delta\theta^v(v_i, v_{i+1}) = k + w_i$. If an edge incident to u_i is switched (Figure 5.4c), the flow on (v_i, v_{i+1}) must be equal to 1 and we get

$$\Delta\theta^v(v_i, v_{i+1}) = \frac{1}{\frac{1}{k} - \frac{1}{k+w_i}} = \frac{k(k+w_i)}{w_i} = \frac{k^2}{w_i} + k > 2k.$$

Note that in any case $\Delta\theta^v(v_i, v_{i+1}) \geq k$. If in any triangle T_i an edge incident to u_i is switched, we have

$$\begin{aligned}\Delta\theta^v(s,t) &= \Delta\theta^v(s, v_1) + \sum_{i=1}^{n} \Delta\theta^v(v_i, v_{i+1}) \\ &> 1 + (n-1)k + 2k = 1 + (n+1)k,\end{aligned}$$

which contradicts $\Delta\theta^v(s,t) = 1 + (n+1)k$. Hence, only the edges (v_i, v_{i+1}) for $i = 1, \ldots, n$ may be switched.

If there is a set S of edges in $\mathcal{N}$ such that removing them from the network yields a maximum flow f in $\mathcal{N} - S$ with throughput $F(\mathcal{N}, f) \equiv 2$, we can construct a solution to the corresponding SSP-instance as follows. Let $x_i = 1$ if $(v_i, v_{i+1}) \in S$ and $x_i = 0$ otherwise. By the argumentation above we have $\Delta\theta^v(v_i, v_{i+1}) = k + w_i$ if $x_i = 1$

and $\Delta\theta^v(v_i, v_{i+1}) = k$ otherwise. Hence, we have

$$\begin{aligned} 1 + (n+1)k &= \Delta\theta^v(s,t) \\ &= \Delta\theta^v(s,v_1) + \sum_{i=1}^{n} \Delta\theta^v(v_i, v_{i+1}) \\ &= 1 + \sum_{i=1}^{n} (k + x_i w_i) \\ &= 1 + nk + \sum_{i=1}^{n} x_i w_i. \end{aligned}$$

and therefore $\sum_{i=1}^{n} x_i w_i = k$ as required by the SSP-instance.

If the SSP-instance has a solution, i. e., $\sum_{i=1}^{n} x_i w_i = k$ for a suitable assignment of the x_i, we define $S := \{(v_i, v_{i+1}) \mid x_i = 1\}$. We claim that after switching these edges the remaining network $\mathcal{N} - S$ admits a power flow with value 2. Setting $\theta^v(s) = 0$ and $\theta^v(v_i) = 1 + \sum_{j=1}^{i-1}(k + x_i w_i)$ induces a feasible electrical flow of 1 on the triangle chain by the arguments above. We further note that

$$\begin{aligned} \Delta\theta^v(s,t) &= \Delta\theta^v(s,v_1) + \sum_{i=1}^{n} \Delta\theta^v(v_i, v_{i+1}) \\ &= 1 + \sum_{i=1}^{n} (k + x_i w_i) \\ &= 1 + nk + \sum_{i=1}^{n} x_i w_i \\ &= 1 + (n+1)k. \end{aligned}$$

Hence, we have $f(s,t) \equiv 1$ and the total flow in $\mathcal{N} - S$ is 2.

The size of the constructed network is linear in $|W|$ and all parameters are polynomial in k. Hence, the reduction from SSP to MTSFP runs in polynomial time. Since SSP is NP-complete [GJ79], this reduction implies that MTSFP is NP-hard even if we restrict ourselves to networks with unit capacities and only one source and one sink. □

5.3 Network Modeling

The model presented in Section 5.1 places no restriction on the network. Our algorithms and proofs are often simpler if the underlying network has a specific form.

Without loss of generality we may assume that in the network $\mathcal{N} := (G, V_G, V_D, \text{cap}, b, \underline{p_d})$ all generators and consumers are degree-1 vertices. We achieve this by adding an edge with infinite capacity and a susceptance of 1 between each generator

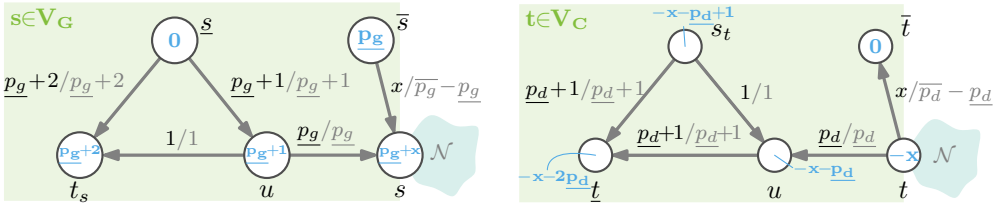

(a) (b)

Figure 5.5: A bounded network can be transformed to an unbounded network by adding substructures to its generator and consumer vertices. (a) A generator $s \in V_G$ in a bounded MTSFP can be transformed to a generator in an unbounded MTSFP by modifying the network $\mathcal{N}$ at the source. Thereby, a generator with non-zero lower bound generation can be replaced by a construction of a cycle with generator $\underline{s}$ and consumer t_s forcing a generation of $\underline{p_g}$ on edge (u, s), and a generator $\bar{s}$ allowing a generation in total of up to $\overline{p_g}$ at vertex s. (b) For consumers t to model the upper bound it suffices to add an edge $(\bar{t}, t)$ and a minimum demand of $\underline{p_d}$ to $\bar{t}$. To model the lower bound, a triangle that configures the voltage angles in such a fashion that there is a feasible power flow only if at least the lower demand is satisfied.

or consumer $v \in (V_G \cup V_D)$ and a new vertex u_v. The new vertex u_v then acts as a generator or consumer and v becomes an intermediate vertex. We use this assumption especially in Section 5.4, where we restrict our network to certain graph classes.

We can shrink the network $\mathcal{N}$ by contracting degree-2 vertices. For this we introduce the *susceptance norm* of a path $\pi(u, v)$, which is defined as

$$\|\pi(u,v)\|_b := \sum_{e \in \pi(u,v)} b(e)^{-1}, \tag{5.14}$$

and gives us a distance metric on power grids. The susceptance norm is a norm, since it fulfills the axioms given by Banach [Ban22].

1. $\|\vec{x}\| \equiv 0$ if and only if $\vec{x} \equiv \vec{0}$ (neutral element),
2. $\|s \cdot \vec{x}\| \equiv |s| \cdot \|\vec{x}\|$ (absolute homogeneity),
3. $\|\vec{x} + \vec{y}\| \leq \|\vec{x}\| + \|\vec{y}\|$ (triangular inequality).

Applying the following lemma we can simplify $\mathcal{N}$ by contracting paths to single edges.

Lemma 5.2. *A simple path π in $\mathcal{N}$ whose internal vertices have degree 2 in $\mathcal{N}$ and are neither generators nor consumers is equivalent to a single edge e with capacity* $\text{cap}(e) := \min_{(u,v)\in\pi} \text{cap}(u, v)$ *and susceptance* $b(e) := 1/\|\pi\|_b$.

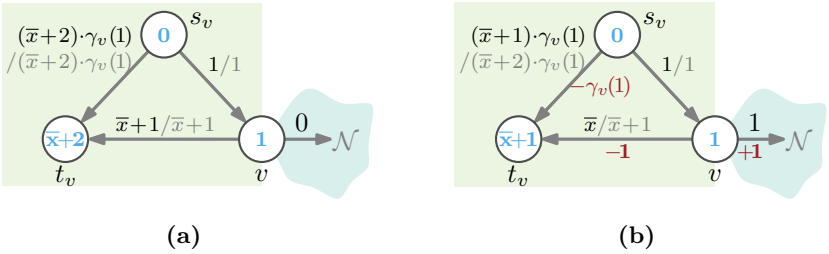

Figure 5.6: Transforming an OTSP-instance to an MTSFP-instance is possible by adding triangles at consumer vertices. The edge $e = (s_v, t_v)$ and the other two edges have susceptances $b(e) = \gamma_v(1)$ and 1, respectively. (a) The maximum flow in a triangle is obtained by injecting no power to the network $\mathcal{N}$ from v. (b) Per injected unit of flow from v to $\mathcal{N}$, there is a decrease in flow value by $\gamma_v(1)$ (red) in a triangle.

Note that if we assume that all generator and consumer vertices have degree 1, they are never internal vertices of any simple path. Note that Lemma 5.2 is equivalent to the transformation Reduction Rule 4.21 presented in Section 4.2.

Lehmann ET AL. [LGH14, LGH15] showed that the bounded MTSFP is NP-hard on cacti (i. e., a graph consisting of edge disjoint cycles). We can transform a bounded MTSFP with network $\mathcal{N} = (G, V_G, V_D, \text{cap}, b, \underline{p_g}, \overline{p_g}, \underline{p_d}, \overline{p_d})$ to an unbounded MTSFP. We model the upper bounds by adding edges $(u, \overline{v})$ with appropriate capacities at vertices $u \in (V_G \cup V_D)$. To model a non-zero lower generation bound $\underline{p_g}$ at a generator, we replace it by the construction shown in Figure 5.5a, which is based on a structure used by Lehmann ET AL. [LGH14]. The cycle with generator $\underline{s}$ and consumer t_s with $\underline{p_d}(t_s) = \underline{p_g} + 2$ forces a flow of $\underline{p_g}$ on the edge (u, s) and the generator $\overline{s}$ is able to add the remaining generation capacity. Note that the cycle can be omitted if $\underline{p_g} \equiv 0$. For consumers we just add an edge $(\overline{t}, t)$ with a capacity of $\overline{p_d}$ to model the upper bound. In addition, the minimum demand is modeled by a triangle for which the voltage angle configuration enforces a minimum demand of $\underline{p_d}$ (Figure 5.5b).

Lemma 5.3. *Every bounded* MTSFP *can be transformed into an unbounded* MTSFP *on a network with size linear in* $|V|$ *and* $|E|$.

Lehmann ET AL. [LGH14, Lemma 2] show that every MTSFP-instance can be transformed to an equivalent OTSP-instance while maintaining the network structure. The idea is basically that we pay for each unit a consumer is not used to its maximum capacity $\overline{p_d}$ meaning $\overline{p_d}(u) - f_{\text{net}}(u) \neq 0$ and we pay $|\overline{p_d}(u) - f_{\text{net}}(u)|$ units. This transformation is done by defining a generator cost function $\gamma\colon V_G \cup V_G' \to \mathbb{R}_{\geq 0}$ with $u \in V_G'$ if $u \in V_D$ and $\gamma_u(1) \equiv 1$ with $u \in V_G'$ and $\gamma_u(1) \equiv 0$ for all $u \in V_G$. In addition, the consumptions are fixed meaning $\underline{p_d}(u) = \overline{p_d}(u) = p_d(u)$ for all $u \in V_D$.

Thus, while maximizing the power flow a generator $u \in V_G'$ produces $\overline{p_d}(u) - f_{\text{net}}(u)$ units of flow.

We present the reverse transformation for OTSP with linear cost functions. Let $\mathcal{N} = (G, V_G, V_D, \text{cap}, b, \underline{p_g}, \overline{p_g}, \underline{p_d}, \overline{p_d})$ be a bounded network, where each consumer $v \in V_D$ has a fixed demand $\underline{p_d}(v) = \underline{p_d}(v) = \overline{p_d}(v)$. At each generator $v \in V_G$ with cost $\gamma_v(1)$ per generated unit of power we add a triangle consisting of v, another generator s_v and a consumer t_v as shown in Figure 5.6. The edge (s_v, t_v) has susceptance $\gamma_v(1)$ and the other two edges have susceptance 1. We denote the resulting network by $\mathcal{N}'$. If v injects no power into the original network (Figure 5.6a), all its generated power flows along (v, t_v) to t_v. The flow in this triangle is then maximized by sending 1 unit from s_v via v to t_v and $(\overline{x}_v + 2) \cdot \gamma_v(1)$ units directly on (s_v, t_v). Per unit of flow injected by v into the original network, the angle difference $\Delta\theta^v(v, t_v)$ decreases by 1 (Figure 5.6b). Therefore, $\Delta\theta^v(s_v, t_v)$ also decreases by 1 and the flow $f(s_v, t_v)$ by $\gamma_v(1)$. Hence, a feasible flow in $\mathcal{N}$ with cost k can be transformed to a feasible flow in $\mathcal{N}'$ with flow value $M - k$, where $M = \sum_{v \in V_G} \left((\overline{p_g}(v) + 2) \cdot \gamma_v(1) + \overline{p_g}(v) + 1\right)$. This leads to the following lemma.

Lemma 5.4. *For every* OTSP*-instance* $\mathcal{N} = (G, V_G, V_D, \text{cap}, b, \underline{p_g}, \overline{p_g}, \underline{p_d}, \overline{p_d})$ *with fixed demands* $p_d(v) = \underline{p_d}(v) = \overline{p_d}(v)$ *and linear cost functions* γ_v *for each consumer* $v \in V_D$ *there is an* MTSFP*-instance* $\mathcal{N}'$ *and a constant* $M \in \mathbb{R}_{\geq 0}$ *such that for every* $k \in \mathbb{R}_{\geq 0}$ *we have* $\text{OPT}_{\text{OTSP}}(\mathcal{N}) \leq k$ *if and only if* $\text{OPT}_{\text{MTSFP}}(\mathcal{N}') \geq M - k$*. Moreover, the size of* $\mathcal{N}'$ *is linear in the size of* $\mathcal{N}$*.*

The previous lemma and the result of Lehmann ET AL. [LGH14, Lemma 2] provide a possibility to interchangeably apply algorithms found for MTSFP to OTSP (and vice versa) by a simple graph transformation.

5.4 MTSF on Source-Sink-Networks

Fisher ET AL. [FOF08] found in their experiments that *Wheatstone Bridges* [Eke01] (bridges or short-cut edges in a cycle with four edges) can be associated with *Braess's Paradox* [BNW05, Nag10, Pal+12], in which adding a line to a network (even with zero cost) can increase the cost of using that network (see Section 2.3). These structures are often removed by switches in their results. In the following, we denote Wheatstone Bridges by *cycle chords* [Gra99, Wes00, p. 225], since a *bridge* in a graph is an edge whose removal disconnects the graph, which is not what we mean here. The structure—meaning cycle and chord together—is denoted by *diamond graph.* An observation of Fisher ET AL. [FOF08] is the following.

Observation 5.5. *The* OTSP *and thus the* MTSFP *try to remove an edge set* S *in such a way that the remaining graph is often chordless.*

We will show in this section that Observation 5.5 does not apply in general. However, Fisher ET AL. [FOF08] empirically show on their test case that this is often the case. Leibfried ET AL. [Lei+15a] prove that placing ideal FACTS in such a way that the remaining grid is a tree results in a MPF, which is equivalent to the MF. This observation indicates that the power flow is equivalent to the graph theoretical flow on trees as only determined by the conservation of flow (KCL, Equation 5.1) [see LGH15, Lemma 4]. However, power grids are meshed (i. e., they contain cycles) for reliability reasons. Each mesh in a power grid has to obey the KVL (Equation 5.5), meaning the sum of all voltage angle differences is zero. These additional constraints are not only the difference to a graph-theoretical flow, but make most of the problems hard to solve even in the DC model. In addition, they lead to Braess's Paradox and make switching beneficial (see Section 2.3).

The idea is to reach a graph-theoretical flow by exploiting the network structure $\mathcal{N}$. The upper and lower bound for MTSF are given by $\mathrm{OPT}_{\mathsf{MFP}}$ and $\mathrm{OPT}_{\mathsf{MPFP}}$, respectively.

Lemma 5.6. $\mathrm{OPT}_{\mathsf{MPFP}} \leq \mathrm{OPT}_{\mathsf{MTSFP}} \leq \mathrm{OPT}_{\mathsf{MFP}}$.

Transmission switching problems formulated as MILP models have highly coupled constraints (see Section 5.1). Cycles add KVL constraints (Equation 5.5) to the problem, which are highly coupled with each other as the sum over the voltage angle differences in each cycle has to be zero (Figure 5.1). Thus, we get the following observation.

Observation 5.7. *The relation* $\mathrm{OPT}_{\mathsf{MPFP}} < \mathrm{OPT}_{\mathsf{MFP}}$ *can only be caused by cycles.*

In this section we study MTSFP on networks that have only one generator vertex s and one consumer vertex t. We call such networks *s-t-networks*. Let $\Pi(u, v)$ denote the set of all paths between two vertices u and v. We denote the smallest capacity of any edge on a path $\pi \in \Pi(u, v)$ by

$$\underline{\mathrm{cap}}(\pi) \coloneqq \min_{(u,v)\in\pi} \mathrm{cap}(u, v). \tag{5.15}$$

From Equations 5.4 and 5.5 we get the following function to calculate the maximum voltage angle difference on any u-v-path $\pi(u, v) \in \Pi(u, v)$.

$$\Delta\theta^v(\pi(u, v)) \coloneqq \|\pi(u, v)\|_b \cdot \underline{\mathrm{cap}}(\pi(u, v)). \tag{5.16}$$

For $\pi_1(u, v), \pi_2(u, v) \in \Pi(u, v)$ we define $\pi_1(u, v) \leq \pi_2(u, v)$ if and only if $\Delta\theta^v(\pi_1(u, v)) \leq \Delta\theta^v(\pi_2(u, v))$.

5.4.1 The Dominating Theta Path (DTP)

The intuition that electricity follows the path of the least resistance leads us towards shortest paths. However, in power grids the shortest path is not always the restricting

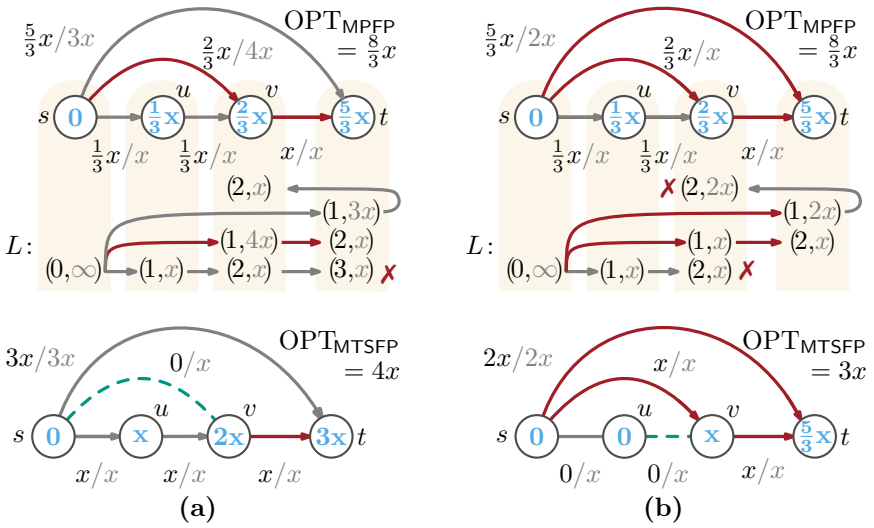

Figure 5.7: A network $\mathcal{N}$ with four vertices and five edges, one generator $V_G = \{s\}$, one consumer $V_D = \{t\}$, capacities $\mathrm{cap}(u, v)$ (gray), susceptance $b(u, v) = 1$ for all $(u, v) \in E$, and voltage angles $\theta^v(u)$ (blue in the vertices) for all vertices $u \in V$. Note for the label calculation that the underlying graph G is undirected. The algorithm computing the DTP saves a set of labels L for each vertex starting at vertex s with label $(0, \infty)$. The red edges represent the DTP from s to t. (a) The cross ✗ means that the label $(3, x)$ is dominated by the label $(2, x)$ at vertex t. In addition, it is not sufficient to compare only the voltage angle differences $\Delta\theta^v$, since we would drop the DTP path $[s, (s, v), v]$ at vertex v, which would lead to incorrect results. Switching edge (s, v) (green dashed edge) results in a solution of the MTSFP. (b) The DTP is not always unique. In addition, for general graphs the switched edge of the MTSFP is not always on the DTP.

path. An s-t-network is often restricted (dominated) by the path with the smallest voltage angle difference. However, it does not seem feasible to give a general bound for that. The smallest voltage angle difference between a vertex u and a vertex v is denoted by $\underline{\Delta\theta^v}(u, v) := \min \Delta\theta^v(\pi(u, v))$ with $\pi(u, v) \in \Pi(u, v)$. We call the path that minimizes $\Delta\theta^v(\pi(u, v))$ Dominating Theta Path (DTP) and denote it by $\pi_{\mathrm{DTP}}(u, v)$. Its value is denoted by $\mathrm{OPT}_{\mathrm{DTP}}(u, v)$. We are mainly interested in s-t-paths, since the power flows from generators s to consumers t.

Note that, unlike shortest paths, a DTP from s to t via another vertex v and a DTP from s to v may have no common edges. For example in the top part of Figure 5.7a a DTP to v goes via u, but not the DTP to t. To compute a DTP we therefore minimize over two objectives $\|\cdot\|_b$ and $\underline{\mathrm{cap}}(\cdot)$. For this we perform a multi-objective search, where we search for Pareto-optimal solutions, i. e., we look for paths that are not dominated by other paths with regards to the objective functions (in our case the susceptance norm $\|\cdot\|_b$ and minimum capacity $\underline{\mathrm{cap}}(\cdot)$). Note that in general multi-

Algorithm 3: Dominating Theta Path (DTP) Algorithm

```
   Data: A network 𝒩 = (G, V_G, V_D, cap, b).
   Result: π(s,t), Δθ^υ(s,t), and D(υ) with υ ∈ V.
1  D(u) := L(u) := ∅   ∀u ∈ V;                                  ▷ Initialization
2  Q := ∅;
3  L(s) := {(0, ∞)};                                            ▷ Special label for source s
4  Q.insert((0, ∞), s, key((0, ∞)));
5  while Q ≠ ∅ do                                               ▷ Visit all vertices
6      (ℓ, u, key) := Q.delMin();
7      D(u) := D(u) ∪ {ℓ};
8      for ∀{u, v} ∈ E⃗ do                                       ▷ Check adjacent vertices
9          cap(π(s, u, v)) := min(ℓ1, cap(u, v));
10         ℓ_new(v) := (ℓ[0] + 1/b(u,v), cap(π(s, u, v)));
11         if isReachable(V \ {v}, ℓ, s) then
12             if ℓ_new(v) ∈ L(v) then
13                 parent(ℓ_new(v)) := parent(ℓ_new(v)) ∪ {ℓ};
14             else if not L(v) dominates ℓ_new(v) then
15                 L(v).deleteDominatedLabels(ℓ_new(v));
16                 Q.deleteDominatedLabels(ℓ_new(v), v);
17                 L(v).insert(ℓ_new(v));
18                 Q.insert(ℓ_new(v), v, key(ℓ_new(v)));
19                 parent(ℓ_new(v)) := {ℓ};
20             end
21         end
22     end
23 end
24 return ( π(s,t) := getPaths(s,t),   ▷ Build paths from parent
           Δθ^υ(s,t) := min_{ℓ∈D(t)}{ℓ[0] · ℓ[1]},
           D(·) );
```

objective search is already NP-hard for two objective functions [GJ79] (see Figure 5.8).

Definition 5.8 (Label Domination Criteria). *Each s-u-path π in $\mathcal{N}$ defines a label $\ell = (\|\pi\|_b, \underline{\mathrm{cap}}(\pi))$ at u. A label $(\|\pi_1\|_b, \underline{\mathrm{cap}}(\pi_1))$* dominates *another label $(\|\pi_2\|_b, \underline{\mathrm{cap}}(\pi_2))$ if $\|\pi_1\|_b \leq \|\pi_2\|_b$ and $\underline{\mathrm{cap}}(\pi_1) \leq \underline{\mathrm{cap}}(\pi_2)$.*

The Pareto set $D(u)$ of labels at a vertex $u \in V$ is then defined as the set of nondominated labels of all s-u-paths (Line 7). These Pareto sets can be computed by a natural extension of Dijkstra's algorithm (see Algorithm 3) known as the *multi-criteria shortest-path* algorithm [Mar84]. At each vertex $u \in V$ a set of nondominated labels $L(u)$ is stored. Note that in general, each label may correspond to multiple s-u-paths. As it is

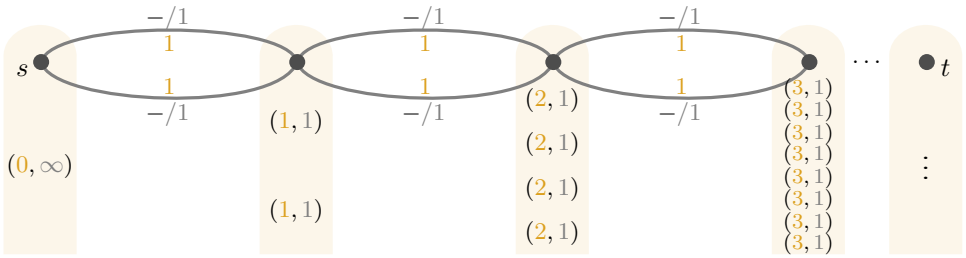

Figure 5.8: An example, where the DTP produces exponential many labels. The edges are given with the susceptances b and capacities cap. The sets of labels are marked at the vertices. The number of labels increases from the source s for each vertex in the chain exponentially by either choosing the upper or lower edge.

necessary to represent all these paths, we store for each label a set of parent-pointers. The latter point to labels that correspond to paths shortened by one vertex. The merging of labels ensures the polynomial size of label sets.

The labels in the priority queue Q are compared by $\|\cdot\|_b$. At the beginning of each iteration a label with the minimum susceptance norm is extracted from Q. This label belongs to a vertex u. Then, new labels for all neighbors of u are computed (Line 10). First, it is checked whether there is a path $\pi(s,u)$ that corresponds to ℓ and does not contain the neighbor v (Line 11, Section 5.4.3). Extending this path to v then still gives a simple path. If the computed label already exists in $L(v)$, the parent-pointers are updated. Otherwise, if it is not dominated, it is added to $L(v)$ and Q (Lines 17 and 18). Before that, all labels dominated by the new labels are removed. Here, only labels at the same vertex are considered, i. e., in Line 16 only the dominated labels at v are removed.

Lemma 5.9. *Algorithm 3 computes a correct* Dominating Theta Path (DTP)*.*

Note that the proof for the next lemma is based on the proof for the *multi-criteria shortest-path* algorithm by Martins [Mar84].

Proof. At any step of Algorithm 3 there is a set of labels $L(u)$ associated with each vertex $u \in V$. We first show that at any step no label in $L(u)$ is dominated by any other label in the same set. After the initialization there is only one label. Hence, it is not dominated.

Suppose that there are no dominated labels in any label set before an iteration. We show that this property still holds after the iteration. First, a label $(\|\pi(s,u)\|_b, \operatorname{cap}(\pi(s,u)))$ with the minimum susceptance norm among all labels in Q is dequeued (Line 6). This label corresponds to a path $\pi(s,u)$ from s to u. Then, the labels for neighbors of u are computed (Line 10 based on Equation 5.16). Since these labels are only added if they are not dominated and labels dominated by them are removed

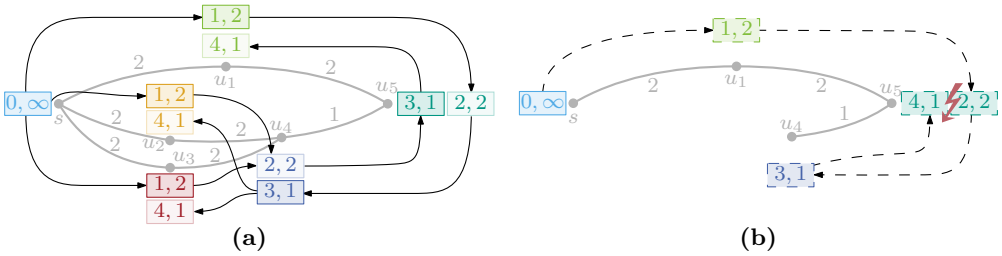

Figure 5.9: A network $\mathcal{N}$ and the corresponding directed graph on the labels computed during the execution of the DTP-algorithm. All edges $(u, v) \in E$ have susceptance $b \equiv 1$. Two labels have the same color if and only if they belong to the same vertex in $\mathcal{N}$. (a) To test whether the label $(4, 1)$ at u_3 shall be inserted into the graph, we search for a rainbow path from the label at s to the new label $(4, 1)$. The slightly colored labels produce no DTP from that particular vertex. (b) The rainbow path avoids cycles and ensures that the paths remain simple.

from $L(v)$, the label sets still do not contain dominated labels. Moreover, the new labels also correspond to simple paths as it is tested whether v already lies on $\pi(s, u)$. Note that previously extracted labels from Q are not removed since their susceptance norm is less than the one of $\ell_{\text{new}}(v)$. In particular, all labels extracted from Q will be present in the final label sets.

Secondly, we prove that in the end we have $D(v) \subseteq L(v)$ for all $v \in V$. Assume that this was not the case. Then, there is a label $\ell \in D(v)$ that is not included in $L(v)$ for some $v \in V$. We pick such a label with the minimum susceptance norm. This label corresponds to a path $\pi(s, v)$. Denote the vertex before v by u. Since the subpath $\pi(s, u)$ from s to u has $\|\pi(s, u)\|_b < \|\pi(s, v)\|_b$, the label for this subpath is present in $L(u)$. But in the iteration in which this label was processed, all neighbors of u were explored. In particular, the label ℓ for v was computed and added to $L(v)$. Moreover, it was never removed from $L(v)$ later, since it is not dominated. This contradicts the existence of ℓ. Since $D(u) \subseteq L(u)$ and $L(u)$ contains no dominated labels, we conclude $D(u) = L(u)$. The DTP is then computed by minimizing over $L(t)$. □

A counterexample for monotone voltage angle paths is given in Figure 5.10 confirming Lemma 5.10.

Lemma 5.10. *The* Dominating Theta Path (DTP) *is not necessarily on a monotone voltage angle path.*

5.4.2 DTP without Merging the Labels

The Algorithm 3 for the DTP can be implemented using the merging of equivalent labels or without merging. Neglecting the merging of labels would mean that we remove Line 11 that avoids cycles and Line 12 that merges the labels. Thus, the

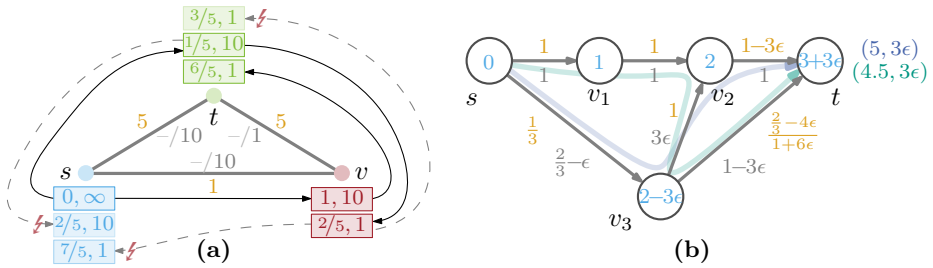

Figure 5.10: The graphs represent two problematic cases. (a) An example that shows that it does not suffice that the labels consist of $(\|\cdot\|_b, \overline{\text{cap}}(\cdot))$, but has to include the set of visited vertices V'. (b) Shows an example that the DTP is not necessarily on a monotone voltage angle path. Let $0 < \epsilon \ll 2/3$ then the green path represents the DTP from s to t.

reachability check is neglected, but we have to add cycle checks that are also done by the reachability test (see Section 5.4.3). The implementation stores a set of visited vertices V' for every label. Using a simple union operation on these set, we are able to check for cycles. In worst-case we have to save $O(|V|)$ elements per vertex in that set. Thus, a label consists in that case of $(\|\cdot\|_b, \overline{\text{cap}}(\cdot), V')$. Note that this method can lead to exponential many labels as exemplified in Figure 5.8. However, the reachability test leads to an exponential running time (see Section 5.4.3 and Equation 5.18).

5.4.3 Reachability Test

Algorithm 3 repeatedly tests whether the new labels correspond to simple paths in the network (Line 11 of Algorithm 3). For this it is checked whether the label at vertex s is reachable from u via parent-pointers from the label ℓ when all labels at v are ignored. The labels and the pointers together form a directed acyclic graph, where the labels have the same color if and only if they belong to the same vertex in network $\mathcal{N}$ (see Figure 5.9). We call a path whose vertices all have different colors a *rainbow path*.

Rainbow s-t-Path s-t-RP(G, c, s, t)	
Instance:	A directed acyclic graph $G = (V, E)$, a coloring $c\colon V \to \mathbb{N}$, and $s, t \in V$.
Question:	Is there an s-t-path π in G such that all vertices of π have different colors?

An algorithm to test whether there is a Rainbow s-t-Path (s-t-RP) in undirected graphs was presented by Uchizawa et al. [Uch+13, Theorem 11]. It runs in $O(k2^k|E||V|)$ time, where k is the number of colors, $|E|$ the number of edges, and $|V|$ the number of vertices in G. We give a different algorithm for directed graphs, which can be implemented to run in $O(k2^k|E|)$ time. The main work is done by Algorithm 4. It

Algorithm 4: computeColors

```
Data: A directed label network 𝒢 = (G = (V, E), c, s), where c : V → ℕ is the coloring
      and s ∈ V is the fixed source of the network, v ∈ V, and a set T ⊆ ℕ of
      forbidden colors.
Result: The intersection of the colors of all rainbow s-v-paths, or ℕ if there are no
        such paths.
1 if c(v) ∈ T then return ℕ ;                          ▷ Not a rainbow path?
2 if s = v then return {c(s)} ;                        ▷ Base case
3 C_T(v) := ℕ;
4 for (u, v) ∈ E do                                    ▷ All incoming edges into v
5 |   C' := computeColors(𝒢, u, T ∪ {c(v)});           ▷ Incoming cut
6 |   C_T(v) := C_T(v) ∩ C';
7 end
8 C_T(v) := C_T(v) ∪ {c(v)};
9 return C_T(v);
```

additionally gets a set T of forbidden colors as input and ignores all vertices of these colors. To decide whether there is a rainbow path from a vertex s to a vertex t, we initially set T to $\emptyset$. We compute for each vertex v a set of colors $C_T(v)$. A color c is in the set $C_T(v)$ if and only if any rainbow s-v-path $\pi(s, v)$ contains a vertex with color c with the additional constraint that no vertex of $\pi(s, v)$ is colored with a color in T (in Algorithm 4 Lines 5 and 6). For each vertex v and all its incoming edges (u, v) we recursively compute all necessary colors for the rainbow paths to u such that $c(v)$ is forbidden. The set $C_T(v)$ is then equal to the intersection of these color sets together with $c(v)$. Throughout the algorithm we use $\mathbb{N}$ to indicate that there is no rainbow path with the given restrictions.

During the execution Algorithm 4 may be called several times with the same parameters. To speed up the computation one may store the results instead of recomputing them every time. Further, we find a relation between $C_T(v)$ and $C_{T'}(v)$ for a vertex v and two sets of forbidden colors T and T'. If every color of a vertex before v in the topological order is either both in T and T' or neither in T nor T', we have $C_T(v) = C_{T'}(v)$. In particular, if no vertex before v is colored by any color in T, we have $C_T(v) = C_\emptyset(v)$. This property can also be used to reduce the number of recursive calls.

Alternatively, the set of colors $C_T(v)$ at a vertex v can be computed by traversing all paths from s to v, checking if no two vertices are colored the same and finally taking the common colors of all rainbow paths. This may be faster if there are only few s-v-paths or if many of the paths can be eliminated quickly because they are not rainbow paths.

5.4.4 Analyses of the DTP

Examples of this algorithm are shown in the upper part of Figure 5.7a and b. Note that there are at most $|E|$ different values of $\underline{\text{cap}}(\cdot)$ since there are at most $|E|$ different labels saved per vertex assuming that we merge and have a penrose-minor free graph with direction. This bound is tight. Consider for example two vertices with $|E|$ parallel lines, where line i has capacity i and susceptance $1/i$.

Lemma 5.11. *For each $u \in V$ we have $|L(u)| \leq |E|$.*

Note that for arbitrary graphs the labels are of the form $(\|\cdot\|_b, \underline{\text{cap}}(\cdot), V')$, which results in exponential many labels. The non-negativity of the susceptance norm and capacity implies that processed labels $D(\cdot)$ will not be removed. This is denoted as *label setting*. In contrast, negativity would imply that there may exist a path such that processed labels have to be updated by labels of vertices on the negative path. In addition, all adjacent labels of the updated labels have to be corrected and so forth. Algorithms working like this are called *label correcting* and do not perform as efficiently as label setting algorithms. The running time of Algorithm 3 depends on the subroutine `isReachable` for which no polynomial bound is known. Note that these tests are easy for labels that correspond to exactly one path, i. e., labels that were not merged. On realistic power grid instances the algorithm performs well since merging is rare. If we use a Fibonacci-heap Q to store labels, the operation `insert` is in $O(1)$, `delMin` is amortized in $O(\log|V|)$ [FT84], `deleteDominatedLabels` is in $O(|E|)$, and `isReachable` (see Section 5.4.3) runs in $O(2^{|V|}|V| \cdot |E|)$ time. The initialization is in $O(|V|)$ time (Lines 1–4). There are $O(|V| \cdot |E|)$ `delMin` operation, since every vertex can have up to $|E|$ labels. There arise $O(|E|^2)$ operations of all other methods, since we do these operation for all incident edges $\sum_{u \in V} \deg(u) = 2|E|$ [Eul41] (Line 8) and each vertex can have at most $|E|$ labels. Thus, the algorithm runs in time

$$\begin{aligned} T &:= O\big(|V| \cdot |E| \cdot T_{\texttt{delMin}} + |E|^2 \cdot \\ &\qquad (T_{\texttt{insert}} + T_{\texttt{isReachable}} + T_{\texttt{deleteDominatedLabels}})\big) && (5.17) \\ &= O\left(|V| \cdot |E| \cdot \log|V| + 2^{|V|}|V| \cdot |E|^3\right). && (5.18) \end{aligned}$$

The following lemma results directly from the previous discussion.

Lemma 5.12. *Algorithm 3 runs in $O\left(2^{|V|}|V| \cdot |E|^3\right)$ time.*

On general graphs we cannot assume that the switched edges are either tight edges (i. e., bottleneck edges that are congested) or on the DTP (in Figure 5.7b edge (u, v) is not on the DTP). In the following, we restrict our graph classes of the network $\mathcal{N}$ to s-t-networks (i. e., there is only one $s \in V_G$ and one $t \in V_D$) and try to solve the MTSFP on them. We identify structures, where it is easy to switch. The following lemma shows at which point it is beneficial to switch on simple cycles.

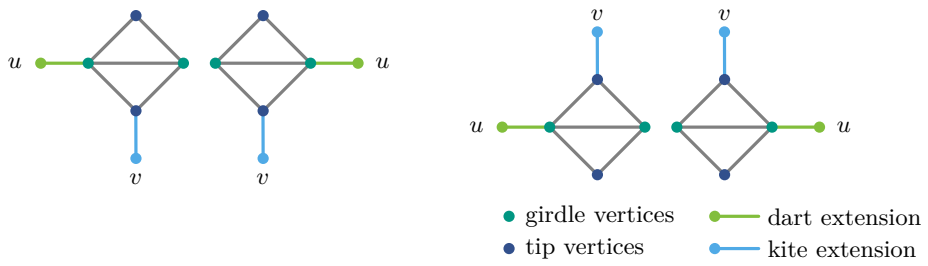

Figure 5.11: All cases show penrose-minors, where u and v are either generators or consumers, but not both the same. They are a combination of a kite graph (i. e., diamond graph with an additional edge on one of the tip vertices) and a dart graph (i. e., diamond graph with an additional edge on one of the girdle vertices).

Lemma 5.13. *Let $\mathcal{N}$ be a simple cycle with one generator s and one consumer t, and let $\pi(s,t) \in \Pi(s,t) \setminus \pi_{\mathsf{DTP}}(s,t)$. The Braess's Paradox exists if and only if* $\mathrm{OPT}_{\mathsf{MPFP}}(\pi(s,t)) > \mathrm{OPT}_{\mathsf{MPFP}}(\mathcal{N})$.

Proof. It suffices to show that removing edge $e_{\min}(\pi_{\mathsf{DTP}}(s,t)) := \arg\min_{e \in \pi_{\mathsf{DTP}}(s,t)} \mathrm{cap}(e)$ results in $\mathrm{OPT}_{\mathsf{MPFP}}(\mathcal{N} - \{e_{\min}\}) > \mathrm{OPT}_{\mathsf{MPFP}}(\mathcal{N})$ and thus, it holds $\mathrm{OPT}_{\mathsf{MTSFP}}(\mathcal{N}) > \mathrm{OPT}_{\mathsf{MPFP}}(\mathcal{N})$. The flow on the path $\pi(s,t)$ is defined by the ratio ${\Delta\theta^v(\pi(s,t))}/{\|\pi(s,t)\|_b}$ (Equations 5.5 and 5.14). The smallest voltage angle difference $\underline{\Delta\theta^v}(s,t)$ restricts the flow on the other path $\pi(s,t)$. Thus, the term ${\underline{\Delta\theta^v}(s,t)}/{\|\pi(s,t)\|_b}$ is the maximum possible flow on path $\pi(s,t)$. The value $\mathrm{OPT}_{\mathsf{MPFP}}(\pi(s,t)) > \mathrm{OPT}_{\mathsf{MPFP}}(\mathcal{N})$ holds if and only if

$$\frac{\Delta\theta^v(\pi(s,t))}{\|\pi(s,t)\|_b} > \underline{\Delta\theta^v}(s,t) \cdot \frac{\|\pi(s,t)\|_b + \|\pi_{\mathsf{DTP}}(s,t)\|_b}{\|\pi(s,t)\|_b \cdot \|\pi_{\mathsf{DTP}}(s,t)\|_b}.$$

Thus, switching an edge $e_{\min}$ on $\pi_{\mathsf{DTP}}(s,t)$ increases the total flow on the cycle and makes switching beneficial. □

We now generalize this result to a more complex graph class. Following the construction in Section 5.3, we assume that all generator and consumer vertices have degree 1. A diamond graph is a simple graph on four vertices and five edges consisting of two triangle facets identified along an edge. Moreover, we denote its degree-3 vertices as *girdle* vertices and its degree-2 vertices as its *tip* vertices. Furthermore, we call the combination of a *kite* and a *dart* graph representing both diamond graphs with an additional edge on one of the tip and the girdle vertices, respectively, a *penrose* graph (Figure 5.11). These additional edges basically represent either a generator edge or a consumer edge, but not both the same. We emphasize this by the following definition.

Definition 5.14 (Penrose Graph)**.** *A* penrose *graph is a kite graph with an additional edge incident to one of the girdle vertices, or similarly, a dart graph with an additional edge on one of the tip vertices.*

Algorithm 5: MTSF Algorithm for Penrose-Minor-Free $\mathcal{N}$

```
Data: A network 𝒩 = (G, V_G, V_D, cap, b).
Result: DTP(s, t), parent: V → V, and ℓ: V → ℝ_≥0 × ℝ_≥0.
S := ∅;
B := blockCutTree(𝒩) ;                                  ▷ Biconnected components
(π, Δθ^v_min, parent, L(·)) := DTP(𝒩);                  ▷ see Algorithm 3
for β ∈ B do
    S' := ∅;
    while L(t) ≠ ∅ do
        S' := S' ∪ e_min(π(s, t));
        if OPT_MPFP(β − S') ≥ OPT_MPFP(β − S) then
            S := S ∪ S';                                ▷ Save switched lines in S
        end
        (π_DTP, Δθ^v_min, parent, ℓ) := DTP(β − S');    ▷ Update
    end
end
return (OPT_MPFP(𝒩 − S), S);
```

A *minor* of a network $\mathcal{N}$ is obtained from $\mathcal{N}$ by contracting and deleting edges, as well as deleting isolated vertices (i. e., vertices without incident edges). A *penrose-minor-free graph* is a graph without a penrose graph as a minor.

In the following, we consider penrose-minor-free graphs with one generator s and one consumer t. Note that each block, i. e., a maximal biconnected subgraph, of such graphs consist of one or more parallel paths. The start and end vertices of the paths act as generator and consumer for the block. Note that the blocks can be considered separately. Let β be a block and u and w the start and end vertices of its paths. The flow value F of an MPF from u to w is $F = \underline{\Delta\theta^v}(u, w) \cdot \sum_{\pi \in \Pi(u,w)} \frac{1}{\|\pi\|_b}$. To increase the flow value, either of the factors has to be increased. Switching cannot increase the sum, but only the angle difference on the DTP. Thus, the following result holds.

Lemma 5.15. *Switching on penrose-minor-free graphs is only beneficial on* DTP*s.*

From Lemma 5.15 we know that we only need to consider edges on a DTP for switching. In Algorithm 5 for each block β we remove the edge with the smallest capacity on $\pi_{\text{DTP}}(s, t)$ in β and update the DTP(s, t). If we get a better value for F, we save it. We repeat this procedure until there is no path from s to t. The correctness of Algorithm 5 follows directly from the correctness of the DTP-Algorithm (Algorithm 3) and Lemma 5.15.

Theorem 5.16. *Algorithm 5 computes a correct* MTSF *on penrose-minor-free graphs with one generator and one consumer.*

Switching is NP-hard in series-parallel graphs, which generalize penrose-minor graphs, and leads to the next lemma that was proven in Section 5.2.2.

Lemma 5.17. MTSFP *is* NP*-hard even if there is only one source and one sink in the network and all edge capacities are* 1*.*

A general observation in power grids is that shortest paths are somehow connected to switching a line, since the betweenness centrality is negatively correlated to switching lines [HB08]. Though switched edges on general graphs are not always on DTPs, Algorithm 3 gives us a new criterion focusing on switching by using DTPs instead of the shortest paths. We define the DTP centrality based on the number of DTPs through an edge.

Definition 5.18. *Let $\mathcal{N}$ be a power grid. The* DTP *betweenness centrality $c_{\mathrm{DTPB}} : E \to \mathbb{R}_{\geq 0}$ is defined by*

$$c_{\mathrm{DTPB}}(e) \coloneqq \frac{1}{m_B} \sum_{s \in V} \sum_{t \in V \setminus \{s\}} \frac{\sigma_{\mathrm{DTP}}(s,t,e)}{\sigma_{\mathrm{DTP}}(s,t)}, \tag{5.19}$$

where $\sigma_{\mathrm{DTP}}(s,t,e)$ is the number of DTP*s between s and t that use e, $\sigma_{\mathrm{DTP}}(s,t)$ is the total number of* DTP*s from s to t and $m_B = |V|(|V|-1)$ is a normalizing constant.*

For directed and undirected graphs, the normalization factor is the same, since the algorithm operates on the directed label graph. However, we normalize the number of DTPs already by the number of DTPs between s and t. Note that in power grids we do not necessarily check all pairs of vertices, but the paths between all generators $s \in V_G$ and consumers $t \in V_D$. Thus, we define the following centrality that differs in the base—meaning generators and consumers instead of all vertices—and normalization constant.

Definition 5.19. *Let $\mathcal{N}$ be a power grid. The switching centrality $c_{\mathrm{S}} : E \to \mathbb{R}_{\geq 0}$ is defined by*

$$c_{\mathrm{S}}(e) \coloneqq \frac{1}{m_B} \sum_{s \in V_G} \sum_{t \in V_D} \frac{\sigma_{\mathrm{DTP}}(s,t,e)}{\sigma_{\mathrm{DTP}}(s,t)}, \tag{5.20}$$

where $\sigma_{\mathrm{DTP}}(s,t,e)$ is the number of DTP*-paths between s and t that use edge e, $\sigma_{\mathrm{DTP}}(s,t)$ is the total number of* DTP*-paths from s to t and $m_B = |V_G| \cdot |V_D|$ is a normalizing constant.*

5.5 Computing one DTP in Polynomial Time

The previous algorithm computes all DTPs between two vertices u and v, but has an exponential running time or uses exponential space dependent on the implementation. In this section, we present a polynomial time algorithm to calculate the DTP. However, instead of calculating all DTPs between two vertices u and v this algorithm computes only one DTP. Thus, it cannot be used for the centrality measurement.

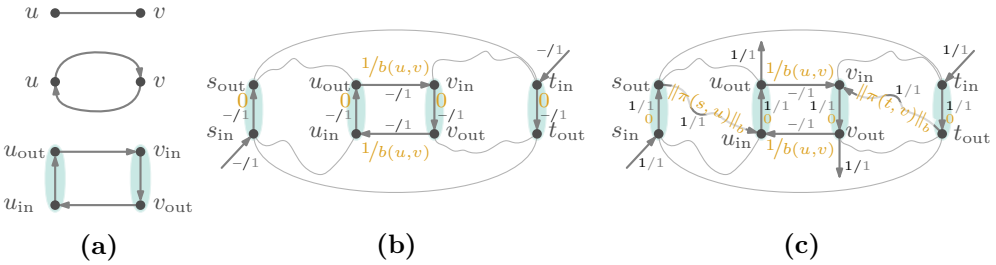

Figure 5.12: The necessary graph transformations to calculate a DTP in polynomial time. (a) The transformation from an undirected graph to a directed graph that is bidirected by transforming edge $\{u, v\}$ to two directed edges $(u, v), (v, u)$. To have a vertex disjoint path, each vertex u is split into two vertices $u_{\text{in}}, u_{\text{out}}$ with one additional edge $(u_{\text{in}}, u_{\text{out}})$. (b) The transformed network $\mathcal{N}''$ with capacities $\text{cap} \equiv 1$ and edges costs $\gamma(u_{\text{out}}, v_{\text{in}}) = 1/b(u_{\text{out}}, v_{\text{in}})$ for an external edge and $\gamma(u_{\text{in}}, u_{\text{out}}) = 0$ for a vertex internal edge. (c) The resulting minimum-cost flow f for an edge $e_{\min} = (u, v)$.

Recall from Section 5.4.1 that a label $(\|\pi(s,u)\|_b, \underline{\text{cap}}(\pi(s,u)))$ consists of the susceptance norm—representing the electrical distance—and the minimum capacity along a path $\pi(s,u)$. Thus, fixing the edge with the smallest capacity and calculating a shortest path from that particular edge to the source and sink vertex using the susceptance norm $\|\cdot\|_b$ is equivalent to the bicriterial shortest path. Assume that one knows an edge $e_{\min}$ on the DTP from s to t with the minimum capacity. We then need to find a shortest s-t-path π via $e_{\min}$, where all edges of π have capacity at least $\text{cap}(e_{\min})$. Let $\mathcal{N}'$ be the network obtained from $\mathcal{N}$ when all edges with capacity smaller than $\text{cap}(e_{\min})$ are removed. Searching for a shortest s-t-path via $e_{\min}$ is then equivalent to searching two disjoint paths π_1 and π_2 from s and t to the endpoints of $e_{\min}$ in $\mathcal{N}'$ such that $\|\pi_1\|_b + \|\pi_2\|_b$ is minimum.

These paths can be found by running a minimum-cost flow algorithm in a suitable graph, which is obtained in the following way. First, we denote the endpoints of $e_{\min}$ by u and v, and remove $e_{\min}$. We replace each undirected edge by directed edges in both directions (bidirected graph). Finally, each vertex w is split into two vertices w_{in} and w_{out}, which are joined by the directed edge $(w_{\text{in}}, w_{\text{out}})$. We call these edges *internal*. The incoming and outgoing edges of w are then placed at w_{in} and w_{out}, respectively. All edges of the resulting graph get a capacity of 1. The cost of the internal edges is set to 0. All other edges correspond to an edge e in the input network, and we set their costs to $1/b(e)$. The vertices s_{out} and t_{out} produce one unit of flow each, while u_{in} and v_{in} consume one unit each. We call the resulting network $\mathcal{N}''$.

Let f be a minimum-cost flow from u to v with flow value 2. We can decompose f into two unit flows from s_{in} and t_{in}, which correspond to disjoint paths π_1 and π_2 from s and t to the endpoints u and v (i. e., endpoints of the removed edge $e_{\min}$).

Algorithm 6: Factor 2-Approximation Algorithm for Cacti

```
Data: A network 𝒩 = (G, V_G, V_D, cap, b).
Result: OPT_MPFP(𝒩 − S), and switched edges S.
S = ∅;
C = dfs (𝒩);
for c ∈ C do
    S = S ∪ {arg min_{∀e∈c}(cap(e))};
end
return (OPT_MFP(𝒩 − S), S);
```

Lemma 5.20. *The shortest s-t-path π via $e_{\min}$ in $\mathcal{N}_{\mathrm{cap}(e_{\min})}$ has susceptance norm $\|\pi\|_b = \mathrm{cost}(f) + \|e_{\min}\|_b$. If the edge on π with the minimum capacity is known, π can be computed in polynomial time.*

Proof. Constructing $\mathcal{N}''$ as described above and computing the minimum-cost flow f is possible in polynomial time. The flow f can be decomposed into two unit flows, e. g., by running a depth-first search. The edge capacities of 1 ensure that these two flows follow two edge-disjoint paths. Since each vertex of $\mathcal{N}''$ has only one incoming or one outgoing edge, these paths are vertex-disjoint as well. Further, they correspond to two paths π_1 and π_2 in $\mathcal{N}'$, where π_1 connects s with an endpoint of $e_{\min}$ and π_2 connects t with the other endpoint of $e_{\min}$. Together with $e_{\min}$ we hence obtain an s-t-path Π via $e_{\min}$ with $\|\pi\|_b = \mathrm{cost}(f) + \|e_{\min}\|_b$. The last property follows immediately from the definition of the costs in $\mathcal{N}''$. As f has minimum cost, the constructed path π has minimum susceptance norm among all s-t-paths via $\|\pi\|_b = \mathrm{cost}(f) + \|e_{\min}\|_b$ in $\mathcal{N}'$. □

Since we assumed that $e_{\min}$ was an edge with minimum capacity on a DTP between s and t, the path π is a DTP. However, $e_{\min}$ is unknown. We therefore repeat this procedure for each edge in the network and pick the path with the smallest angle difference. Lemma 5.20 then guarantees that this results in a DTP.

5.6 Approximation Algorithm on Cacti

Lehmann ET AL. [LGH14] showed that the bounded MTSFP on cacti is NP-hard by using a reduction from subset sum. Subset sum is weakly NP-hard and a fully polynomial-time approximation scheme (FPTAS) exists [Kel+03]. In this section, we present an approximation algorithm for MTSFP on cacti with approximation factor 2. Recall from Section 5.3 that it is always possible to transform a bounded MTSFP into an unbounded MTSFP (Lemma 5.3).

In the following, we assume that our underlying graph G of $\mathcal{N}$ is a cactus. Unlike in Section 5.4 we allow multiple generators and consumers. The basic idea for our

algorithm (Algorithm 6) is to remove from each cycle the edge with the smallest capacity. Since we presume that $\mathcal{N}$ is a cactus, cycles are independent concerning the voltage angle difference, since they do not share an edge. Cycle detection can be done via a depth-first search (DFS) in $O(|V|)$ time, where $|V|$ is the number of vertices. Finding the edge with minimum capacity in each cycle is done during the DFS. Note that the remaining structure is a tree that is equivalent to a Maximum Spanning Tree (MaxST). The running time of MaxST is in general $O(|E|\ \alpha(|E|, |V|))$ [Cha00], where α is the inverse of the Ackermann function (i. e., α grows very slowly). Note that MaxST on cacti runs also in $O(|V|)$ time. The maximum flow on trees can be realized in $O(|V|)$ time by using the pseudoflow algorithm [Hoc08]. Thus, the algorithm runs in $O(|V|)$ time.

Lemma 5.21. *Let $\mathcal{N} = (G, V_G, V_D, \mathrm{cap}, b)$ be a power grid and let S be the set* $\arg\min_{\forall e \in c} \mathrm{cap}(e)$ *of switched edges for all cycles $c \in C$. Then there exist a feasible electrical flow f' on $\mathcal{N} - S$ such that $F(f') = 1/2\ \mathrm{OPT}_{\mathsf{MF}}(\mathcal{N})$.*

Proof. Let $f^\star$ be a MF with value $\mathrm{OPT}_{\mathsf{MFP}}$ on $\mathcal{N}$. By reducing the flow on each edge by one half (see Equation 5.21), we get a flow f on $\mathcal{N}$ with a value of $1/2\ \mathrm{OPT}_{\mathsf{MF}}$. Applying Algorithm 6 returns a set of switched edges $S = \bigcup_{c \in C} \arg\min_{\forall e \in c} \mathrm{cap}(e)$. We decompose each cycle $c \in C$ into an edge $e_{\min}$ having the smallest capacity on the cycle c (Equation 5.22) and into the remaining part denoted as path π. Since the flow on $e_{\min}$ is $1/2 f^\star(e_{\min})$ it can be rerouted on the remaining part π of c (Equation 5.23). We denote the rerouted flow by f'. For any $e \in \pi$ we have

$$|f(e)| = |1/2\ f^\star(e)| \leq 1/2\ \mathrm{cap}(e), \tag{5.21}$$

$$|f(e_{\min})| \leq 1/2\ \mathrm{cap}(e_{\min}) \leq 1/2\ \mathrm{cap}(e), \tag{5.22}$$

$$|f'(e)| = |f(e_{\min}) + f(e)| \leq \mathrm{cap}(e). \tag{5.23}$$

□

Recall that $\mathrm{OPT}_{\mathsf{MFP}}$ is an upper bound for $\mathrm{OPT}_{\mathsf{MTSFP}}$ and that MFP and MTSFP are equal on trees. Thus, from Lemma 5.21 follows Theorem 5.22.

Theorem 5.22. *Algorithm 6 is a factor 2-approximation algorithm for the* MFP *and* MTSFP *problem on cacti.*

Note that an approximation ratio of $1/2$ does not provide a good guarantee in the worst case. However, compared to other heuristics it gives guarantees and can be used as an initial step for heuristics.

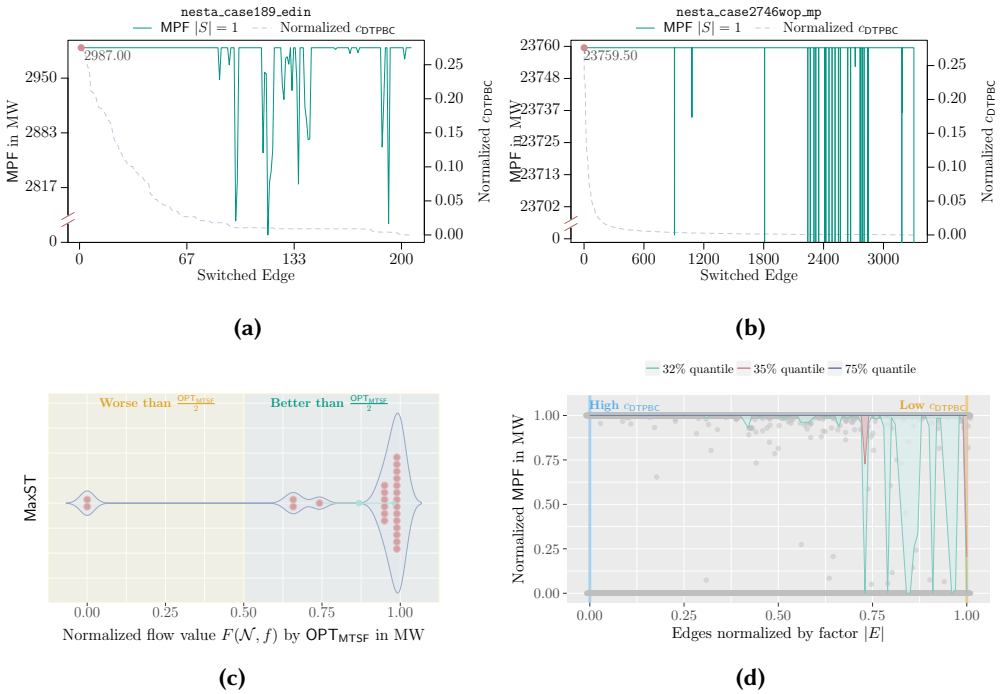

Figure 5.13: Simulation evaluation using the data from Table 5.2 for (c) and aggregating the results from Figures C.1–C.3 into (d) including (a) and (b). (a) and (b) show the `nesta_case189_edin` and `2746wop_mp`, respectively, with the gray dashed line being the centrality of the edges (x-axis) and the green line the MPF (y-axis). (c) The 2-approximation on cacti using MaxST is tested on arbitrary graphs. The global optimum OPT_{MaxST} is reached at 1 and the proven factor for cacti is at $1/2$. The green left (with range) and right point show the mean and median, respectively. (d) The aggregated data are normalized with regards to the edges and MPF using $|E|$ and the MPF of each of the network. The edges are ranked from highest to lowest c_{DTPB}. The quantiles show that 32 % of the test cases give worse results than the green line while switching an edge with low centrality.

5.7 Simulations

We simulated[4] our DTP betweenness centrality and 2-approximation algorithms for penrose-minor-free graphs and cacti, respectively, on arbitrary graphs. By arbitrary graph we mean the NESTA benchmark sets [CGS14], which are based on the IEEE benchmark sets [Alb+79, AS74, Bil70, Cro15, Dem+77, GJ03, Gri+99, Jos+16, LB10, Les+11, Mat13, Uni14, WWS13, ZMT11] and incorporate realistic data such as thermal line limits. Note that we run our simulations on arbitrary power grids, since there are not a lot of benchmark sets presenting cacti namely `nesta_case3_lmbd`, `4_gs`,

[4] https://i11www.iti.kit.edu/projects/mtsf/index

and 9_wscc or s-t-networks available. Recall from Section 5.1 that we have a disjoint set of generators and consumers. This theoretical assumption cannot be found in any benchmark set and realistic power grid. Thus, we have to modify the data in such a way that we still provide a realistic benchmark set and comply with the assumptions to avoid infinite generator production at buses having both generators and consumers (see Equations 5.2 and 5.3). In addition, we only allow to consume a real power demand p_d at a real power generator (see bus data's column three in the IEEE Common Data Format [Pie+73]). All other consumers have an infinite maximum demand (Equation 5.12). The results for the problems in Section 5.1 are shown in Table 5.2.

For the 2-approximation, we use MaxST (Section 5.6) on different benchmark data sets and compare the results with the MILP from Section 5.1. The algorithm MaxST gives very good results even though operating on arbitrary graphs (see Table 5.2). Nearly all—meaning 93 %—of the results are better than the approximation factor and 82 % are at most 7 % from the optimum value $\mathrm{OPT}_{\mathsf{MTSFP}}$ (see Figure 5.13c). Note that 36 % of the results even reach the optimal value (cases equal to $\mathrm{OPT}_{\mathsf{MTSFP}}$ have gray markers in Table 5.2). Thus, the expected quality on arbitrary graphs is much better than the proven approximation ratio of 2 on cacti (Section 5.6). There are two cases worse than the approximation factor, because there is no feasible power flow for the resulting networks $\mathcal{N} - S_{\mathsf{MaxST}}$. There are three cases in which the number of switched lines in the 2-approximation is greater than $\mathrm{OPT}_{\mathsf{MTSFP}}$.

The DTP is exact for s-t-penrose-minor-free graphs. There is no benchmark case providing this structure. However, since the DTP represents a distance measure, which marks interesting paths for switching, we introduced the DTP-betweenness centrality in Definition 5.18. To estimate the relation of the power flow and the different edges having different centrality values c_{DTPB} for the different benchmark cases with different assorted characteristics, we calculated the MPF for the network after removing a single edge e with centrality $c_{\mathsf{DTPB}}(e)$ from the network and decreasingly order the normalized edges by the centrality. Note that we normalized the MPF and edge index by the network's $\mathrm{OPT}_{\mathsf{MPFP}}$ value and $|E|$, respectively. The normalization is necessary to aggregate all cases from Figures C.1–C.3 into one plot. The 32 % and 35 % quantiles in Figure 5.13d show cut points where the MPF decreases while switching an edge. These quantiles show that 32 % of the test cases at low centrality result in worse results than the plotted line. This effect happens mainly with edges having a small c_{DTPB} (i. e., the normalized edge index is close to 1). For the 35 % quantile there are only deflections at edges with low centrality. Note, that the line at zero represents nesta_case57_ieee, nesta_case2383wp_mp, and nesta_case3012wp_mp, where switching of an edge leads to a network with no feasible MPF. Note that deflection at edges with low centrality motivates the algorithm also for ROP, since edges with low centrality are more essential for the power grid to get into a stable operation and should be considered first.

Table 5.2: The PF, MPF, MTSF and OTS models from Section 5.1 are evaluated on the NESTA benchmark sets [CGS14]. The parameters $|V|$, $|E|$, and $|S_{\mathcal{P}}|$ represent the number of vertices, edges and switched edges for a problem $\mathcal{P}$, respectively, and the optimal solutions are given in $\text{OPT}_{\mathcal{P}}$. Since OTSP minimizes the cost, the flow value F_{OTSP} is shown, too. The maximum possible generation is given in the last column (marked red if it is larger than the OPT_{MFP}). The yellow rows mark the interesting cases where OPT_{MPFP} is smaller than the $\text{OPT}_{\text{MTSFP}}$.

NESTA Case	$\lvert V\rvert$	$\lvert E\rvert$	$\lvert S_{\text{MTSFP}}\rvert$	$\lvert S_{\text{OTSP}}\rvert$	$\lvert S_{\text{MaxST}}\rvert$	OPT_{OTSP} in \$	F_{OTSP}	OPT_{PF}	OPT_{MPFP}	$\text{OPT}_{\text{MTSFP}}$	$\text{OPT}_{\text{MaxST}}$	OPT_{MFP}	max Gen
3_lmbd	3	3	1	1	1	5 638.97	315	315.00	353.53	4 000.00	4 000.00	4 000.00	4 000.00
4_gs	4	4	0	1	1	109.99	500	500.00	969.00	969.00	719.00	969.00	1 639.00
5_pjm	5	6	0	1	3	14 991.30	1000	1 000.00	1 448.39	1 448.39	1 356.00	1 530.00	1 530.00
6_c	6	7	4	1	4	22.77	107.5	107.50	370.00	370.00	248.00	370.00	1 002.00
6_ww	6	11	6	6	6	3 046.41	210	210.00	332.80	360.00	360.00	470.00	530.00
9_wscc	9	9	6	0	2	5 216.03	315	315.00	770.00	770.00	770.00	770.00	820.00
14_ieee	14	20	15	7	10	231.41	259	259.00	425.00	425.00	425.00	425.00	425.00
24_ieee_rts	24	38	28	10	18	61 001.20	2850	2 850.00	3 405.00	3 405.00	3 405.00	3 405.00	3 405.00
29_edin	29	99	55	54	79	29 669.40	56325.9	56 325.90	81 597.50	81 603.40	76 158.80	82 384.80	82 384.80
30_as	30	41	32	10	15	767.60	283.4	283.40	435.00	435.00	435.00	435.00	435.00
30_fsr	30	41	30	14	15	565.21	189.2	189.20	335.00	335.00	322.20	335.00	335.00
30_ieee	30	41	34	12	19	152.67	283.4	283.40	390.00	390.00	252.00	390.00	884.00
39_epri	39	46	35	7	17	95 578.30	6254.23	6 254.23	7 227.00	7 227.00	7 227.00	7 227.00	7 367.00
57_ieee	57	80	75	25	40	1 125.14	1250.8	1 250.80	1 377.00	1 377.00	1 377.00	1 377.00	1 377.00
73_ieee_rts	73	120	87	34	56	183 004.00	8550	8 550.00	10 215.00	10 215.00	10 215.00	10 215.00	10 215.00
89_pegase	89	210	145	70	142	5 733.37	5733.37	5 733.37	9 921.23	9 921.23	9 718.23	9 921.23	9 921.23
118_ieee	118	186	150	—	92	—	—	4 242.00	7 119.00	7 119.00	6 830.00	7 134.00	7 134.00
162_ieee_dtc	162	284	269	77	154	3 904.81	7239.06	7 239.06	8 296.00	8 296.00	7 931.00	8 296.00	9 685.00
189_edin	189	206	71	62	62	783.95	1367.83	1 367.83	2 987.00	2 987.00	2 987.00	2 987.00	3 012.00
300_ieee	300	411	290	—	185	—	—	23 527.20	31 568.00	31 568.00	30 504.00	31 735.00	32 492.00
2736sp_mp	2736	3269	2518	545	1307	991 228.00	18074.5	18 074.50	20 246.70	20 246.70	20 010.70	20 246.70	20 246.70
2737sop_mp	2737	3269	2536	630	1305	621 780.00	11267.2	11 267.20	14 677.90	14 677.90	14 537.20	14 677.90	14 677.90
2746wop_mp	2746	3307	2547	649	1349	861 568.00	18960	18 960.00	23 759.50	23 759.50	—	23 759.50	23 759.50
2746wp_mp	2746	3279	2487	594	1318	1 261 620.00	24873	24 873.00	27 618.70	27 618.70	—	27 618.70	27 618.70
3120sp_mp	3120	3693	2793	—	1513	—	—	21 181.50	25 406.00	25 406.00	24 856.50	25 406.00	25 406.00

5.8 Conclusion

This paper is the first to provide algorithms with provable guarantees for MTSFP on certain graph structures and shrinks the gap between theory and practice. In addition, it provides an extensive theoretical analysis of the MTSFP, builds connections to related problems and shows how to simplify the network including the transformations from a bounded to an unbounded MTSFP, and the equivalence of OTSP and MTSFP. We introduce an exact algorithm for networks with one generator and one consumer for certain network structures and show when it becomes NP-hard on s-t-networks. On that base, we define a new centrality measure based on Dominating Theta Paths (DTPs) representing the s-t-path with the smallest voltage angle difference. For multiple generators and sinks in the network, we give a 2-approximation for cacti. At the end, the complementing evaluation rounds off the theoretical results. The simulations show very good results on the NESTA benchmark set with arbitrary graph structures, i. e., the results are in nearly all cases either optimal or very close to the optimum.

However, there are many open problems. It is unknown if the reachability test can be done in polynomial time and, if not, if there is still a polynomial time algorithm for DTP (see discussion in Section 5.4.3). Another open question is if there is a PTAS on cacti. The current idea is a rounding based algorithm. There are many other open problems such as the complexity and the existence of algorithms while fixing a set of edges as non-switchable (motivated by TNEP), as well as minimizing or constraining the number of switches. In addition, we used a linearization of the AC-model denoted by DC-model. Though, we could not easily transfer our results directly to AC-power grids, the general idea can be applied as a heuristic since it is based on the fact that the power flow uses the path with the smallest resistance, which makes sense also with the AC-model. However, the evaluation of that will be part of our future research.

6 Continuous Control Units[1]

Ideal FACTS Placement – A Susceptance Scaling Approach

Future power grids will offer enhanced controllability due to the increased availability of power flow control units such as FACTS and switches. Contrary to switches that offer a discrete decision, FACTS allow to manipulate the power flow continuously by changing a line parameter in a certain range. As the installation of control units in the power grid is an expensive investment, we are interested in using few controllers to achieve high controllability. In particular, two questions arise: How many flow control units are necessary to obtain globally optimal power flows? And if fewer flow control units are available, what can we achieve with them?

Using steady state IEEE benchmark data sets, we explore experimentally that a small number of controllers placed at certain grid buses (i. e., vertices) or lines (i. e., edges) already suffices to achieve globally optimal power flows. With globally optimal power flows, we mean power flows that have the same value as the minimum cost flows using a graph-theoretical flow. We present a graph-theoretical explanation for this behavior. To answer the second question we perform a set of experiments that explore the existence and costs of feasible power flow solutions at increased loads with respect to the number of flow control units in the grid. We observe that adding a small number of flow control units reduces the flow costs and extends the existence of feasible solutions at increased load. The central task of any electrical power infrastructure is the reliable and cost-efficient supply of electrical energy to industry and population on a national or even continental scale. Future power grids and their usage are subject to fundamental changes due to the shift towards renewable distributed energy production and the installation of new power flow control units, which offer increased control, but make the grid operation more demanding. Not only do these changes lead to a much larger number of independent power producers (IPP), which are highly distributed in the network, but they also cause very different patterns of energy flow. For example, regions with off-shore wind farms may sometimes produce enough energy to supply remote consumers, but at other times they are consumers themselves. In particular, this may require long-distance energy transmission and frequent flow direction changes. Most of the existing power grids, however, were not designed for such transmission patterns. The current strategy to cope with these changes is to either extend the grid with additional transmission lines, or to install advanced control units to facilitate better utilization of the existing infrastructure.

[1] This chapter is partly published in [Lei+15a, Lei+15b, Mch+15].

(S1) Extending the grid with additional transmission lines.

(S2) Installing control units such as Flexible AC Transmission Systems (FACTS) [Hin93] to enhance the grid utilization.

In this chapter, we consider the latter option and study the advantageous effects of making selected vertices or edges of a power grid controllable, both in terms of the minimum number of controllable units needed for achieving maximum flow control and in terms of the operation costs and the existence of feasible power flows at critical line capacities. We discuss the placement of control units on vertices and edges, which we call *flow control vertex* (FCV) and *flow control edge* (FCE), respectively.

In abstract terms, we assume that a *flow-control unit* that is a FCV is able to flexibly distribute the entire power flow at the placed vertex among its incident edges, as long as Kirchhoff's current law—that is equivalent to the *flow-conservation property* meaning the in-flow to the vertex equals its out-flow—is satisfied. In terms of FCE, we assume that a flow-control unit can only flexibly control the power flow on one edge by changing the voltage angle difference for that particular edge (see Figure 6.1b and c). These flow control units can be realized using power electronics devices known as *Flexible* AC *Transmission Systems* (FACTS), which are a class of power systems that have the capabilities to control various electrical parameters [GH99, Hin93]. More specifically for FCV, since we are interested in controlling the real power flow on the edges incident to a particular vertex that has a FCV, we can realize our flow control units by installing on each (but one) incident edge a *unified power flow controller* (UPFC), which is a FACTS that is able to control the voltage magnitude and angle and consequently has control of the real and reactive power flow on the particular edge by changing the voltage angle difference [GH99, Nor+97]. In terms of FCEs, this would be a UPFC on that particular edge. Recall that in Chapter 4, we introduced the geometrical interpretation of a feasible electrical flow. A FACTS is able to change the voltage angle difference, which can be modeled by a continuously changeable susceptance b. In the geometrical setting this basically means that we are able to change the aspect ratio of a rectangle by resizing it in one dimension (e. g., in our examples it represents the height; see Figure 6.1).

One of the most important tasks in operating a power grid is to control the energy production of each power generator such that supply and demand are balanced and the resulting power flow does not exceed the thermal line limits of the power lines. Among all solutions we are interested in one that minimizes the total energy production and transmission cost. This is called *Economic Dispatch Problem* (EDP). The Optimal Power Flow Problem (OPFP) solves EDP in power grids without FACTS [Car62]. The methods to solve OPFP have subsequently been refined and generalized, see the recent surveys by Frank et al. [FSR12a, FSR12b]. However, the standard OPFP does not incorporate flow control units and cannot exploit the extended flow control possibilities

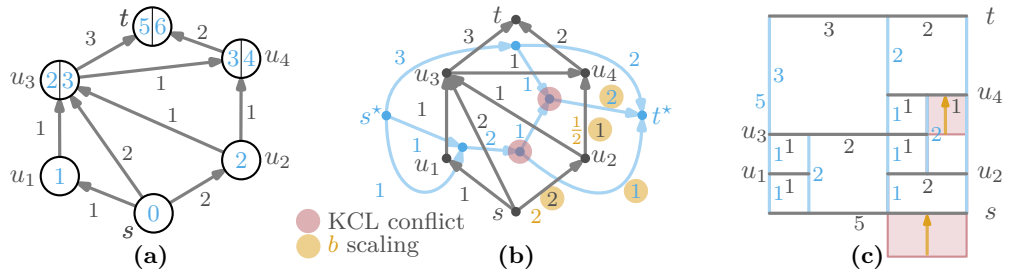

Figure 6.1: We use the example graph of Felsner [Fel13, p.18] that was already used in Chapter 4 to show the geometric analogies for the FACTS placement. A FACTS placement basically represents a susceptance scaling. (a) Shows a feasible flow that is not a feasible electrical flow, since the voltage angles $\theta^v(u)$ at each vertex $u \in V$ are not unique. This is illustrated at vertices $u_3, u_4, t \in V$, where for example vertex u_3 has two voltage angle labels $\theta^v{}_1(u_3) = 2$ and $\theta^v{}_2(u_3) = 3$. (b) The corresponding flows are shown in the primal graph G and the dual graph $G^\star$ (see Chapter 4 for more information). The flows on the two graphs do not map on the associated edges. A mapping of the primal flow would result in KCL conflicts in the dual graph $G^\star$. Applying the shown susceptance scaling results in a feasible electrical flow. (c) This is the geometric interpretation (see Section 4.3.3 for more information) of the susceptance scaling, where each edge corresponds to a rectangle. A susceptance scaling is a scaling of a rectangle's aspect ratio by resizing it in one dimension (here we define it as a height scaling). The scaling reduces the height of the bottom right square of size 2×2 to a rectangle of size 1×2 and the center right square of size 1×1 to a rectangle of size 2×1. The mentioned susceptance scaling removes the conflicts that are highlighted by the red areas.

to obtain globally optimal solutions. Recall from Section 3.3.1 that electrical elements such as FACTS can be modeled by the admittance matrix and incorporated into the standard flow analysis. However, it usually models fixed parameters for the electrical elements. In addition, the standard objective does not incorporate these components or flow control in general.

Hence, we propose in Section 6.2.2 a new hybrid DC-based model for power flows in power grids that combines traditional grid elements (i. e., vertices and edges) with some flow-control units (meaning FCVs and FCEs). In order to answer our questions on the effects of installing flow control units, we solve the EDP in our hybrid model using a linear programming (LP) formulation. Our LP combines a standard graph-theoretical network flow model, which already satisfies Kirchhoff's current law at all vertices, with additional constraints for Kirchhoff's voltage law in those parts of the grid that are not equipped with flow control units. Thus we are able to obtain feasible electrical flows that minimize, similarly to OPFP, the overall flow costs in terms of generation and transmission costs.

Using the well-known IEEE power systems test cases, we performed simulation experiments related to two key questions, which take into account that the FACTS

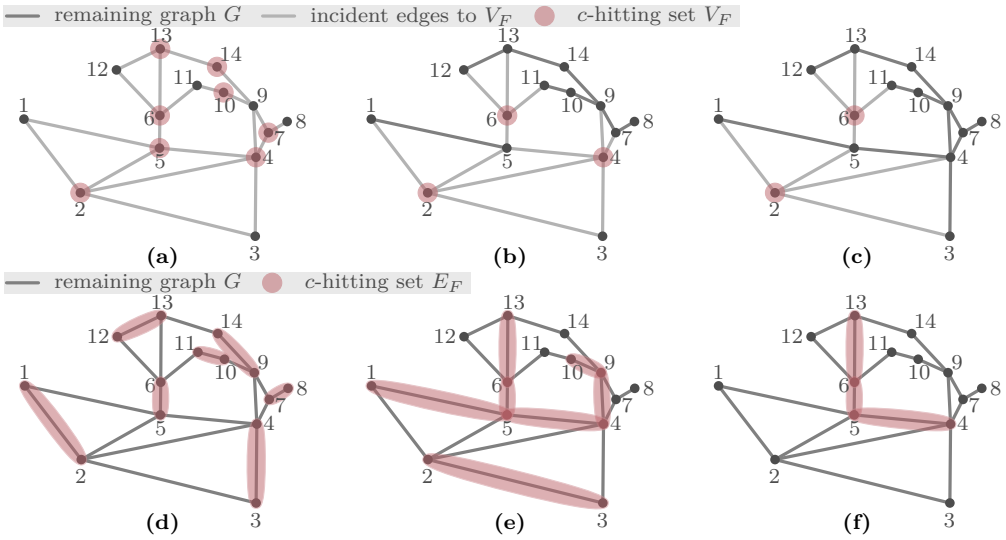

Figure 6.2: The IEEE 14 bus benchmark case is a graph G with 14 vertices and 20 edges [Uni14]. The vertices (respectively edges) in the vertex hitting set ${V_F}^c$ (respectively edge hitting set ${E_F}^c$) are marked red •. Edges that are affected by a vertex hitting set have a light gray color and the remaining graph that we call *native power grid* has a dark gray color. (a) The 1-pumpkin hitting set (i. e., vertex cover) has $|{V_F}^{c=1}| = 8$ vertices and the remaining graph G is empty. (b) The 2-pumpkin hitting set (i. e., feedback vertex set) has $|{V_F}^{c=2}| = 3$ vertices and the remaining graph is a forest. (c) The 3-pumpkin hitting set (i. e., diamond hitting set) has only $|{V_F}^{c=3}| = 2$ vertices and the remaining graph is a cactus graph. (d)–(f) Represent the same results as (a)–(c), but on edges and the set is denoted by ${E_F}^c$. We get the following sizes for the hitting set sizes $|{E_F}^{c=1}| = 7$, $|{E_F}^{c=2}| = 7$, and $|{E_F}^{c=3}| = 3$.

needed for realizing our flow control units in reality constitute a significant and expensive investment and hence their number should be as small as possible.

(Q1) How many flow control units are required and where do they have to be placed in order to obtain a lower bound for the operating costs?

(Q2) If the number of available flow control units is given, do we still see a positive effect on the operating costs and on the operability of the grid during peak periods of the grid?

In Section 6.5 we address the first question. In our simulations we determine the minimum number of flow control vertices necessary to achieve the same solution quality as in a power grid in which each vertex is controllable and which clearly admits an upper bound on what can be achieved with the network topology. Interestingly, it turns out that a relatively small number of flow control units are sufficient for this. In fact, we can prove a theorem stating a structural graph-theoretic property, which, if

met by the placement of flow control units, implies the optimality of the power flow and serves as a theoretical explanation of the observed behavior. Section 6.6 deals with the second question of operating a power grid close to its capacity limits, which becomes increasingly relevant as the consumption of electrical energy grows faster than the grid capacities. Our experiments indicate that installing few flow control units in a power grid is sufficient not only to achieve lower costs compared to a solution of OPFP, but also allows to operate the grid at capacities for which no feasible solution of OPFP exists any more.

6.1 Preliminaries

In this section we recall some basic notions from graph theory. Although, for technical reasons, the graphs we use for modeling power grids are directed, when considering the topology of the network, we always consider the underlying undirected graph. Thus, in the following let $G = (V, \overleftrightarrow{E})$ be an undirected graph (see Section 3.1).

The graph G is *connected* if it contains a path between any two vertices. A *connected component* of G is a maximal connected subgraph of G (maximal with respect to inclusion). A *cactus* is a graph where every edge is contained in at most one cycle. A *tree* is a connected graph that does not contain a cycle. A *forest* consists of multiple connected components, where each connected component constitutes a tree.

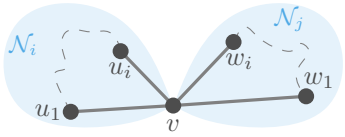

Figure 6.3: A cutvertex v decomposes the network $\mathcal{N}$ into at least two networks $\mathcal{N}_i$ and $\mathcal{N}_j$.

A *cut vertex* (also known as articulation point) is a vertex of a graph whose removal increases the number of connected components (see Figure 6.3). Note from Figure 6.3 that any path from vertex u_i to vertex w_i passes through the cut vertex v. A *biconnected component* is a maximal subgraph that does not have a cut vertex. Biconnected components are also called nonseparable graphs. Such nonseparable graphs with at least three edges have the following properties: The nullity $n > 0$ (see Section 4.1), $\deg(v) \geq 2$ for all vertices $v \in V$, and each edge lies on a cycle. The decomposition of a graph into its nonseparable graphs is unique [SR61, p.38]. Note that a biconnected component of a forest is either *trivial* in the sense that it consists of a single vertex, or it consists of a single edge. Similarly, a biconnected component of a cactus is trivial, a single edge, or a cycle.

In the following we introduce two special hitting sets that are the Vertex Cover Problem (VCP) and the Feedback Vertex Set Problem (FVSP), which we will generalize in the next paragraph.

Vertex Cover Problem VCP(G, k)

Instance: A graph $G = (V, \overleftrightarrow{E})$, and parameter $k \in \mathbb{N}$.

Question: Is there a vertex cover VC(G) of size at most k such that one endpoint of each edge $\{u, w\} \in \overleftrightarrow{E}$ belongs to a subset of ${V_F}^{c=1} \subseteq V$ with $|{V_F}^{c=1}| \leq k$?

Feedback Vertex Set Problem FVSP(G, k)

Instance: A graph $G = (V, \overleftrightarrow{E})$, and parameter $k \in \mathbb{N}$.

Question: Is there a feedback vertex set FVS(G) of size at most k such that at least one vertex of each cycle $c \in C$ belongs to a subset of ${V_F}^{c=2} \subseteq V$ with $|{V_F}^{c=2}| \leq k$?

A *vertex hitting set* of $G = (V, E)$ with respect to a class of graphs $\mathcal{G}$ is a set of vertices $V_F \subseteq V$ such that $G - V_F \in \mathcal{G}$. We will only be interested in hitting sets with respect to forests and cacti. The former is also called *feedback vertex set*. Naturally, one is interested in finding a set V_F that is as small as possible. A generalization of vertex cover and feedback vertex set is called c-pumpkin hitting set. A *minor* H of a graph G is a graph that can be obtained from G by deletion of vertices and edges or by contraction of edges. A graph that has no c-pumpkin minor for $c = 1$ is an empty graph (i. e., vertex cover; see Figure 6.2a), for $c = 2$ is a forest (i. e., feedback vertex set; see Figure 6.2b), and for $c = 3$ is a cactus (i. e., diamond hitting set; see Figure 6.2c). We call a subset of vertices ${V_F}^c$ c-pumpkin hitting set if there is a vertex subset ${V_F}^c \subseteq V(G)$ such that $G - {V_F}^c$ consists of no c-pumpkin minor (see Figure 6.4 for different c-minors). In addition, we try to minimize the size of the c-pumpkin hitting set. The general problem definition is given below.

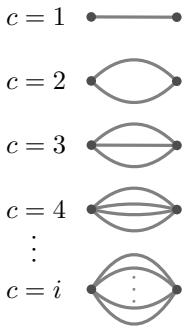

Figure 6.4: Forbidden c-pumpkin minors for different values of c with $c \in \mathbb{N}_{>0}$.

c-Pumkin Hitting Set Problem p-c-Hit(G, c, k) [Jor+11a, Jor+11b]

Instance: A graph G, parameter $c \in \mathbb{N}_{>0}$, and $k \in \mathbb{N}$.

Question: Is there a c-pumpkin hitting set ${V_F}^c \subseteq V$ of size $|{V_F}^c| \leq k$ such that $G - {V_F}^c$ consists of no c-pumpkin minor?

Note that the problem of finding a c-pumpkin hitting set is already NP-hard for all $c \geq 1$ [Jor+11a, Jor+11b]. Analogous to vertex hitting set, we define the *edge hitting set* $E_F \subseteq E$ such that $G - E_F \in \mathcal{G}$ and a c-pumpkin hitting set is denoted by ${E_F}^c \subseteq E(G)$.

An Exact Model for (Special) Hitting Sets. In general a *set system* (also known as hypergraph or range space) is a tuple (V, S), where V is the set of elements such as vertices and S is the set of subsets of V that is not necessarily a power set meaning $\mathcal{P}(V)$. The latter would imply an exponential size of S with $|S| = 2^{|V|}$. A *hitting set* $V_F \subseteq V$ is a set that has at least one element in each subset of S meaning $V_F \cap S_i \neq \emptyset$ for all $S_i \in S$ with $i \in \mathbb{N}$ (see Equation 6.1b) and thus, a hitting set highly depends on the definition of the set S. One possibility to define the set of subsets is $S = \bigcup_{e_i \in E} \{S_i \cap V \mid S_i = e_i, e_i = \{u, v\}\}$, which represent the set of subsets for vertex cover. The hitting set problem is defined by Equation 6.1.

$$\text{minimize} \quad \sum_{v \in V} z(v), \tag{6.1a}$$

$$\text{subject to}$$

$$\sum_{v \in S_i} z(v) \geq 1 \qquad \forall S_i \in S, \tag{6.1b}$$

where $z \colon V \to \{0, 1\}$ is a decision variable that is $z(v) = 1$ if v is in the hitting set $v \in V_F$ and 0 otherwise. The latter represents basically the integrality constraint that explains why this is an ILP. The solution to the above defined ILP dependent on S is a hitting set ${V_F}^{c=1}$ that is a 1-pumpkin hitting set (i. e., vertex cover) [Cyg+15, p.60].

Now, we are interested in hitting sets such that the remaining graph has no c-pumpkin minor. Thus, we have to generalize the definition of S with subsets $S_i \in S$ such that S_i is a connected component (also known as block) that is not c-pumpkin minor free. We are looking for all such connected components. This is quite similar to the Traveling Salesman Problem (TSP) approach that is generating subtour elimination constraints meaning if the tour does not have the correct length then the tour represents a subtour that is excluded from the solution set. However, we add a restriction to the structure of S_i that is a connected component that has at least one c-pumpkin minor. Thus, in each solver callback we add new sets S_i with $S_i \subseteq V \setminus \bigcup_{v \in V} \{v \mid z(v) = 1\}$. For c-pumpkins with $c = 2$ or $c = 3$ we use block-cut trees to identify the set of maximum biconnected components and check by the ratio of the number of vertices to the number of edges whether each new connected component β is large enough. This means that for $c = 2$, we have $|V(\beta)| - 1 < |E(\beta)|$ that excludes trees and for $c = 3$ we have $|V(\beta)| < |E(\beta)|$ that excludes simple cycles. This can be extend to any $c \in \mathbb{N}$ (see Figure 6.4). The substructure exclusion leads to exponentially many constraints. Thus, a common way to solve this ILP is by using techniques such as column generation.

6.2 A Hybrid Mathematical Model for the Placement of Continuous Control Units

In this section we introduce three graph-theoretic flow models for optimal power flows. We propose a *hybrid model* that combines the flow model and the electrical flow model in order to handle power grids with flow control units. Our models are based on the DC power grid model [Ham07, SJA09, ZMT11], which is commonly used as an approximation of AC grids [OCS04, Pur+05]. An overview of the simplifications is given in Section 3.3.2. We model a power grid $\mathcal{N}$ as a graph $G = (V, E)$, where V is the set of vertices and $E \subseteq \binom{V}{2}$ is the set of edges. The underlying power grid is an undirected graph. We model the undirected graph using a directed graph by replacing the undirected edges $\{u, v\}$ by two directed edges $(u, v), (v, u) \in E$ that are directed to either vertices of the original edge. However, in some cases we neglect for the notational convenience the orientation and use the undirected edge that is denoted by $\overleftrightarrow{e} \in \overleftrightarrow{E}$, where $\overleftrightarrow{e}$ is the undirected edge of e. The vertices represent the buses, some of which may be special generator and consumer vertices, and the edges represent the branches, which may be transmission lines between the incident vertices or transformers. There is a subset $V_G \subseteq V$ of the vertices that represent generator vertices. We define the functions $\underline{p_g}, \overline{p_g} \colon V_G \to \mathbb{R}_{\geq 0}$ that represent the minimum and maximum supply for each generator, respectively. In this chapter, we assume that the lower generation bound is zero meaning $\underline{p_g} \equiv 0$. Further, there is a subset $V_D \subseteq V \setminus V_G$ of consumer vertices. We define the functions $\underline{p_d}, \overline{p_d} \colon V_D \to \mathbb{R} \cup \{\infty\}$ that represents the minimum and maximum real power demand, respectively. We assume that the demands are fixed meaning $\underline{p_d}(u) = \overline{p_d}(u) = p_d(u)$ for each consumer $u \in V_D$. Without loss of generality, we assume that $V_G \cap V_D = \emptyset$.

6.2.1 The Objective Function

Each generator $u \in V_G$ is equipped with a convex cost function $\gamma_u : \mathbb{R} \to \mathbb{R}_{\geq 0}$ with $\gamma_u > 0$ that is assumed to be piecewise linear (see Equation 6.2).

$$\gamma_u(x) = \max\{a_i x + c_i \mid (a_i, c_i) \in F_u\}, \tag{6.2}$$

where F_u is the set of all piecewise linear functions of γ_u and $a_i \leq a_{i+1}$ for $i \in \mathbb{N}$.

Each edge $e \in E$ has a thermal line limit that is modeled by a capacity function $\mathrm{cap} \colon E \to \mathbb{R}$ restricting the real power. Further, each edge causes a certain loss of power depending on the physical edge parameters and the actual power flow on that edge. These losses are again approximated as a convex, piecewise linear function $\ell_e \colon \mathbb{R} \to \mathbb{R}_{\geq 0}$ for each edge $e \in E$ (see Equation 6.3).

$$\ell_e(x) = \max\{a_i x + c_i \mid (a_i, c_i) \in F_e\}, \tag{6.3}$$

where F_e is the set of all piecewise linear functions of ℓ_e and $a_i \leq a_{i+1}$ for $i \in \mathbb{N}$.

A *flow* f in a power grid $\mathcal{N}$ is a function $f : V \times V \to \mathbb{R}$ that complies with the skew symmetry property $f(u,v) = -f(v,u)$ for all $u, v \in V$. For every vertex u in $V(G)$, we define its *net out-flow* $f_{\text{net}}(u) \coloneqq \sum_{\{u,v\} \in \overrightarrow{E}} f(u,v)$. For a flow f, we further define two types of cost functions. The total *generator cost* is a function $c_g : \mathbb{R} \to \mathbb{R}_{\geq 0}$ that is defined in Equation 6.4 and the total *line loss* is a function $c_\ell : \mathbb{R} \to \mathbb{R}_{\geq 0}$ that is defined in Equation 6.5.

$$c_g(f) = \sum_{u \in V_G} \gamma_u(f_{\text{net}}(u)), \tag{6.4}$$

$$c_\ell(f) = \sum_{(u,v) \in E} \ell_{(u,v)}(|f(u,v)|)\,. \tag{6.5}$$

To obtain the overall cost for a flow f, we weight these two terms with $\lambda \in [0,1]$ such that the objective function represents a multi-criteria objective (see Equation 6.6) weighted with λ.

$$c_\lambda(f) = \lambda \cdot c_g(f) + (1-\lambda) \cdot c_\ell(f). \tag{6.6}$$

Our goal is to minimize this objective function c_λ in different models.

6.2.2 Power Flow Models

The most basic model is the *flow model*, where f has to satisfy the constraints given in the Equations 6.7–6.10. We call a flow satisfying these constraints *feasible*. Equation 6.10 models the thermal line limits or real power capacities of all edges and is called *capacity constraint*. Equation 6.7 models the zero net out-flow for intermediate vertices, i. e., vertices that are neither generators nor consumers. Equation 6.8 models that all consumer demands are satisfied and is called *demand constraint*. Finally, Equation 6.9 models that all generators respect their production limits and is called *generator constraint*. The Equations 6.7–6.9 are called *flow conservation constraints*.

$$f_{\text{net}}(v) = 0 \qquad v \in V \setminus (V_G \cup V_D), \tag{6.7}$$

$$f_{\text{net}}(v) = -p_d(v) \qquad v \in V_D, \tag{6.8}$$

$$0 \leq f_{\text{net}}(v) \leq \overline{p_g}(v) \qquad v \in V_G, \tag{6.9}$$

$$|f(u,v)| \leq \text{cap}(u,v) \qquad \forall (u,v) \in E. \tag{6.10}$$

The flow model (i. e., Equations 6.7–6.10) neglects some physical properties of electrical flows, in particular Kirchhoff's voltage law. Thus, the computed power flows can only be applied to power grids where every vertex is a control vertex. In contrast, the *electrical flow model*, e. g., according to Zimmerman ET AL. [ZMT11], models the power flow using the same set of constraints as the flow model, but additionally requires the existence of a suitable voltage angle assignment $\theta^v : V \to \mathbb{R}$ such that

for each edge $\{u, v\} \in \overleftrightarrow{E}$ the power flow specific constraint holds (see Equation 6.11). The power flow constraint basically represents Kirchhoff's Voltage Law (KVL) that is combined with Ohm's law. More details can be found in Chapter 4.

$$f(u, v) = b(u, v)(\theta^v(v) - \theta^v(u)), \tag{6.11}$$

where the *susceptance* $b(u, v)$ is a function $b\colon E \to \mathbb{R}$. This is equivalent to restricting the model to feasible flows that also satisfy the KVL, or, in other words, no flow control units are used. This yields a model that matches the situation in the traditional power grid existing today. We call a feasible flow f a *feasible electrical flow* if there exists a voltage angle assignment θ^v satisfying Equation 6.11. We are now able to give a complete definition of the power grid by the tuple $\mathcal{N} = (G = (V, E), V_G, V_D, \mathrm{cap}, b, \gamma_{u\in V_G}, \ell_{e\in E}, \underline{p_g}, \overline{p_g}, p_d)$.

Recall from the introduction that flow control vertices (FCVs) and flow control edges (FCEs) can be technically realized by UPFCs, which are FACTS. Ideal FACTS as introduced by Griffin ET AL. [GAG96] are often used to simplify the modeling of FACTS by using a linear model and assuming a complete and independent control of the real and reactive power. Our flow control units are ideal FACTS that control the power flow to all incident edges in terms of FCVs and the power flow on that particular edge in terms of FCEs. The flow model—in contrast to the electrical model—assumes flow control units at each vertex or each edge, whereas the electrical model assumes no immediate control of the power flow. Instead, the grid is balanced by changing the generator outputs only. In the following, we propose a *hybrid model* that combines the flow model and the electrical flow model in order to handle power grids with flow control vertices (resp. edges) at a subset of selected vertices (resp. edges).

6.2.3 Flow Control Units on Vertices

In this section, we focus on continuous flow control units that are placed on vertices. As mentioned above, we call them flow control vertices (in short FCVs). Let $V_F \subseteq V$ be a subset of vertices of G. We denote by G_{V_F} the power network obtained from G by considering all vertices in V_F as flow control vertices. We call any subgraph $G' = G[V']$ induced by a subset $V' \subseteq V \setminus V_F$ of the vertices without controllers a *native power grid* of G. A flow f on G is a *feasible electrical flow* for a native power grid $G' \subseteq G$ if there exists a voltage angle assignment $\theta^v\colon V \to \mathbb{R}$ such that every edge in G' satisfies Equation 6.11. In this case we call θ^v a *feasible (voltage) angle assignment* for G'.

A feasible flow f is a *feasible electrical flow for* G_{V_F} if and only if f is a feasible electrical flow for the *maximal native power grid* $G - V_F = G[V \setminus V_F]$. Intuitively, this models the fact that a power flow in G_{V_F} must be a feasible flow and that it satisfies the Kirchhoff's voltage law in the maximum native power grid.

Obviously, if $V_F \subseteq V_F'$ and f is a feasible electrical flow for G_{V_F}, then f is also a feasible electrical flow for $G_{V_F'}$. Hence the minimum value of the cost c_λ does not increase when adding more flow control buses.

We note that each of the models can easily be expressed as a Linear Programming (LP), and thus in all three models an optimal solution can be computed efficiently [BJS04]; see Equation 6.12. However, the flow model can be reduced to a special minimum cost network flow problem, for which efficient exact optimization algorithms exist [Gol97]. We describe this reduction in the Section 6.2.5.

We present the problem formulation as an Integer Linear Programming (ILP) formulation (see Equation 6.12). Though Equation 6.12 has only linear constraints—which would imply that we have an ILP—the objective function has two piecewise linear cost functions, where the decision of which piece we select is done by an integer variable. Thus, the whole program is an ILP. In the ILP, we minimize the generation costs c_g and losses c_ℓ shown in Equation 6.12a under flow and electrical constraints. The main flow constraints comprise the conservation of flow (Equation 6.12b), demand and generator constraints (Equations 6.12d and 6.12e), and capacity constraints (Equation 6.12f). Whereas the electrical constraints describe the electrical feasibility for the native power grid shown in Equation 6.12c. Recall that each consumer $u \in V_D$ has a fixed power demand $p_d(u) \in \mathbb{R}$ and $V_F \subseteq V$ is the set of flow control vertices.

$$\underset{f}{\text{minimize}} \quad c_\lambda(f) = \lambda \cdot c_g(f) + (1-\lambda) \cdot c_\ell(f) \tag{6.12a}$$

subject to

$$f_{\text{net}}(v) = 0 \qquad \forall v \in V \setminus (V_G \cup V_D) \tag{6.12b}$$

$$f(u,v) = b(u,v)(\theta^v(u) - \theta^v(v)) \quad \begin{cases} \forall \{u,v\} \in E \text{ s.t. } u,v \notin V_F & \text{for FCVs} \\ \forall \{u,v\} \in E \setminus E_F & \text{for FCEs} \end{cases} \tag{6.12c}$$

$$f_{\text{net}}(v) = -p_d(v) \qquad v \in V_D \tag{6.12d}$$

$$0 \le f_{\text{net}}(v) \le \overline{p_g}(v) \qquad v \in V_G \tag{6.12e}$$

$$|f(u,v)| \le \text{cap}(u,v) \qquad \forall (u,v) \in E. \tag{6.12f}$$

However, note that the ILP represents the hybrid model, which solves the feasibility problem only. A proper problem definition and an overview of related problems will be given in Section 6.3. In addition, different possibilities to place control units are given in Section 6.5. The latter will make extensive use of the above formulation.

6.2.4 Flow Control Units on Edges

We define analogously to the set of *flow control vertices* (FCVs) the set of *flow control edges* (FCEs) that is denoted by $E_F \subseteq E$. FCEs are edges with ideal FACTS controlling

flow on them. We denote by G_{E_F} the subgraph of G that contains all edges of E_F and their incident vertices.

In the standard *flow model* the flow on all edges can be manipulated, i. e., it is like having a FACTS on every edge in a power grid. In case of FCEs this means $E_F = E$. The standard flow model asks to find a flow, i. e., it neglects Equation 6.11. In the DC *flow model* [ZMT11] the flow on edges cannot be controlled, which translates to $E_F = \emptyset$ in case of FCEs. The DC *flow model* requires to find a feasible electrical flow, i. e., Equation 6.11 satisfied for all edges $e \in E \setminus E_F$. The *hybrid model* is formalized in Equation 6.12 as an LP, the flow model and the DC flow model are combined and it is required to find a flow on G_{V_F} such that Equation 6.11 holds only for edges that are not in E_F.

Since an *ideal FACTS* [GAG96] is technically realized on transmission lines, it is more realistic to consider FCEs instead of FCVs. However, we can easily translate the described models designed for FCVs to models on FCEs by simply replacing V_F by E_F and G_{V_F} by G_{E_F} and vice versa (see Equation 6.12c).

Recall that the EDP is the problem of generating the required amount of power while obtaining minimum operation cost and meeting the constraints in Equations 6.7–6.9. The objective function $c_\lambda(f)$ describing the operation cost is a weighted function of generator costs $c_g(f)$ and transmission line losses $c_\ell(f)$, where $\lambda \in [0, 1]$ is the weight factor (see Equations 6.6 and 6.12a). The overall optimization problem is given in Equation 6.12 as an LP.

6.2.5 Reduction to MinCostFlow

Let $\mathcal{N} = (G = (V, E), s, t, \text{cap}, a)$ be a *s-t flow network* consisting of a directed (multi-) graph G, two dedicated source and sink vertices $s, t \in V$, edge capacities $\text{cap}\colon E \to \mathbb{R}_{\geq 0}$, and edge costs $a\colon E \to \mathbb{R}_{\geq 0}$. A *flow* f in $\mathcal{N}$ is a function $f\colon E \to \mathbb{R}_{\geq 0}$ and it is called *feasible* if it satisfies the capacity constraint in Equation 6.10 and a flow conservation constraint similar to Equation 6.7 that is given in Equation 6.13.

$$\sum_{(u,v)\in E} f(u,v) - \sum_{(v,u)\in E} f(v,u) = 0 \qquad \forall v \in V \setminus \{s,t\}. \tag{6.13}$$

The *flow value* $F(\mathcal{N})$ of a flow f is the total flow from s to t, i. e., $F(\mathcal{N}) = \sum_{(u,t)\in E} f(u,t) = \sum_{(s,u)\in E} f(s,u)$. A feasible flow f with maximum value is called a *maximum flow* in $\mathcal{N}$ and denoted by $\text{MF}(\mathcal{N})$. For a given flow value x the *min-cost s-t flow problem* is to find a feasible flow f of value $F(\mathcal{N}) = x$ such that the cost $c_{\mathcal{N}}(f) = \sum_{e\in E} a(e) \cdot f(e)$ is minimized.

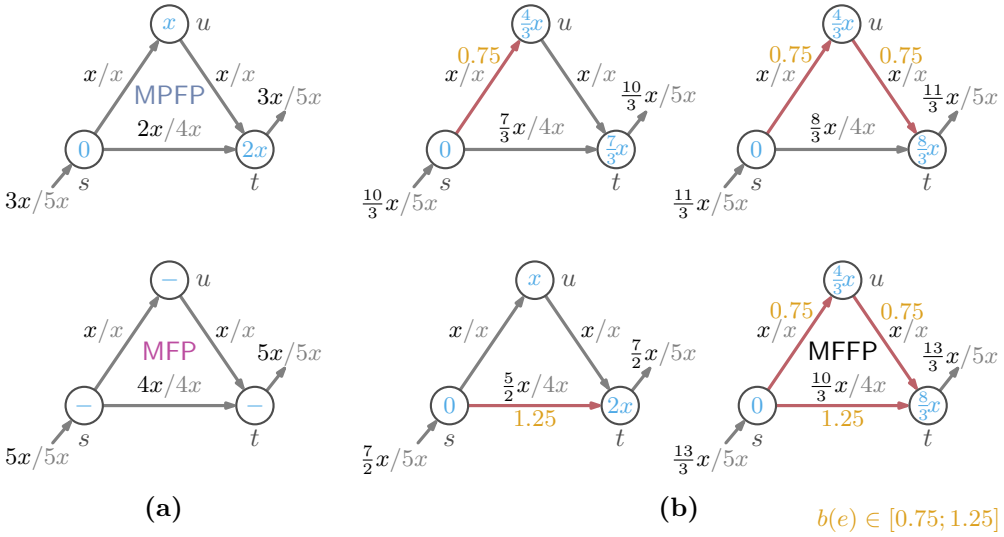

Figure 6.5: A small example graph with three vertices, three edges, one source s, and one sink t. We label each vertex $u \in V$ that is represented by a cycle ○ with a voltage angle $\theta^v(u)$. On the edges, we write the flow f and the edge's capacity cap in the form f/cap. Note that the susceptance on the black edges is fixed to $b \equiv 1$ and when placing FACTS (red edges) the susceptance is in the range $b(e) \in [0.75; 1.25]$ for all $e \in E_F$. (a) The top graph shows an MPF($\mathcal{N}$) with a value of $\text{OPT}_{\text{MPFP}}(\mathcal{N}) = 3x$. The bottom graph shows a MF($\mathcal{N}$) with a value of $\text{OPT}_{\text{MFP}}(\mathcal{N}) = 5x$. (b) Different placement of FACTS and their best susceptance scaling for this situation result in different values for the resulting flow. However, the best placement is shown in the bottom right yielding a MFF($\mathcal{N}$) with a value of $\text{OPT}_{\text{MFFP}}(\mathcal{N}) = {}^{13}/_{3} \cdot x$.

Min-cost s-t Flow Problem

Instance: A network $\mathcal{N}$, parameter $x \in \mathbb{R}$, and $k \in \mathbb{R}_{\geq 0}$.

Question: Is there a feasible flow f of value $F(\mathcal{N}) = x$ such that $c_{\mathcal{N}}(f) \leq k$?

In Section 3.2, we discussed some approaches to tackle the problem. In order to transform the graph $G = (V, E)$ of a power grid into an s-t flow network $\mathcal{N}$, we first add a new source vertex s and a new sink vertex t to V. Each generator $u \in V_G$ is connected by a directed edge (s, u) with capacity $\text{cap}(s, u) = \overline{p_g}(u)$ to the source s. Each consumer $u \in V_D$ is connected by a directed edge (u, t) with capacity $\text{cap}(u, t) = p_d(u)$ to the sink t. Further, we replace each original undirected edge $\{u, v\} \in E$ by two directed edges (u, v) and (v, u), whose capacities $\text{cap}(u, v) = \text{cap}(v, u)$ are given by their common thermal limit $\text{cap}(\{u, v\})$. Recall from the introduction of Section 6.2 that this represents a bidirected graph.

Next, we define the edge costs. It is well known that a convex, piecewise linear edge cost function h can easily be modeled in a flow network by replacing the respective

edge (u, v) with as many copies as the linear pieces of the cost function. The edge capacities are defined by the differences between consecutive breakpoints of h and sum up to $\mathrm{cap}(u, v)$; the individual costs correspond to the costs as defined by the linear pieces between the breakpoints. Thus for ease of presentation we refrain from explicitly modeling convex piecewise linear cost functions in $\mathcal{N}$. We rather assume that the flow cost z_λ is given for each edge $(u, v) \in E$ with $u \neq s$ and $v \neq t$ by the weighted loss function $z_\lambda((u, v), f) \coloneqq (1 - \lambda) \cdot \ell_{\{u,v\}}(f(u, v))$, where λ is the weight parameter of Equation 6.6. The edges (s, u) from the source s to a generator $u \in V_G$ have cost $z_\lambda((s, u), f) \coloneqq \lambda \cdot \gamma_u(f(s, u))$ and the edges incident to the sink t have cost 0. Then the objective function to be minimized is $z_\lambda(f) \coloneqq \sum_{e \in E} z_\lambda(e, f)$. Finally, we set the target flow value x to the total demand $\sum_{u \in V_D} p_d(u)$ of all consumers. By construction, every feasible minimum-cost flow in $\mathcal{N}$ is a feasible minimum-cost flow in the underlying power grid G and vice versa.

6.3 Complexity

In the above section we gave no restriction on the control unit's ability. The latter means that a FACTS is able to adjust the flow arbitrarily. However, a realistic FACTS is only able to adjust the voltage angle difference within a limited range. Since the proposed hybrid model does not incorporate a limitation of the power flow scaling, we could instead use the DC-model and allow to adjust the susceptances $b(u, v)$ arbitrarily, where either u or v is in V_F for FCVs or $(u, v) \in E_F$ for FCEs. The limitation for adjusting the voltage angle difference can be modeled by a real interval $I_e \in \mathcal{I}(\mathbb{R}_{\geq 0})$ that depends on the edge e, where $\mathcal{I}(\mathbb{R}_{\geq 0})$ is the set of all real intervals and $\mathcal{I}(\mathbb{R}_{\geq 0})$ is a semiring (i. e., a ring without additive inverse) of sets. Thus, the interval I_e is a subset of $\mathbb{R}$ that is defined by the two elements x and y with $x, y \in I_e$ and $z \in \mathbb{R}$ such that $x \leq z \leq y$, which implies that $z \in I_e$. The difference now is that either edges incident to a vertex V_F for FCVs or all edges in $e \in E_F$ for FCEs have a variable susceptance $b \colon E \to \mathcal{I}(\mathbb{R}_{\geq 0})$, $(u, v) \mapsto \mathcal{I}(\mathbb{R}_{\geq 0})$ with u or v in V_F, or $b \colon E_F \to \mathcal{I}(\mathbb{R}_{\geq 0})$, respectively. An example that shows different scalings for a triangle graph is given in Figure 6.5. Figure 6.5 shows different susceptance scaling of the same graph that lead to different power flows by either allowing more flow, but fixing the voltage angles, changing the voltage angles and fixing the flows, or both.

This modeling would change the linear program Equation 6.12 to a quadratic program, since Equation 6.12c is a quadratic constraint with variables f, θ^v, and b. More precisely, it represents a bilinear constraint. In Equation 6.14 we use a bilinear form, where $\mu_{\text{bilin}} \colon V \times V \to \mathbb{R}$ with $(u, v) \mapsto b(u, v) \cdot (\theta^v(v) - \theta^v(u))$. The latter bilinear

form is skew-symmetric.

$$f(u,v) = b(u,v)(\theta^v(v) - \theta^v(u)) \tag{6.14a}$$
$$f(u,v) = b(u,v) \cdot \theta^v(v) - b(u,v) \cdot \theta^v(u) \tag{6.14b}$$
$$f(u,v) = \mu_{\text{bilin}}(b(u,v), \theta^v(v) - \theta^v(u)) \tag{6.14c}$$

Thus, we have one quadratic constraint (i. e., the KVL combined with Ohm's law). However, the other constraints and—in terms of maximizing the throughput—also the objective stays linear. In the first problem, we assume a given placement of the FACTS and are just interested in the susceptance scaling, which is NP-hard under the condition that there are quadratic constraints and the objective is linear [Sahni,1974]. The proof uses a reduction from the Partition Problem. For more precise information about the complexity of quadratic programming refer to Garey and Johnson [GJ79, p.245, MP2] and Ausiello et al. [Aus+99, p.447, MP5].

Maximum FACTS Flow Problem with E_F MFFP($\mathcal{N}, E_F$)	
Instance:	A network $\mathcal{N}$, and a set $E_F \subseteq E$.
Objective:	Find a susceptance setting $b \in I_e$ for all $e \in E_F$ such that $\text{OPT}_{\text{MPFP}}(\mathcal{N})$ is maximum among all choices of b.

Problem Definitions. We can now give different level of granularity for the problem definition of the Maximum FACTS Flow Problem (MFFP). Recall from Chapter 4 the Maximum Power Flow Problem MPFP($\mathcal{N}$) and its value $\text{OPT}_{\text{MPFP}}(\mathcal{N})$. For simplicity and for consistency reasons, we only consider FCEs. However, all formulations can be translated to FCVs, too. The first placement problem MFFP($\mathcal{N}, k$) considers the problem with a fixed number of FACTS—meaning $|E_F| = k$—and is defined by $\text{OPT}_{\text{MFFP}}(\mathcal{N}, k) := \max_{E_F \subseteq E, b \in I_b} \text{OPT}_{\text{MPFP}}(\mathcal{N})$ with $|E_F| = k$. The optimization problem is defined as follows.

Maximum FACTS Flow Problem with k-FACTS MFFP($\mathcal{N}, k$)	
Instance:	A network $\mathcal{N}$, and parameter $k \in \mathbb{N}$.
Objective:	Find a set $E_F \subseteq E$ of FACTS with $\lvert E_F \rvert = k$ and a susceptance setting $b \in I_e$ for all $e \in E_F$ such that $\text{OPT}_{\text{MPFP}}(\mathcal{N})$ is maximum among all choices of E_F and b.

Note that if $|E_F| = |E| = k$ and the susceptance is defined in $b(e) \in [0, \infty]$ for all $e \in E_F$ the value of $\text{OPT}_{\text{MFFP}}(\mathcal{N}, k) = \text{OPT}_{\text{MFP}}(\mathcal{N})$. Assume, we have no limitation on the number of FACTS we can place. The problem to get the maximum possible flow for a network $\mathcal{N}$ by allowing as many FACTS as possible (i. e., some k) is called MFFP($\mathcal{N}$)

and its value is denoted by $\mathrm{OPT}_{\mathsf{MFFP}}(\mathcal{N}) := \max_k \mathrm{OPT}_{\mathsf{MFFP}}(\mathcal{N}, k)$. The problem is defined as follows.

Maximum FACTS Flow Problem MFFP($\mathcal{N}$)	
Instance:	A network $\mathcal{N}$.
Objective:	Find a set $E_F \subseteq E$ of FACTS with $\lvert E_F\rvert = k$, $0 \leq k \leq \lvert E\rvert$, and a susceptance setting $b \in I_e$ for all $e \in E_F$ such that $\mathrm{OPT}_{\mathsf{MPFP}}(\mathcal{N})$ is maximum among all choices of E_F, b, and k.

In the simulations, where we allow a susceptance range of $b(e) \in [0, \infty]$, we will see that a small number of control units suffices to get $\mathrm{OPT}_{\mathsf{MFP}}(\mathcal{N})$. However, dependent on the susceptance interval I_e and the network's underlying graph structure, the $\mathrm{OPT}_{\mathsf{MFFP}}(\mathcal{N})$ does not necessarily have the same value as the $\mathrm{OPT}_{\mathsf{MFP}}(\mathcal{N})$ meaning $\mathrm{OPT}_{\mathsf{MFFP}}(\mathcal{N}) \leq \mathrm{OPT}_{\mathsf{MFP}}(\mathcal{N})$.

In the simulations, we will be interested in the problem of finding the minimum number of control units, which we call MNFP($\mathcal{N}$). Its value is denoted by $\mathrm{OPT}_{\mathsf{MNFP}}(\mathcal{N}) := \min_{\mathrm{OPT}_{\mathsf{MFFP}}(\mathcal{N},k)=\mathrm{OPT}_{\mathsf{MFFP}}(\mathcal{N})} k$.

Minimum Number of FACTS Problem MNFP($\mathcal{N}$)	
Instance:	A network $\mathcal{N}$, and a parameter $k \in \mathbb{N}$.
Objective:	Find a set $E_F \subseteq E$ of FACTS and a susceptance setting $b \in I_e$ with $e \in E_F$ such that $k = \lvert E_F\rvert$ is minimum among all choices of $\mathrm{OPT}_{\mathsf{MFFP}}(\mathcal{N})$.

From Lemma 5.6, we know the bounds of MTSFP. A similar relationship holds for the MFFP, which we describe in Lemma 6.1.

Lemma 6.1. $\mathrm{OPT}_{\mathsf{MPFP}}(\mathcal{N}) \leq \mathrm{OPT}_{\mathsf{MFFP}}(\mathcal{N}) \leq \mathrm{OPT}_{\mathsf{MFP}}(\mathcal{N})$.

In addition, we can give the following relationship between the aforementioned problems that is given by the problem definition itself.

Lemma 6.2. $\mathsf{MPFP}(\mathcal{N}) \subseteq \mathsf{MFFP}(\mathcal{N}, k) \subseteq \mathsf{MFFP}(\mathcal{N}) \subseteq \mathsf{MNFP}(\mathcal{N})$.

Note that the KVL constraint is a bilinear constraint that can be reformulated as shown in Equations 6.14a–6.14c

Overview. For trees (see Table 6.1–1) any of the aforementioned problems is polynomial time solvable, since we reach $\mathrm{OPT}_{\mathsf{MFP}}(\mathcal{N})$ without any control units. We will discuss this in more detail in Section 6.5.2. While increasing the structural complexity of a graph by allowing cycles, Lehmann et al. [LGH15, pp.10ff., Theorem 4] show that the problem is already NP-hard for cacti with maximum degree of 3 by reduction from Subset Sum Problem (SSP; see Section 5.2.2). In Table 6.1–3, we give a short

overview. For the most general graph structure—meaning an arbitrary graph—the problem is strongly NP-hard. The latter was shown by Lehmann ET AL. [LGH15, pp. 7, Theorem 1] by reduction from *exact cover by 3-set problem* (i. e., given a set U and a set of subsets $M \subseteq \mathcal{P}(U)$ with $|M| = 3$ the decision problem is whether there is a set $M' \subseteq M$ such that $\bigcup\{X \mid X \in M'\} = U$) and an overview on that is given in Table 6.1–5. Note that Lehmann ET AL. [LGH15] implemented this by a choice network and focused on the problem MFFP($\mathcal{N}, E_F$), where the position of the FACTS is predefined.

Table 6.1: Overview of known results on the complexity of the MFF and OFF problem. The complexity increases from top to bottom as shown in the hardness column. Note that the main points that influence the complexity of the problem are the graph structure of G, the number of generators V_G, the number of consumers V_D, the susceptance b, and the capacity cap.

	Problem	Network Properties						Complexity		Algorithms		
		Graph Structure	Example	$\lvert V_G \rvert$	$\lvert V_D \rvert$	b	cap	Hardness	Reference	Name	b	cap
1	MFFP and OFFP	tree graphs	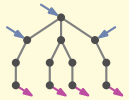	∞	∞	–	–	polynomial-time solvable	Lemma 4.9, Theorem 6.5, Section 3.2 p. 30	MF	∞	∞
2	MFFP and OFFP	series-parallel graphs		∞	∞	∞	∞	–	–	–	–	–
3	MFFP and OFFP	cacti with maximum degree of 3		∞	∞	∞	∞	NP-hard	[LGH15, pp.10, Theorem 4]	–	–	–
4	MFFP and OFFP	planar graph with max degree of 3	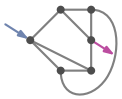	∞	∞	∞	∞	–	–	–	–	–
5	MFFP and OFFP	arbitrary graphs	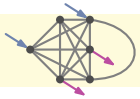	∞	∞	∞	∞	strongly NP-hard	[LGH15, pp.7, Theorem 1]	–	–	–

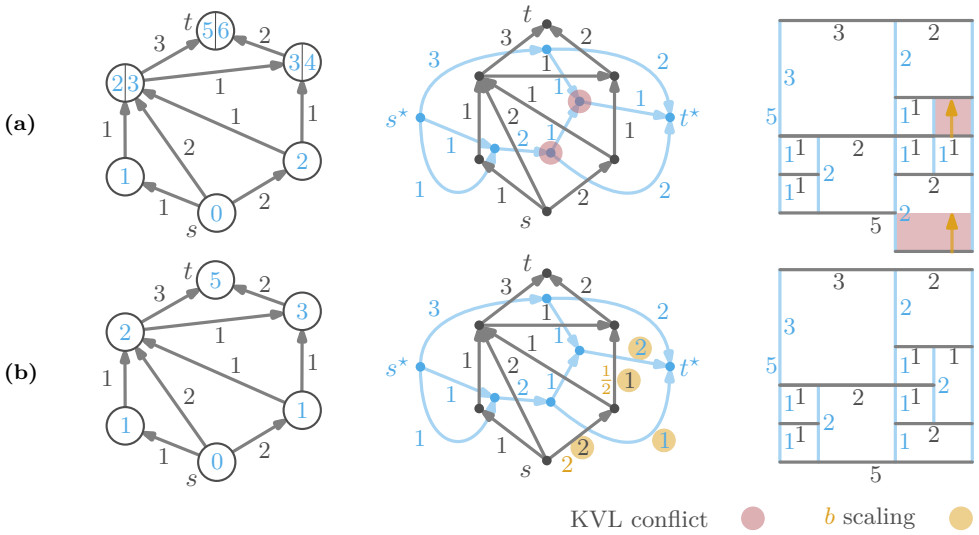

Figure 6.6: The graph from Figure 6.1 [Fel13, p.18, Figure 18], where we split the KVL conflict step (a) that is a KCL conflict in the dual graph $G^\star$ from the susceptance scaling step (b). If not described otherwise, we have unit susceptances b with $b \equiv 1$. In (a) the KVL conflict is visible in all three representations. Whether it is the left graph that shows the conflict by non-unique voltage angle θ^v assignments, or in the middle representation with the KCL conflicts in the dual graph $G^\star$, or the rectangle conflicts in the geometric representation on the right side. However, the susceptance scalings shown in (b) and indicated with the arrows ↑ for the geometric interpretation in the right most figure in (a) fix these conflicts in all three representations.

6.4 Planar Problem Reinterpretation

Recall from Section 5.3 that we defined a single source and single sink planar power flow in terms of simultaneous flows in the primal graph G and dual graph $G^\star$. The definition of simultaneous flows is given in Section 4.3.2. We adjust the problem formulation for FACTS in the following, while allowing a susceptance range of $[0, \infty]$ for all edges $e \in E$.

s-t-DC Feasibility Problem with FACTS s-t-DC-FEAS-FACTS$(G, G^\star, \mu_{\text{dual}})$

Instance: A plane s-t-graph G and its dual $G^\star$, subsets $E_1 \subseteq E(G)$ and $E_2 \subseteq E(G^\star)$, and a bijection $\mu_{\text{dual}} \colon E_1 \to E_2$.

Objective: Find KCL-feasible flows f_G and $f_{G^\star}$ in G and $G^\star$ with $F(G) \neq 0$ and $F(G^\star) \neq 0$ such that for every edge $e \in E$ we have $f_G(e) = f_{G^\star}(\mu_{\text{dual}}(e))$.

Table 6.2: IEEE benchmark set with $|V|$, $|E|$, $|V_G|$, and p_d representing number of buses, number of transmission lines, number of generators and total power demand, respectively.

case	$\|V\|$	$\|E\|$	$\|V_G\|$	p_d
case6	6	11	3	210.00
case9	9	9	3	315.00
case14	14	20	5	259.00
case30	30	41	6	189.20
case39	39	46	10	6254.23
case57	57	78	7	1250.80
case118	118	179	54	4242.00

Instead of demanding that the bijection of the flows holds for all edges, we relax this property to edges in $E \setminus E_F$. In Figure 6.6, we apply a feasible flow f on the primal graph G and show that an adjustment of the susceptances transforms f into a feasible power flow. However, the assumption to $[0, \infty]$ is quite strong. Thus, restricting the height scaling would lead to the same formulation as in Chapter 4.

6.5 Placing Flow Control Buses

In this section we seek to answer the question of how many flow control buses are necessary to obtain a globally optimal solution. Recall that the flow model is a relaxation of the physical model and uses fewer constraints. Therefore, optimal solutions in the flow model are at least as good as in the physical model.

Given a power grid $G = (V, E)$, we say that making the vertices in V_F flow control vertices achieves *full control* if the objective value of an optimal energy flow for the grid G_{V_F} is the same as the objective value of an optimal solution in the flow model (or equivalently in the hybrid network G_V, where every vertex is a flow control vertex). Our experiments indicate that in the IEEE instances a small fraction of the vertices is often sufficient to achieve full control as was already indicated in Figure 6.1. Afterwards we give a graph-theoretical explanation of this behavior.

6.5.1 Experiments

For our evaluation we use the IEEE benchmark data sets [Uni14, ZM11] shown in Table 6.2. There each case is named according to the number of buses $|V|$. The number of generators and the number of edges are denoted by $|V_G|$ and $|E|$, respectively.

To obtain piecewise linear functions for generator costs γ_u for all $u \in V_G$ and line losses ℓ_e for all $e \in E$, we simply sample the cost functions using a specified number of sampling points. Note further that our approach requires convex cost functions,

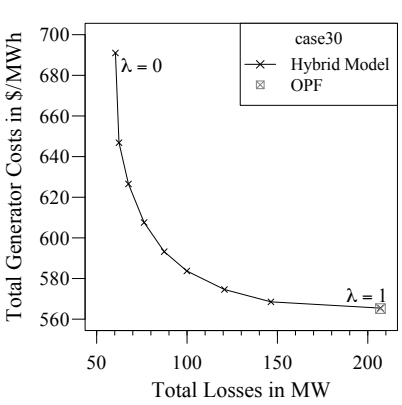

(a) Total costs c_g and losses c_ℓ for the IEEE benchmark data with 30 buses, where the square cross marks the solution computed by OPF.

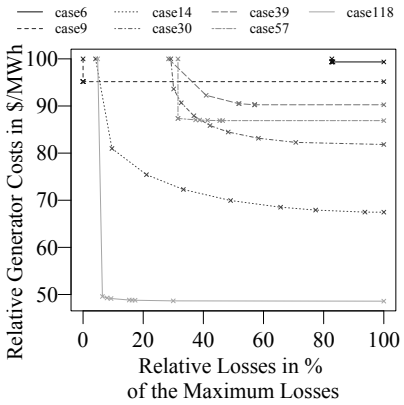

(b) Relative costs and losses for the IEEE benchmark data sets.

Figure 6.7: Trade-off of generator costs c_g and losses c_ℓ normalized to the maximum generator cost ($\lambda = 0$) and the maximum loss ($\lambda = 1$) as λ varies from 0 to 1.

but this is fine in practice [WW96]; in particular the functions are convex for the IEEE benchmark instances.

We performed our experiments on an AMD Opteron 6172 processor running openSUSE 12.2. Our implementation is written in Python 2.7.3 and uses PYPOWER [Lin11], a Python port of MATPOWER [ZMT09, ZMT11], for computing solutions for the OPFP. For computing solutions and minimizing the number of control buses in our hybrid model we use the (integer) linear programming solver Gurobi 6.0.0 [GUR13].

First, we observe that the value of λ, which controls the weighting of costs and losses in the objective value, has a significant effect on the objective values of generator costs and line losses. Figure 6.7a shows the trade-off for the IEEE instance `case30` (the plots for the other instances can be found in Appendix D). The OPF solution, which ignores losses, is typically at the far end of the spectrum with high losses and is comparable to our solution with $\lambda = 1$. As can be seen in Figure 6.7b, where the costs and losses are normalized to the maximum cost and the maximum loss per instance, the same trade-off behavior is present in all instances. It thus makes sense to allow the operator of a power grid to choose the value of λ in order to model the true operation costs.

On the other hand, it may then be the case that the number of flow control vertices to achieve full control of the network varies depending on the choice of λ. Figure 6.8 shows for different values of λ the relative number of control vertices necessary to achieve full control in each of the instances. In most cases less than 15% of all vertices need to be controllers to achieve full control. For the cases with 6 vertices and 14 vertices this percentage is slightly bigger, which is mainly an artifact stemming from the small total size. As can be seen, the required number of units is relatively stable

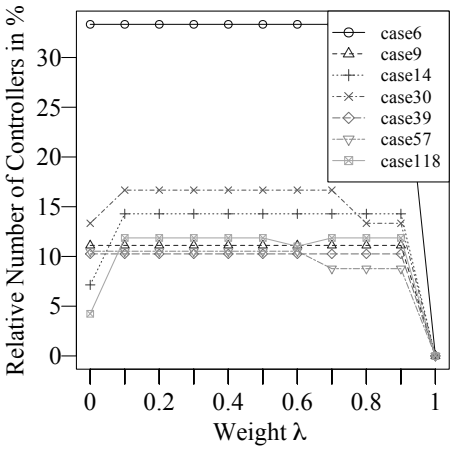

Figure 6.8: Relative number of controllers for achieving full control in the IEEE instances as λ varies from 0 to 1.

but drops to zero for $\lambda = 1$, i. e., when only the generator costs are considered. This is due to the fact that all IEEE instances have basically unlimited line capacities and thus do not restrict the possible flows.

In order to make a useful prediction on the number of vertices required for full control that applies to all choices of λ, in the following we take for each instance the maximum of the smallest possible number of vertices to achieve full control over all values of λ and refer to this as the number of vertices for achieving full control of the instance. This conservative choice ensures that the numbers we compute are certainly an upper bound for achieving full control, independent of the actual choice of λ.

6.5.2 Structure of Optimal Solutions

As we have seen in our experimental evaluation, often a small number of flow control vertices is sufficient to ensure that solutions in the hybrid model are the same as in the flow model. In the following we provide a theoretical explanation of this property and link it to structural properties of power grids. Farivar and Low [FL13] give similar structural results on spanning trees, but using a different model.

A first observation is that flow control vertices influence all incident edges. Thus, if every edge is incident to a flow control vertex, i. e., the set $V_F{}^c$ is a *vertex cover* of G (i. e., $c = 1$), no edge in the network is affected by the constraint Equation 6.11). Then the flow model and the hybrid model are equivalent and full control is achieved. However, it is generally not true that power grids admit small vertex covers; as shown in Figure 6.9, all instances require more than 40% of their vertices for a vertex cover. In the following, we show a much stronger result, namely that it suffices for becoming

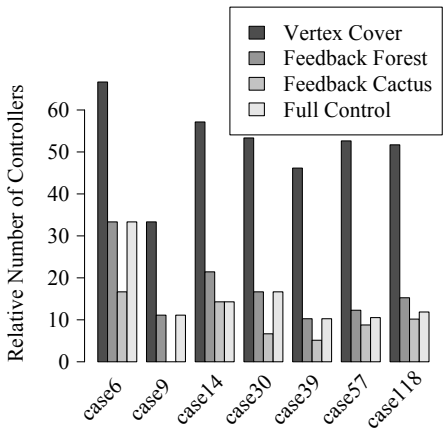

Figure 6.9: Comparison of the number of vertices which need to be removed from the network to get a tree (i. e., 2-pumpkin hitting set) or a cactus (i. e., 3-pumpkin hitting set), with the worst number of controllers to have full control in the network (i. e., equivalent costs to the graph-theoretical flow).

independent of Equation 6.11 that the native power grid $G - {V_F}^c$ is an acyclic network (i. e., $c = 2$). Moreover, if $\lambda = 1$, (line losses are neglected) and edge capacities are ignored, it even suffices that $G - {V_F}^c$ is a so-called *cactus* graph, in which every edge is part of at most one cycle (i. e., $c = 3$).

Lemma 6.3. *Let $H = (V, E)$ be a native power grid and let v be a vertex whose removal disconnects H into connected components with vertex sets $C_1, \ldots, C_k$. Then a flow f is a feasible electrical flow for H if and only if it is a feasible electrical flow for $H_i = H[C_i \cup \{v\}]$ for $i = 1, \ldots, k$.*

Proof. Clearly, if $\theta^v(u)$ is a feasible voltage angle assignment for all $u \in V(H)$, then its restriction to $C_i \cup \{v\}$ is a feasible angle assignment for H_i. Conversely, assume that ${\theta^v}_i$ is a feasible angle assignment for H_i. Define ${\theta^v}_i' = {\theta^v}_i - {\theta^v}_i(v)$. Since for every edge in H_i the voltage angles of the endpoints are changed by the same value, $\theta^{v\prime}$ is a feasible voltage angle assignment for H_i. Further, ${\theta^v}_i'(v) = 0$ for every H_i, which means that the function $\theta^v \colon V \to \mathbb{R}$, where $\theta^v(u) \mapsto {\theta^v}_i'(u)$ for $u \in C_i$ is well-defined. Note that the restriction of θ^v to any of the H_i coincides with ${\theta^v}_i'$. Since every edge of H belongs to exactly one of the H_i, it follows that θ^v is a feasible voltage angle assignment for H. □

Iteratively applying Lemma 6.3 yields the following.

Corollary 6.4. *A flow in a native power grid is electrically feasible if and only if it is electrically feasible for each biconnected component of the power grid.*

We observe that if $G - {V_F}^c$ is a forest (i. e., $c = 2$), then each biconnected component H consists of a single edge $\{u, v\}$. Then $\theta^v(u) = {}^{f(u,v)}/_{b(u,v)}$ and $\theta^v(v) = 0$ are feasible voltage angles for any flow f in $G - {V_F}^{c=2}$. Thus, we conclude with the following theorem.

Theorem 6.5. *Let H be a native power grid that is a forest. Then every flow f is a feasible electrical flow on H.*

Thus, when V_F is a *feedback vertex set* of G, i. e., $G - {V_F}^{c=2}$ is a forest, then every flow on G is a feasible electrical flow for $G - {V_F}^{c=2}$, and thus any feasible flow for $G_{{V_F}^{c=2}}$ is electrically feasible for $G_{{V_F}^{c=2}}$. It follows that the flow model and the hybrid model are equivalent in this case. In particular, whenever V_F is a feedback vertex set, instead of solving the LP for the hybrid model, we can rather assume the flow model and compute an optimal solution using a, potentially more efficient, flow algorithm. It follows from Theorem 6.5 that this solution is optimal also in the hybrid model.

Figure 6.9 shows for each of our instances the relative number of vertices necessary to obtain a vertex cover (i. e., $c = 1$), a feedback vertex set (i. e., $c = 2$) with respect to forests, and the number of vertices necessary to obtain full control. In all instances a vertex cover is two to three times larger than a feedback vertex set (for forests) and the vertex set necessary for full control. Comparing the relative number of controllers for full control with the size of a feedback vertex sets shows that the number to get an optimal placement is in many cases smaller than the size of a feedback vertex set. Thus, in the optimal solutions, the native power grid does not always represent a forest, but can also include cycles. A closer inspection showed that this is in particular the case for instances that are operated far from their capacity limits.

We now consider what happens when cycles exist in a native power grid. To this end, we start with the simplest case of a power grid that consists of a single cycle C. We say that two flows f and f' on a network $G = (V, E)$ are *equivalent* if for each vertex $v \in V$ we have $f_{\text{net}}(v) = {f_{\text{net}}}'(v)$.

Lemma 6.6. *Let C be a native power grid that is a cycle. For every flow f there exists a unique equivalent flow f' that is a feasible electrical flow for C.*

Proof. Let $v_1, \ldots, v_n$ be the vertices of C as they occur along the cycle, i. e., $f(v_i, v_j) = 0$ unless v_i and v_j are neighbors on the cycle. Assume we wish to change the amount of flow from v_1 to v_2 by a fixed amount Δ and obtain an equivalent flow. The net out-flow conservation at the vertices then uniquely determines the change of flow along the remaining edges. Hence, every flow f' equivalent to f is obtained from f by choosing some amount Δ and setting $f'(v_i, v_{i+1}) = f(v_i, v_{i+1}) + \Delta$ and $f'(v_{i+1}, v_i) = f(v_{i+1}, v_i) - \Delta$, where $v_{n+1} = v_1$.

Now the existence of a suitable offset Δ and the associated feasible voltage angles can be expressed as a linear system of equations. Namely, for edge (v_i, v_{i+1}) with $i =$

$1, \ldots, n$ and $v_{n+1} = v_1$, we have the following equation.

$$b(v_i, v_{i+1}) \cdot \theta^v(v_i) - b(v_i, v_{i+1}) \cdot \theta^v(v_{i+1}) - \Delta = f(v_i, v_{i+1}) .$$

It is readily seen that the n equations are linearly independent, and hence a solution exists. Moreover, dividing each of the equations by $b(v_i, v_{i+1})$ and summing them up

$$\begin{pmatrix} b(v_1,v_2) & -b(v_1,v_2) & 0 & \ldots & -1 \\ 0 & b(v_2,v_3) & -b(v_2,v_3) & \ldots & -1 \\ & & \ldots & \ddots & \vdots \\ 0 & & \ldots & b(v_n,v_1) & -1 \\ -b(v_n,v_1) & & \ldots & & \end{pmatrix} \begin{pmatrix} \theta^v(u_1) \\ \theta^v(u_2) \\ \vdots \\ \theta^v(u_n) \\ \Delta \end{pmatrix} = \begin{pmatrix} f(v_1,v_2) \\ f(v_2,v_3) \\ \vdots \\ f(v_n,v_1) \end{pmatrix}$$

yields $-\sum_{i=1}^{n} 1/b(v_i,v_{i+1)}\Delta = \sum_{i=1}^{n} f(v_i,v_{i+1})/b(v_i,v_{i+1})$, which shows that the value Δ is uniquely determined. □

Note however, that the equivalent flow f' whose existence is guaranteed by Lemma 6.6 does not necessarily satisfy the capacity constraints (see Equation 6.10). Also the evaluation of f' in terms of line losses may change. If neither of these is a limiting factor, e.g., if $\lambda = 1$ and line capacities are sufficiently large, we can show a stronger version of Theorem 6.5. Recall that a cactus is a graph where every edge belongs to at most one cycle.

Theorem 6.7. *Let $G_{V_F{}^c}$ be a power grid with flow control vertices at the vertices in $V_F{}^c$ such that the maximum native power grid $G - V_F{}^c$ is a cactus (i. e., $c = 3$) and every edge of $G - V_F{}^{c=3}$ that lies on a cycle has infinite capacity. For any feasible flow f there exists an equivalent feasible flow f' that is a feasible electrical flow for $G_{V_F{}^{c=3}}$.*

Proof. We first construct an equivalent flow f' as follows. For each biconnected component C of $G - V_F{}^{c=3}$ that is a cycle, we consider the restriction f_C of f to C. By Lemma 6.6, there exists a unique flow f'_C equivalent to f_C that is electrically feasible for C. We now define flow

$$f'(u,v) = \begin{cases} f'_C(u,v) & \text{if } u, v \text{ are on a cycle } C, \\ f(u,v) & \text{otherwise.} \end{cases}$$

Note that changing the flow f along the edges of a cycle C to the values determined by f'_C preserves the net out-flow at every vertex, and hence f' is a flow equivalent to f. We claim that f' is a feasible electrical flow. To see this, observe that each block of $G - V_F{}^{c=3}$ is either a single edge or a cycle C. In the former case, f' is trivially feasible on the block. In the latter, we have that f' coincides on C with f'_C, which is a feasible electrical flow. By Corollary 6.4 f' is a feasible electrical flow. □

Let $e_1, \ldots, e_k$ be the edges of a cycle in $G_{V_F^{c=3}}$ and f_i be a flow on an edge e_i in cycle C. We abbreviate the susceptance $b(e_i)$ on an edge in a cycle by b_i. The maximum susceptance is denoted by $b_{\max}$ with $b_{\max} = \max_{1 \leq i \leq k}(b_i)$ for all $i = 1, \ldots, k$. The minimum susceptance $b_{\min}$ is defined analogously. In practice, the requirement for infinite capacity in Theorem 6.7 is unnecessary. In fact, we can bound the sufficiently large capacities of Theorem 6.7 by rearranging the equation of the proof of Lemma 6.6 such that the change of flow is bounded by the ratio of maximum to minimum susceptance times the average flow in the cycle C that is

$$\Delta = -\frac{\sum_{i=1}^{k} \frac{f_i}{b_i}}{\sum_{i=1}^{k} \frac{1}{b_i}} \leq \frac{b_{\max}}{b_{\min}} \cdot \frac{\left(\sum_{i=1}^{k} f_i\right)}{k}. \tag{6.15}$$

We refer back to Figure 6.9, which in addition to the previously mentioned parameters also shows the size of a minimum diamond hitting set (i. e., $c = 3$, where the native power grid represents a cactus). In all cases the number of vertices for full control is between the sizes of c-pumpkin hitting sets with c equal to 2 (i. e., forests) and 3 (i. e., cacti). For the cases 14, 57 and 118, the minimum number of controllers for achieving full control indeed results in a native power grid that forms a cactus (i. e., $c = 3$), although they do not necessarily achieve the smallest hitting number due to some influence of line capacities.

6.6 Grid Operation Under Increasing Loads

In the previous section we have seen that typically selecting a small fraction of the vertices as flow control vertices suffices to achieve full control in the network. In this section we study what happens when even fewer flow control vertices are available and whether few flow control vertices allow a better utilization of the existing infrastructure in the presence of increasing loads.

To measure the controllability in the presence of very few flow control vertices, we simulate a load increase by a factor ρ in the power grid by decreasing all line capacities by the factor $1/\rho$. This has the effect that the overall demand remains constant and thus any change of costs is due to flow redirections. It is then expected that, once the load increases, the network without flow control vertices will require significantly higher operating costs, since the main criterion for determining the generator outputs becomes the overall feasibility of the flow rather than the cost-efficient generation of the energy. At some point, the load increases to a level where, by means of changing only the generator outputs, a feasible energy flow cannot be found. We compare the operation costs to solutions in power grids with a small number of flow control vertices. Specifically, our plots show two things. First, the operation costs for various small numbers of flow control vertices and, second, the operation costs and the number of

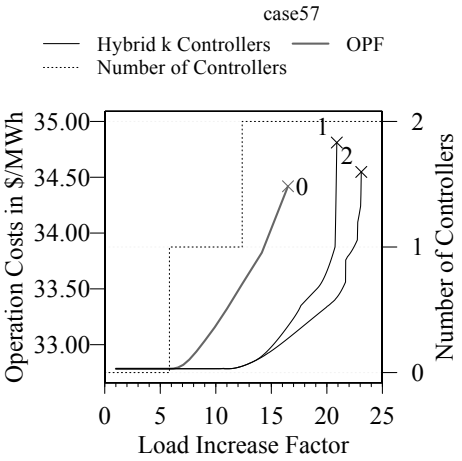

Figure 6.10: Operation costs of `case57` for OPF and the hybrid model with 1 and 2 control vertices with respect to the load factor ρ.

flow control vertices necessary for achieving full control in the network with respect to the load increase factor ρ.

Of course these operation costs again vary depending on the value of λ. Since most related work ignores line losses, we consider only the case $\lambda = 1$, i. e., only generation costs are taken into account. Varying λ changes the objective value, but it does not influence the existence of solutions with a certain number of flow control vertices. Recall from the plot in Figure 6.8 that, if the load increase ρ is small, full control can be achieved without flow control vertices for $\lambda = 1$. In the IEEE instances all lines have very large capacities, often much larger than even the total demand in the network, e. g., the thermal line limit cap of each edge is 9 900 MW, whereas the total demand is $p_d = 259$ MW in the `case14` and $p_d = 1\,250.8$ MW in the `case57`. To better highlight the interesting parts, similar to the work by Melo Lima ET AL. [Mel+03], we first scale all line capacities such that the smallest capacity is equal to the total demand of the consumers as given in Table 6.2. This changes neither the existence nor the cost of solutions. We increase the load until the flow model becomes infeasible; at this point a feasible solution cannot be achieved by adding flow control vertices and adding additional lines to the network becomes unavoidable.

Figure 6.10 shows the results of our experiment for the power grid `case57`. To improve readability, all costs have been rescaled by the total demand in the network, and thus give the cost per MWh. The black curve shows the operation cost with sufficient control vertices for full control. The dotted staircase curve shows the number of flow control vertices that are necessary to achieve full control. Moreover, for each number of flow control vertices from 1 up to the number required at the point when further load increase makes the instance infeasible, we show the optimal operation

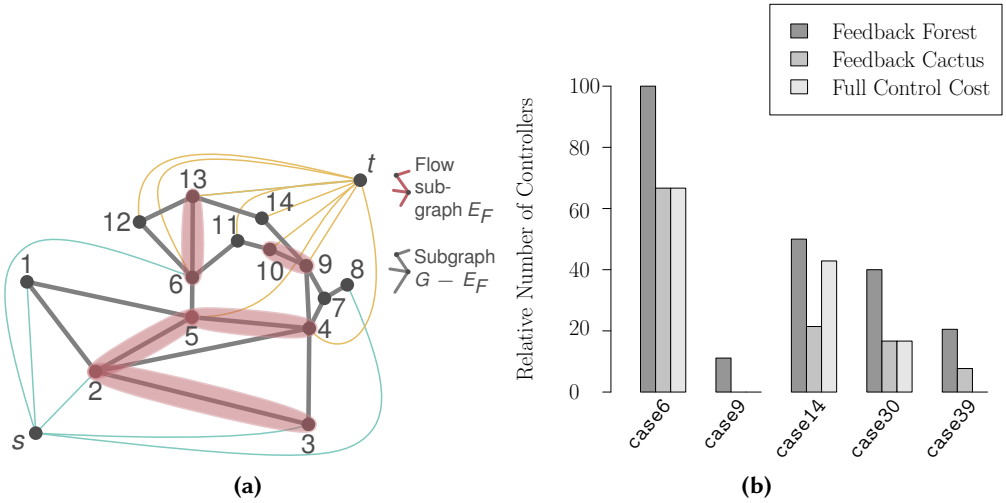

Figure 6.11: (a) IEEE benchmark `case14` including the minimum numbers of controllers for $\lambda = 0.5$, where the bold normal lines represent $G - E_F$ and the bold dashed lines represent FCEs E_F. (b) Comparing of the minimum feedback set sizes for forests and cacti with the necessary number of FCEs for full control. Cases 9 and 39 need zero FCEs, which is equivalent to Figure 6.9.

costs with this number of flow control vertices. Finally, the bold gray curve shows the operation cost with OPF, i. e., without any control vertices. The plots for the other IEEE instances can be found in Appendix D.

As expected, increasing loads result in increasing operation costs. Interestingly, very few control vertices suffice for increasing the maximal feasible operation point. This is emphasized by the curve for two control vertices in Figure 6.10, which continues to a load increase of factor 23.09, whereas OPF works only for up to an increase of roughly 17.27 and exhibits a significant increase in operation costs at higher loads. In contrast, when using flow control vertices, the costs start to increase much later and more moderately. Interestingly, the solution with one control vertex remains roughly equivalent to the solution with two control vertices until shortly before the end of its feasibility range. This example shows that control vertices indeed increase the feasible operation point and also decrease the corresponding operation costs even if there are only very few controllers available.

6.7 Evaluation of Placing Flow Control Edges

In this section, we transfer our previous theoretical results from Section 6.5.2 to FCEs. Thereby, we answer Question 1: How many FCEs are necessary to achieve the lower

bound for the operation cost, which happens in case each line is a FCE. We call this operation cost a *full control cost*.

In Figure 6.11a the graph of the IEEE `case14` with the different subgrids is shown for the placement of FCEs, that induces the operation cost equal to the full control cost. We observe that the subgrid $G - {E_F}^c$ (graph G where the edges of E_F are removed) forms a *cactus* (i. e., $c = 3$; graph where each edge lies in at most one cycle). In other examples, we observed that $G - {E_F}^c$ can be even simpler, forming a *forest* (i. e., $c = 2$; a graph without any cycle). If $G - {E_F}^c$ is a cactus (resp. forest) and ${E_F}^c$ is the smallest such set, set ${E_F}^c$ is called *minimum diamond* (resp. *forest*) *hitting set*.

In our experiments, summarized in Figure 6.11b, we compared the number of FCEs necessary for achieving the full control cost to the size of minimum forest and diamond hitting sets. In `case6`-`case30` the number of edges for the full control cost is between the minimum size of a forest hitting set and that of a diamond hitting set. In addition, `case6`, `case9` and `case30` achieve full control cost with FCE size equal to the size of a diamond hitting set. For `case39`, full control is achieved with fewer FCEs than the diamond hitting set size. Unfortunately computing the optimal number of FCEs for the larger IEEE test cases is prohibitively expensive with our current integer linear programming formulation.

The following two theorems provide theoretical evidence for our empirical observations. They explain why the number of FCEs to achieve full control cost and the size of minimum diamond/forest hitting set are related. This relation and the fact that power grids are not dense networks, i. e., their forest hitting set is not large, suggests that the relatively small number of FCEs are enough to achieve the full control cost. Farivar and Low [FL13] give similar structural results on spanning trees, but using a different model.

Theorem 6.8. *Let $G - {E_F}^c$ be a forest (i. e., $c = 2$). Then every flow f is a feasible electrical flow on $G_{{E_F}^{c=2}}$.*

Theorem 6.9. *Let $G_{{E_F}^c}$ be a power grid with FCEs at the edges in ${E_F}^c$ such that $G - {E_F}^c$ is a cactus (i. e., $c = 3$) and every edge of $G - {E_F}^{c=3}$ that lies on a cycle has infinite line limits (or suitably bounded, see Equation 6.15). For any flow f there exists a flow f' with identical cost that is electrically feasible for G_{E_F}.*

The proofs for these theorems can be directly derived from Section 6.5.2 by replacing the set of flow control vertices ${V_F}^c$ with the set of flow control edges ${E_F}^c$.

6.8 Effect of FCEs in Comparision to FCVs

In this section we evaluate Question 2. For this reason, we increase the load by a factor ρ until the model becomes infeasible. For the hybrid model this happens when adding more FCEs does not extend the operability.

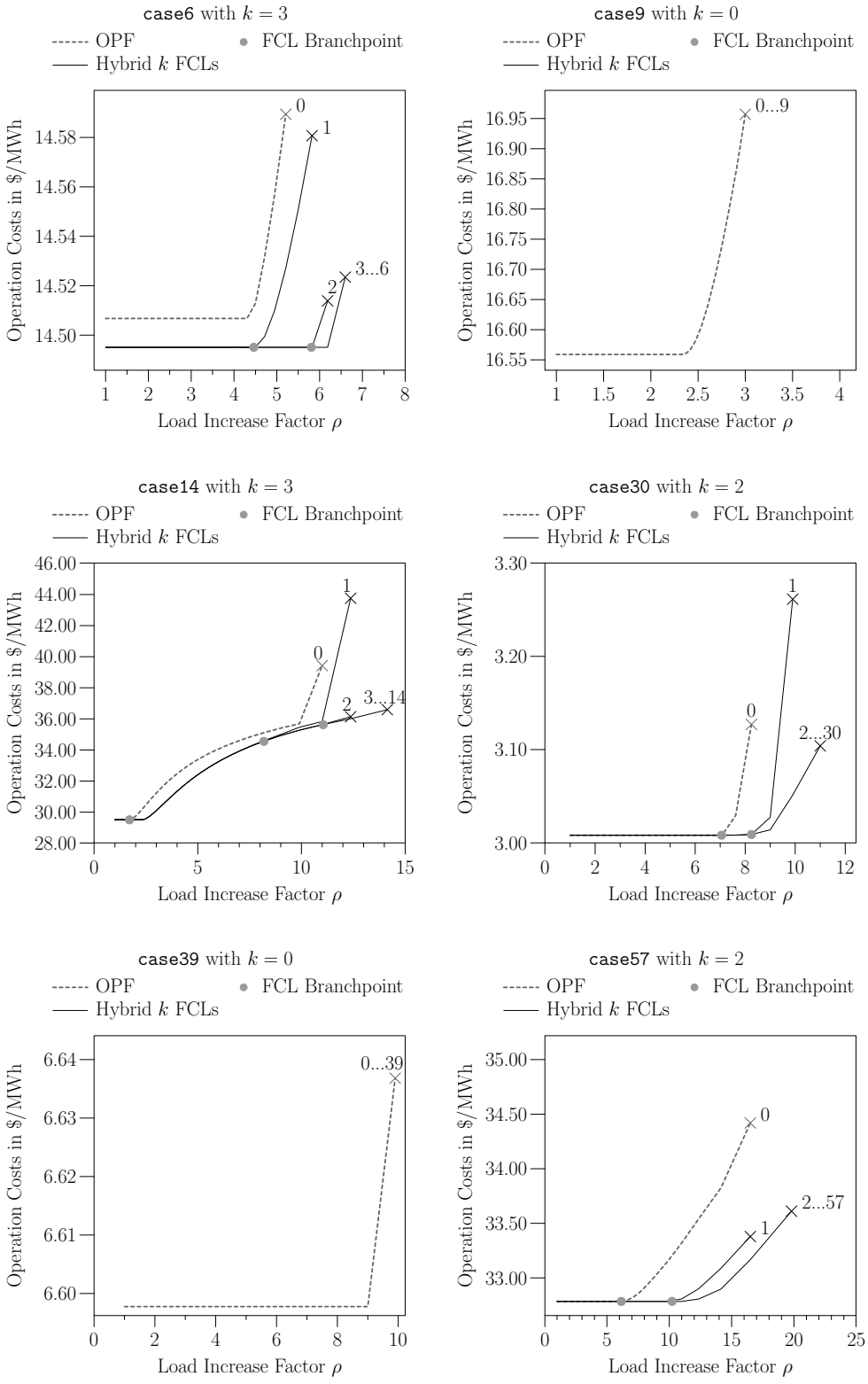

Figure 6.12: Overview of operation costs for `case6` to `case57` for OPFP (0 FCEs) and the hybrid model with respect to load increase factor ρ, where k is the upper bound for FCEs. The numbers on the curves represent the number of FCEs for that specific curve. Cases 9 and 39 need zero FCEs, equivalent to the results for FCVs.

Table 6.3: Comparison of the previous model using FCVs and the current model using FCEs. To compute the number of FACTS in case of FCVs, we compute the total number of edges incident to the vertices holding FCVs.

Dependency of Control Units Number		case6	case9	case14	case30	case39
FCEs	Feedback Edge Set	6	1	7	12	8
	Diamond Hitting Set	4	0	3	5	3
	Full Control	4	0	6	5	0
FCVs	Feedback Edge Set	2	1	3	5	4
	FACTS	9	2	11	21	15
	Diamond Hitting Set	1	0	2	2	2
	FACTS	5	0	8	10	5
	Full Control	2	1	2	5	4
	FACTS	9	3	8	23	15

Figure 6.12 show the experimental results for the IEEE power grids `case6` to `case57`. The behavior is the same as for FCVs meaning that the operation cost and the range of operability increase when increasing the load factor ρ. Interestingly, the number of FCEs does not increase substantially. For the `case14` there is a maximum of three FCEs necessary instead of two FCVs and for the `case57` the number of maximum FCEs remains the same as for FCVs. Similar behavior can be observed for the remaining cases. Recall that FCVs control flow on all incident edges, which can be realized by placing FACTS on all of these edges. Thus, in case of FCVs the number of necessary FACTS actually depends on the degree of the vertices holding the FCVs and results in large number of FACTS as indicated in Table 6.3.

6.9 Conclusion

Assuming the existence of special vertices that control the flow on all their incident transmission lines, we have presented a hybrid model for including some flow control vertices. In this model, we have shown that relatively few control vertices suffice for achieving full control. Further, we scaled the load of the network and showed that even fewer flow control vertices improve the loadability and have a lower cost increase compared to OPF.

A more realistic assumption is the placement of flow control units on edges, which we call FCEs. Here, we were able to transfer the results of FCVs and make some similar observations.

Our work shows the benefits of augmenting power grids with flow control devices. Using our theoretical model, we were able to explain our empirical observations on controller placement with graph-theoretical means. While this also explains previous observations of Gerbex ET AL. [GCG01], the main drawback is that the model is based on several strong, simplifying assumptions such as neglecting line losses.

7 Transmission Network Expansion Planning[1]

The Wind Farm Cabling Problem – A Greenfield Approach

Sustainability is an important aspect of the goal of improving and preserving the existence of human society. Accordingly, renewable energy sources play an important role. The renewable energy act EEG 2017 aims for 40% to 45% of electricity to be produced from renewable energy producers to gross electricity consumption until 2025 and 55% to 60% until 2035 [Jus16]. Thus, it is expected that the current trend of adding renewable energy producers, will continue [ALH01, IWR16, Jus14].

Wind farms transform wind energy into electrical energy and present an important and one of the most promising renewable energy producers (Chapter 1) for today's and future power grid. In contrast to traditional power plants, which produce the power in a centralized way (see Figure 1.1 on Page 2), wind farms aggregate the power of multiple wind turbines, each injecting power at around 33 kV (medium voltage level), e. g., the Hornsea Project One offshore wind farm is planned to have up to 240 turbines [Ltd16f]. As the number of wind turbines increases, algorithms for planning a wind farm cabling have to handle this amount of wind turbines. If we consider for instance a wind turbine of 3.6 MW then the number of wind turbines increases worldwide from 2014 to 2015 by 38% (see Table 7.1). The biggest planned offshore wind farm so far with approximately 300 turbines is the Hornsea Project Three [Ltd16g]. In total, the European grid has 3 344 connected turbines on 82 offshore wind farms [asb16]. The onshore wind farms Terra-Gen with 617 turbines and Gansu with more than 3 500 turbines represent two of the largest onshore wind farm projects in North America and China, respectively. Table 7.1 shows that the annual potential of offshore power production compared to the current annual electricity consumption worldwide is about 80% larger [ALH01]. Thus, satisfying a reasonable portion of the annual consumption of electricity with wind energy seems to be possible and reducing the cabling costs is important to reduce the trade-off between usage and expenses for wind farms [LHF08]. Since it is expected that the trend of adding renewable energy sources, such as wind turbines, will continue and accelerate [ALH01, IWR16, Jus14], the number of wind turbines and wind farms will increase. This gives an indicator for realistic instance sizes.

In this chapter, we focus on network planning for wind farms due to a high potential of cost savings [Fra+05] and a rapidly increasing number of planned projects [IWR16, Ltd16c]. The design process of a wind farm includes a variety of decisions that influence the construction and operation costs [Lun06]. Typical layout and design factors are presented in [Cam+09] such as the turbine locations, terrain, landowner requirements,

[1] This chapter is partly published in [Leh+17, Weg17].

Table 7.1: The roughly installed offshore wind power (status February 2016)[Gmb16, IWR16] increases significantly from 2014 to 2015. The number of turbines $|V_G|$ is based on the total power and assumes that all wind turbines have a power rating of 3.6 MW, which matches today's dominating Siemens SWT-3.6 turbines. In the last three columns the annual consumption of electricity (El. Cons.) and total energy consumption (Tot. E.) is compared to the potential offshore wind energy (Max. Pot.), respectively [Ene16, GM93].

	2015		2014		2015		—
					El. Cons.	Tot. E.	Max. Pot.
	in MW	$\lvert V_G \rvert$	in MW	$\lvert V_G \rvert$	in $^{\text{TW h}}/_{\text{a}}$	in $^{\text{TW h}}/_{\text{a}}$	in $^{\text{TW h}}/_{\text{a}}$
World	12 100	3 362	8 800	2 444	20 568	160 240	36 990
Europe	11 000	3 056	8 050	2 237	3 291	20 930	8 480
UK	5 100	1 417	4 500	1 250	312	2 080	986
Germany	3 300	917	1 050	292	521	3 550	237
Denmark	1 300	362	1 300	362	—	—	550
North America	0	—	0	—	4 342	28 450	9 860
South America	0	—	0	—	1 279	9 850	5 660
Asia	1 100	306	710	198	8 608	65 420	7 210
Australia	0	—	0	—	220	1 470	4 110

and wind profiles, to name a few. A large fraction of the investment is needed for the cables, cable laying and substations [Fra+05]. Thus, reducing the cabling costs reduces the trade-off between usage and expenses of wind farms [LHF08]. We focus on network planning for wind farms due to a high potential of cost savings [Fra+05] and an increasing number of planned projects [IWR16, Ltd16c].

Wind farms are organized in a hierarchical fashion; compare Figures 2.2 and 7.1. Turbines in a wind farm are usually grouped into *circuits* representing connected components attached to a *collector point*, which represents a substation. Circuits are combined at a substation to a local wind turbine grid known as *collector system*. Each collector system is connected to a collector point and from there using a transmission system, possibly via multiple substations [Ltd16a], to a unique substation representing the *grid access point* of the wind farm. The grid access point is connected to the grid itself via the *point of common connection* (PCC). The wind farm network usually forms a tree network (i. e., it is acyclic) [Ltd16b], sometimes a cactus network (i. e., each edge is contained in at most one cycle) [Ltd16e] or less commonly a meshed network [Ltd16d]. During the construction of on- or offshore wind farms the cabling of turbines and substations represents one important design question, while the location of the wind turbines is already fixed. Within this design question, typical cabling

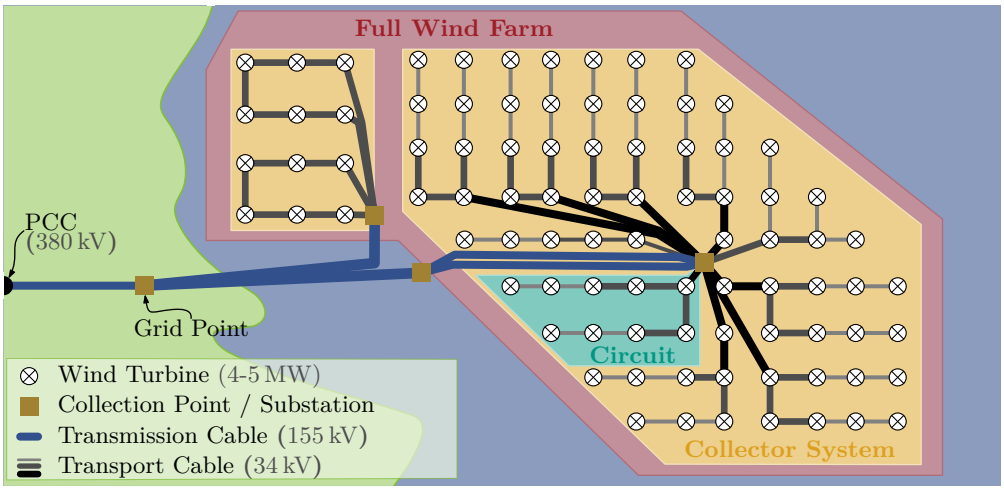

Figure 7.1: The wind farm topology typically consists of wind turbines ⊗ and substations ■. The latter are connected with consecutive substations using the transmission system ▬. The last substation represents the *grid point* ■—building the access to the (usually) high-voltage AC power grid—building the interface to the PCC ●. Wind turbines forming a connected component are called circuit. Multiple circuits connected to a substation constitute a collector system. Cables interconnecting turbines and connecting turbines with substations are called *transport cables* ≡. Both shown collector systems are the Alpha Ventus (left) and Borkum Riffgrund I (right) with 12 (60 MW) and 78 turbines (312 MW), respectively.

problem layers are the cabling of turbines within a circuit with one or multiple cable types known as *Circuit Problem* (CP), the cabling of multiple independent circuits with one substation to a collector system, known as *Substation Problem* (SP), and the cabling during the consideration of multiple—not necessarily fixed—substations known as *Full Farm Problem* (FFP). A simple example that describes different cabling for SP with their costs is given in Figure 7.2. It also shows that a redundant cabling design has a significant impact on the overall costs and that—when allowing multiple cable types—the minimum spanning tree does not necessarily present an optimal solution to the wind farm cabling problem (see Figure 2.2).

We study the problem of computing a cabling in a wind farm with minimum costs allowing different cable types and provide a model formulation using three different levels of granularity, where the highest level represents the whole wind farm. This is a greenfield approach for Transmission Network Expansion Planning (TNEP). The algorithmic issues for wind farm planning with multiple cable types are in general NP-hard (see Section 2). To solve this NP-hard problem, we propose to use simulated annealing (SA), a well-known heuristic approach [OL96, pp.532ff., Section 5]. We

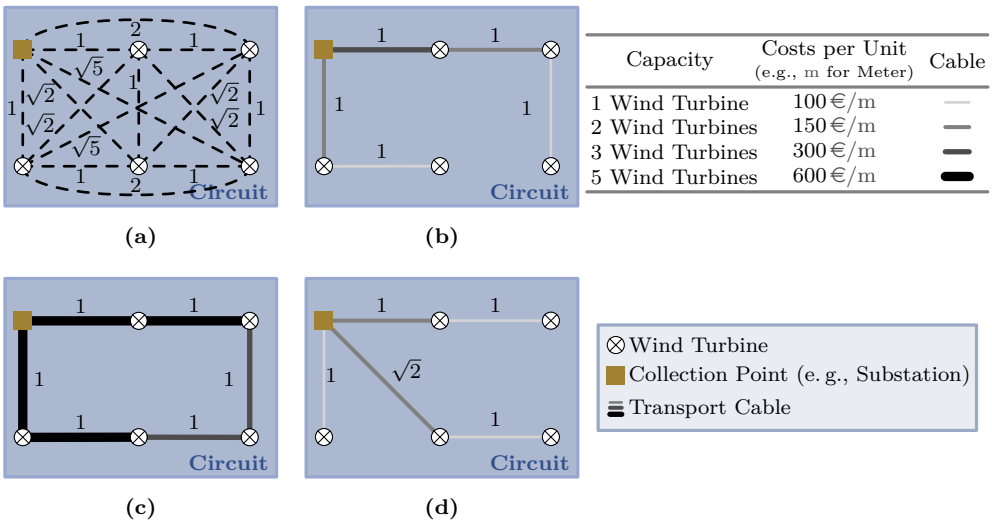

Figure 7.2: The circuit of a wind farm in this small example has five wind turbines ⊗, one substation ■, and four possible cable types and one additional option to lay no cable type at all. Each cable type has a maximum capacity of power it is able to carry, which is shown in the table on the upper right corner. Since we assume that each turbine produces the same amount of power, we define the capacity in terms of connected turbines to a particular cable. (a) The circuit with its 15 possible cabling connections that represent a complete graph. Every possible connection has a certain length that is shown at each connection. (b) A Minimum Spanning Tree (MST) of this circuit has costs of about 800 €. (c) A circuit that is cabled using a simple cycle has costs of about 3 000 €. (d) One best possible cabling costs about 662 € and constitutes a star-shaped cabling.

introduce a first formal hierarchical structure definition of the wind farm problem. To evaluate our algorithm, we demonstrate on a large variety of benchmark sets the performance of our simulated annealing algorithm. In the following section we formalize the problem structure.

7.1 A Mathematical Model for the Wind Farm Cabling Problem

The cable layout problem for a wind farm considers multiple—not necessarily fixed—substations and different cable types. A *cable layout* of a wind farm determines which entities are connected by cables, and for each of them a *cable type*. A *valid* cable layout for a wind farm interconnects turbines and turbines with substations in such a way that, in the end, all turbines are connected through a path to a substation. Further, a valid cable layout has to support a power flow from the turbines to the

collector point in such a way that (i) the thermal limits of the cables are respected, and (ii) the substation capacities are satisfied. Our goal is to find a valid cable layout that minimizes the construction costs, which depend on the lengths and the chosen cable types.

Cable Specific Definitions. Before we model the wind farm cabling problem, we need some preliminaries. Let K denote a set of cable types and let $\text{cap}, \gamma\colon K \to \mathbb{R}_{\geq 0} \cup \{\infty\}$ denote two functions that assign to each cable type $\kappa \in K$ a maximum capacity $\text{cap}(\kappa)$ and a cost $\gamma(\kappa)$ per unit of length. For $\kappa_1, \kappa_2 \in K$ we define $\kappa_1 < \kappa_2$ if and only if $\text{cap}(\kappa_1) < \text{cap}(\kappa_2)$ and $\gamma(\kappa_1) < \gamma(\kappa_2)$. Without loss of generality, we assume that $<$ is a strict total ordering on K (it never makes sense to use a more expensive cable with same or lower capacity). We further assume that there exist two special cable types $\kappa_0, \kappa_\infty \in K$ with $\text{cap}(\kappa_0) = \gamma(\kappa_0) = 0$ and $\text{cap}(\kappa_\infty) = \gamma(\kappa_\infty) = \infty$, where the former allows to easily model connections that are not used and the latter is used to make every instance feasible, though possibly with infinite costs.

Topology and Flows. A bidirected graph is a graph $G = (V, E)$ with vertex set V and edge set E that contains each edge in both directions. We use $\overleftrightarrow{E}$ to denote the underlying undirected edge set, and for $e \in E$ we denote by $\overleftrightarrow{e} \in \overleftrightarrow{E}$ the underlying undirected edge, i.e., $\overleftrightarrow{(u,v)} = \overleftrightarrow{(v,u)} = \{u, v\}$. A *flow* on a bidirected graph $G = (V, E)$ is a function $f\colon E \to \mathbb{R}$ satisfying the skew-symmetry property $f(u,v) = -f(v,u)$ for all $(u,v) \in E$. We denote the *net out-flow* of each vertex u in V as $f_{\text{net}}(u) = \sum_{(u,v)\in E} f(u,v)$.

Wind Farm Cabling Model. We are now ready to present our model of the general wind farm cabling problem called Full Farm Problem (FFP). An instance of this problem is given by a weighted, bidirected graph $G = (V, E, \text{len})$, where the vertex set $V = V_D \cup V_G$ is the union of the set V_D of substations and the set V_G of turbines, the set E of edges models the possible connections in the wind farm, and $\text{len}\colon \overleftrightarrow{E} \to \mathbb{R}_{\geq 0}$ defines the lengths of the connections. Further, we are given a set K of cable types and for each turbine $u \in V_G$ the amount $p_g(u) \in \mathbb{R}_{\geq 0}$ of power it supplies with fixed minimum, maximum, and current power generation with $\underline{p_g}(u) = \overline{p_g}(u) = p_g(u)$, respectively. In addition, there is for each $w \in V_D$ its minimum, maximum, and current capacity $\underline{p_d}(w), \overline{p_d}(w), p_d(w) \in \mathbb{R}_{\geq 0}$. We assume that the minimum substation capacity is zero meaning $\underline{p_d} \equiv 0$.

A solution to such an instance is a pair (κ, f) where $\kappa\colon \overleftrightarrow{E} \to K$ is a cable assignment and f is a flow on G satisfying the *conservation of flow* and the *edge capacity* constraints. The conservation of flow (Equations 7.1–7.3) describes the flow at each vertex including the production of wind turbines (Equation 7.2) and capacity restrictions at substations (Equation 7.3). The capacity restrictions of substations should be in general described

by $\sum_{(u,v)\in E} \max\big(0, f(u,v)\big) \leq p_d(v)$ for all $v \in V_D$. However, we assume that there is no positive flow leaving any substation (Equation 7.3). The edge capacity constraints (Equation 7.4) require that the flow on each edge respects the thermal limits of the chosen cable type.

$$\sum_{u\in V} f_{\text{net}}(u) = 0, \tag{7.1}$$

$$f_{\text{net}}(u) = -p_g(u) \qquad u \in V_G, \tag{7.2}$$

$$f_{\text{net}}(u) \leq p_d(u) \qquad u \in V_D, \tag{7.3}$$

$$|f(e)| \leq \text{cap}(\kappa(\overleftrightarrow{e})) \qquad e \in E. \tag{7.4}$$

We call a pair (κ, f) satisfying these properties *valid*. The total cost $c(\kappa, f)$ is given in Equation 7.5.

$$c(\kappa, f) = \sum_{\overleftrightarrow{e}\in\overleftrightarrow{E}} \big(\gamma(\kappa(\overleftrightarrow{e})) \cdot \text{len}(\overleftrightarrow{e})\big)\,. \tag{7.5}$$

Our goal is to find a valid pair $(\kappa^\star, f^\star)$ of minimum total cost for FFP with input $\mathcal{N} = (G, K, \text{cap}, \gamma, p_g, p_d)$. We denote the optimum cost of such a solution by $\text{OPT}_{\text{FFP}}(\mathcal{N}) := \min c(\kappa, f)$.

> Full Farm Problem FFP($\mathcal{N}$)
>
> *Instance:* A network corresponding to the whole wind farm $\mathcal{N} = (G, K, \text{cap}, \gamma, p_g, p_d)$.
>
> *Objective:* Find a valid pair (κ, f) that minimizes the total cost $c(\kappa, f)$ while complying with Equations 7.1–7.4.

We note that our model only requires f to be a *combinatorial flow*, i. e., it satisfies Kirchhoff's current law (KCL), and not necessarily an *electrical flow* (power flow) satisfying also Kirchhoff's voltage law (KVL). However, this is not a restriction in our setting. First of all, our heuristics mainly produce tree networks, and it is known that in this setting every combinatorial flow is also a power flow (see Theorem 6.5 on Page 162). While our mixed-integer linear program can also produce network topologies that are not trees, this happens only rarely.

Transformation to a Minimum Cost Flow Problem. In the following we transform this problem into a minimum cost flow problem on the input graph G, but with non-convex staircase cost functions (see Figure 7.3b). For this, we first observe that, given a flow f on G satisfying Equations 7.1–7.3, it is easy to construct a cable assignment κ of minimum cost such that (κ, f) is valid. Namely, for each edge $\overleftrightarrow{e} \in \overleftrightarrow{E}$, we define $\kappa_f(\overleftrightarrow{e}) = \min\{\kappa \in K \mid |f(e)| \leq \text{cap}(\kappa)\}$, i. e., $\kappa_f(\overleftrightarrow{e})$ is the cable type with the smallest capacity (and by our assumption on K also with the smallest cost) whose

Cable type	Capacity cap	Cost per unit γ
1	5	20
2	8	25
3	12	27
4	15	41

(a)

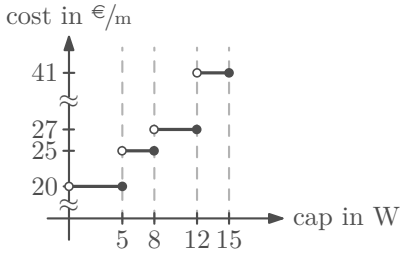

(b)

Figure 7.3: The cable types for our experiments are based on Berzan ET AL. [Ber+]. The cost for a cable on an edge is the product of the cost per length γ (e. g., in Euro €/m) and the euclidean distance (e. g., in meter m). Note that each cable has a certain capacity cap (e. g., using real power in Watt W). (a) The cable types in tabular form. (b) The diagram's x-axis represents the cable capacity (e. g., in terms of real power in W) and its y-axis represents the costs γ (e. g., in €/m). The cable types in a diagram illustrate the non-convex staircase cost function. If the line ends with a dark filled cycle the value is included and otherwise it is not.

capacity is large enough so that Equation 7.4 is satisfied for f. Note that the cost associated with edge $\overleftrightarrow{e} = \{u, v\}$ then is $\gamma(\kappa_f(\overleftrightarrow{e})) \cdot \text{len}(\overleftrightarrow{e})$. Thus, by using for each edge $e \in E$ the cost function $\gamma_e \colon \mathbb{R} \to \mathbb{R}_{\geq 0}$ as

$$\gamma_e(x) = \min\{\gamma(\kappa) \mid \kappa \in K, |x| \leq \text{cap}(\kappa)\} \cdot \text{len}(e), \tag{7.6}$$

the problem becomes equivalent to a minimum-cost flow problem $\mathcal{N} = (G, \gamma_e, p_g, p_d)$ on the bidirected graph $G = (V, E)$ where the cost of x units of flow along an edge is $\gamma_e(x)$. An optimal solution is a flow $f^\star$ minimizing $\sum_{e \in E} \gamma_e(f^\star(e))$. As above, we denote the optimal cost by $\text{OPT}_{\text{FFP}}(\mathcal{N})$.

MINIMUM COST FLOW PROBLEM $\text{MCFP}_{\text{FFP}}(\mathcal{N})$

Instance: A flow network $\mathcal{N} = (G, \gamma_e, p_g, p_d)$.

Objective: Find a feasible flow f such that the sum of the cost over all edges $\sum_{e \in E} \gamma_e(f(e))$ is minimized.

We note that, generally, γ_e forms a stair-case function, and thus this problem is NP-hard [YK12] and that this transformation generalizes to the case where an individual set of cable types $K_{\overleftrightarrow{e}}$ is specified for each edge $\overleftrightarrow{e} \in \overleftrightarrow{E}$. In our simulations we use the same set of cable types for all edges. Further, factors such as wind strength and turbulences affect all turbines with the same maximum power rating in the wind farm equally [Ltd16c]. Thus, a nominal power can be used to dimension the cabling and $p_g(u) = 1$ can be set for all $u \in V_G$.

The optimization of the transmission system's export cables is not considered for the FFP, since it is separately improvable. However, if the substations are flexible,

Table 7.2: The generated benchmark sets for our simulations. The sets $\mathcal{N}_1 \dots \mathcal{N}_4$ are the sets with a restricted edge set E resembling realistic wind farms in the sense of allowed cabling. The benchmark set $\mathcal{N}_5$ represents a complete graph vertex-equivalent to $\mathcal{N}_3$. The parameters $\beta, V_G, V_D, \xi, \delta, k$, and ϵ represent the shape aspect ratio, set of turbines, set of substations, substation capacity tightness, substation capacity variance, k-nearest neighbor, and value for the inclusion of shortcut edges E', respectively.

Benchmark Set	β min	β max	$\lvert V_G\rvert$ min	$\lvert V_G\rvert$ max	$\lvert V_D\rvert$ min	$\lvert V_D\rvert$ max	$\lvert V_G\rvert/\lvert V_D\rvert$ min	$\lvert V_G\rvert/\lvert V_D\rvert$ max	ξ min	ξ max	δ	k	ϵ	$\lvert\mathcal{N}_i\rvert$	run $\left\lceil \frac{\min}{\mathcal{N}_i} \right\rceil$	T_0
$\mathcal{N}_1$ small/single	0.7	1	10	80	1	1	–	–	–	–	–	6	1.1	500	2	0.01
$\mathcal{N}_2$ small	0.7	1	10	80	2	7	10	20	0.83	1	0	6	1.1	500	2	0.01
$\mathcal{N}_3$ medium	0.5	1	80	200	4	10	10	20	0.83	1	0	6	1.1	1 000	30	0.01
$\mathcal{N}_4$ large	0.4	1	200	1 000	10	40	10	50	0.83	1	0	6	1.1	1 000	30	0.01
$\mathcal{N}_5$ medium/complete	0.5	1	80	200	4	10	10	20	0.83	1	0	$(\lvert V\rvert - 1)$	–	1 000	30	0.01

export cables have to be considered. We call that problem flexible FFP (fFFP) and its optimum value is denoted by $\mathrm{OPT}_{\mathsf{fFFP}}(\mathcal{N}(k))$. Hierarchical-wise we consider two special cases: the Substation Problem (SP) and the Circuit Problem (CP) regarding the cabling layout of a single collector system with $\mathrm{OPT}_{\mathsf{SP}}(\mathcal{N})$ and circuit with $\mathrm{OPT}_{\mathsf{CP}}(\mathcal{N})$, respectively. Note that the problem is the same, but the network changes. For the wind farm cabling problem hierarchy holds that

$$\mathrm{OPT}_{\mathsf{FFP}}(\mathcal{N}) \leq \sum_{j \in V_D} \mathrm{OPT}_{\mathsf{SP}}(\mathcal{N}(j)) \leq \sum_{j \in V_D} \sum_{i \in \mathbb{N}} \mathrm{OPT}_{\mathsf{CP}}(\mathcal{N}(j,i)).$$

Note that the CP is already NP-hard [YK12]. In order to provide a good solution, we need a heuristic which is described in the following section.

7.2 Simulated Annealing-based Approach

The layout problem for multiple cable types is NP-hard [YK12]. Thus, this optimization problem becomes impracticable using combinatorial methods as the problem size grows. However, meta-heuristics such as simulated annealing (SA) [Čer85, KGV83] are promising probabilistic approaches—especially for large search spaces—even though they do not necessarily find an optimum, but often a very good solution. SA is often used for optimization problems where the search space is discrete such as the cabling problem. The Metropolis algorithm [Met+53] and the cooling schedule represent two characteristic methods of the SA algorithm. The SA approach calculates a finite set of solutions S (since the number of iteration is finite). A solution at time $t \in \mathbb{N}$ is denoted by $s_t \in S$, where each solution is a tuple $s_t = (\mathcal{N}^t, f^t)$ with a flow network $\mathcal{N}$ at time t, where the underlying graph G changes dependent on t denoted by $G^t = (V, E^t)$ with $E^t \subseteq E$. By using Equation 7.6, we have a real-valued cost function for our SA

approach, which is defined in Equation 7.7.

$$c(s_t) = \sum_{e \in E^t} \gamma_e(f(e)). \tag{7.7}$$

We call a solution *feasible* if the flow f is feasible and the graph G^t is connected. The global optimum for problem $\mathcal{P}$ (see Section 7.1) minimizing the total cost $c(s^\star)$ is a feasible solution $s^\star = (\mathcal{N}^\star, f^\star)$ with $s^\star \in S$ and cost $\mathrm{OPT}(s^\star)$. For each edge $\overleftrightarrow{e} \in \overleftrightarrow{E}$, we denote the *neighborhood* $N_G(\overleftrightarrow{e})$ as the set of *adjacent* edges that are connected to either endpoints u, v of $\overleftrightarrow{e} = \{u, v\}$ with $N_G(\overleftrightarrow{e}) \subsetneq \overleftrightarrow{E} - \{\overleftrightarrow{e}\}$ (an edge $\overleftrightarrow{e_1} \in N_G(\overleftrightarrow{e_2})$ if and only if $\overleftrightarrow{e_2} \in N_G(\overleftrightarrow{e_1})$). We write $N(\overleftrightarrow{e})$ instead of $N_G(\overleftrightarrow{e})$ if the underlying graph G is unambiguous. In a similar fashion, we define the neighborhood of solutions, where we denote that solution $s_1 \in S$ is neighbor of solution $s_2 \in S$ by $s_1 \in S(s_2)$. The *cooling schedule* is a non-increasing monotone function $T\colon \mathbb{N} \to (0, \infty)$, where $T(t)$ is the temperature at time t. The cooling of an object at time $t \in \mathbb{N}$ (Equation 7.8) is also influenced by the thermal conductivity and capacity represented by the factor τ.

$$T(t+1) = (1-\tau) \cdot T(t) \tag{7.8}$$

It influences the probability $\mathcal{W}_{s_1 s_2} \in \mathbb{R}_{\geq 0}$ of accepting a worse solution s_2 from s_1. All possible probabilities are assumed to be $\sum_{s_2 \in S(s_1)} \mathcal{W}_{s_1 s_2} = 1$. We introduce a *dynamic cooling schedule* in the following. In Equation 7.9, we define the *activity* μ_t.

$$\mu_{t+1} = \alpha_{\text{smooth}} \mathcal{W}_{\text{Norm}} + (1 - \alpha_{\text{smooth}})\mu_t, \tag{7.9}$$

where the initial activity $\mu_{t=0} = 1$, the impact of the current probability fluctuations and the normalized probability are denoted by α_{smooth} and

$$\mathcal{W}_{\text{Norm}}[s_{t+1} \mid s_{t+1} \in S(s_t)] \approx \exp(^{-\Delta c}/_{T(t)c(s_t)}),$$

respectively, where $\Delta c = c(s_{t+1}) - c(s_t)$ represents the cost difference between the present and the next cost value (often considered as energy). Thus, we adjust the cooling schedule in Equation 7.8 to a dynamic cooling schedule $T(t+1) = (1-\mu\tau) \cdot T(t)$.

An SA algorithm always starts with an initial solution $s_{t=0} \in S$. The set of instances is denoted by $\mathcal{I}$. Further, we denote as an *instance* $I \in \mathcal{I}$ a sequence of solutions starting with an arbitrary but fixed solution $s_{t=0}$, where $I = (s_t, \bar{s}, T)$, with $\bar{s}$ representing the best feasible solution found so far. Note that the standard SA approach holds only one instance. The encoding is a representation of a solution candidate $s_t \in S$. Our representation $R = (\theta, H)$ is a tuple representing a *potential field* $\theta\colon V \to \mathbb{N}, u \mapsto x$ with $x \in \{1, \ldots, |V|\}$ representing a strict order on the set of turbines using the distance function $\mathrm{len}(\{u, j\})$, and *edge cuts* $H \subsetneq E$ with $G = G - H$ representing the edges that are not considered as possible cable routes (see Figure 7.4a). The potential field avoids to lay cables to vertices having a smaller potential.

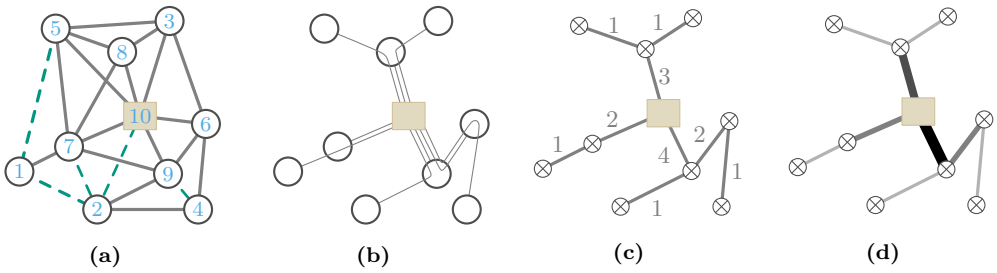

Figure 7.4: Given an example graph $G = (V, E)$ with vertex set $V = \{1, \ldots, 10\}$, with a substation $j \in V_D$ represented by squares ■, set of turbines V_G represented by cycles ⊗ and set of edges E represented by gray lines. (a) The encoded graph G is shown in the initial representation, where the cut set H is represented by the green dashed lines and the potential field θ is represented by the indices in the vertices. (b) The intermediate path representation used by the evaluation, where for each turbine $u \in V_G$ the path to the substation $w \in V_D$ is shown with $\pi(u, w) = (v_0 = u, v_1, \ldots, v_\ell = w)$, where $\{v_i, v_{i+1}\} \in \overleftrightarrow{E}$ for $i = 0, 1, \ldots, \ell$. (c) The cables are labeled with the maximum cable flow, which depends on the number of attached turbines. (d) The different cable types are represented by different diameters and colors presenting different cable types for the transport cables ═. Note that this is an adoption from Lehmann [Leh16].

The set of turbines closest to substation j is denoted by ${V_G}^j$. The turbines $u \in {V_G}^j$ are ordered by distance $\text{len}(\{u, j\})$ for each $j \in V_D$ separately and their rank represents the initial potential $\theta(u)$ and H is empty. To evaluate the result, the total cost $c(s)$ of a solution candidate s is calculated. However, the representation R does not provide a solution in the from $s = (\mathcal{N}, f)$. Therefore, we decode R to a path representation (see Figure 7.4b), in which we define for each turbine $u \in {V_G}^j$ a simple path $\pi(u, j) = (v_0 = u, v_1, \ldots, v_\ell = j)$, where $\{v_i, v_{i+1}\} \in \overleftrightarrow{E}$ for $i = 0, 1, \ldots, \ell$. The result is used to calculate the flow by $f(v_i, v_{i+1}) = -\sum_{v_i \in \pi(u,j)} p_g(u)$ for all $u \in V_G$ and $j \in V_D$ (see Figure 7.4c). If the flow f is valid, a solution $s = (\mathcal{N}, f)$ exists (see Figure 7.4d).

For the wind farm planning we introduce new methods to the *diversification*—increasing the SA search space exploration—and *intensification*—improving a solution—phase to improve the solution quality. In the diversification, the standard SA algorithm iteratively mutates and evaluates one solution at a time. To increase the diversity of the search space exploration, we allow multiple independent instances $I_k = (s_t^k, \overline{s}^k, T^k, \tau^k, \mu^k)$ of SA computations with $I_k \in \mathcal{I}$ each starting with a different random seed k. An *activity threshold* $\overline{\mu}$ stops a sequence of solutions once it stagnates and falls below that activity. Further, we introduce a counter tracking the number of iterations and resetting the instance to the best feasible solution $\overline{s}^k$ or apply *branching* at $\overline{s}^k$. Further, we restrict $|\mathcal{I}|$ to stabilize the computation time per instance and call instances *mature* for removal, when they reach a minimum number of mutations. Due to the fact that different solutions with similar good energy levels provide

good partial solutions, we use *crossings* to generate new solutions based on the best parts of two solutions. From the biological evolution, crossing provides a technique known from evolutionary computing. We use only solutions $s_1, s_2 \in S$ that have a high compatibility, i. e., small minimum cuts $F(s_1, s_2)$ among all solutions in S. To compute such a minimum cut, we use a complete graph $G_{s_1,s_2} = (V_D, \binom{|V_D|}{2})$ with edge capacities $\text{cap}\colon E \to \mathbb{N}, (u, v) \mapsto |V_G{}^u(s_1) \cap V_G{}^v(s_2)|$, with $u, v \in V_D$, and $V_G{}^x(s_i)$ being the set of all turbines connected to substation $x \in V_D$ of solution $s_i \in S$. The assignment of the potential function θ of two solutions becomes fuzzy within the cut region of the two partitions. Thus, we assign $\theta(v) = \lceil (\theta_{s_1}(v) + \theta_{s_2}(v))/2 \rceil$, sort the vector of potentials, and use the indices of the vector as new potentials. For an edge $e\colon (u, v)$ with $u, v \in V_G{}^x(s_1) \cap V_G{}^x(s_2)$ and $x \in V_D$, i. e. both vertices are assigned to the same substation in both solutions, we have $e \in H$ if $e \in H_{s_1} \cup H_{s_2}$. With the symmetric case, we get two new representation.

The intensification method mutates a representation R by modifying either the potential field θ or the set of cuts H. We use *swapping* techniques to change the potential field. Either we swap the potential of two distinct vertices $u, v \in V_G$ randomly or we change the potential field with regard to a potential change of a vertex u. The cut-based modification is another method using random edges. Whether we add or remove an edge to the set of cuts H depends on the cardinality of H set to $O(\sqrt{|V|})$.

7.3 Benchmark Generation

For our thorough evaluation, we have to generate wind farms of different sizes as there are no published benchmark sets or generators for wind farms so far. In addition, current wind farms provide only a limited size and complexity.

We introduce numerical parameters which characterize a typical wind farm. We define the shape of a wind farm to be an ellipse described by the aspect ratio $\beta \in (0, 1]$. The size of the shape is set such that its area is equal to $|V_G|$. Placing the turbines within this shape is done using poisson disc sampling [Bri07], a random point placement strategy in which all points are tightly placed within a minimum distance to each other (in our case 1). If the new randomly generated point violates the minimum pairwise distance, the whole farm is scaled up by an $\epsilon > 0$. The substations are placed in the same way with a minimum pairwise distance of $\sqrt{|V_G|/|V_D|}$.

The substation capacities are characterized by the *substation capacity tightness* ξ (see Equation 7.10), which roughly states how flexible turbines can be shifted to different substations without violating the substation capacity $\overline{p_d}$. If the substation capacity is tight meaning $\xi = 1$ then there is no flexibility at all and our assumption is that it is hard to find any feasible solution.

$$\sum_{u \in V_D} f_{\text{net}}(u) = \frac{\sum_{v \in V_G} p_g(v)}{\xi} \tag{7.10}$$

The *substation capacity variance* δ restricts the net flow at each substation and thus, defines $\underline{p_d}$ and $\overline{p_d}$ (see Equation 7.11).

$$f_{\text{net}}(u) \in \left[(1-\delta)\frac{|V_G|}{\xi|V_D|},\ \delta\frac{|V_G|}{\xi|V_D|} \right] \quad \forall u \in V_D \tag{7.11}$$

We call the substation capacity *tight* if $\xi = 1$ as the supply meets the substation capacity. However, the individual substation capacities are chosen randomly in this interval while making sure that their sum is equal to $\sum_{v \in V_G} p_g(v)/\xi$. Since G is a complete graph our generator has the ability to connect all pairs of vertices (except for export cable in the transmission system). However, we apply a preprocessing in which we assume that direct connections over long distances (dependent on the cable types K) are uncommon, which is a valid assumption for real world instances. Given a set of vertices we add for each vertex $u \in V$ edges to the k-nearest neighbors (k-NN) based on the euclidean distance. In addition, we add shortcut edges between any vertex pair having no edge in $\overleftrightarrow{E}$ but are fairly near to each other, which is described by Equation 7.12.

$$\overleftrightarrow{E}' := \{\{u,w\} \notin \overleftrightarrow{E} : \text{len}(u,v) + \text{len}(v,w) > \epsilon \cdot \text{len}(u,w)\}, \tag{7.12}$$

where $\{u,v\}, \{v,w\} \in \overleftrightarrow{E}$. We denoted the set of edges by $\overleftrightarrow{E} = \overleftrightarrow{E} \cup \overleftrightarrow{E}'$.

Even thought the generator is able to handle distinct sets of cable types for each edge, we generate graphs using the same set of cables for all edges, which is standard in practice. Throughout our experiments, we use the cables from Berzan ET AL. [Ber+] obtaining their data from domain experts (see Figure 7.3).

7.4 Simulations

In this section we run simulations of our SA approach and compare instances with similar turbine to substation ratio. In an analysis we compare the performance influence of the benchmark data on our SA heuristic and MIXED-INTEGER LINEAR PROGRAM (MILP) based on Section 7.1 subject to different criteria such as instance size $|V|$, number of substations $|V_D|$ and the *substation capacity tightness* measuring the ratio of maximum supply and demand. Our code is written in C++14, based on OGDF 2015.05 [Chi+13], Gurobi 6.5 [Gur16], Qt 5.5; compiled with the GCC 4.8.3 with `-O3 -march=native`. The experiment runs on a 64-bit with four 12-core CPU of AMD 6172, clocked at 2.1 GHz, with 256 GB RAM running OpenSUSE 13.2.

In order to ensure comparability, all simulations are evaluated in single-thread mode. The upper bound of the MILP after 1 hour serves as our *reference solution*. For our experiments, we use the benchmark sets $\mathcal{N}_\ell$ with $\ell = \{1, \ldots, 5\}$ (see Table 7.2) generated by benchmark generator for wind farms; see Section 7.3. In general we

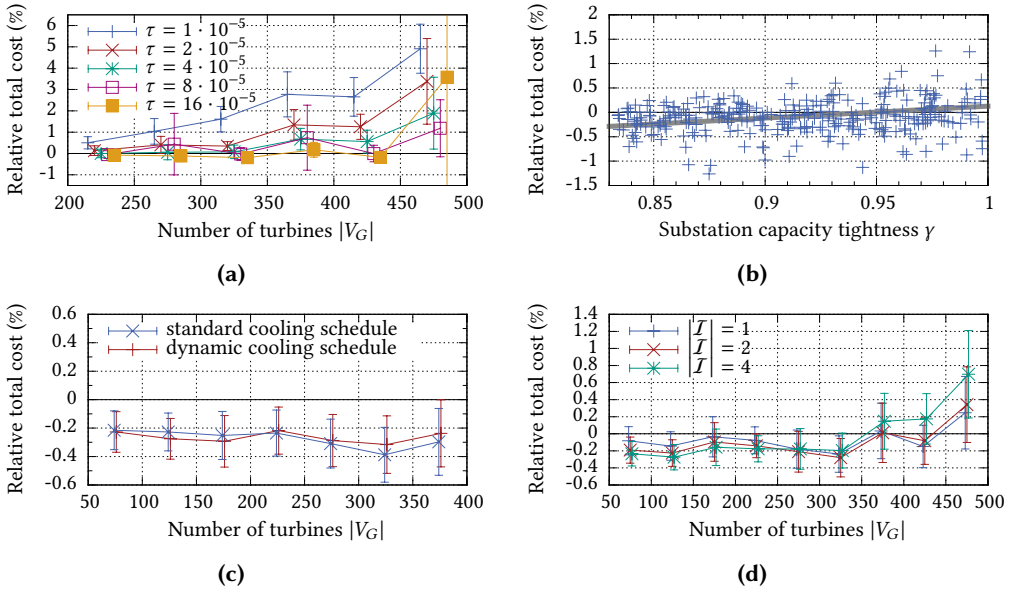

Figure 7.5: Comparison of our SA algorithm with the MILP. (a) The value of τ has to be chosen in relation to the network size. (b) A tighter substation capacity decreases the performance of our SA approach, where for $\xi < 0.83$ it is better. (c) Different cooling schedules have different influence on the quality. (d) Multi-instance SA performs better for networks ≤ 450.

use the benchmark sets $\mathcal{N}_1$ to $\mathcal{N}_4$, since they work on a restricted set of edges. Note that this is already a heuristic restriction of the solution space and thus improves the running time for both the MILP and the SA algorithm. For the small benchmark sets $\mathcal{N}_1$ and $\mathcal{N}_2$ with shorter running times the parameter $\tau = 10^{-5}$ represents a good value for the cooling schedule. Whereas for the longer running times $\tau = 10^{-6}$ results in better solutions as the temperature is reduced more slowly. By default, the SA algorithm uses a single SA instance, a dynamic cooling schedule and no crossings.

For the MILP we observe different gaps after one hour running time dependent on the wind farm size. For small networks $\mathcal{N}_1$ and $\mathcal{N}_2$, the average gap was about 22 %, for networks $\mathcal{N}_3$ it was 30 – 31 %, and for $\mathcal{N}_4$ it reaches 32 %. Benchmark instances with up to 13 turbines are solvable to optimality in less than an hour.

Note that the parameter τ influences the cooling schedule and is relevant to achieve good results (see Figure 7.5a). However, our SA algorithm performs for $\mathcal{N}_1$ with one substation better than the MILP for 48.2 % of all benchmarks with a better average relative cost of 0.44 %. In all other cases it performs 1.77 % worse than the MILP. Note that our SA algorithm takes only 2 min for small networks (see Table 7.2). However, for multiple substations our algorithm outperforms the MILP in about half of all benchmarks with a better average relative cost of 0.29 %. For the other cases it

performs 0.41 % worse. The network size influences the time each iteration of the SA algorithm takes, i. e. an increasing network size results in a decreasing number of iterations for the same amount of time. For the medium and large benchmark sets $\mathcal{N}_3$ with up to 200 and $\mathcal{N}_4$ with up to 500 turbines, both evaluated with value $\tau = 10^{-6}$, our SA outperforms the MILP in 7.9 % of the cases due to a too short intensification time. Thus, we increase τ to at least 10^{-5} (see Figure 7.5a).

The complexity of the problem can be increased by the substation capacity tightness ξ (see Figure 7.5b). For $\xi = 0.83$ the capacities can be up to 20 % more than the turbine supply and for $\xi = 1$ there is no variability in the number of turbines per collector system. For medium benchmark networks and parameter value $\tau = 8 \cdot 10^{-5}$ the simulations show that the instances are more difficult to solve for $\xi = 1$, whereas more flexibility ($\xi = 0.83$) improves the results. Our algorithm finds better solution for instances with $\xi < 0.85$ than the MILP, where for $\xi > 0.95$ the MILP is better on average. For the dynamic cooling schedule a larger value for τ is better, since the factor μ drastically decreases the resulting temperature difference. By comparing the dynamic with the standard static cooling schedule, we use $2^k \cdot 10^{-5}$ and $2^k \cdot 10^{-7}$ with $k \in \{0, 1, \ldots, 7\}$, respectively. In addition, we use for each group $|V_G|$ the value τ minimizing the average relative performance of our algorithm. The results are shown in Figure 7.5c. However, the difference between the standard and dynamic cooling schedule is never larger than 0.1 %. In Figure 7.5c the dynamic cooling schedule is more applicable for networks with up to 200 turbines, while the standard cooling schedule is slightly better for larger networks. The dynamic cooling schedule has a slight advantage when not optimizing τ.

For all previous simulations, our SA algorithm runs one instance. Multiple instances (see Figure 7.5d) increase the diversification, but the total running time is distributed among all SA instances in $\mathcal{I}$ resulting in a shorter intensification phase. The results of the experiments are aggregated using $\tau = 8 \cdot 10^{-5}$ for small and $\tau = 16 \cdot 10^{-5}$ for large instances. For small networks multiple SA instances are better, but for larger instances few SA instances should be used. The reason is that the diversification phase explores more of the search space with multiple SA instances, but the intensification phase for large networks is too short to find or improve good solutions.

7.5 Conclusion

In this chapter, we introduced the wind farm cabling problem and provided model formulations for the four hierarchical layers. Since the cabling problem is already NP-hard for the smallest problem layer, we introduced a novel simulated annealing (SA) to cope with the wind farms cabling problem. In this context, we introduce different criteria and strategies to adapt the standard SA algorithm to the cabling problem. In an extensive experimental study, we compared our SA algorithm, induced by

different criteria and strategies, with the Mixed-integer Linear Program (MILP) by using various benchmark data sets, which we generated to enable comparability and to overcome the shortcomings of the current literature. The latter used a small set of small-sized networks, which can lead to falsifications of the results, since the configuration of the algorithm is improved with regards to one specific data set. We are the first that work on a great variety of benchmark data sets. In our simulations we studied the influence of different wind farm properties on our algorithm and MILP. Our SA algorithm demonstrates excellent performance on a variety of benchmark sets and outperforms the MILP in benchmark instances with up to 450 turbines in a smaller fraction of time. It is worth noting that we will do some future endeavors in improving our tuning parameters and adapting the SA algorithm by improving and adding strategies and tuning parameters.

8 Conclusion

In this thesis, we identified a bunch of problems in energy networks. We analyzed the problems and networks such that we were able to design algorithms that give certain guarantees or bounds. In addition, we evaluated the algorithms on the IEEE benchmark data set or on self-generated instances. In this chapter, we briefly recapitulate the main results of this thesis in Section 8.1. There are still many ideas and open questions, which we were not able to tackle during that time. Thus, we give an outlook of what can be done in the future by outlining a few of the remaining ideas and open problems in Section 8.2.

8.1 Summary

One of the most fundamental problems that is part of nearly all problems that incorporate the power grid is the feasibility problem for electrical flows. We gave a first comprehensive analysis of electrical flows. We showed the duality of the two Kirchhoff's laws known as Kirchhoff's Current Law and Kirchhoff's Voltage Law that separates the relationship between current and voltage by using two graphs. We also show different possible representations that increase the understanding of electrical flows leading to different properties in electrical networks. We think that one of the most interesting properties is the balancing property that basically shows that all paths from one vertex to another vertex have the same length. We developed first algorithms for the feasibility problem on s-t-planar biconnected graphs that can be seen as a s-t electrical flow decomposition. Using the superposition principle, we can compute all s-t electrical flows and combine them into one electrical flow. The algorithmic idea that uses the duality has the potential to be used in dynamic scenarios, since a topology change does not need a full new recomputation of the flow, but can start from an already existing solution.

The second content chapter is about Maximum Transmission Switching Flow (MTSF) that can be seen as a discrete manipulation of the electrical network topology. We are the first that develop algorithms with provable guarantees on certain graph structures and shrink the gap between theory and practice. With the theoretical analysis of this problem, we are able to build connections to related problems. We showed network simplifications including transformations from the bounded to the unbounded MTSF and the equivalence between Optimal Transmission Switching (OTS) and MTSF. We introduced exact algorithms for networks with one generator and one demand for certain graph structures. We also show when the problem becomes

already NP-hard on *s*-*t* networks. Though the algorithms are only designed for special graph structures, we evaluate them on general power grids. For the *s*-*t* algorithm, which we called Dominating Theta Path (DTP), we defined a new centrality. The results of the centrality seem to give a hint on which edges are critical, since there are edges where the electrical network degenerates and we realized that these edges are the ones with a low centrality.

The third chapter is about the continuous manipulation of the electrical network topology. We motivate this by placing FACTS either at vertices or at edges. For that problem, we present a hybrid model for including flow control vertices or edges. We were able to show that it suffices to place a relatively small number of flow control units to reach the same solution as the graph-theoretical flow solution that is equivalent to placing these units everywhere. In addition to that, we even saw that fewer flow control buses improve the loadability and even have lower cost increase compared to Optimal Power Flow (OPF). We were able to explain our empirical observations on controller placement with graph-theoretical means.

We focused in the last part of this work on transmission network expansion planning on the green field. This particular problem represents a layout problem and was motivated by the wind farm cabling problem. We assumed that the turbines have fixed positions and that there are multiple cables types. We want to find a cabling of the wind farm such that the overall cabling costs are minimized. This is in general an NP-hard problem. We give a first proper model and decompose the wind farm cabling problem into multiple subproblems, each remaining NP-hard for multiple cable types. We developed a meta-heuristic known as simulated annealing algorithm, which we compare to the MILP by using various benchmark sets that we generated to enable comparability and to overcome the shortcoming of the current literature. We could see good results in the simulations for medium to large wind farms.

8.2 Outlook

For the electrical flow feasibility problem there remain several further investigations and proofs to explain the properties of such an electrical flow in depth. Furthermore, it would be interesting to evaluate whether the assumptions we make—meaning biconnectivity and planarity—are reasonable assumptions for the problem. We think that planarity should be a reasonable assumption following the statement of Cain et al. [COC12, p.13] and even the biconnectivity assumption for an *s*-*t* subgraph should be reasonable, since the electrical flow takes a path with the least resistance. However, it might lead to some error, which will be interesting to evaluate in simulations.

For Maximum Transmission Switching Flow (MTSF), which is a discrete manipulation of the power grid topology, it is unknown to us whether the reachability test can be done in polynomial time and if not, whether there is a polynomial time

algorithm that finds all Dominating Theta Paths (DTPs) from one source s to one sink t. Another open question to us is whether there is a Polynomial Time Approximation Scheme (PTAS) on cacti. It would be also interesting to see whether the complexity changes and whether there are algorithms when we define a set of edges as non-switchable (motivated by TNEP). Other interesting problems are the minimization and the constraining of the number of switches.

For the manipulation of the power grid topology using control units a complexity analysis would give the problem more structure and would increase the understanding of the problem. It would be even interesting if we can adopt the methods and algorithm from MTSF such that they work for the susceptance scaling, too. It is also unknown to us if the bilinearity will help us to some extent.

For both problems it would be interesting if the recent findings in the electrical flow feasibility also help in developing better algorithms for the discrete and continuous manipulation in power grids. In addition, a comparison to more realistic network models such as AC model is another main evaluation.

For the wind farm cabling there are many open questions concerning complexity and algorithms that give certain guarantees. In addition, so far we completely omit electrical flows in the wind farm cabling, since we more or less assume that the resulting networks are tree-like and thus, a graph-theoretical flow is a reasonable assumption. It would be worth investigating whether the results are electrically feasible and to incorporate electrical flows in general.

Bibliography

[AF09] Joes M. Arroyo and Federico J. Fernández. **A Genetic Algorithm Approach for the Analysis of Electric Grid Interdiction with Line Switching**. In *15th International Conference on Intelligent System Applications to Power Systems*, pages 1–6, 2009. DOI: 10.1109/ISAP.2009.5352849.
Cited on page 19.

[Ake60] Sheldon B. Akers. **The Use of Wye-Delta Transformations in Network Simplification**. *Operations Research* 8:3, pages 311–323, 1960. DOI: 10.1287/opre.8.3.311.
Cited on pages 14, 15, 77, 79.

[Alb+79] Paul F. Albrecht, Murty P. Bhavaraju, Billie E. Biggerstaff, Roy Billinton, Gunnar E. Jorgensen, Norbjorn D. Reppen, and Paul B. Shortley. **IEEE Reliability Test System**. *IEEE Transactions on Power Apparatus and Systems* PAS-98:6, pages 2047–2054, 1979. ISSN: 0018-9510. DOI: 10.1109/TPAS.1979.319398.
Cited on pages 6, 134.

[ALH01] Thomas Ackermann, Ralf Leutz, and Jens Hobohm. **World-wide offshore wind potential and European projects**. In *Power Engineering Society Summer Meeting*. Volume 1 of, pages 4–9, 2001. ISBN: 0-7803-7173-9. DOI: 10.1109/PESS.2001.969970.
Cited on pages 103, 171.

[AMO93] Ravindra K. Ahuja, Thomas L. Magnanti, and James B. Orlin. **Network Flows: Theory, Algorithms, and Applications**. Upper Saddle River, NJ, USA: Prentice-Hall, Inc., 1993, Upper Saddle River, NJ, USA. ISBN: 0-13-617549-X.
Cited on page 30.

[AO89] R. K. Ahuja and James B. Orlin. **A Fast and Simple Algorithm for the Maximum Flow Problem**. *Oper. Res.* 37:5, pages 748–759, 1989. ISSN: 0030-364X. DOI: 10.1287/opre.37.5.748.
Cited on page 71.

[APC90] Stefan Arnborg, Andrzej Proskurowski, and Derek G. Corneil. **Forbidden minors characterization of partial 3-trees**. *Discrete Mathematics* 80:1, pages 1–19, 1990. ISSN: 0012-365X. DOI: 10.1016/0012-365X(90)90292-P.
Cited on page 15.

[Arc+00] Dan Archdeacon, Charles J. Colbourn, Isidoro Gitler, and J. Scott Provan. **Four-terminal reducibility and projective-planar wye-delta-wye-reducible graphs**. *Journal of Graph Theory* 33:2, pages 83–93, 2000. ISSN: 0364-9024.
Cited on page 16.

[Ari+09] Sergio Arianos, Ettore Bompard, Anna Carbone, and Fei Xue. **Power grid vulnerability: A complex network approach**. *Chaos: An Interdisciplinary Journal of Nonlinear Science* 19:1, pages 013119-1–013119-6, 2009. DOI: 10.1063/1.3077229.
Cited on page 19.

[AS74] Ongun Alsacc and Brian Stott. **Optimal Load Flow with Steady-State Security**. *IEEE Transactions on Power Apparatus and Systems* PAS-93:3, pages 745–751, 1974. ISSN: 0018-9510. DOI: 10.1109/TPAS.1974.293972.
Cited on pages 6, 134.

[AS84] Avinash Agrawal and Appaajosyula Satyanarayana. **An $O(|E|)$ Time Algorithm for Computing the Reliability of a Class of Directed Networks**. *Operations Research* 32:3, pages 493–515, 1984. DOI: 10.1287/opre.32.3.493.
Cited on page 16.

[AS85] Avinash Agrawal and Appaajosyula Satyanarayana. **Network reliability analysis using 2-connected digraph reductions**. *Networks* 15:2, pages 239–256, 1985. DOI: 10.1002/net.3230150209.
Cited on page 16.

[asb16] WindEurope asbl/vzw. **The european offshore wind industry – Key trends and statistics 1st half 2016**. https://windeurope.org/wp-content/uploads/files/about-wind/statistics/WindEurope-mid-year-offshore-statistics-2016.pdf, Accessed: 2016-10-24. *@ONLINE*. 2016.
Cited on page 171.

[Aus+99] Giorgio Ausiello, Marco Protasi, Alberto Marchetti-Spaccamela, Giorgio Gambosi, Pierluigi Crescenzi, and Viggo Kann. **Complexity and Approximation: Combinatorial Optimization Problems and Their Approximability Properties**. 1st. Berlin, Heidelberg: Springer-Verlag, 1999, Berlin, Heidelberg. ISBN: 3-54065431-3.
Cited on pages 25, 111, 153.

[Bai+15] Yang Bai, Haiwang Zhong, Qing Xia, and Yang Wang. **A conic programming approach to optimal transmission switching considering reactive power and voltage security**. In *IEEE Power Energy Society General Meeting*, pages 1–5, 2015. DOI: 10.1109/PESGM.2015.7285833.
Cited on page 18.

[Bai+17] Yang Bai, Haiwang Zhong, Qing Xia, and Chongqing Kang. **A Two-Level Approach to AC Optimal Transmission Switching With an Accelerating Technique**. *IEEE Transactions on Power Systems* 32:2, pages 1616–1625, 2017. ISSN: 0885-8950. DOI: 10.1109/TPWRS.2016.2582214.
Cited on page 19.

[Ban22] Stefan Banach. **Sur les opérations dans les ensembles abstraits et leur application aux équations intégrales**. fre. *Fundamenta Mathematicae* 3:1, pages 133–181, 1922. URL: http://eudml.org/doc/213289.
Cited on page 117.

[Bat+98] Giuseppe Di Battista, Peter Eades, Roberto Tamassia, and Ioannis G. Tollis. **Graph Drawing: Algorithms for the Visualization of Graphs**. 1st. Upper Saddle River, NJ, USA: Prentice Hall PTR, 1998, Upper Saddle River, NJ, USA. ISBN: 0133016153.
Cited on page 96.

[Bax16] Rodney J. Baxter. **Exactly solved models in statistical mechanics**. Elsevier, 2016.
Cited on page 14.

[BB11] Clayton Barrows and Seth Blumsack. **Optimal transmission switching analysis and marginal switching results**. In *IEEE Power and Energy Society General Meeting*. PESGM, pages 1–3, 2011. DOI: 10.1109/PES.2011.6039669.
Cited on page 19.

[BB12] Clayton Barrows and Seth Blumsack. **Transmission Switching in the RTS-96 Test System**. *IEEE Transactions on Power Systems* 27:2, pages 1134–1135, 2012. ISSN: 0885-8950. DOI: 10.1109/TPWRS.2011.2170771.
Cited on pages 19, 104.

[BBB12] Clayton Barrows, Seth Blumsack, and Russell Bent. **Computationally efficient optimal Transmission Switching: Solution space reduction**. In *IEEE Power and Energy Society General Meeting*. PESGM, pages 1–8, 2012. DOI: 10.1109/PESGM.2012.6345550.
Cited on pages 106, 107.

[BBB13] Clayton Barrows, Seth Blumsack, and Russell Bent. **Using Network Metrics to Achieve Computationally Efficient Optimal Transmission Switching**. In *Proceedings of the 46th Hawaii International Conference on System Sciences*. HICSS, pages 2187–2196, 2013. DOI: 10.1109/HICSS.2013.590.
Cited on page 19.

[BC75] J. Wesley Barnes and Robert M. Crisp Jr. **Linear Programming: A Survey of General Purpose Algorithms**. *American Institute of Industrial Engineers Transactions* 8:1, pages 212–221, 1975. DOI: 10.1080/05695557508975428.
Cited on pages 51, 58.

[BDD89] Timothy J. Bertram, Kendall D. Demaree, and Lisa C. Dangelmaier. **An integrated package for real-time security enhancement**. In *Conference Papers Power Industry Computer Application Conference*, pages 18–24, 1989. DOI: 10.1109/PICA.1989.38969.
Cited on page 18.

[Bed61] S. Bedrosian. **Converse of the star-mesh transformation**. *IRE Transactions on Circuit Theory* 8:4, pages 491–493, 1961. ISSN: 0096-2007, 2331-3854. DOI: 10.1109/TCT.1961.1086832.
Cited on page 14.

[Ber+] Constantin Berzan, Kalyan Veeramachaneni, James McDermott, and Una-May O'Reilly. **Algorithms for cable network design on large-scale wind farms**. http://thirld.com/files/msrp_techreport.pdf, Accessed: 2016-01-04.
Cited on pages 22, 177, 182.

[BG88] Rainer Bacher and Hans Glavitsch. **Loss reduction by network switching**. *IEEE Transactions on Power Systems* 3:2, pages 447–454, 1988. ISSN: 0885-8950. DOI: 10.1109/59.192895.
Cited on page 18.

[Bil70] Glenn W. Bills. **On-line stability analysis study, RP 90-1**. Tech. rep. North American Rockwell Information Systems Co., Anaheim, CA (USA), 1970.
Cited on pages 6, 134.

[BJS04] Mokhtar S. Bazaraa, John J. Jarvis, and Hanif D. Sherali. **Linear Programming and Network Flows**. Wiley-Interscience, 2004. ISBN: 0-47148599-3.
Cited on page 149.

[BK98] Therese Biedl and Goos Kant. **A better heuristic for orthogonal graph drawings**. *Computational Geometry* 9:3, pages 159–180, 1998. ISSN: 0925-7721. DOI: 10.1016/S0925-7721(97)00026-6.
Cited on page 83.

[Bla+11] Gerardo Blanco, Fernando Olsina, Francisco Garcés, and Christian Rehtanz. **Real Option Valuation of FACTS Investments Based on the Least Square Monte Carlo Method**. *IEEE Transactions on Power Systems* 26:3, pages 1389–1398, 2011. DOI: 10.1109/TPWRS.2010.2094211.
Cited on page 20.

[BM87] Anastasios G. Bakirtzis and Athanasios P. Sakis Meliopoulos. **Incorporation of Switching Operations in Power System Corrective Control Computations**. *IEEE Transactions on Power Systems* 2:3, pages 669–675, 1987. ISSN: 0885-8950. DOI: 10.1109/TPWRS.1987.4335192.
Cited on page 18.

[BNW05] Dietrich Braess, Anna Nagurney, and Tina Wakolbinger. **On a Paradox of Traffic Planning**. *Transportation Science* 39:4, pages 446–450, 2005. ISSN: 1526-5447. DOI: 10.1287/trsc.1050.0127.
Cited on pages 4, 17, 119.

[BNX09] Ettore Bompard, Roberto Napoli, and Fei Xue. **Analysis of structural vulnerabilities in power transmission grids**. *International Journal of Critical Infrastructure Protection* 2:1, pages 5–12, 2009. ISSN: 1874-5482. DOI: 10.1016/j.ijcip.2009.02.002.
Cited on page 19.

[Bol98] Béla Bollobás. **Modern Graph Theory**. Springer New York, 1998. ISBN: 978-0-38798488-9.
Cited on page 106.

[BPG01a] Silvio Binato, Mário V. F. Pereira, and Sérgio Granville. **A new Benders decomposition approach to solve power transmission network design problems**. *IEEE Transactions on Power Systems* 16:2, pages 235–240, 2001. ISSN: 0885-8950. DOI: 10.1109/59.918292.
Cited on pages 2, 103, 107.

[BPG01b] Silvio Binato, Mário Veiga F. Pereira, and Sérgio Granville. **A New Benders Decomposition Approach to Solve Power Transmission Network Design Problems**. *IEEE Power Engineering Review* 21:5, pages 62–62, 2001. ISSN: 0272-1724. DOI: 10.1109/MPER.2001.4311380.
Cited on page 103.

[Bra68] Dietrich Braess. **Über ein Paradoxon aus der Verkehrsplanung (engl. Over a paradox in the traffic planning)**. *Unternehmensforschung* 12:1, pages 258–268, 1968. ISSN: 1432-5217. DOI: 10.1007/BF01918335.
Cited on pages 4, 17.

[Bri07] Robert Bridson. **Fast poisson disk sampling in arbitrary dimensions**. In *ACM SIGGRAPH Sketches*. SIGGRAPH, page 22. San Diego, California: ACM, 2007. ISBN: 978-1-4503-4726-6. DOI: 10.1145/1278780.1278807.
Cited on page 181.

[But21] Stephen Butterworth. **Notes on Earth Capacity Effects in Alternating-Current Bridges**. *Proceedings of the Physical Society of London* 34:1, pages 8–16, 1921. DOI: 10.1088/1478-7814/34/1/302.
Cited on pages 77, 81.

[BV19] Daniel Bienstock and Abhinav Verma. **Strong NP-hardness of AC power flows feasibility**. *CoRR* abs/1512.07315, 2019. arXiv: 1512.07315. URL: https://arxiv.org/abs/1512.07315.
Cited on pages 25, 54, 55.

[Cam+09] Ernst H. Camm, Michael R. Behnke, Oscar Bolado, Math H. J. Bollen, Mitch Bradt, C. Brooks, Wayne A. Dilling, Mike Edds, W. J. Hejdak, D. Houseman, Stanley A. Klein, F. Li, J. Li, Philippe Maibach, T. Nicolai, J. Patino, Subbaiah V. Pasupulati, Nader Samaan, Steven W. Saylors, T. Siebert, Travis M. Smith, Michael Starke, and Reigh A. Walling. **Wind power plant collector system design considerations: IEEE PES wind plant collector system design working group**. In *IEEE Power Energy Society General Meeting*. PESGM, pages 1–7, 2009. ISBN: 978-1-4244-4241-6. DOI: 10.1109/PES.2009.5275322.
Cited on page 171.

[Can+17] José M. Cano, Md. Rejwanur R. Mojumdar, Joaquín G. Norniella, and Gonzalo A. Orcajo. **Phase shifting transformer model for direct approach power flow studies**. *International Journal of Electrical Power & Energy Systems* 91, pages 71–79, 2017. ISSN: 0142-0615. DOI: 10.1016/j.ijepes.2017.03.007.
Cited on page 47.

[Car62] J. Carpentier. **Contribution to the Economic Dispatch Problem**. *Bulletin de la Société Franccoise des Électriciens* 3:8, pages 431–437, 1962.
Cited on pages 13, 140.

[Car79] J. L. Carpentier. **Optimal power flows**. *International Journal of Electrical Power & Energy Systems* 1:1, pages 3–15, 1979. ISSN: 0142-0615. DOI: 10.1016/0142-0615(79)90026-7.
Cited on page 13.

[CE17] Hsien-Chih Chang and Jeff Erickson. **Untangling Planar Curves**. *Discrete & Computational Geometry* 58:4, pages 889–920, 2017. ISSN: 1432-0444. DOI: 10.1007/s00454-017-9907-6.
Cited on pages 14, 15.

[Ced55] I. Cederbaum. **Invariance and Mutual Relations of Electrical Network Determinants**. *Journal of Mathematics and Physics* 34:1-4, pages 236–244, 1955. DOI: 10.1002/sapm1955341236.
Cited on page 64.

[Čer85] V. Černý. **Thermodynamical approach to the traveling salesman problem: An efficient simulation algorithm**. *Journal of Optimization Theory and Applications* 45:1, pages 41–51, 1985. ISSN: 1573-2878. DOI: 10.1007/BF00940812.
Cited on page 178.

[CES04] Li-Jun Cai, István Erlich, and Georgios C. Stamtsis. **Optimal Choice and Allocation of FACTS Devices in Deregulated Electricity Market using Genetic Algorithms**. In *IEEE Power Systems Conference and Exposition*. Volume 1 of PES, pages 201–207, 2004. ISBN: 0-7803-8718-X. DOI: 10.1109/PSCE.2004.1397562.
Cited on page 20.

[CGS14] Carleton Coffrin, Dan Gordon, and Paul Scott. **NESTA, The NICTA Energy System Test Case Archive**. *CoRR* abs/1411.0359, 2014. arXiv: 1411.0359. URL: http://arxiv.org/abs/1411.0359.
Cited on pages 134, 136.

[CH15] Carleton Coffrin and Pascal Van Hentenryck. **Transmission system restoration with co-optimization of repairs, load pickups, and generation dispatch**. *International Journal of Electrical Power & Energy Systems* 72:Supplement C. The Special Issue for 18th Power Systems Computation Conference, pages 144–154, 2015. ISSN: 0142-0615. DOI: 10.1016/j.ijepes.2015.02.027.
Cited on page 109.

[CH91] Joel E. Cohen and Paul Horowitz. **Paradoxical behaviour of mechanical and electrical networks**. *Nature* 352:6337, pages 699–701, 1991. ISSN: 1476-4687. DOI: 10.1038/352699a0.
Cited on page 17.

[Cha00] Bernard Chazelle. **A Minimum Spanning Tree Algorithm with inverse-Ackermann Type Complexity**. *J. ACM* 47:6, pages 1028–1047, 2000. ISSN: 0004-5411. DOI: 10.1145/355541.355562.
Cited on page 133.

[Chi+13] Markus Chimani, Carsten Gutwenger, Michael Jünger, Gunnar W. Klau, Karsten Klein, and Petra Mutzel. "The open graph drawing framework (OGDF)." In *Handbook of Graph Drawing and Visualization*. Ed. by Roberto Tamassia. CRC Press, 2013. Chap. 17, pages 543–569.
Cited on page 182.

[Cho+06] Jaeseok Choi, Timothy D. Mount, Robert J. Thomas, and Roy Billinton. **Probabilistic reliability criterion for planning transmission system expansions**. *IEE Proceedings - Generation, Transmission and Distribution* 153:6, pages 719–727, 2006. ISSN: 1350-2360. DOI: 10.1049/ip-gtd:20050205.
Cited on pages 2, 18, 103.

[Chr+11] Paul Christiano, Jonathan A. Kelner, Aleksander Madry, Daniel A. Spielman, and Shang-Hua Teng. **Electrical Flows, Laplacian Systems, and Faster Approximation of Maximum Flow in Undirected Graphs**. In *Proceedings of the Forty-third Annual ACM Symposium on Theory of Computing*. STOC, pages 273–282. San Jose, California, USA: ACM, 2011. ISBN: 978-1-4503-0691-1. DOI: 10.1145/1993636.1993674.
Cited on page 91.

[COC12] Mary B. Cain, Richard P. O'Neill, and Anya Castillo. **History of Optimal Power Flow and Formulations – Optimal Power Flow Paper 1**. Tech. rep. FERC, 2012, pages 1–36. URL: https://www.ferc.gov/industries/electric/indus-act/market-planning/opf-papers/acopf-1-history-formulation-testing.pdf.
Cited on pages 13, 26, 33, 46, 48, 49, 58, 74, 85, 188, 274.

[Cof+14] Carleton Coffrin, Hassan L. Hijazi, Karsten Lehmann, and Pascal Van Hentenryck. **Primal and dual bounds for Optimal Transmission Switching**. In *Proceedings of the 18th Power Systems Computation Conference*. PSCC, pages 1–8, 2014. DOI: 10.1109/PSCC.2014.7038446.
Cited on pages 3, 103.

[Cro15] Mariesa L. Crow. **Computational Methods for Electric Power Systems**. Third Edition. CRC Press, 2015. ISBN: 978-1-49871160-9.
Cited on pages 6, 134.

[CW14] Florin Capitanescu and Louis Wehenkel. **An AC OPF-based heuristic algorithm for optimal transmission switching**. In *Proceedings of the 18th Power Systems Computation Conference*. PSCC, pages 1–6, 2014. DOI: 10.1109/PSCC.2014.7038445.
Cited on page 18.

[Cyg+15] Marek Cygan, Fedor V. Fomin, Lukasz Kowalik, Daniel Lokshtanov, Daniel Marx, Marcin Pilipczuk, Michal Pilipczuk, and Saket Saurabh. **Parameterized Algorithms**. 1st. Springer Publishing Company, Incorporated, 2015. ISBN: 3319212745.
Cited on page 145.

[Dem+77] Benjamin Dembart, Albert M. Erisman, Esko G. Cate, Michael A. Epton, and Herman Dommel. **Power system dynamic analysis: Phase I. Final report**. Tech. rep. Boeing Computer Services, Inc., Seattle, Wash.(USA). Energy Technology Applications Div., 1977.
Cited on pages 6, 134.

[DF57] George B. Dantzig and Delbert R. Fulkerson. **On the Max-Flow Min-Cut Theorem of Networks**. In *Linear Inequalities and Related Systems*. Ed. by Harold William Kuhn and Albert William Tucker. Volume 38 of, pages 215–222. Princeton: Princeton University Press, 1957. ISBN: 978-1-40088198-7. DOI: 10.1515/9781400881987-013.
Cited on page 30.

[DK15] Payman Dehghanian and Mladen Kezunovic. **Impact assessment of transmission line switching on system reliability performance**. In *18th International Conference on Intelligent System Application to Power Systems*. ISAP, pages 1–6, 2015. DOI: 10.1109/ISAP.2015.7325581.
Cited on page 18.

[DK67] Eugene P. Durbin and David M. Kroenke. **The Out-of-kilter algorithm: A Primer**. Tech. rep. https://apps.dtic.mil/docs/citations/AD0663370. Santa Monica, CA: RAND Corporation, 1967. URL: https://www.rand.org/content/dam/rand/pubs/research_memoranda/2008/RM5472.pdf.
Cited on page 31.

[DM15] Lino Demasi and Bojan Mohar. **Four Terminal Planar Delta-Wye Reducibility via Rooted $K_{2,4}$ Minors**. In *Proceedings of the Twenty-sixth Annual ACM-SIAM Symposium on Discrete Algorithms*. SODA '15, pages 1728–1742. San Diego, California: Society for Industrial and Applied Mathematics, 2015. URL: http://dl.acm.org/citation.cfm?id=2722129.2722244.
Cited on page 16.

[dMP99] Vander M. da Costa, Nelson Martins, and José L. R. Pereira. **Developments in the Newton Raphson power flow formulation based on current injections**. *IEEE Transactions on Power Systems* 14:4, pages 1320–1326, 1999. ISSN: 0885-8950. DOI: 10.1109/59.801891.
Cited on page 13.

[DO11] Sudipta Dutta and Thomas J. Overbye. **A clustering based wind farm collector system cable layout design**. In *IEEE Power and Energy Conference at Illinois*. PECI, pages 1–6, 2011. ISBN: 978-1-4244-8052-4. DOI: 10.1109/PECI.2011.5740480.
Cited on page 22.

[Don+05] Vaibhav Donde, Vanessa López, Bernard Lesieutre, Ali Pinar, Chao Yang, and Juan Meza. **Identification of severe multiple contingencies in electric power networks**. In *Proceedings of the 37th Annual North American Power Symposium*, pages 59–66, 2005. ISBN: 0-7803-9255-8. DOI: 10.1109/NAPS.2005.1560502.
Cited on page 52.

[Dor01] Marco Dorigo. **Advances in artificial life: 6th european conference, ECAL Prague, Czech Republic**. In. Ed. by Jozef Kelemen and Petr Sosík, pages 11–22. Berlin, Heidelberg: Springer Berlin Heidelberg, 2001. ISBN: 978-3-540-44811-2. DOI: 10.1007/3-540-44811-X_2.
Cited on page 22.

[Dör17] Maximilian Dörrbecker. **Map of the offshore wind power farms in the German Bight**. https://en.wikipedia.org/wiki/File:Map_of_the_offshore_wind_power_farms_in_the_German_Bight.png#/media/File:Map_of_the_offshore_wind_power_farms_in_the_German_Bight.png, Accessed: 2017-05-17. *@ONLINE*. 2017.
Cited on page 3.

[dR08] Vander M. da Costa and Arlei L. S. Rosa. **A comparative analysis of different power flow methodologies**. In *IEEE/PES Transmission and Distribution Conference and Exposition: Latin America*, pages 1–7, 2008. DOI: 10.1109/TDC-LA.2008.4641868.
Cited on page 13.

[Dub86] Pradeep Dubey. **Inefficiency of Nash Equilibria**. *Mathematics of Operations Research* 11:1, pages 1–8, 1986. DOI: 10.1287/moor.11.1.1.
Cited on page 17.

[DV01] Markus Doll and Johannes F. Verstege. **Congestion management in a deregulated environment using corrective measures**. In *Conference Proceedings (Cat. No.01CH37194) – IEEE Power Engineering Society Winter Meeting*. Volume 2 of, pages 393–398, 2001. DOI: 10.1109/PESW.2001.916873.
Cited on page 19.

[EK72] Jack Edmonds and Richard M. Karp. **Theoretical Improvements in Algorithmic Efficiency for Network Flow Problems**. *J. ACM* 19:2, pages 248–264, 1972. ISSN: 0004-5411. DOI: 10.1145/321694.321699.
Cited on pages 12, 31, 71.

[Eke01] Stig Ekelöf. **The genesis of the Wheatstone bridge**. *Engineering Science and Education Journal* 10:1, pages 37–40, 2001. ISSN: 0963-7346. DOI: 10.1049/esej:20010106.
Cited on page 119.

[Els17] Marc Elsberg. **Blackout**. Thorndike Press, 2017. ISBN: 978-1-43284242-0.
Cited on page 1.

[Ene16] Enerdata. **Global energy statistical yearbook 2016**. https://yearbook.enerdata.net, Accessed: 2016-11-17. *@ONLINE*. 2016.
Cited on page 172.

[ent18] entsoe. **TYNDP 2018 Projects Sheets (166)**. https://tyndp.entsoe.eu/tyndp2018/projects/projects, Accessed: 2019-06-05. *@ONLINE*. 2018.
Cited on pages 2, 3.

[ent19a] entsoe. **North-South interconnections in Western Europe–regional planning**. https://tyndp.entsoe.eu/2016/insight-reports/north-south-interconnection-western/, Accessed: 2019-06-05. *@ONLINE*. 2019.
Cited on page 2.

[ent19b] entsoe. **Project 132 – HVDC Line A-North**. https://tyndp.entsoe.eu/tyndp2018/projects/projects/132, Accessed: 2019-06-05. *@ONLINE*. 2019.
Cited on page 2.

[ent19c] entsoe. **Project 235 - HVDC SuedLink Brunsbüttel/Wilster to Großgartach/Grafenrheinfeld**. https://tyndp.entsoe.eu/tyndp2018/projects/projects/235, Accessed: 2019-06-05. *@ONLINE*. 2019.
Cited on page 2.

[Epi66] G. V. Epifanov. **Reduction of a plane graph to an edge by star-triangle transformations**. *Doklady Akademii Nauk SSSR* 166:1, pages 19–22, 1966. URL: http://mi.mathnet.ru/dan31994.
Cited on pages 14, 81.

[ET76] Shimon Even and Robert Endre Tarjan. **Computing an st-numbering**. *Theoretical Computer Science* 2:3, pages 339–344, 1976. ISSN: 0304-3975. DOI: 10.1016/0304-3975(76)90086-4.
Cited on page 95.

[Eul41] Leonhard Euler. **Solutio problematis ad geometriam situs pertinentis**. *Commentarii academiae scientiarum Petropolitanae* 8, pages 128–140, 1741. URL: http://eulerarchive.maa.org//pages/E053.html.
Cited on page 127.

[EW66] L. R. Esau and K. C. Williams. **On teleprocessing system design, Part II: A method for approximating the optimal network**. *IBM Systems Journal* 5:3, pages 142–147, 1966. ISSN: 0018-8670. DOI: 10.1147/sj.53.0142.
Cited on page 22.

[Fel13] Stefan Felsner. **Rectangle and Square Representations of Planar Graphs**. In *Thirty Essays on Geometric Graph Theory*. Ed. by János Pach, pages 213–248. New York, NY: Springer, 2013. ISBN: 978-1-4614-0110-0. DOI: 10.1007/978-1-4614-0110-0_12.
Cited on pages 57, 71, 87, 89, 90, 91, 94, 95, 96, 141, 157.

[Feo85] Thomas A. Feo. **Efficient reduction of planar networks for solving certain combinatorial problems**. *University of California, Berkeley*. Working Paper, 1985.
Cited on page 14.

[FF56] Lester R. Ford and Delbert R. Fulkerson. **Maximal Flow through a Network**. *Canadian Journal of Mathematics* 8:0, pages 399–404, 1956. ISSN: 1496-4279. DOI: 10.4153/cjm-1956-045-5.
Cited on pages 91, 93.

[FL13] Masoud Farivar and Steven H. Low. **Branch Flow Model: Relaxations and Convexification – Part II**. *IEEE Transactions on Power Systems* 28:3, pages 2565–2572, 2013. ISSN: 0885-8950. DOI: 10.1109/TPWRS.2013.2255318.
Cited on pages 21, 160, 167.

[FMR95] Hubert de Fraysseix, Patrice Ossona de Mendez, and Pierre Rosenstiehl. **Bipolar orientations revisited**. *Discrete Applied Mathematics* 56:2. Fifth Franco-Japanese Days, pages 157–179, 1995. ISSN: 0166-218X. DOI: 10.1016/0166-218X(94)00085-R.
Cited on page 95.

[FOF08] Emily B. Fisher, Richard P. O'Neill, and Michael C. Ferris. **Optimal Transmission Switching**. *IEEE Transactions on Power Systems* 23:3, pages 1346–1355, 2008. ISSN: 0885-8950. DOI: 10.1109/TPWRS.2008.922256.
Cited on pages 4, 5, 18, 103, 106, 119, 120.

[Fou96] Robert Fourer. **AMPL:A modeling language for mathematical programming**. 2nd ed. San Francisco, California: San Francisco, California : Scientific Pr., 1996, San Francisco, California.
Cited on page 33.

[Fra+05] Bengt Frankén, Henrik Breder, Mikael Dahlgren, and Erik K. Nielsen. **Collection grid topologies for off-shore wind parks**. In *18th International Conference and Exhibition on Electricity Distribution*. CIRED, pages 1–5, 2005. ISBN: 978-0-86341-534-0. DOI: 10.1049/cp:20051326.
Cited on pages 171, 172.

[FRC12] J. David Fuller, Raynier Ramasra, and Amanda Cha. **Fast Heuristics for Transmission-Line Switching**. *IEEE Transactions on Power Systems* 27:3, pages 1377–1386, 2012. ISSN: 0885-8950. DOI: 10.1109/TPWRS.2012.2186155.
Cited on page 18.

[FSR12a] Stephen Frank, Ingrida Steponavice, and Steffen Rebennack. **Optimal Power Flow: A Bibliographic Survey I**. *Energy Systems* 3:3, pages 221–258, 2012. ISSN: 1868-3967. DOI: 10.1007/s12667-012-0056-y.
Cited on pages 13, 140.

[FSR12b] Stephen Frank, Ingrida Steponavice, and Steffen Rebennack. **Optimal Power Flow: A Bibliographic Survey II**. *Energy Systems* 3:3, pages 259–289, 2012. ISSN: 1868-3967. DOI: 10.1007/s12667-012-0057-x.
Cited on pages 13, 140.

[FT84] Michael L. Fredman and Robert E. Tarjan. **Fibonacci Heaps And Their Uses In Improved Network Optimization Algorithms**. In *25th Annual Symposium on Foundations of Computer Science*, pages 338–346, 1984. DOI: 10.1109/SFCS.1984.715934.
Cited on page 127.

[Ful61] Delbert R. Fulkerson. **An out-of-kilter method for minimal-cost flow problems**. *Journal of the Society for Industrial and Applied Mathematics* 9:1, pages 18–27, 1961. ISSN: 0368-4245, 2168-3484. DOI: 10.1137/0109002.
Cited on page 31.

[Gab+86] Harold N. Gabow, Zvi Galil, Thomas Spencer, and Robert E. Tarjan. **Efficient algorithms for finding minimum spanning trees in undirected and directed graphs**. *Combinatorica* 6:2, pages 109–122, 1986. ISSN: 1439-6912. DOI: 10.1007/BF02579168.
Cited on page 22.

[GAG96] Julie Griffin, Djordje R. Atanackovic, and Francisco D. Galiana. **A study of the impact of flexible AC transmission system devices on the economic-secure operation of power systems**. In *Proceedings of the 12th Power Systems Computation Conference*. PSCC, pages 1077–1082, 1996.
Cited on pages 6, 148, 150.

[Gao+18] Shilin Gao, Hua Ye, Yanling Du, and Haitao Liu. **A general decoupled AC/DC power flow algorithm with VSC-MTDC**. In *13th IEEE Conference on Industrial Electronics and Applications (ICIEA)*, pages 1779–1784, 2018. DOI: 10.1109/ICIEA.2018.8397997.
Cited on page 41.

[GCG01] Stéphane Gerbex, Rachid Cherkaoui, and Alain J. Germond. **Optimal location of multi-type FACTS devices in a power system by means of genetic algorithms**. *IEEE Transactions on Power Systems* 16:3, pages 537–544, 2001. DOI: 10.1109/59.932292.
Cited on pages 20, 170.

[GH99] Laszlo Gyugyi and Narain G. Hingorani. **Understanding FACTS. Concepts and Technology of Flexible AC Transmission Systems**. Wiley-IEEE Press, 1999.
Cited on page 140.

[Git91] Isidoro Gitler. **Delta-wye-delta Transformations: Algorithms and Applications**. AAINN68979. PhD dissertation. Waterloo, Ont., Canada: University of Waterloo, 1991. ISBN: 0-315-68979-X.
Cited on pages 16, 17.

[GJ03] John J. Grainger and William D. Stevenson Jr. **Power System Analysis**. McGraw-Hill, 2003. ISBN: 978-0-07058515-7.
Cited on pages 6, 134.

[GJ79] Michael R. Garey and David S. Johnson. **Computers and Intractability: A Guide to the Theory of NP-Completeness**. New York, NY, USA: W. H. Freeman & Co., 1979, New York, NY, USA. ISBN: 0-71671044-7.
Cited on pages 25, 57, 71, 111, 114, 116, 122, 153.

[GK03] Branko Grünbaum and Volker Kaibel. **Convex polytopes**. 2. ed. / prepared by Volker Kaibel. Includes bibliographical references and index. - Previous ed.: s.l.: Wiley, 1967. New York: Springer, 2003, New York, XVI, 466 S. ISBN: 978-0-38700424-2. DOI: 10.1007/978-1-4613-0019-9.
Cited on page 14.

[GL99] Fred W. Glover and Manuel Laguna. **Handbook of combinatorial optimization: Volume 1–3**. In. Ed. by Ding-Zhu Du and Panos M. Pardalos, pages 2093–2229. Boston, MA: Springer US, 1999. ISBN: 978-1-46130303-9. DOI: 10.1007/978-1-4613-0303-9_33.
Cited on page 22.

[Gla85] Hans Glavitsch. **Switching as means of control in the power system**. *International Journal of Electrical Power & Energy Systems* 7:2, pages 92–100, 1985. ISSN: 0142-0615. DOI: 10.1016/0142-0615(85)90014-6.
Cited on pages 18, 19.

[GM93] Andrew D. Garrad and Hermann G. Matthies. **Study of offshore wind energy in the European Community (EC). JOULE I (JOUR 0072). Executive summary. Offshore wind turbines**. 1993. URL: https://books.google.de/books?id=SximQwAACAAJ.
Cited on page 172.

[Gmb16] Internationales Wirtschaftsforum Regenerative Energien (IWR) / IWR.de GmbH. **Windparks**. http://www.offshore-windindustrie.de/windparks, Accessed: 2016-10-25. *@ONLINE*. 2016.
Cited on page 172.

[GMM92] Francisco D. Galiana, Donald T. McGillis, and Miguel A. Marin. **Expert systems in transmission planning**. *Proceedings of the IEEE* 80:5, pages 712–726, 1992. ISSN: 0018-9219. DOI: 10.1109/5.137226.
Cited on pages 2, 103.

[Gol97] Andrew V. Goldberg. **An Efficient Implementation of a Scaling Minimum-Cost Flow Algorithm**. *Journal of Algorithms* 22:1, pages 1–29, 1997. ISSN: 0196-6774. DOI: 10.1006/jagm.1995.0805.
Cited on page 149.

[Gon+12] Francisco M. González-Longatt, Peter Wall, Pawel Regulski, and Vladimir Terzija. **Optimal electric network design for a large offshore wind farm based on a modified genetic algorithm approach**. *IEEE Systems Journal* 6:1, pages 164–172, 2012. ISSN: 1932-8184. DOI: 10.1109/JSYST.2011.2163027.
Cited on page 22.

[Gor19] Alice Gordenker. **Japan's incompatible power grids**. https://www.japantimes.co.jp/news/2011/07/19/reference/japans-incompatible-power-grids/#.XtZpBC-w01I, Accessed: 2019-08-28. *@ONLINE*. 2019.
Cited on page 31.

[Gra+06] Gianpietro Granelli, Mario Montagna, Fabio Zanellini, Paola Bresesti, Riccardo Vailati, and Mario Innorta. **Optimal Network Reconfiguration for Congestion Management by Deterministic and Genetic Algorithms**. *Electric Power Systems Research* 76:6–7, pages 549–556, 2006. ISSN: 0378-7796. DOI: 10.1016/j.epsr.2005.09.014.
Cited on page 104.

[Gra+18] Alban Grastien, Ignaz Rutter, Dorothea Wagner, Franziska Wegner, and Matthias Wolf. **The Maximum Transmission Switching Flow Problem**. In *Proceedings of the Ninth International Conference on Future Energy Systems*. e-Energy, pages 340–360. Karlsruhe, Germany: ACM, 2018. ISBN: 978-1-4503-5767-8. DOI: 10.1145/3208903.3208910.
Cited on pages 6, 7, 8, 94, 103, 113, 275.

[Gra99] ISGCI: Information System on Graph Class Inclusions. **List of Small Graphs**. http://www.graphclasses.org/smallgraphs.html, Verion: 2.0, Accessed: 2017-12-03. *@ONLINE*. 1999.
Cited on page 119.

[Gri+99] Cliff Grigg, Peter Wong, Paul Albrecht, Ron Allan, Murty Bhavaraju, Roy Billinton, Quan Chen, Clement Fong, Suheil Haddad, Sastry Kuruganty, Wenyuan Li, Rana Mukerji, Dee Patton, Narayan Rau, Dag Reppen, Alex Schneider, Mohammed Shahidehpour, and Chanan Singh. **The IEEE Reliability Test System-1996. A report prepared by the Reliability Test System Task Force of the Application of Probability Methods Subcommittee**. *IEEE Transactions on Power Systems* 14:3, pages 1010–1020, 1999. ISSN: 0885-8950. DOI: 10.1109/59.780914.
Cited on pages 6, 134.

[Gro+19] Martin Gross, Marc E. Pfetsch, Lars Schewe, Martin Schmidt, and Martin Skutella. **Algorithmic results for potential-based flows: Easy and hard cases**. *Networks* 73:3, pages 306–324, 2019. DOI: 10.1002/net.21865.
Cited on pages vii, 273.

[GS] Isidoro Gitler and Feliú Sagols. **On terminal delta-wye reducibility of planar graphs**. *Networks* 57:2, pages 174–186. DOI: 10.1002/net.20399.
Cited on page 17.

[GT01] Jonathan L. Gross and Thomas W. Tucker. **Topological graph theory**. Courier Corporation, 2001.
Cited on pages 26, 74.

[GT14] Andrew V. Goldberg and Robert E. Tarjan. **Efficient Maximum Flow Algorithms**. *Commun. ACM* 57:8, pages 82–89, 2014. ISSN: 0001-0782. DOI: 10.1145/2628036.
Cited on page 12.

[GT89] Andrew V. Goldberg and Robert E. Tarjan. **Finding Minimum-cost Circulations by Canceling Negative Cycles**. *J. ACM* 36:4, pages 873–886, 1989. ISSN: 0004-5411. DOI: 10.1145/76359.76368.
Cited on pages 12, 31, 71.

[GT90] Andrew V. Goldberg and Robert E. Tarjan. **Finding Minimum-Cost Circulations by Successive Approximation**. *Mathematics of Operations Research* 15:3, pages 430–466, 1990. DOI: 10.1287/moor.15.3.430.
Cited on pages 12, 31.

[GTT89] Andrew V. Goldberg, Éva Tardos, and Robert E. Tarjan. **Network Flow Algorithms**. Tech. rep. Princeton University NJ Department of Computer Science, 1989. URL: https://www.researchgate.net/publication/235021228_Network_Flow_Algorithms.
Cited on pages 30, 31.

[GUR13] Inc. GUROBI Optimization. **GUROBI OPTIMIZER – State of the Art Mathematical Programming Solver**. http://www.gurobi.com/products/gurobi-optimizer/gurobi-overview, Accessed 2013-08-06. *@ONLINE*. 2013.
Cited on pages 13, 159.

[Gur16] Inc. Gurobi Optimization. **Gurobi optimizer reference manual**. http://www.gurobi.com, Accessed: 2017-01-14. *@ONLINE*. 2016.
Cited on pages 8, 13, 66, 182.

[Hag15] Hossein Haghighat. **Loading margin calculation with line switching: A decomposition method**. *International Journal of Electrical Power & Energy Systems* 64:Supplement C, pages 104–111, 2015. ISSN: 0142-0615. DOI: 10.1016/j.ijepes.2014.07.019.
Cited on page 5.

[Ham07] Donald J. Hammerstrom. **AC Versus DC Distribution Systems – Did We Get it Right?** In *IEEE Power Engineering Society General Meeting*, pages 1–5. IEEE, 2007. ISBN: 1-4244-1296-X. DOI: 10.1109/PES.2007.386130.
Cited on pages 54, 146.

[HB08] Paul Hines and Seth Blumsack. **A Centrality Measure for Electrical Networks**. In *Proceedings of the 41st Annual Hawaii International Conference on System Sciences*. HICSS, pages 185–185, 2008. DOI: 10.1109/HICSS.2008.5.
Cited on pages 19, 130.

[HCB11] Pascal Van Hentenryck, Carleton Coffrin, and Russell Bent. **Vehicle routing for the last mile of power system restoration**. In *Proceedings of the 17th Power Systems Computation Conference*. PSCC, 2011.
Cited on page 109.

[Hed+08] Kory W. Hedman, Richard P. O'Neill, Emily B. Fisher, and Shmuel S. Oren. **Optimal Transmission Switching: Sensitivity Analysis and Extensions**. *IEEE Transactions on Power Systems* 23:3, pages 1469–1479, 2008. ISSN: 0885-8950. DOI: 10.1109/TPWRS.2008.926411.
Cited on page 18.

[Hed+09] Kory W. Hedman, Richard P. O'Neill, Emily B. Fisher, and Shmuel S. Oren. **Optimal Transmission Switching With Contingency Analysis**. *IEEE Transactions on Power Systems* 24:3, pages 1577–1586, 2009. ISSN: 0885-8950. DOI: 10.1109/TPWRS.2009.2020530.
Cited on page 18.

[Hed+10] Kory W. Hedman, Michael C. Ferris, Richard P. O'Neill, Emily B. Fisher, and Shmuel S. Oren. **Co-Optimization of Generation Unit Commitment and Transmission Switching With $N-1$ Reliability**. *IEEE Transactions on Power Systems* 25:2, pages 1052–1063, 2010. ISSN: 0885-8950. DOI: 10.1109/TPWRS.2009.2037232.
Cited on page 107.

[Hed+11] Kory W. Hedman, Richard P. O'Neill, Emily B. Fisher, and Shmuel S. Oren. **Smart Flexible Just-in-Time Transmission and Flowgate Bidding**. *IEEE Transactions on Power Systems* 26:1, pages 93–102, 2011. ISSN: 0885-8950. DOI: 10.1109/TPWRS.2010.2047660.
Cited on page 18.

[Her+12] Alain Hertz, Odile Marcotte, Asma Mdimagh, Michel Carreau, and Franccois Welt. **Optimizing the design of a wind farm collection network**. *INFOR: Information Systems and Operational Research* 50:2, pages 95–104, 2012. DOI: 10.3138/infor.50.2.095.
Cited on page 22.

[HG91] Maurice Huneault and Francisco D. Galiana. **A survey of the optimal power flow literature**. *IEEE Transactions on Power Systems* 6:2, pages 762–770, 1991. ISSN: 08858950. DOI: 10.1109/59.76723.
Cited on page 13.

[HHK13] Reza Hemmati, Rahmat-Allah Hooshmand, and Amin Khodabakhshian. **State-of-the-art of transmission expansion planning: Comprehensive review**. *Renewable and Sustainable Energy Reviews* 23, pages 312–319, 2013. ISSN: 1364-0321. DOI: 10.1016/j.rser.2013.03.015.
Cited on pages 2, 109.

[Hin93] Narain G. Hingorani. **Flexible AC transmission**. *IEEE Spectrum* 30:4, pages 40–45, 1993. ISSN: 0018-9235. DOI: 10.1109/6.206621.
Cited on page 140.

[HK71] Michael Held and Richard M. Karp. **The traveling-salesman problem and minimum spanning trees: Part II**. *Mathematical Programming* 1:1, pages 6–25, 1971. ISSN: 1436-4646. DOI: 10.1007/BF01584070.
Cited on page 22.

[Hoc08] Dorit S. Hochbaum. **The Pseudoflow Algorithm: A New Algorithm for the Maximum-Flow Problem**. *Operations Research* 56:4, pages 992–1009, 2008. DOI: 10.1287/opre.1080.0524.
Cited on page 133.

[Hof19] Remco van der Hofstad. **Random Graphs and Complex Networks**. https://www.win.tue.nl/~rhofstad/NotesRGCN.pdf, Accessed: 2019-09-13. *@ONLINE*. 2019.
Cited on page 18.

[HOO10] Kory W. Hedman, Shmuel S. Oren, and Richard P. O'Neill. **Optimal transmission switching: When economic efficiency and financial transmission rights markets collide**. In *Proceedings of the 6th Conference on Economics of Energy Markets Conference*, 2010.
Cited on page 104.

[HOO11a] Kory W. Hedman, Shmuel S. Oren, and Richard P. O'Neill. **A review of transmission switching and network topology optimization**. In *IEEE Power and Energy Society General Meeting*. PESGM, pages 1–7, 2011. DOI: 10.1109/PES.2011.6039857.
Cited on pages 4, 18, 104.

[HOO11b] Kory W. Hedman, Shmuel S. Oren, and Richard P. O'Neill. **Optimal transmission switching: Economic efficiency and market implications**. *Journal of Regulatory Economics* 40:2, page 111, 2011. ISSN: 1573-0468. DOI: 10.1007/s11149-011-9158-z.
Cited on page 104.

[HT74] John Hopcroft and Robert Tarjan. **Efficient Planarity Testing**. *Journal of the ACM* 21:4, pages 549–568, 1974. ISSN: 0004-5411. DOI: 10.1145/321850.321852.
Cited on page 96.

[IS04] Lucio Ippolito and Pierluigi Siano. **Selection of optimal number and location of thyristor-controlled phase shifters using genetic based algorithms**. *IEE Proceedings – Generation, Transmission and Distribution* 151:5, pages 630–637, 2004. DOI: 10.1049/ip-gtd:20040800.
Cited on page 21.

[IWR16] Internationales Wirtschaftsforum Regenerative Energien (IWR) / IWR.de GmbH. **Offshore-windparks europa**. http://www.offshore-windindustrie.de/windparks/europa, Accessed: 2016-10-25. *@ONLINE*. 2016.
Cited on pages 171, 172.

[Jas19] Markus Jaschinsky. **Netzfrequenz (engl. grid frequency)**. https://www.netzfrequenz.info/aktuelle-netzfrequenz-full, Accessed: 2019-05-12. *@ONLINE*. 2019.
Cited on pages 31, 32.

[Jor+11a] Gwenaël Joret, Christophe Paul, Ignasi Sau, Saket Saurabh, and Stéphan Thomassé. **Hitting and Harvesting Pumpkins**. In *Algorithms – ESA 2011*. Ed. by Camil Demetrescu and Magnús M. Halldórsson, pages 394–407. Berlin, Heidelberg: Springer Berlin Heidelberg, 2011. ISBN: 978-3-642-23719-5. DOI: 10.1007/978-3-642-23719-5_34.
Cited on pages 144, 246.

[Jor+11b] Gwenaël Joret, Christophe Paul, Ignasi Sau, Saket Saurabh, and Stéphan Thomassé. **Hitting and Harvesting Pumpkins**. *CoRR* abs/1105.2704, 2011. arXiv: 1105.2704. URL: http://arxiv.org/abs/1105.2704.
Cited on pages 144, 246.

[Jos+16] Cédric Josz, Stéphane Fliscounakis, Jean Maeght, and Patrick Panciatici. **AC power flow data in MATPOWER and QCQP format: iTesla, RTE snapshots, and PEGASE**. *CoRR* abs/1603.01533, 2016. arXiv: 1603.01533. URL: http://arxiv.org/abs/1603.01533.
Cited on pages 6, 134.

[Jün+10] Michael Jünger, Thomas M. Liebling, Denis Naddef, George L. Nemhauser, William R. Pulleyblank, Gerhard Reinelt, Giovanni Rinaldi, and Laurence A. Wolsey (editors). **50 Years of Integer Programming 1958-2008 – From the Early Years to the State-of-the-Art**. Springer, 2010. ISBN: 978-3-54068274-5. DOI: 10.1007/978-3-540-68279-0.
Cited on page 19.

[Jus14] Bundesministerium der Justiz und für Verbraucherschutz. **Gesetz für den Ausbau erneuerbarer Energien (Erneuerbare-Energien-Gesetz – EEG 2014) § 1 Zweck und Ziel des Gesetzes (engl. Act for the expansion of the renewable energy (German renewable energy sources act – EEG 2014) § 1 aim and goal of the act)**. http://www.gesetze-im-internet.de/eeg_2014/__1.html, Accessed: 2016-10-24. *@ONLINE*. 2014.
Cited on pages 1, 3, 171.

[Jus16] Bundesministerium der Justiz und für Verbraucherschutz. **Gesetz für den Ausbau erneuerbarer Energien (Erneuerbare-Energien-Gesetz – EEG 2017)**. http://www.gesetze-im-internet.de/eeg_2014/__1.html, Accessed: 2016-11-03. *@ONLINE*. 2016.
Cited on page 171.

[JWV15] Masood Jabarnejad, Jianhui Wang, and Jorge Valenzuela. **A Decomposition Approach for Solving Seasonal Transmission Switching**. *IEEE Transactions on Power Systems* 30:3, pages 1203–1211, 2015. ISSN: 0885-8950. DOI: 10.1109/TPWRS.2014.2343944.
Cited on page 18.

[Kal59] R. E. Kalman. **On the general theory of control systems**. *IRE Transactions on Automatic Control* 4:3, pages 110–110, 1959. ISSN: 0096-199X. DOI: 10.1109/TAC.1959.1104873.
Cited on page 68.

[Kan+02] Tapas Kanungo, David M. Mount, Nathan S. Netanyahu, Christine D. Piatko, Ruth Silverman, and Angela Y. Wu. **An efficient k-means clustering algorithm: Analysis and implementation**. *IEEE Transactions on Pattern Analysis and Machine Intelligence* 24:7, pages 881–892, 2002. ISSN: 0162-8828. DOI: 10.1109/TPAMI.2002.1017616.
Cited on page 22.

[Kav+09] Telikepalli Kavitha, Christian Liebchen, Kurt Mehlhorn, Dimitrios Michail, Romeo Rizzi, Torsten Ueckerdt, and Katharina A. Zweig. **Survey: Cycle Bases in Graphs Characterization, Algorithms, Complexity, and Applications**. *Comput. Sci. Rev.* 3:4, pages 199–243, 2009. ISSN: 1574-0137. DOI: 10.1016/j.cosrev.2009.08.001.
Cited on page 63.

[Kel+03] Hans Kellerer, Renata Mansini, Ulrich Pferschy, and Maria G. Speranza. **An efficient fully polynomial approximation scheme for the Subset-Sum Problem**. *Journal of Computer and System Sciences* 66:2, pages 349–370, 2003. ISSN: 0022-0000. DOI: 10.1016/S0022-0000(03)00006-0.
Cited on page 132.

[Ken99] Arthur E. Kennelly. **The Equivalence of Triangles and Three-Pointed Stars in Conducting Networks**. *Electrical World and Engineer* 34:12, pages 413–414, 1899.
Cited on page 79.

[KGD13] Mojtaba Khanabadi, Hassan Ghasemi, and Meysam Doostizadeh. **Optimal Transmission Switching Considering Voltage Security and $N-1$ Contingency Analysis**. *IEEE Transactions on Power Systems* 28:1, pages 542–550, 2013. ISSN: 0885-8950. DOI: 10.1109/TPWRS.2012.2207464.
Cited on page 5.

[KGV83] Scott Kirkpatrick, C. Daniel Gelatt, and Mario P. Vecchi. **Optimization by simulated annealing**. *Science* 220:4598, pages 671–680, 1983. ISSN: 1095-9203. DOI: 10.1126/science.220.4598.671.
Cited on page 178.

[Kir47] Gustav Robert Kirchhoff. **Über die Auflösung der Gleichungen, auf welche man bei der Untersuchung der linearen Vertheilung galvanischer Ströme geführt wird**. *Annalen der Physik* 148:12, pages 497–508, 1847. DOI: 10.1002/andp.18471481202.
Cited on pages 12, 18, 57, 59, 63.

[Kle67] Morton Klein. **A Primal Method for Minimal Cost Flows with Applications to the Assignment and Transportation Problems**. *Management Science* 14:3, pages 205–220, 1967. DOI: 10.1287/mnsc.14.3.205.
Cited on pages 12, 31.

[KM80] Hans-Jürgen Koglin and Hermann Müller. **Overload reduction through corrective switching actions**. In *International Conference on Power System Monitoring and Control*. Volume 24 of, pages 159–164, 1980.
Cited on page 18.

[KMR97] David R. Karger, Rajeev Motwani, and Gurumurthy D. S. Ramkumar. **On approximating the longest path in a graph**. *Algorithmica* 18:1, pages 82–98, 1997. ISSN: 1432-0541. DOI: 10.1007/BF02523689.
Cited on pages 107, 113.

[Koc+16] Burak Kocuk, Hyemin Jeon, Santanu S. Dey, Jeff Linderoth, James Luedtke, and Xu Andy Sun. **A Cycle-Based Formulation and Valid Inequalities for DC Power Transmission Problems with Switching**. *Operations Research* 64:4, pages 922–938, 2016. DOI: 10.1287/opre.2015.1471.
Cited on pages 6, 110, 113.

[KSK10] Amin Khodaei, Mohammad Shahidehpour, and Saeed Kamalinia. **Transmission Switching in Expansion Planning**. *IEEE Transactions on Power Systems* 25:3, pages 1722–1733, 2010. ISSN: 0885-8950. DOI: 10.1109/TPWRS.2009.2039946.
Cited on page 18.

[KV00] Bernhard Korte and Jens Vygen. **Combinatorial Optimization: Theory and Algorithms**. 1th. Springer Publishing Company, Incorporated, 2000. ISBN: 3-540-67226-5.
Cited on page 75.

[LB10] Fangxing Li and Rui Bo. **Small test systems for power system economic studies**. In *IEEE Power and Energy Society General Meeting*. PESGM, pages 1–4, 2010. DOI: 10.1109/PES.2010.5589973.
Cited on pages 6, 134.

[Leh+17] Sebastian Lehmann, Ignaz Rutter, Dorothea Wagner, and Franziska Wegner. **A Simulated-Annealing-Based Approach for Wind Farm Cabling**. In *Proceedings of the Eighth International Conference on Future Energy Systems*. e-Energy '17, pages 203–215. Shatin, Hong Kong: ACM, 2017. ISBN: 978-1-4503-5036-5. DOI: 10.1145/3077839.3077843.
Cited on pages 7, 9, 171, 275.

[Leh16] Sebastian Lehmann. **Simulated Annealing-Based Heuristics for Wind Farm Cabling Problems**. Master's thesis. Karlsruhe Institute of Technology, Germany, 2016.
Cited on page 180.

[Leh63] Alfred Lehman. **Wye-Delta Transformation in Probabilistic Networks**. *Journal of the Society for Industrial and Applied Mathematics* 11:3, pages 773–805, 1963. ISSN: 03684245.
Cited on pages 14, 15, 16.

[Lei+15a] Thomas Leibfried, Tamara Mchedlidze, Nico Meyer-Hübner, Martin Nöllenburg, Ignaz Rutter, Peter Sanders, Dorothea Wagner, and Franziska Wegner. **Operating Power Grids with Few Flow Control Buses**. In *Proceedings of the ACM Sixth International Conference on Future Energy Systems*. e-Energy, pages 289–294. ACM, 2015. ISBN: 978-1-4503-3609-3. DOI: 10.1145/2768510.2768521.
Cited on pages 7, 8, 76, 86, 103, 120, 139.

[Lei+15b] Thomas Leibfried, Tamara Mchedlidze, Nico Meyer-Hübner, Martin Nöllenburg, Ignaz Rutter, Peter Sanders, Dorothea Wagner, and Franziska Wegner. **Operating Power Grids with Few Flow Control Buses**. *CoRR* abs/1505.05747, 2015. arXiv: 1505.05747. URL: http://arxiv.org/abs/1505.05747.
Cited on pages 7, 8, 139.

[Les+11] Bernard C. Lesieutre, Daniel K. Molzahn, Alex R. Borden, and Christopher L. DeMarco. **Examining the limits of the application of semidefinite programming to power flow problems**. In *49th Annual Allerton Conference on Communication, Control, and Computing (Allerton)*, pages 1492–1499, 2011. DOI: 10.1109/Allerton.2011.6120344.
Cited on pages 6, 134.

[LGH14] Karsten Lehmann, Alban Grastien, and Pascal Van Hentenryck. **The Complexity of DC-Switching Problems**. *CoRR* abs/1411.4369, 2014. arXiv: 1411.4369. URL: http://arxiv.org/abs/1411.4369.
Cited on pages 5, 18, 110, 113, 118, 119, 132, 275.

[LGH15] Karsten Lehmann, Alban Grastien, and Pascal Van Hentenryck. **The Complexity of Switching and FACTS Maximum-Potential-Flow Problems**. *CoRR* abs/1507.04820, 2015. arXiv: 1507.04820. URL: http://arxiv.org/abs/1507.04820.
Cited on pages 18, 76, 86, 108, 118, 120, 154, 155, 156.

[LGH16] Karsten Lehmann, Alban Grastien, and Pascal Van Hentenryck. **AC-Feasibility on Tree Networks is NP-Hard**. *IEEE Transactions on Power Systems* 31:1, pages 798–801, 2016. ISSN: 0885-8950. DOI: 10.1109/TPWRS.2015.2407363.
Cited on pages 6, 25, 33, 45, 49, 104.

[LHF08] Dong D. Li, Chao He, and Yang Fu. **Optimization of internal electric connection system of large offshore wind farm with hybrid genetic and immune algorithm**. In *Third International Conference on Electric Utility Deregulation and Restructuring and Power Technologies*. DRPT, pages 2476–2481, 2008. ISBN: 978-7-900714-13-8. DOI: 10.1109/DRPT.2008.4523827.
Cited on pages 171, 172.

[Li+13] W. Q. Li, W. M. Guo, G. J. Liu, M. Yang, X. S. Han, and X. K. Zhang. **A bilevel approach to transmission switching**. In *IEEE International Conference of IEEE Region 10 (TENCON)*. TENCON, pages 1–4, 2013. DOI: 10.1109/TENCON.2013.6718479.
Cited on pages 4, 19, 103.

[Lin11] R. Lincoln. **PYPOWER 4.0.0**. https://pypi.python.org/pypi/PYPOWER/4.0.0, accessed 2015-01-01. *@ONLINE*. 2011.
Cited on pages 47, 159.

[LL12] Javad Lavaei and Steven H. Low. **Zero Duality Gap in Optimal Power Flow Problem**. *IEEE Transactions on Power Systems* 27:1, pages 92–107, 2012. ISSN: 0885-8950. DOI: 10.1109/TPWRS.2011.2160974.
Cited on page 45.

[LO73] Marinus C. van Lier and Ralph H. J. M. Otten. **Planarization by Transformation**. *IEEE Transactions on Circuit Theory* 20:2, pages 169–171, 1973. ISSN: 0018-9324. DOI: 10.1109/TCT.1973.1083633.
Cited on page 14.

[Ltd16a] 4C Offshore Ltd. **BARD 1 substation**. http://www.4coffshore.com/windfarms/substation-bard-1-substation--sid101.html, Accessed: 2016-11-04. *@ONLINE*. 2016.
Cited on page 172.

[Ltd16b] 4C Offshore Ltd. **BARD offshore 1 offshore wind farm**. http://www.4coffshore.com/windfarms/bard-offshore-1-germany-de23.html, Accessed: 2017-04-19. *@ONLINE*. 2016.
Cited on page 172.

[Ltd16c] 4C Offshore Ltd. **Global offshore wind farms database**. http://www.4coffshore.com/offshorewind/, Accessed: 2016-10-24. *@ONLINE*. 2016.
Cited on pages 171, 172, 177.

[Ltd16d] 4C Offshore Ltd. **Global tech I offshore wind farm**. http://www.4coffshore.com/windfarms/global-tech-i-germany-de09.html, Accessed: 2017-04-19. *@ONLINE*. 2016.
Cited on page 172.

[Ltd16e] 4C Offshore Ltd. **Trianel windpark Borkum I offshore wind farm**. http://www.4coffshore.com/windfarms/trianel-windpark-borkum-i-germany-de27.html, Accessed: 2017-04-19. *@ONLINE*. 2016.
Cited on page 172.

[Ltd16f] DONG Energy Hornsea Project One (UK) Ltd. **Hornsea project one**. https://assets.dongenergy.com/DONGEnergyDocuments/horns/Hornsea%20Project%20One%20project%20summary.pdf, Accessed: 2016-10-24. *@ONLINE*. 2016.
Cited on page 171.

[Ltd16g] DONG Energy Hornsea Project One (UK) Ltd. **Hornsea project three**. http://www.dongenergy.co.uk/uk-business-activities/wind-power/offshore-wind-farms-in-the-uk/hornsea-project-three-development, Accessed: 2016-10-24. *@ONLINE*. 2016.
Cited on page 171.

[Lun06] Stefan Lundberg. **Evaluation of wind farm layouts**. *European Power Electronics and Drives Journal* 16:1, pages 14–21, 2006. DOI: 10.1080/09398368.2006.11463608.
Cited on page 171.

[LWO12] Cong Liu, Jianhui Wang, and James Ostrowski. **Heuristic Prescreening Switchable Branches in Optimal Transmission Switching**. *IEEE Transactions on Power Systems* 27:4, pages 2289–2290, 2012. ISSN: 0885-8950. DOI: 10.1109/TPWRS.2012.2193489.
Cited on page 19.

[LYX09] Huang Lingling, Fu Yang, and Guo Xiaoming. **Optimization of electrical connection scheme for large offshore wind farm with genetic algorithm**. In *International Conference on Sustainable Power Generation and Supply*, pages 1–4, 2009. DOI: 10.1109/SUPERGEN.2009.5348118.
Cited on page 22.

[Mäk+14] Olli Mäkelä, Joseph Warrington, Manfred Morari, and Göran Andersson. **Optimal transmission line switching for large-scale power systems using the Alternating Direction Method of Multipliers**. In *Proceedings of the 18th Power Systems Computation Conference*. PSCC, pages 1–6, 2014. DOI: 10.1109/PSCC.2014.7038447.
Cited on page 19.

[Mar67] James Martin. **Design of real-time computer systems**. Prentice-Hall, 1967.
Cited on page 22.

[Mar84] Ernesto Q. V. Martins. **On a multicriteria shortest path problem**. *European Journal of Operational Research* 16:2, pages 236–245, 1984. ISSN: 0377-2217. DOI: 10.1016/0377-2217(84)90077-8.
Cited on pages 122, 123.

[Mat13] The University Of Edinburgh – School of Mathematics. **Power System Test Case Archive**. http://www.maths.ed.ac.uk/optenergy/NetworkData/, Verion: March 31, 2013, Accessed: 2018-01-11. *@ONLINE*. 2013.
Cited on pages 6, 134.

[Max65] James Clerk Maxwell. **VIII. A dynamical theory of the electromagnetic field**. *Philosophical Transactions of the Royal Society of London* 155, pages 459–512, 1865. DOI: 10.1098/rstl.1865.0008.
Cited on page 12.

[Mch+15] Tamara Mchedlidze, Martin Nöllenburg, Ignaz Rutter, Dorothea Wagner, and Franziska Wegner. **Towards Realistic Flow Control in Power Grid Operation**. In *Energy Informatics*. Ed. by Sebastian Gottwalt, Lukas König, and Hartmut Schmeck, pages 192–199. Cham: Springer International Publishing, 2015. ISBN: 978-3-319-25876-8.
Cited on pages 7, 8, 139.

[MEA99] J.A. Momoh, M.E. El-Hawary, and R. Adapa. **A review of selected optimal power flow literature to 1993. II. Newton, linear programming and interior point methods**. *IEEE Transactions on Power Systems* 14:1, pages 105–111, 1999. ISSN: 0885-8950. DOI: 10.1109/59.744495.
Cited on page 20.

[Mel+03] Flavio Guilherme de Melo Lima, Francisco D. Galiana, Ivana Kockar, and Jorge Munoz. **Phase shifter placement in large-scale systems via mixed integer linear programming**. *IEEE Transactions on Power Systems* 18:3, pages 1029–1034, 2003. DOI: 10.1109/TPWRS.2003.814858.
Cited on pages 20, 165.

[Met+53] Nicholas Metropolis, Arianna W. Rosenbluth, Marshall N. Rosenbluth, Augusta H. Teller, and Edward Teller. **Equation of state calculations by fast computing machines**. *The Journal of Chemical Physics* 21:6, pages 1087–1092, 1953. DOI: 10.1063/1.1699114.
Cited on page 178.

[MH19] Daniel K. Molzahn and Ian A. Hiskens. **A Survey of Relaxations and Approximations of the Power Flow Equations**. Volume 4 of. 2019, pages 1–221. ISBN: 978-1-68083540-3. DOI: 10.1561/3100000012.
Cited on page 13.

[MTB89] Elham B. Makram, Katherine P. Thorton, and Homer E. Brown. **Selection of lines to be switched to eliminate overloaded lines using a Z-matrix method**. *IEEE Transactions on Power Systems* 4:2, pages 653–661, 1989. ISSN: 0885-8950. DOI: 10.1109/59.193839.
Cited on page 18.

[MWH86] Abdulhalem A. Mazi, Bruce F. Wollenberg, and Morten H. Hesse. **Corrective Control of Power System Flows by Line and Bus-Bar Switching**. *IEEE Transactions on Power Systems* 1:3, pages 258–264, 1986. ISSN: 0885-8950. DOI: 10.1109/TPWRS.1986.4334990.
Cited on pages 18, 19.

[Nag10] Anna Nagurney. **The Negation of the Braess Paradox as Demand Increases: The Wisdom of Crowds in Transportation Networks**. *EPL (Europhysics Letters)*, 2010. ISSN: 0295-5075. DOI: 10.1209/0295-5075/91/48002.
Cited on page 119.

[Nor+97] Mojtaba Noroozian, Lennart Ängquist, Mehrdad Ghandhari, and Göran Andersson. **Use of UPFC for optimal power flow control**. *IEEE Transactions on Power Delivery* 12:4, pages 1629–1634, 1997. ISSN: 0885-8977. DOI: 10.1109/61.634183.
Cited on page 140.

[Nov+12] Alexander Novitskiy, Dorothee Arlt, Jens Wolling, and Dirk Westermann. **Freileitungen oder Erdkabelleitungen? – Eine Metastudie über die Kriterien und Ergebnisse von Untersuchungen zum Netzausbau**. Universitätsverlag Ilmenau, 2012, page 150. ISBN: 978-3-86360-029-7.
Cited on page 48.

[OCS04] Thomas J. Overbye, Xu Cheng, and Yan Sun. **A comparison of the AC and DC power flow models for LMP calculations**. In *Proceedings of the 37th Annual Hawaii International Conference on System Sciences*. HICSS, pages 1–9. IEEE, 2004. ISBN: 0-7695-2056-1. DOI: 10.1109/HICSS.2004.1265164.
Cited on page 146.

[OJ05] Weerakorn Ongsakul and Peerapol Jirapong. **Optimal Allocation of FACTS Devices to Enhance Total Transfer Capability using Evolutionary Programming**. In *IEEE International Symposium on Circuits and Systems*. Volume 5 of ISCAS, pages 4175–4178, 2005. DOI: 10.1109/ISCAS.2005.1465551.
Cited on page 20.

[Oka55] S. Okada. **Topologic and Algebraic Foundations of Network Synthesis**. *Proceedings of Symposim on Modern Network Synthesis* 5, pages 283–322, 1955.
Cited on page 63.

[OL96] Ibrahim H. Osman and Gilbert Laporte. **Metaheuristics: A bibliography**. *Annals of Operations Research* 63:5, pages 511–623, 1996. ISSN: 1572-9338. DOI: 10.1007/BF02125421.
Cited on pages 22, 173.

[ONe+05] Richard P. O'Neill, Ross Baldick, Udi Helman, Michael H. Rothkopf, and William Stewart. **Dispatchable transmission in RTO markets**. *IEEE Transactions on Power Systems* 20:1, pages 171–179, 2005. ISSN: 0885-8950. DOI: 10.1109/TPWRS.2004.841168.
Cited on page 18.

[ONe+10] Richard P. O'Neill, Kory W. Hedman, Eric A. Krall, Anthony Papavasiliou, and Shmuel S. Oren. **Economic analysis of the $N-1$ reliable unit commitment and transmission switching problem using duality concepts**. *Energy Systems* 1:2, pages 165–195, 2010. ISSN: 1868-3975. DOI: 10.1007/s12667-009-0005-6.
Cited on page 18.

[OPT93] James B. Orlin, Serge A. Plotkin, and Éva Tardos. **Polynomial dual network simplex algorithms**. *Mathematical Programming* 60:1, pages 255–276, 1993. ISSN: 1436-4646. DOI: 10.1007/BF01580615.
Cited on page 31.

[Orl97] James B. Orlin. **A polynomial time primal network simplex algorithm for minimum cost flows**. *Mathematical Programming* 78:2, pages 109–129, 1997. ISSN: 1436-4646. DOI: 10.1007/BF02614365.
Cited on pages 12, 31.

[OWL12] James Ostrowski, Jianhui Wang, and Cong Liu. **Exploiting Symmetry in Transmission Lines for Transmission Switching**. *IEEE Transactions on Power Systems* 27:3, pages 1708–1709, 2012. ISSN: 0885-8950. DOI: 10.1109/TPWRS.2012.2187121.
Cited on page 19.

[OWL14] James Ostrowski, Jianhui Wang, and Cong Liu. **Transmission Switching With Connectivity-Ensuring Constraints**. *IEEE Transactions on Power Systems* 29:6, pages 2621–2627, 2014. ISSN: 0885-8950. DOI: 10.1109/TPWRS.2014.2315434.
Cited on page 19.

[Pal+12] Marco G. Pala, Samuel Baltazar, Peng Liu, Hermann Sellier, Benoît Hackens, Frederico R. Martins, Vincent Bayot, Xavier Wallart, Ludovic Desplanque, and Serge Huant. **Transport Inefficiency in Branched-Out Mesoscopic Networks: An Analog of the Braess Paradox**. *Physical Review Letters* 108, page 076802, 2012. DOI: 10.1103/PhysRevLett.108.076802.
Cited on pages 17, 119.

[PB83] J. Scott Provan and Michael O. Ball. **The Complexity of Counting Cuts and of Computing the Probability that a Graph is Connected**. *SIAM Journal on Computing* 12:4, pages 777–788, 1983. DOI: 10.1137/0212053.
Cited on page 15.

[Pes+68] John Peschon, Dean S. Piercy, William F. Tinney, Odd J. Tveit, and Michael Cuenod. **Optimum Control of Reactive Power Flow**. *IEEE Transactions on Power Apparatus and Systems* PAS-87:1, pages 40–48, 1968. ISSN: 0018-9510. DOI: 10.1109/TPAS.1968.292254.
Cited on page 13.

[PH12] Tanvi Potluri and Kory W. Hedman. **Impacts of topology control on the ACOPF**. In *IEEE Power and Energy Society General Meeting*. PESGM, pages 1–7, 2012. DOI: 10.1109/PESGM.2012.6345676.
Cited on page 103.

[Pie+73] H. E. Pierce, Harry W. Colborn, D. W. Coleman, E. A. Marriage, J. C. Richard, L. J. Rindt, L. J. Rubino, G. W. Stagg, T. P. Traub, J. Vandergrift, C. E. Winn, and C. C. Young. **Common Format For Exchange of Solved Load Flow Data**. *IEEE Transactions on Power Apparatus and Systems* PAS-92:6, pages 1916–1925, 1973. ISSN: 0018-9510. DOI: 10.1109/TPAS.1973.293571.
Cited on page 135.

[Pin+10] Ali Pinar, Juan Meza, Vaibhav Donde, and Bernard Lesieutre. **Optimization Strategies for the Vulnerability Analysis of the Electric Power Grid**. *SIAM Journal on Optimization* 20:4, pages 1786–1810, 2010. DOI: 10.1137/070708275.
Cited on page 52.

[PJH16] Farzaneh Pourahmadi, Mohammad Jooshaki, and Seyed H. Hosseini. **A dynamic programming-based heuristic approach for optimal transmission switching problem with $N-1$ reliability criterion**. In *International Conference on Probabilistic Methods Applied to Power Systems*. PMAPS, pages 1–7, 2016. DOI: 10.1109/PMAPS.2016.7764208.
Cited on page 18.

[Pol83] Themistocles Politof. **A Characterization and Efficient Reliability Computation of Delta-Y Reducible Networks**. AAI8413557. PhD dissertation. University of California, Berkeley, 1983.
Cited on page 15.

[PP03] Claude M. Penchina and Leora J. Penchina. **The Braess paradox in mechanical, traffic, and other networks**. *American Journal of Physics* 71:5, pages 479–482, 2003. DOI: 10.1119/1.1538553.
Cited on page 17.

[PP97] Eric I. Pas and Shari L. Principio. **Braess' paradox: Some new insights**. *Transportation Research Part B: Methodological* 31:3, pages 265–276, 1997. ISSN: 0191-2615. DOI: 10.1016/S0191-2615(96)00024-0.
Cited on pages 17, 18, 19, 106.

[PS86] Themistocles Politof and Appaajosyula Satyanarayana. **Efficient algorithms for reliability analysis of planar networks - a survey**. *IEEE Transactions on Reliability* 35:3, pages 252–259, 1986. ISSN: 0018-9529. DOI: 10.1109/TR.1986.4335427.
Cited on page 16.

[PS90] Themistocles Politof and Appaajosyula Satyanarayana. **A linear-time algorithm to compute the reliability of planar cube-free networks**. *IEEE Transactions on Reliability* 39:5, pages 557–563, 1990.
Cited on page 16.

[PST92] Themistocles Politof, Appaajosyula Satyanarayana, and L. Tung. **An $O(n \cdot \log(n))$ Algorithm to Compute the All-Terminal Reliability of $(K_5, K_{2,2,2})$ Free Networks**. *IEEE Transactions on Reliability* 41:4, pages 512–517, 1992. ISSN: 0018-9529. DOI: 10.1109/24.249577.
Cited on page 16.

[Pur+05] Konrad Purchala, Leonardo Meeus, Daniel Van Dommelen, and Ronnie Belmans. **Usefulness of DC power flow for active power flow analysis**. In *IEEE Power Engineering Society General Meeting*, pages 2457–2462. IEEE, 2005. ISBN: 0-7803-9157-8. DOI: 10.1109/PES.2005.1489581.
Cited on pages 50, 51, 54, 55, 146.

[PV12] Sarah Peters and Mark Vondracek. **Counterintuitive Behavior in Mechanical Networks**. *The Physics Teacher* 50:6, pages 359–362, 2012. DOI: 10.1119/1.4745689.
Cited on page 17.

[Rei83] Kurt Reidemeister. **Knot theory**. BCS Associates Moscow, Idaho, 1983.
Cited on page 14.

[RIM95] Jacqueline G. Rolim, Malcolm R. Irving, and Luiz Jairo B. Machado. **SECTE – An Expert System For Voltage Control, Including Topological Changes**. *IFAC Symposium on Control of Power Plants and Power Systems* 28:26, pages 177–182, 1995. ISSN: 1474-6670. DOI: 10.1016/S1474-6670(17)44753-7.
Cited on page 18.

[RM12] Allan H. Robbins and Wilhelm C. Miller. **Circuit Analysis: Theory and Practice**. Fifth Edition. Cengage Learning, 2012. ISBN: 1-28540192-1.
Cited on page 34.

[RM99] Jacqueline G. Rolim and Luiz J. B. Machado. **A study of the use of corrective switching in transmission systems**. *IEEE Transactions on Power Systems* 14:1, pages 336–341, 1999. ISSN: 0885-8950. DOI: 10.1109/59.744552.
Cited on page 18.

[Roc84] R. Tyrrell Rockafellar. **Network Flows and Monotropic Optimization**. Wiley-Interscience, 1984. ISBN: 1-886529-06-X.
Cited on page 68.

[Roh+12] Martin Rohden, Andreas Sorge, Marc Timme, and Dirk Witthaut. **Self-Organized Synchronization in Decentralized Power Grids**. *Physical Review Letters* 109, page 064101, 2012. DOI: 10.1103/PhysRevLett.109.064101.
Cited on page 35.

[Ros24] A. Rosen. **A new network theorem**. *Journal of the Institution of Electrical Engineers* 62:335, pages 916–918, 1924. DOI: 10.1049/jiee-1.1924.0120.
Cited on pages 77, 81.

[RT86] Pierre Rosenstiehl and Robert E. Tarjan. **Rectilinear planar layouts and bipolar orientations of planar graphs**. *Discrete & Computational Geometry* 1:4, pages 343–353, 1986. ISSN: 1432-0444. DOI: 10.1007/BF02187706.
Cited on pages 89, 96.

[Sah74] Sartaj Sahni. **Computationally Related Problems**. *SIAM Journal on Computing* 3:4, pages 262–279, 1974. DOI: 10.1137/0203021.
Cited on page 111.

[Sch03] Alexander Schrijver. **Combinatorial Optimization: Polyhedra and Efficiency**. Springer, 2003. ISBN: 3-540-44389-4.
Cited on page 73.

[SF14] Milad Soroush and J. David Fuller. **Accuracies of Optimal Transmission Switching Heuristics Based on DCOPF and ACOPF**. *IEEE Transactions on Power Systems* 29:2, pages 924–932, 2014. ISSN: 0885-8950. DOI: 10.1109/TPWRS.2013.2283542.
Cited on page 18.

[SG88] Gilbert Schnyder and Hans Glavitsch. **Integrated security control using an optimal power flow and switching concepts**. *IEEE Transactions on Power Systems* 3:2, pages 782–790, 1988. ISSN: 0885-8950. DOI: 10.1109/59.192935.
Cited on pages 4, 104.

[SG90] Gilbert Schnyder and Hans Glavitsch. **Security enhancement using an optimal switching power flow**. *IEEE Transactions on Power Systems* 5:2, pages 674–681, 1990. ISSN: 0885-8950. DOI: 10.1109/59.54580.
Cited on pages 4, 18, 104.

[SGV03] Nikhlesh K. Sharma, Arindam Ghosh, and Rajiv K. Varma. **A novel placement strategy for FACTS controllers**. *IEEE Transactions on Power Delivery* 18:3, pages 982–987, 2003. DOI: 10.1109/TPWRD.2003.813874.
Cited on page 21.

[Sha87] Louis W. Shapiro. **An Electrical Lemma**. *Mathematics Magazine* 60:1, pages 36–38, 1987. ISSN: 0025570X, 19300980. URL: http://www.jstor.org/stable/2690136.
Cited on pages 11, 13, 57, 66.

[SJ67] Albert M. Sasson and Fernando J. Jaimes. **Digital Methods Applied to Power Flow Studies**. *IEEE Transactions on Power Apparatus and Systems* PAS-86:7, pages 860–867, 1967. ISSN: 0018-9510. DOI: 10.1109/TPAS.1967.291753.
Cited on page 12.

[SJA09] Brian Stott, Jorge Jardim, and Ongun Alsacc. **DC Power Flow Revisited**. *IEEE Transactions on Power Systems* 24:3, pages 1290–1300, 2009. DOI: 10.1109/TPWRS.2009.2021235.
Cited on page 146.

[SR61] Sundaram Seshu and Myril B. Reed. **Linear graphs and electrical networks**. Addison-Wesley Publishing Company, 1961.
Cited on pages 11, 13, 27, 28, 47, 57, 59, 61, 63, 64, 65, 66, 69, 75, 76, 143.

[ST90] Appaajosyula Satyanarayana and L. Tung. **A characterization of partial 3-trees**. *Networks* 20:3, pages 299–322, 1990. DOI: 10.1002/net.3230200304.
Cited on page 15.

[ST93] Appaajosyula Satyanarayana and Ralph Tindell. **Efficient Algorithms for the Evaluation of Planar Network Reliability**. Tech. rep. Stevens Institute of Technology, Hoboken NJ, Department of Electrical Engineering and Computer Science, 1993.
Cited on pages 14, 16, 81.

[Sto74] Brian Stott. **Review of load-flow calculation methods**. *Proceedings of the IEEE* 62:7, pages 916–929, 1974. ISSN: 0018-9219. DOI: 10.1109/PROC.1974.9544.
Cited on page 13.

[Str18] Steven H. Strogatz. **Nonlinear Dynamics and Chaos: With Applications to Physics, Biology, Chemistry, and Engineering**. CRC Press, 2018. ISBN: 9780429961113.
Cited on page 35.

[SV05] Wei Shao and Vijay Vittal. **Corrective Switching Algorithm for Relieving Overloads and Voltage Violations**. *IEEE Transactions on Power Systems* 20:4, pages 1877–1885, 2005. ISSN: 0885-8950. DOI: 10.1109/TPWRS.2005.857931.
Cited on page 18.

[Sve13] Harald G. Svendsen. **Planning tool for clustering and optimised grid connection of offshore wind farms**. *Energy Procedia* 35, pages 297–306, 2013. ISSN: 1876-6102. DOI: 10.1016/j.egypro.2013.07.182.
Cited on page 22.

[SW73] Huntington S. Swanson and Robert E. D. Woolsey. **An "Out-of-Kilter" Network Tutorial**. *SIGMAP Bull.* 13, pages 34–40, 1973. ISSN: 0163-5786. DOI: 10.1145/1216978.1216980.
Cited on page 31.

[SW85] Appaajosyula Satyanarayana and R. Kevin Wood. **A Linear-Time Algorithm for Computing K-Terminal Reliability in Series-Parallel Networks**. *SIAM Journal on Computing* 14:4, pages 818–832, 1985. DOI: 10.1137/0214057.
Cited on pages 16, 81.

[Tar97] Robert E. Tarjan. **Dynamic trees as search trees via euler tours, applied to the network simplex algorithm**. *Mathematical Programming* 78:2, pages 169–177, 1997. ISSN: 1436-4646. DOI: 10.1007/BF02614369.
Cited on page 31.

[TC14a] Marc Timme and Jose Casadiego. **Revealing networks from dynamics: An introduction**. *Journal of Physics A: Mathematical and Theoretical* 47:34, page 343001, 2014. DOI: 10.1088/1751-8113/47/34/343001.
Cited on page 35.

[TC14b] Santiago P. Torres and Carlos A. Castro. **Practical heuristic approach to solve the Optimal Transmission Switching problem for Smart Grids**. In *IEEE PES Transmission Distribution Conference and Exposition - Latin America*. PES T D-LA, pages 1–6, 2014. DOI: 10.1109/TDC-LA.2014.6955256.
Cited on page 19.

[TI12] Chin Yen Tee and Marija D. Ilić. **Optimal investment decisions in transmission expansion**. In *North American Power Symposium*. NAPS, pages 1–6, 2012. ISBN: 978-1-4673-2308-6. DOI: 10.1109/NAPS.2012.6336421.
Cited on page 20.

[Tim18] Marc Timme. **Collective Dynamics of Power Grids –Paradoxes and Challenges for Data Analysis and Modeling**. In *Modern Computational Science – Energy of the Future*. Ed. by Stefan Harfst and Alexander K. Hartmann, pages 231–260. Oldenburg: BIS-Verlag der Carl von Ossietzky Universität Oldenburg, 2018. ISBN: 978-3-81422370-4.
Cited on page 35.

[Tra02] Lorenzo Traldi. **A note on delta-wye-delta reductions of plane graphs**. *Congressus Numerantium* 158, pages 213–220, 2002.
Cited on page 14.

[Tru89] Klaus Truemper. **On the delta-wye reduction for planar graphs**. *Journal of Graph Theory* 13:2, pages 141–148, 1989. DOI: 10.1002/jgt.3190130202.
Cited on pages 14, 82, 83, 84, 85.

[Uch+13] Kei Uchizawa, Takanori Aoki, Takehiro Ito, Akira Suzuki, and Xiao Zhou. **On the Rainbow Connectivity of Graphs: Complexity and FPT Algorithms**. *Algorithmica* 67:2, pages 161–179, 2013. ISSN: 1432-0541. DOI: 10.1007/s00453-012-9689-4.
Cited on page 125.

[Uni14] Department of Electrical Engineering University of Washington. **Power Systems Test Case Archive**. http://www.ee.washington.edu/research/pstca/, accessed 2014-12-2. *@ONLINE*. 2014.
Cited on pages 6, 134, 142, 158.

[Vai89] Pravin M. Vaidya. **Speeding-up linear programming using fast matrix multiplication**. In *30th Annual Symposium on Foundations of Computer Science*, pages 332–337, 1989. DOI: 10.1109/SFCS.1989.63499.
Cited on pages 51, 58.

[Val79] Leslie G. Valiant. **The Complexity of Enumeration and Reliability Problems**. *SIAM Journal on Computing* 8:3, pages 410–421, 1979. DOI: 10.1137/0208032.
Cited on page 15.

[Ver05] Dirk Vertigan. **The Computational Complexity of Tutte Invariants for Planar Graphs**. *SIAM Journal on Computing* 35:3, pages 690–712, 2005. DOI: 10.1137/S0097539704446797.
Cited on page 15.

[Ver10] Abhinav Verma. **Power Grid Security Analysis: An Optimization Approach**. PhD dissertation. Columbia University, 2010. ISBN: 978-1-124-17436-5. URL: http://www.columbia.edu/~dano/theses/verma.pdf.
Cited on pages 25, 53, 68.

[Voß09] Stefan Voß. **Capacitated minimum spanning trees**. In *Encyclopedia of Optimization*. Ed. by Christodoulos A. Floudas and Panos M. Pardalos, pages 347–357. Boston, MA: Springer US, 2009. ISBN: 978-0-38774759-0. DOI: 10.1007/978-0-387-74759-0_62.
Cited on page 22.

[VP12] Jonas C. Villumsen and Andrew B. Philpott. **Investment in electricity networks with transmission switching**. *European Journal of Operational Research* 222:2, pages 377–385, 2012. ISSN: 0377-2217. DOI: 10.1016/j.ejor.2012.05.002.
Cited on page 18.

[VR06] Greg Valiant and Tim Roughgarden. **Braess's Paradox in Large Random Graphs**. In *Proceedings of the 7th ACM Conference on Electronic Commerce*. EC '06, pages 296–305. Ann Arbor, Michigan, USA: ACM, 2006. ISBN: 1-59593-236-4. DOI: 10.1145/1134707.1134740.
Cited on page 18.

[VTL79] Jacobo Valdes, Robert E. Tarjan, and Eugene L. Lawler. **The Recognition of Series Parallel Digraphs**. In *Proceedings of the Eleventh Annual ACM Symposium on Theory of Computing*. STOC, pages 1–12. Atlanta, Georgia, USA: ACM, 1979. DOI: 10.1145/800135.804393.
Cited on page 15.

[Wag15] Donald K. Wagner. **Delta–wye reduction of almost-planar graphs**. *Discrete Applied Mathematics* 180, pages 158–167, 2015. ISSN: 0166-218X. DOI: 10.1016/j.dam.2014.07.014.
Cited on page 16.

[Weg17] Franziska Wegner. **Netzwerkplanung in Windparks – Die Lücke zwischen Aufwand und Nutzen schließen**. Karlsruher Transfer (KT): Ausgabe 53, Oktober 2017. Magazine. 2017.
Cited on page 171.

[Wes00] Douglas B. West. **Introduction to Graph Theory**. 2nd ed. Prentice Hall, 2000. ISBN: 0-13014400-2.
Cited on page 119.

[WH56] J. B. Ward and H. W. Hale. **Digital Computer Solution of Power-Flow Problems [includes discussion]**. *Transactions of the American Institute of Electrical Engineers. Part III: Power Apparatus and Systems* 75:3, pages 398–404, 1956. ISSN: 0097-2460. DOI: 10.1109/AIEEPAS.1956.4499318.
Cited on page 13.

[Whi31] Hassler Whitney. **Non-Separable and Planar Graphs**. *Proceedings of the National Academy of Sciences of the United States of America* 17:2, pages 125–127, 1931. ISSN: 00278424.
Cited on page 75.

[Whi32] Hassler Whitney. **Congruent Graphs and the Connectivity of Graphs**. *American Journal of Mathematics* 54:1, pages 150–168, 1932. ISSN: 00029327, 10806377. DOI: 10.2307/2371086.
Cited on page 27.

[Whi35] Hassler Whitney. **On the abstract properties of linear dependence**. *American Journal of Mathematics* 57:3, pages 509–533, 1935. DOI: 10.2307/2371182.
Cited on pages 63, 75, 76, 85.

[Wit+16] Dirk Witthaut, Martin Rohden, Xiaozhu Zhang, Sarah Hallerberg, and Marc Timme. **Critical Links and Nonlocal Rerouting in Complex Supply Networks**. *Phys. Rev. Lett.* 116, page 138701, 2016. DOI: 10.1103/PhysRevLett.116.138701.
Cited on page 2.

[Wru+96] Joseph N. Wrubel, Paul S. Rapcienski, Kuang-Li Lee, Boris S. Gisin, and George W. Woodzell. **Practical experience with corrective switching algorithm for on-line applications**. *IEEE Transactions on Power Systems* 11:1, pages 415–421, 1996. ISSN: 0885-8950. DOI: 10.1109/59.486127.
Cited on pages 18, 19.

[WT12] Dirk Witthaut and Marc Timme. **Braess's paradox in oscillator networks, desynchronization and power outage**. *New Journal of Physics* 14:8, page 083036, 2012.
Cited on page 17.

[WW96] Allen J. Wood and Bruce F. Wollenberg. **Power Generation, Operation, and Control**. Wiley, 1996. ISBN: 978-0-47158699-9.
Cited on pages 42, 43, 47, 159.

[WWS13] Allen J. Wood, Bruce F. Wollenberg, and Gerald B. Sheblé. **Power Generation, Operation, and Control**. Third. Wiley, 2013. ISBN: 978-1-11873391-2.
Cited on pages 6, 134.

[Xia+16] Ruosong Xiao, Yingmeng Xiang, Lingfeng Wang, and Kaigui Xie. **Bulk power system reliability evaluation considering optimal transmission switching and dynamic line thermal rating**. In *International Conference on Probabilistic Methods Applied to Power Systems*. PMAPS, pages 1–5, 2016. DOI: 10.1109/PMAPS.2016.7764210.
Cited on page 104.

[YGJ08] Hyejin Youn, Michael T. Gastner, and Hawoong Jeong. **Price of Anarchy in Transportation Networks: Efficiency and Optimality Control**. *Phys. Rev. Lett.* 101, page 128701, 2008. DOI: 10.1103/PhysRevLett.101.128701.
Cited on page 17.

[YK12] Masoud Yaghini and Mohammad R. Akhavan Kazemzadeh. **A simulated annealing algorithm for unsplittable capacitated network design**. *International Journal of Industiral Engineering & Producion Research* 23, pages 91–100, 2012. ISSN: 2008-4889.
Cited on pages 22, 177, 178.

[YL08] Won Y. Yang and Seung C. Lee. **Circuit Systems with MATLAB and PSpice**. In, pages 256–261. John Wiley & Sons, 2008. ISBN: 978-0-47082240-1.
Cited on page 34.

[Yu04] Yaming Yu. **Forbidden minors for wye-delta-wye reducibility**. *Journal of Graph Theory* 47:4, pages 317–321, 2004. DOI: 10.1002/jgt.20039.
Cited on page 16.

[Yu06] Yaming Yu. **More Forbidden Minors for Wye-Delta-Wye Reducibility**. *Electronic Journal of Combinatorics* 13:1, 2006. ISSN: 1077-8926. URL: https://www.combinatorics.org/ojs/index.php/eljc/article/download/v13i1r7/pdf.
Cited on page 16.

[YZX14] Zhifang Yang, Haiwang Zhong, and Qing Xia. **Optimal transmission switching based on auxiliary induce function**. In *IEEE Power and Energy Society General Meeting | Conference Exposition*. PESGM, pages 1–5, 2014. DOI: 10.1109/PESGM.2014.6938949.
Cited on page 19.

[ZCB04] Menghua Zhao, Zhe Chen, and Frede Blaabjerg. **Optimization of electrical system for a large DC offshore wind farm by genetic algorithm**. In *Nordic Workshop on Power and Industrial Electronics*, 2004.
Cited on page 22.

[ZCB09] Menghua Zhao, Zhe Chen, and Frede Blaabjerg. **Optimisation of electrical system for offshore wind farms via genetic algorithm**. *IET Renewable Power Generation* 3:2, pages 205–216, 2009. ISSN: 1752-1416. DOI: 10.1049/iet-rpg:20070112.
Cited on page 22.

[ZCH06] Menghua Zhao, Zhe Chen, and Jesper Hjerrild. **Analysis of the behaviour of genetic algorithm applied in optimization of electrical system design for offshore wind farms**. In *IECON - 32nd Annual Conference on IEEE Industrial Electronics*, pages 2335–2340, 2006. DOI: 10.1109/IECON.2006.347333.
Cited on page 22.

[ZM11] Ray D. Zimmerman and Carlos E. Murillo-Sanchez. **MATPOWER User's Manual**. http://www.pserc.cornell.edu/matpower/. 2011.
Cited on pages 43, 47, 50, 158.

[ZMT09] Ray D. Zimmerman, Carlos E. Murillo-Sanchez, and Robert J. Thomas. **MATPOWER's Extensible Optimal Power Flow Architecture**. In *IEEE Power & Energy Society General Meeting*, pages 1–7. IEEE, 2009. ISBN: 978-1-4244-4241-6. DOI: 10.1109/PES.2009.5275967.
Cited on page 159.

[ZMT11] Ray D. Zimmerman, Carlos E. Murillo-Sanchez, and Robert J. Thomas. **MATPOWER: Steady-State Operations, Planning, and Analysis Tools for Power Systems Research and Education**. *IEEE Transactions on Power Systems* 26:1, pages 12–19, 2011. ISSN: 0885-8950. DOI: 10.1109/TPWRS.2010.2051168.
Cited on pages 6, 134, 146, 147, 150, 159.

[ZS17] Shijia Zhao and Chanan Singh. **Studying the Reliability Implications of Line Switching Operations**. *IEEE Transactions on Power Systems* 32:6, pages 4614–4625, 2017. ISSN: 0885-8950. DOI: 10.1109/TPWRS.2017.2679541.
Cited on page 18.

[ZW14] Chi Zhang and Jianhui Wang. **Optimal Transmission Switching Considering Probabilistic Reliability**. *IEEE Transactions on Power Systems* 29:2, pages 974–975, 2014. ISSN: 0885-8950. DOI: 10.1109/TPWRS.2013.2287999. Cited on page 18.

List of Figures

1.1 Change of the power grid hierarchical structure. 2
1.2 The offshore wind farms of the German Bight in the north sea. 3

2.1 Common network reduction rules. 14
2.2 The complexity of wind farm cabling problems. 21

3.1 Simple description of the feasibility problem. 32
3.2 The relationship between voltage and current. 34
3.3 Time varying AC sinusoid curves with different voltage angle differences. 36
3.4 Relationship between conductivity and the material's atomic structure. 38
3.5 The Pi-equivalent circuit model for a transmission line 47
3.6 Difference between the AC and DC model 54

4.1 The image and kernel of the incidence matrix **I**. 61
4.2 Linear maps of the incidence matrix **I**. 62
4.3 The image and kernel of the circuit matrix **B**. 64
4.4 A simple polytope example. 67
4.5 TUM counter example. 68
4.6 The combined incidence and circuit matrix structure. 69
4.7 Combinatorial dual graphs. 74
4.8 The series-parallel-contraction and contraction of superfluous edges. 77
4.9 The delta-wye- and wye-delta-transformations. 80
4.10 A grid graph. 81
4.11 An extended grid graph. 82
4.12 The delta-wye-reducibility of the smallest extended grid graph. . . . 83
4.13 The delta-wye-reducibility of a general extended grid graph. 85
4.14 Different representation for the power flow feasibility problem. . . . 87
4.15 The geometric interpretation of a susceptance scaling. 91
4.16 The property of balancing. 94
4.17 KCL Conflict Resolution. 98

5.1 A simple switching example that compares MF, MPF, and MTSF. . . 105
5.2 The Braess's Paradox highly depends on the network's parameters. . 106
5.3 A network constructed from SSP. 114
5.4 Possible ways to switch in a triangle in a network constructed from SSP 115

5.5 The transformation of an unbounded into a bounded network. 117
5.6 Transformation from an OTSP- to an MTSFP-instance. 118
5.7 An example and counterexample for the DTP calculation. 121
5.8 An example, where the DTP produces exponential many labels. . . . 123
5.9 The directed label graph after an DTP-algorithm execution. 124
5.10 DTP problematic cases. 125
5.11 A description of penrose-minors. 128
5.12 Necessary graph transformation to calculate a polynomial algorithm. 131
5.13 Simulation results for switching. 134

6.1 Geometric interpretation of the susceptance scaling. 141
6.2 Different vertex and edge hitting sets for the IEEE 14 system. 142
6.3 A cutvertex decomposes the network. 143
6.4 Forbidden c-pumpkin minors for different values of c with $c \in \mathbb{N}_{>0}$. . 144
6.5 The influence of susceptance scaling. 151
6.6 Different interpretations for the KVL conflict and resolution. 157
6.7 Trade-off of generator costs c_g and losses c_ℓ 159
6.8 Comparison of the relative number of controller. 160
6.9 Comparison of the size of different c-pumpkin hitting sets. 161
6.10 Operation costs of `case57`. 165
6.11 Minimum number of controllers to reach full control. 166
6.12 Overview of operation costs while placing FACTS. 168

7.1 The description of the wind farm topology. 173
7.2 A circuit cabling example showing different cabling. 174
7.3 An example set of cable types. 177
7.4 The simulated annealing representation used within this work. 180
7.5 Comparison of our SA algorithm with the MILP. 183

C.1 Results of the simulations for the DTP betweenness centrality on `nesta_case3_lmbd` to `nesta_case24_ieee_rts`. 260
C.2 Results of the simulations for the DTP betweenness centrality on cases `nesta_case30_as` to `nesta_case118_ieee`. 261
C.3 Results of the simulations for the DTP betweenness centrality on cases `nesta_case162_ieee` to `nesta_case3012wp_mp`. 262

D.1 Trade-off of generator costs and costs of the losses depending as λ varies from 0 to 1. The square cross marks the solution computed by OPF. 264
D.2 Operation costs of `case6` to `case118` for OPF and the hybrid model with their control buses with respect to the load factor ρ. 265

List of Tables

3.1 Specification of the different power grid vertex types. 42
3.2 Comparison of the different AC models. 46

5.1 Overview of results on the complexity of switching. 110
5.2 Switching Results using the NESTA Benchmark Sets. 136

6.1 Overview of results on the complexity of FACTS placement. 156
6.2 IEEE Benchmark Set Structure. 158
6.3 Comparison of the FCV and FCE Model. 169

7.1 Installed offshore wind farm power 172
7.2 Values of the generated benchmark data set. 178

Glossary

Acronyms and Abbreviations

AC	Alternating Current	10, 11, 33
CMST	Capacitated Minimum Spanning Tree	11
DC	Direct Current	8, 10, 33–35, 37
DCOPF	Direct Current Optimal Power Flow	8
DCOTS	Direct Current Optimal Transmission Switching	8
EDP	Economic Dispatch Problem	3, 8
FACTS	Flexible AC Transmission Systems	1, 8–11, 37
FEAS	Feasibility Problem	2, 33, 34, 37
FVSP	Feedback Vertex Set Problem	38
KCL	Kirchhoff's Current Law	2, 9, 34, 37
KVL	Kirchhoff's Voltage Law	2
MCFP	Minimum Cost Flow Problem	2, 35, 39
MCND	Multicommodity Capacitated Network Design	12
MFF	Maximum FACTS Flow	37
MFP	Maximum Flow Problem	2, 5, 34
MILP	Mixed-integer Linear Program	12
MNSP	Minimum Number of Switches Problem	36
MPF	maximum power flow	35–37
MPFP	Maximum Power Flow Problem	35, 36
MST	Minimum Spanning Tree	11, 12
MTSF	Maximum Transmission Switching Flow	35, 36
MTSFP	Maximum Transmission Switching Flow Problem	35, 36
OPF	Optimal Power Flow	11

OPFP	Optimal Power Flow Problem	2, 3
OTS	Optimal Transmission Switching	9
OTSP	Optimal Transmission Switching Problem	8, 35
SFP	Simultaneous Flow Problem	34
VNLP	Voltage Normalized Lossless Real Power Flow	34
SPP	Shortest Path Problem	5
SSP	Subset Sum Problem	38
s-*t*-RP	Rainbow *s*-*t*-Path	38
TNEP	Transmission Network Expansion Planning	7, 8
VCP	Vertex Cover Problem	38

fFFP — The flexible full farm problem represents the cabling of multiple collector systems with substation locations. In this problem layer the location of the substation is not fix and has to be computed, too. Note that the assignment of turbines is neither fixed to a circuit nor to a substation. The Substation Problem and Circuit Problem are subproblems. See Figure 7.1 for more information.

FFP	The Full Farm Problem represents the cabling of multiple collector systems with fix substation locations. Note that the assignment of turbines is neither fixed to a circuit nor to a substation. The Substation Problem and Circuit Problem are subproblems. See Figure 7.1 for more information.	11, 39
SP	The Substation Problem is a cabling of multiple independent circuits with one preassigned substation. This represents the cable layout of a single collector system of a substation in the wind farm. Note that the turbines are not assigned to a circuit. Thus, the Circuit Problem can be seen as a subproblem if the turbine to substation assignment is computed. See Figure 7.1 for more information.	11

CP	Circuit Problem (CP) is the smallest problem layer in the wind farm layout problem hierarchy. In this problem layer only the cable layout of a circuit—a connected component connected to a substation—is considered, where turbines are either connected to other turbines or to a preassigned substation. See Figure 7.1 for more information.	11, 12
GA	Genetic Algorithm	12, 13
Gurobi Optimizer	Gurobi is a solver that can solve optimization problems formulated as an Linear Programming (LP) or an MILP (MILP).	3
ILP	Integer Linear Programming	8
QT	Quality Threshold is a clustering algorithm.	12
RTS	reliability test system	9
SA	Simulated Annealing	12

Model

ω	The velocity of the angle (here voltage angle θ^v and current angle θ^i) rotation is defined by the angular frequency $\omega := {}^{d\theta}/_{dt}$. Thus, it describes how the phase changes of a sinusoid function. In a time-invariant setting, we have a constant rotation velocity meaning $\omega := {}^{d\theta}/_{dt} = 2 \cdot \pi \mathrm{f}$. In the Argand diagram (see Figure 3.2) the rotation speed of the voltage vector v and current vector i (counter-clock-wise) is meant.	41, 42, 45
s	The complex power function $s \colon V \to \mathbb{C}$ is the sum of the real and reactive power. For time varying models, the function is called instantaneous electric power, which is a function $s \colon V \times \mathbb{R} \to \mathbb{C}$ representing the instantaneous power at vertex $u \in V$ for timestamp $t \in \mathbb{R}$. It is usually denoted by p, but the additional parameter separates the constant term $s(u)$ clearly from the time varying term $s(u, t)$.	41–43, 46
$\overline{s}$	The apparent power maximum $\overline{s}$ is a total thermal line limitation in terms of power.	46
i	The current is a function $i \colon V \to \mathbb{R}$ that represents the electrons that move through an element per second an thus, is measured in Ampere A. The time varying function (in a dynamic network setting) of current is defined by $i \colon V \times \mathbb{R} \to \mathbb{R}$ that represents the instantaneous current $i(u, t)$ at vertex $u \in V$ for timestamp $t \in \mathbb{R}$.	41–44, 46–48
θ^i	The current angle is a function $\theta^i \colon V \to \mathbb{R}$ at a vertex $u \in V$ that represents an initial potential at a vertex u. The current angle θ^i is the initial angle between the current vector and the x-axis in the Argand diagram (see Figure 3.2).	41, 42, 47
$\overline{i}$	The current power maximum $\overline{i}$ is a total thermal line limitation in terms of current i.	48

I_{RMS}		The root-mean-squared (RMS) value of a current magnitude $\lvert i(u)\rvert$ at vertex $u \in V$ is defined by $\lvert i(u)\rvert/\sqrt{2}$. It represents the effective value of a sinusoid current waveform. Note that the RMS value is only used for time varying sinusoid functions and not for DC or AC models, where we assume time invariance and thus, the functions become constant over time.	41
C		The set C is called the set of cycles for a graph G.	38
	c	A *cycle* is a path $\pi(s,t) \in \Pi(s,t)$, where the first and the last vertex are identical meaning $s = t$. A cycle is called *simple* if no vertex is visited twice with the exception of s and t.	38
Δ-Y		The delta-wye transformation transforms a triangle to a star by adding one vertex into the center and adding edges from the center to the already existing vertices.	3–5
E_F		The set of facts buses.	36, 37
V_F		The set of facts buses. A *vertex hitting set* of $G = (V,E)$ with respect to a class of graphs $\mathcal{G}$ is a set of vertices $V_F \subseteq V$ such that $G - V_F \in \mathcal{G}$. We call a subset of vertices ${V_F}^c$ c-pumpkin hitting set if there is a vertex subset ${V_F}^c \subseteq V(G)$ such that $G - {V_F}^c$ consists of no c-pumpkin minor.	38
f		The flow f is a function $f\colon E \to \mathbb{R}$ satisfying the skew-symmetry property.	33–37, 39
	F	The flow value $F(\mathcal{N}, f)$ of a network $\mathcal{N}$ and some flow f is defined by $F(\mathcal{N}, f) \coloneqq \sum_{u \in V_G} f_{\text{net}}(u)$.	34–37
	f_{net}	The net flow $f_{\text{net}}(u)$ at a vertex $u \in V$ is defined by the sum of all incident edges $f_{\text{net}}(u) \coloneqq \sum_{\{u,v\} \in \overrightarrow{E}} f(u,v)$.	35
G		The topological structure of a power grid is a graph $G = (V,E)$, where the set V is the set of vertices and the set E is the set of edges.	6, 33–35, 37–39
	cubic graph	A cubic graph (also known as trivalent graph) is a 3-regular graph, where all vertices have a degree of three.	6

$G^\star$	A dual graph $G^\star$ of a planar graph G with a fixed planar embedding $\mathcal{E}$ is a graph that has for each face of G a vertex and whenever two faces are incident to each other in graph G these two vertices representing the faces are connected by an edge in the dual graph $G^\star$. There is a one-to-one correspondence between the edges of the primal graph G and the edges of the dual graph $G^\star$.	34, 37
E	The set E of edges (in the power grid denoted as branches) represents curves that interconnect to points such as transmission lines or cables.	6, 12, 33–39
$\overleftrightarrow{E}$	The set $\overleftrightarrow{E}$ of undirected edges that is represented by unordered pairs of vertices $\{u, w\} \in \overleftrightarrow{E}(G)$.	35, 36, 38
Y-Δ graph	The Y-Δ graph is a topological structure of the power grid that can be reduced to a vertex by the following reduction rules: degree 1 and self-loop deletion, series and parallel contraction, and Y-Δ transformations.	5, 6
tri-sub-graph	Is a minimal non-trivial 3-attached subgraph.	6
V	The set V of vertices (in the power grid denoted as buses) represent points such as transmission line junctions.	4–6, 33, 38, 48
$\mathcal{N}$	A network $\mathcal{N}$ represents a power grid with electrical parameters such as $\mathcal{N} = (G, V_G, V_D, \text{cap}, b, \underline{p_g}, \overline{p_g}, \underline{p_d}, \overline{p_d})$ for the DC-network. See Chapter 3 for other example networks.	33–37, 39
cap	The capacity is in general a function $\text{cap}\colon \overleftrightarrow{E} \to \mathbb{R}_{\geq 0}$ representing the (thermal line) limits of an edge. For the wind farm cabling problem the capacity is a function $\text{cap}\colon K \to \mathbb{R}_{\geq 0} \cup \{\infty\}$.	33–35, 39
V_D	The set V_D of consumer vertices is a subset of the set V of vertices. It represents the set of sinks.	33–35

y	The admittance is a function $y\colon \overleftrightarrow{E} \to \mathbb{C}$ (Equation 3.9), where $y(u, v)$ (Equation 3.9) is defined by the conductance $g(u, v)$ (Equation 3.11) and the susceptance $b(u, v)$ (Equation 3.12) that define how easy the current is able to flow through an element such as a transmission line $\{u, v\} \in \overleftrightarrow{E}$.	43, 46
g	The conductance g is a function $g\colon \overleftrightarrow{E} \to \mathbb{R}$ defined by $g(u, w) := {r(u,w)}/{(r(u,w)^2 + x(u,w)^2)}$ for all $\{u, w\} \in \overleftrightarrow{E}$. Note that for DC models it is simply the reciprocal of the resistance r. Roughly speaking it represents how easy an electron is able to pass a material.	33, 43–48
x	The reactance is a function $x\colon \overleftrightarrow{E} \to \mathbb{R}_{\geq 0} \cup \{\infty\}$ representing the imaginary part of the impedance. Note that for DC models it is simply the reciprocal of the b. Roughly speaking it represents how easy an electron is able to pass a material.	33
r	The resistance is a function $r\colon \overleftrightarrow{E} \to \mathbb{R}_{\geq 0} \cup \{\infty\}$ representing the real part of the impedance. Note that for DC models it is simply the reciprocal of the g. Roughly speaking it represents how easy an electron is able to pass a material.	33
b	The susceptance is a function $b\colon \overleftrightarrow{E} \to \mathbb{R}_{\geq 0}$ defined by $b(u, w) := {-x(u,w)}/{(r(u,w)^2 + x(u,w)^2)}$ for all $\{u, w\} \in \overleftrightarrow{E}$. Note that for DC models it is simply the reciprocal of the reactance x. Roughly speaking it represents how easy an electron is able to pass a material.	33–37, 43–48
V_G	The set V_G of generator vertices is a subset of the set V of vertices. It represents the set of sources.	33–35
$\overline{q_d}$	The demands' reactive power upper bound at vertex $u \in V_D$.	33
$\underline{q_d}$	The demands' reactive power lower bound at vertex $u \in V_D$.	33
$\overline{q_g}$	The generators' reactive power upper bound at vertex $u \in V_G$.	33
$\underline{q_g}$	The generators' reactive power lower bound at vertex $u \in V_G$.	33
$\overline{q}$	The reactive power maximum $\overline{q}$ is the imaginary part of the thermal line limitation.	46–48
$\underline{q}$	The reactive power minimum $\underline{q}$ is the imaginary part of the thermal line limitation.	47, 48

$\overline{p_d}$	The demands' real power upper bound at vertex $u \in V_D$.	33–35
$\underline{p_d}$	The demands' lower real power bound at vertex $u \in V_D$.	33–35
p_g	The generators' real power output at vertex $u \in V_G$.	33, 39
$\overline{p_g}$	The generators' real power upper bound at vertex $u \in V_G$.	33–35
$\underline{p_g}$	The generators' real power lower bound at vertex $u \in V_G$.	33–35
$\Pi(u, w)$	The set of all paths between two vertices u and w with $u, w \in V$ is denoted by $\Pi(u, w)$.	
$\pi(u, w)$	A path starting at u and ending at w with $u, w \in V$ is denoted by $\pi(u, w)$.	6
q	The reactive power q is also called phantom power and represents the imaginary part of the complex power s.	41–43, 45–48
p	The real power p is also called active power and represents the real part of the complex power s.	41, 42, 45–48
p_d	The demands' real power at vertex $u \in V_D$.	33, 39
$\overline{p}$	The real power maximum $\overline{p}$ is the real part of the thermal line limitation in terms of power.	46–48
$\underline{p}$	The real power minimum $\underline{p}$ is the real part of the thermal line limitation in terms of power.	47, 48
S	Set of switched edges S with $S \subseteq \overleftrightarrow{E}$. Note that for a static analysis with one timestamp the switch is in OFF-state for these edges. Roughly speaking the transmission line is temporary removed from the topology.	35, 36
$z(u, v)$	The function $z\colon \overleftrightarrow{E} \to \{0, 1\}$ is $z(u, v) = 0$ if an edge is switched and $z(u, v) = 1$ otherwise.	36
t	A timestamp represents a point in time.	41, 42, 45

v		The voltage is a function $v\colon V \to \mathbb{R}$ that represents the push of current i and is measured in Volt. Note that we will talk some times of a voltage drop at an element $(u, w) \in E$. Then voltage is a function $v\colon E \to \mathbb{R}$. If we use the vertex based definition, we just neglect the reference point, which is ground 0.	41–48
θ^v		The voltage angle (also called phase angle or theta angle) is a function $\theta^v\colon V \to \mathbb{R}$ at a vertex u that represents a potential at a vertex u. The voltage angle is the angle between the voltage vector and the x-axis in the Argand diagram (see Figure 3.2).	41, 42, 45, 47
	$\overline{\Delta\theta^v}$	The voltage angle difference's upper bound $\overline{\Delta\theta^v}$ restricts the flow.	33, 45–48
	$\underline{\Delta\theta^v}$	The voltage angle difference's lower bound $\underline{\Delta\theta^v}$ restricts the flow.	33, 45–48
$\overline{v}$		The voltage magnitude's $\lvert v(u)\rvert$ upper bound is denoted by $\overline{v}$.	33, 45–48
$\underline{v}$		The voltage magnitude's $\lvert v(u)\rvert$ lower bound is denoted by $\underline{v}$.	33, 45–48
V_{RMS}		The root-mean-squared (RMS) value of a voltage magnitude $\lvert v(u)\rvert$ is defined by $\lvert v(u)\rvert/\sqrt{2}$ at vertex $u \in V$. It represents the effective value of the voltage. Note that the RMS value is only used for time varying sinusoid functions.	41
K		The set of cable types is denoted by K. See cabletype κ for a detailed specification of a cable type and for an example set of cable types see Figure 7.3.	39
	κ	A cabletype is denoted by κ. Each cable type has a thermal limit cap and a cost per unit γ, where the unit can be meter m. See for example Figure 7.3.	39
c		The total cost c is defined by the costs of the transport and export cables and is defined in Equation 7.5.	39
	γ	A cable type is among other things defined by its cost. The cost function is defined by $\gamma\colon K \to \mathbb{R}_{\geq 0}$ and is non-convex.	39

Y-Δ	The wye-delta transformation transforms a star with three edges to a triangle by removing the star's center and its incident edges, and adding edges such that the remaining vertices build a complete graph that is a triangle.	3–5

Units

A	The unit of electrical current is called *Ampere* (in short C). It is one of the seven SI base units and describes how much coulomb of current flows through a point per second ($^{\mathrm{C}}/_{\mathrm{s}}$).
C	The *Coulomb* corresponds to 6.24×10^{18} electrons and was introduced since the amount of one electron is simply to small. It is equal to the unit As and represents a SI derived unit of electric charge.
Hz	One Hz corresponds to one s^{-1}. It is used in terms of frequencies.
J	The unit of energy and thus, work is measured in *Joule*. From an electrical point of view it represents the electrical current density. It is a SI derived unit measuring the (electrical) energy or work that is done $\mathrm{N\,m} = \mathrm{V\,A\,s} = \mathrm{W\,s} = {}^{\mathrm{kg\,m^2}}/_{\mathrm{s^2}}$.
Ω	The unit of electrical impedance z, resistance r, and reactance x is called *Ohm*. It is a derived SI unit from ${}^{\mathrm{V}}/_{\mathrm{A}} = {}^{\mathrm{kg\,m^2}}/_{\mathrm{A^2 s^3}}$.
Ωm	The unit of resistivity ρ is $\Omega\,\mathrm{m}$. It represents the property how well a material resists electric current. It is reciprocal to the electrical conductivity σ and is a derived SI unit from ${}^{\mathrm{kgm^3}}/_{\mathrm{A^2 s^3}}$. Note that another definition is $\rho := r\frac{A}{\ell}$, where A is the area (wired gauge) and ℓ the length of the material.
π	The ratio of a circle's circumference to its diameter.
$2 \cdot \pi$	A full period T that corresponds to a full cycle rotation of a vector in the Argand diagram that corresponds to 2π (see Figure 3.2).
SI	The International System of Units (SI) is a metric system that helps to prevent conversion problems as it specify the seven base units that are ampere A, candela cd, kelvin K, kilogram kg, metre m, mole mol, and seconds s.

S
: The unit of electrical admittance y, conductance g, and susceptance b is Siemens S. It is a derived SI unit from $^{1}/_{\Omega} = {}^{A}/_{V} = {}^{A^2 s^3}/_{kg\,m^2}$. It also shows that Siemens is reciprocal to Ohm.

$^{S}/_{m}$
: The unit of conductivity σ is $^{S}/_{m}$. It represents the property how well a material (conductor) conducts electric current. It is reciprocal to the electrical resistivity ρ and is a derived SI unit from $^{A^2 s^3}/_{kg\,m^3}$.

VA
: The unit of the complex and apparent power is Volt Ampere VA. For more information see Watt W.

VAr
: The unit of the reactive power is Volt Ampere reactive VAr. For more information see Watt W.

V
: The unit of voltage v is called *Volt* representing a potential difference and a electromotive force in electrical circuits. It is a SI derived unit measuring either the work that is done on one ampere or an alternative formulation the force that take effect on an electrical charge $^{W}/_{A} = {}^{J}/_{C} =$ Nm/As.

W
: The unit of power such as real power p is measured in *Watt*. It is a SI derived unit measuring the (electrical) energy conversion per second (representing a degree of efficiency) that is done $^{J}/_{s} = {}^{kg\,m^2}/_{s^3}$. Note that it is used for the real power. For the complex power and reactive power the units V A and VAr are used, respectively.

kV
: One kV corresponds to 1 000 V.

kW
: One kW corresponds to 1 000 W.

kWh
: One kWh corresponds to 3.6 MJ. It basically describes that one kW is in average used over one hour of time. Note that this is a non-SI unit and mainly used for electricity bills.

mWh
: One mW corresponds to 10^{-3} W and thus, a mWh corresponds to 3.6 J.

MW
: One MW corresponds to 1 000 000 W.

MWh
: One MW corresponds to 10^{6} W.

A Problem Definitions

A.1 Flow Feasibility Problems

All feasibility problems check if there is a feasible electrical flow such that the demand can be satisfied. From the combinatorial nature of the problems it makes more sense to formulate the problems as decision problems.

The next problem definition is introduced in Section 3.2 on Page 30.

Flow Feasibility Problem FEAS($\mathcal{N}$)	
Instance:	A flow network $\mathcal{N} = (G, s, t, \text{cap}, \underline{p_g}, \overline{p_g}, \underline{p_d}, \overline{p_d})$.
Question:	Is there a feasible flow f complying with the constraints in Equations 3.1–3.4?

The next problem definition is introduced in Section 3.3.1 on Page 45.

Alternating Current Feasibility Problem AC FEAS($\mathcal{N}$)	
Instance:	An AC network $\mathcal{N} = (\, G = (V, E), V_G, V_D, \text{cap}, r, x, b, g, \underline{\Delta\theta^v}, \overline{\Delta\theta^v}, \underline{v}, \overline{v}, \underline{p_g}, \overline{p_g}, \underline{q_g}, \overline{q_g}, \underline{p_d}, \overline{p_d}, \underline{q_d}, \overline{q_d}\,)$.
Question:	Is there a feasible electrical flow complying with one of these model constraints in Table 3.2?

The next problem definition is introduced in Section 3.3.2 on Page 51.

Direct Current Feasibility Problem DC FEAS($\mathcal{N}$)	
Instance:	A DC network $\mathcal{N} = (\, G, V_G, V_D, \text{cap}, b, \underline{p_g}, \overline{p_g}, \underline{p_d}, \overline{p_d}\,)$.
Question:	Is there a feasible electrical flow complying with the Equations 3.33–3.38?

The next problem definition is introduced in Section 4.1 on Page 66.

Direct Current Feasibility Problem DC-FEAS($\mathcal{N}$)	
Instance:	An exact bounded network $\mathcal{N} = (G, V_G, V_D, \text{cap}, b, \underline{p_g}, \overline{p_g}, \underline{p_d}, \overline{p_d})$, i. e., $p_g \equiv \underline{p_g} \equiv \overline{p_g}$ and $p_d \equiv \underline{p_d} \equiv \overline{p_d}$.
Question:	Is there a feasible electrical flow f (see Equations 4.7, 4.9 and 4.10)?

The next problem definition is introduced in Section 3.3.3 on Page 53.

Voltage Normalized Lossless Real Power Flow Feasibility Problem	
Instance:	A VNLP network $\mathcal{N} = (G, V_G, V_D, \text{cap}, b, \underline{p_g}, \overline{p_g}, \underline{p_d}, \overline{p_d})$.
Question:	Is there a feasible electrical flow complying with Equations 3.43a–3.43f?

The next problem definition is introduced in Section 4.3.2 on Page 87.

Simultaneous Flow Problem [1] SFP($\mathcal{N}$)	
Instance:	Two graphs G_1 and G_2, subsets $E_1 \subseteq E(G_1)$ and $E_2 \subseteq E(G_2)$, and a bijection $\mu_{\text{SFP}} \colon E_1 \to E_2$.
Question:	Are there nonzero KCL-feasible flows f_{G_1} and f_{G_2} in G_1 and G_2 such that for every edge $e \in E_1$ we have $f_{G_1}(e) = f_{G_2}(\mu_{\text{SFP}}(e))$?

The next problem definition is introduced in Section 4.3.2 on Page 88.

s-t Planar DC FEAS($\mathcal{N}$)	
Instance:	A plane s-t-graph G, its dual graph $G^\star$, and the corresponding bijection $\mu_{\text{dual}} \colon E(G) \to E(G^\star)$.
Question:	Are there simultaneous flows on G and $G^\star$ such that $f_G(e) = f_{G^\star}\big(\mu_{\text{dual}}(e)\big) \cdot b(e)$ for all $e \in E(G)$?

A.2 Flow Optimization Problems

The next problem definition is introduced in Section 3.2 on Page 30.

[1] After showing our results to Guido Brückner, he mentioned the SFP generalization to us. We would like to thank him for that generalization of the biconnected planar s-t-DC FEAS-problem.

Maximum Flow Problem MFP($\mathcal{N}$)	
Instance:	A flow network $\mathcal{N} = (G, s, t, \text{cap}, \underline{p_g}, \overline{p_g}, \underline{p_d}, \overline{p_d})$.
Objective:	Is there a feasible flow f that maximizes the flow value $F(\mathcal{N}, f)$.

The next problem definition is introduced in Section 3.2 on Page 31.

Minimum Cost Flow Problem MCFP($\mathcal{N}$)	
Instance:	A flow network $\mathcal{N} = (G, s, t, \text{cap}, \underline{p_g}, \overline{p_g}, \underline{p_d}, \overline{p_d})$ and a cost function γ_e.
Objective:	Find a feasible flow f such that the sum of the cost over all edges $\sum_{e \in E} \gamma_e(f(e))$ is minimized.

The next problem definition is introduced in Section 4.1 on Page 66.

Direct Current Maximum Power Flow Problem DC-MPFP($\mathcal{N}$)	
Instance:	A network $\mathcal{N} = (G, V_G, V_D, \text{cap}, b, \underline{p_g}, \overline{p_g}, \underline{p_d}, \overline{p_d})$.
Objective:	Find a feasible electrical flow f (see Equations 4.7, 4.9 and 4.10) such that the flow value $F(\mathcal{N})$ is maximum among all choices of f.

A.3 Discrete Placement Problems

The next problem definition is introduced in Section 5.1 on Page 107.

Maximum Transmission Switching Flow Problem MTSFP($\mathcal{N}$)	
Instance:	A network $\mathcal{N}$.
Objective:	Find a set $S \subseteq \overleftrightarrow{E}$ of switched edges such that $\text{OPT}_{\text{MPFP}}(\mathcal{N} - S)$ is maximum among all choices of switched edges S.

The next problem definition is introduced in Section 5.2 on Page 112.

k-Maximum Transmission Switching Flow Problem k-MTSFP($\mathcal{N}, k$)	
Instance:	A network $\mathcal{N}$ and $k \in \mathbb{Q}_{\geq 0}$.
Question:	Is it possible to remove a set of edges S such that there is an electrically feasible flow f in $\mathcal{N} - S$ with flow value $F(\mathcal{N} - S, f) \geq k$?

The next problem definition is introduced in Section 5.1 on Page 108.

Optimal Transmission Switching Problem OTSP($\mathcal{N}$)	
Instance:	A network $\mathcal{N}$.
Objective:	Find a set $S \subseteq E$ and an electrically feasible flow f in $\mathcal{N} - S$ such that the sum of the generation costs $\sum_{u \in V_G} \gamma_u (f_{\text{net}}(u))$ is minimized.

The next problem definition is introduced in Section 5.2 on Page 111.

MTSF Problem with Fixed Switches MTSFP($\mathcal{N}, S$)	
Instance:	A network $\mathcal{N}$ and a set $S \subseteq \overleftrightarrow{E}$.
Objective:	Find a switching $z(e) \in \{0, 1\}$ for all $e \in S$ such that $\text{OPT}_{\text{MPFP}}(\mathcal{N} - \{e \mid e \in S \wedge z(e) = 0\})$ is maximum among all choices of z.

The next problem definition is introduced in Section 5.2 on Page 111.

MTSF Problem with k-Switches MTSFP($\mathcal{N}, k$)	
Instance:	A network $\mathcal{N}$ and a parameter $k \in \mathbb{N}$.
Objective:	Find a set $S \subseteq \overleftrightarrow{E}$ of switches with $\lvert S \rvert = k$ such that $\text{OPT}_{\text{MPFP}}(\mathcal{N} - S)$ is maximum among all choices of S.

The next problem definition is introduced in Section 5.2 on Page 112.

Minimum Number of Switches Problem under MTSF MNSP($\mathcal{N}, k$)	
Instance:	A network $\mathcal{N}$ and $k \in \mathbb{N}$.
Question:	Is it possible to remove a set of edges $S \subseteq E$ such that $k = \lvert S \rvert$ is minimum among all choices of $\text{OPT}_{\text{MTSFP}}(\mathcal{N})$?

A.4 Continuous Placement Problems

The next problem definition is introduced in Section 6.2.5 on Page 151.

Min-cost s-t Flow Problem	
Instance:	A network $\mathcal{N}$, parameter $x \in \mathbb{R}$, and $k \in \mathbb{R}_{\geq 0}$.
Question:	Is there a feasible flow f of value $F(\mathcal{N}) = x$ such that $c_{\mathcal{N}}(f) \leq k$?

The next problem definition is introduced in Section 6.3 on Page 153.

MAXIMUM FACTS FLOW PROBLEM WITH E_F MFFP($\mathcal{N}, E_F$)

Instance: A network $\mathcal{N}$, and a set $E_F \subseteq E$.

Objective: Find a susceptance setting $b \in I_e$ for all $e \in E_F$ such that $\text{OPT}_{\text{MPFP}}(\mathcal{N})$ is maximum among all choices of b.

The next problem definition is introduced in Section 6.3 on Page 153.

MAXIMUM FACTS FLOW PROBLEM WITH k-FACTS MFFP($\mathcal{N}, k$)

Instance: A network $\mathcal{N}$, and parameter $k \in \mathbb{N}$.

Objective: Find a set $E_F \subseteq E$ of FACTS with $|E_F| = k$ and a susceptance setting $b \in I_e$ for all $e \in E_F$ such that $\text{OPT}_{\text{MPFP}}(\mathcal{N})$ is maximum among all choices of E_F and b.

The next problem definition is introduced in Section 6.3 on Page 154.

MAXIMUM FACTS FLOW PROBLEM MFFP($\mathcal{N}$)

Instance: A network $\mathcal{N}$.

Objective: Find a set $E_F \subseteq E$ of FACTS with $|E_F| = k$, $0 \leq k \leq |E|$, and a susceptance setting $b \in I_e$ for all $e \in E_F$ such that $\text{OPT}_{\text{MPFP}}(\mathcal{N})$ is maximum among all choices of E_F, b, and k.

The next problem definition is introduced in Section 6.3 on Page 154.

MINIMUM NUMBER OF FACTS PROBLEM MNFP($\mathcal{N}$)

Instance: A network $\mathcal{N}$, and a parameter $k \in \mathbb{N}$.

Objective: Find a set $E_F \subseteq E$ of FACTS and a susceptance setting $b \in I_e$ with $e \in E_F$ such that $k = |E_F|$ is minimum among all choices of $\text{OPT}_{\text{MFFP}}(\mathcal{N})$.

The next problem definition is introduced in Section 6.4 on Page 157.

s-t-DC Feasibility Problem with FACTS s-t-DC-FEAS-FACTS$(G, G^\star, \mu_{\text{dual}})$

Instance: A plane s-t-graph G and its dual $G^\star$, subsets $E_1 \subseteq E(G)$ and $E_2 \subseteq E(G^\star)$, and a bijection $\mu_{\text{dual}} \colon E_1 \to E_2$.

Objective: Find KCL-feasible flows f_G and $f_{G^\star}$ in G and $G^\star$ with $F(G) \neq 0$ and $F(G^\star) \neq 0$ such that for every edge $e \in E$ we have $f_G(e) = f_{G^\star}(\mu_{\text{dual}}(e))$.

A.5 Others

The next problem definition is introduced in Section 5.2.2 on Page 114.

Subset Sum Problem SSP(W, k)

Instance: A finite set of numbers $W = \{w_1, w_2, \ldots, w_n\}$ with $w_i \in \mathbb{N}$ and a $k \in \mathbb{N}$.

Question: Is there a set of elements $x_1, \ldots, x_n \in \{0, 1\}$ such that $\sum_{j=1}^{n} w_j x_j = k$?

The next problem definition is introduced in Section 5.4.3 on Page 125.

Rainbow s-t-Path s-t-RP(G, c, s, t)

Instance: A directed acyclic graph $G = (V, E)$, a coloring $c \colon V \to \mathbb{N}$, and $s, t \in V$.

Question: Is there an s-t-path π in G such that all vertices of π have different colors?

The next problem definition is introduced in Section 6.1 on Page 144.

c-Pumkin Hitting Set Problem p-c-Hit(G, c, k) [Jor+11a, Jor+11b]

Instance: A graph G, parameter $c \in \mathbb{N}_{>0}$, and $k \in \mathbb{N}$.

Question: Is there a c-pumpkin hitting set ${V_F}^c \subseteq V$ of size $|{V_F}^c| \leq k$ such that $G - {V_F}^c$ consists of no c-pumpkin minor?

The next problem definition is introduced in Section 6.1 on Page 144.

VERTEX COVER PROBLEM VCP(G, k)

Instance: A graph $G = (V, \overleftrightarrow{E})$, and parameter $k \in \mathbb{N}$.

Question: Is there a vertex cover VC(G) of size at most k such that one endpoint of each edge $\{u, w\} \in \overleftrightarrow{E}$ belongs to a subset of ${V_F}^{c=1} \subseteq V$ with $|{V_F}^{c=1}| \leq k$?

The next problem definition is introduced in Section 6.1 on Page 144.

FEEDBACK VERTEX SET PROBLEM FVSP(G, k)

Instance: A graph $G = (V, \overleftrightarrow{E})$, and parameter $k \in \mathbb{N}$.

Question: Is there a feedback vertex set FVS(G) of size at most k such that at least one vertex of each cycle $c \in C$ belongs to a subset of ${V_F}^{c=2} \subseteq V$ with $|{V_F}^{c=2}| \leq k$?

The next problem definition is introduced in Section 7.1 on Page 176.

FULL FARM PROBLEM FFP($\mathcal{N}$)

Instance: A network corresponding to the whole wind farm $\mathcal{N} = (G, K, \text{cap}, \gamma, p_g, p_d)$.

Objective: Find a valid pair (κ, f) that minimizes the total cost $c(\kappa, f)$ while complying with Equations 7.1–7.4.

The next problem definition is introduced in Section 7.1 on Page 177.

MINIMUM COST FLOW PROBLEM $\text{MCFP}_{\text{FFP}}(\mathcal{N})$

Instance: A flow network $\mathcal{N} = (G, \gamma_e, p_g, p_d)$.

Objective: Find a feasible flow f such that the sum of the cost over all edges $\sum_{e \in E} \gamma_e(f(e))$ is minimized.

B Fundamentals

B.1 Instantaneous Curves

$$I_{\mathrm{RMS}}(u) = |i(u)| \cdot \frac{1}{\sqrt{2}} \tag{B.1a}$$

$$V_{\mathrm{RMS}}(u) = |v(u)| \cdot \frac{1}{\sqrt{2}} \tag{B.1b}$$

$$i(u,t) = |i(u)| \cdot \sin(\omega t - \theta^{i}(u)) \tag{B.1c}$$

$$v(u,t) = |v(u)| \cdot \sin(\omega t - \theta^{v}(u)) \tag{B.1d}$$

$$\begin{aligned} p(u) &= I_{\mathrm{RMS}}(u) \cdot V_{\mathrm{RMS}}(u) \cdot \cos(\theta^{v}(u) - \theta^{i}(u)) \\ &= \frac{1}{2}|v(u)||i(u)| \cdot \cos(\theta^{v}(u) - \theta^{i}(u)) \end{aligned} \tag{B.1e}$$

$$\begin{aligned} q(u) &= I_{\mathrm{RMS}}(u) V_{\mathrm{RMS}}(u) \cdot \sin(\theta^{v}(u) - \theta^{i}(u)) \\ &= \frac{1}{2}|v(u)||i(u)| \cdot \sin(\theta^{v}(u) - \theta^{i}(u)) \end{aligned} \tag{B.1f}$$

$$q(u,t) = -q(u) \cdot \sin(2 \cdot (\omega t - (\theta^{v}(u) - \theta^{i}(u)))) \tag{B.1g}$$

$$p(u,t) = p(u) \cdot (1 + \cos(2 \cdot (\omega t - (\theta^{v}(u) - \theta^{i}(u))))) \tag{B.1h}$$

$$s(u,t) = v(u,t) \cdot i(u,t) \tag{B.1i}$$

$$s(u,t) = p(u,t) + q(u,t) \tag{B.1j}$$

B.2 Complex Power Injection

The complete derivation of the trigonometric relationship from Equation 3.7 on Page 35 is given in Equation B.2. We emphasize the decoupled parts of the real power p and reactive power q.

$$
\begin{aligned}
s(u,t) &= v(u,t) \cdot i(u,t)^{\star} && \text{(B.2a)}\\
&= \big(\mathcal{R}e(v(u,t)) + \mathbf{j}\mathcal{I}m(v(u,t))\big) \cdot \big(\mathcal{R}e(i(u,t)) - \mathbf{j} \cdot \mathcal{I}m(i(u,t))\big) && \text{(B.2b)}\\
&= \underbrace{\mathcal{R}e(v(u,t)) \cdot \mathcal{R}e(i(u,t)) + \mathcal{I}m(v(u,t)) \cdot \mathcal{I}m(i(u,t))}_{=:p(u)} \\
&\quad - \mathbf{j} \cdot \underbrace{\big(\mathcal{R}e(v(u,t)) \cdot \mathcal{I}m(i(u,t)) - \mathcal{I}m(v(u,t)) \cdot \mathcal{R}e(i(u,t))\big)}_{=:q(u)} && \text{(B.2c)}\\
&= |v(u)||i(u)| \cos\big(\theta^v(u) + \omega t\big) \cos\big(\theta^i(u) + \omega t\big) \\
&\quad + |v(u)||i(u)| \sin\big(\theta^v(u) + \omega t\big) \sin\big(\theta^i(u) + \omega t\big) \\
&\quad - \mathbf{j} \cdot |v(u)||i(u)| \cos\big(\theta^v(u) + \omega t\big) \sin\big(\theta^i(u) + \omega t\big) \\
&\quad + \mathbf{j} \cdot |v(u)||i(u)| \sin\big(\theta^v(u) + \omega t\big) \cos\big(\theta^i(u) + \omega t\big) && \text{(B.2d)}\\
&= |v(u)||i(u)| \Big(\cos\big(\theta^v(u) + \omega t - \theta^i(u) - \omega t\big) + \mathbf{j} \cdot \sin\big(\theta^v(u) + \omega t - \theta^i(u) - \omega t\big)\Big) && \text{(B.2e)}\\
&= \underbrace{|v(u)||i(u)| \cos\big(\theta^v(u) - \theta^i(u)\big)}_{=p(u)} + \mathbf{j} \cdot \underbrace{|v(u)||i(u)| \sin\big(\theta^v(u) - \theta^i(u)\big)}_{=q(u)} && \text{(B.2f)}
\end{aligned}
$$

B.3 Complex Power Flow

The complete derivation of the complex power flow on an edge from Equation 3.18 on Page 43 is given in Equation B.3.

$$
\begin{aligned}
s(u,w) &= v(u)\cdot i(u,w)^{\star} && \text{(B.3a)}\\
&= v(u)\cdot y(u,w)^{\star}\cdot\left(v(w)^{\star}-v(u)^{\star}\right) && \text{(B.3b)}\\
&= \left(\mathcal{R}e(v(u))+\mathbf{j}\cdot\mathcal{I}m(v(u))\right)\left(g(u,w)-\mathbf{j}\cdot b(u,w)\right)\\
&\quad\cdot\left(\mathcal{R}e(v(w))-\mathbf{j}\cdot\mathcal{I}m(v(w))-\mathcal{R}e(v(u))+\mathbf{j}\cdot\mathcal{I}m(v(u))\right)\\
&= \Big(\mathcal{R}e(v(u))\,g(u,w)+\mathcal{I}m(v(u))\,b(u,w)-\mathbf{j}\big(\mathcal{R}e(v(u))\,b(u,w)-\mathcal{I}m(v(u))\,g(u,w)\big)\Big)\\
&\quad\cdot\left(\mathcal{R}e(v(w))-\mathbf{j}\cdot\mathcal{I}m(v(w))-\mathcal{R}e(v(u))+\mathbf{j}\cdot\mathcal{I}m(v(u))\right)\\
&= g(u,w)\mathcal{R}e(v(u))\,\mathcal{R}e(v(w))-\mathbf{j}\cdot g(u,w)\mathcal{R}e(v(u))\,\mathcal{I}m(v(w))\\
&\quad-g(u,w)\mathcal{R}e(v(u))^2+\mathbf{j}\cdot g(u,w)\mathcal{R}e(v(u))\,\mathcal{I}m(v(u))\\
&\quad-\mathbf{j}\cdot b(u,w)\mathcal{R}e(v(u))\,\mathcal{R}e(v(w))-b(u,w)\mathcal{R}e(v(u))\,\mathcal{I}m(v(w))\\
&\quad+\mathbf{j}\cdot b(u,w)\mathcal{R}e(v(u))^2+b(u,w)\mathcal{R}e(v(u))\,\mathcal{I}m(v(u))\\
&\quad+\mathbf{j}\cdot g(u,w)\mathcal{R}e(v(w))\,\mathcal{I}m(v(u))+g(u,w)\mathcal{I}m(v(u))\,\mathcal{I}m(v(w))\\
&\quad-\mathbf{j}\cdot g(u,w)\mathcal{R}e(v(u))\,\mathcal{I}m(v(u))-g(u,w)\mathcal{I}m(v(u))^2\\
&\quad+b(u,w)\mathcal{R}e(v(w))\,\mathcal{I}m(v(u))-\mathbf{j}\cdot b(u,w)\mathcal{I}m(v(u))\,\mathcal{I}m(v(w))\\
&\quad-b(u,w)\mathcal{R}e(v(u))\,\mathcal{I}m(v(u))+\mathbf{j}b(u,w)\mathcal{I}m(v(u))^2\\
&= \left.\begin{array}{l} g(u,w)\big(\mathcal{R}e(v(u))\,\mathcal{R}e(v(w))+\mathcal{I}m(v(u))\,\mathcal{I}m(v(w))-\mathcal{R}e(v(u))^2-\mathcal{I}m(v(u))^2\big)\\ +b(u,w)\big(\mathcal{R}e(v(w))\,\mathcal{I}m(v(u))-\mathcal{R}e(v(u))\,\mathcal{I}m(v(w))\big)\end{array}\right\}=:p(u,w)\\
&\quad\left.\begin{array}{l} +\mathbf{j}\cdot\Big(g(u,w)\big(\mathcal{R}e(v(w))\,\mathcal{I}m(v(u))-\mathcal{R}e(v(u))\,\mathcal{I}m(v(w))\big)\\ +b(u,w)\big(\mathcal{R}e(v(u))^2+\mathcal{I}m(v(u))^2-\mathcal{R}e(v(u))\,\mathcal{R}e(v(w))-\mathcal{I}m(v(u))\,\mathcal{I}m(v(w))\big)\Big)\end{array}\right\}=:q(u,w)\\
& && \text{(B.3c)}
\end{aligned}
$$

B.4 Complex Current Flow

The complete derivation of the complex current flow on an edge from Equation 3.23 on Page 44 is given in Equation B.4.

$$
\begin{aligned}
i(u,w) &= \big(g(u,w) + \mathbf{j}\cdot b(u,w)\big)\big(v(w) - v(u)\big) \\
&= \Big(g(u,w) + \mathbf{j}\cdot b(u,w)\Big)\Big(\mathcal{R}e(v(w)) + \mathbf{j}\cdot \mathcal{I}m(v(w)) - \mathcal{R}e(v(u)) - \mathbf{j}\cdot \mathcal{I}m(v(u))\Big) \\
&= \begin{array}{rrrrr}
 & g(u,w)\cdot\mathcal{R}e(v(w)) & + & \mathbf{j}\cdot g(u,w)\cdot\mathcal{I}m(v(w)) & - \\
 & g(u,w)\cdot\mathcal{R}e(v(u)) & - & \mathbf{j}\cdot g(u,w)\cdot\mathcal{I}m(v(u)) & + \\
\mathbf{j}\cdot & b(u,w)\cdot\mathcal{R}e(v(w)) & + & \mathbf{j}^2\cdot b(u,w)\cdot\mathcal{I}m(v(w)) & - \\
\mathbf{j}\cdot & b(u,w)\cdot\mathcal{R}e(v(u)) & - & \mathbf{j}^2\cdot b(u,w)\cdot\mathcal{I}m(v(u)) &
\end{array} \\
&= \underbrace{g(u,w)\big(\mathcal{R}e(v(w)) - \mathcal{R}e(v(u))\big) + b(u,w)\big(\mathcal{I}m(v(u)) - \mathcal{I}m(v(w))\big)}_{=:\mathcal{R}e(i(u,w))} + \\
&\quad \mathbf{j}\cdot\Big(\underbrace{g(u,w)\big(\mathcal{I}m(v(w)) - \mathcal{I}m(v(u))\big) + b(u,w)\big(\mathcal{R}e(v(w)) - \mathcal{R}e(v(u))\big)}_{=:\mathcal{I}m(i(u,w))}\Big)
\end{aligned}
\tag{B.4}
$$

B.5 Formulations

B.5.1 Polar PQV Formulation

The real and reactive parts of the complex power flow equation from Equation B.3c are transformed separately to the polar form. The real power PQV formulation is used in Equation 3.19a on Page 44. The reactive power PQV formulation is used in Equation 3.20a on Page 44.

$$
\begin{aligned}
p(u,w) = \;& g(u,w)\Big(\mathcal{R}e(v(u))\,\mathcal{R}e(v(w)) + \mathcal{I}m(v(u))\,\mathcal{I}m(v(w)) - \mathcal{R}e(v(u))^2 - \mathcal{I}m(v(u))^2\Big) \\
& + b(u,w)\Big(\mathcal{R}e(v(w))\,\mathcal{I}m(v(u)) - \mathcal{R}e(v(u))\,\mathcal{I}m(v(w))\Big) \\
= \;& g(u,w)\Big(|v(u)||v(w)|\cos\big(\theta^v(u)+\omega t\big)\cos\big(\theta^v(w)+\omega t\big) \\
& \quad + |v(u)||v(w)|\sin\big(\theta^v(u)+\omega t\big)\sin\big(\theta^v(w)+\omega t\big) \\
& \quad - |v(u)|^2 \underbrace{\big(\cos^2(\theta^v(u)+\omega t) + \sin^2(\theta^v(u)+\omega t)\big)}_{=1}\Big) \\
& + b(u,w)\Big(|v(u)||v(w)|\cos\big(v(w)+\omega t\big)\sin\big(v(u)+\omega t\big) \\
& \quad - |v(u)||v(w)|\cos\big(v(u)+\omega t\big)\sin\big(v(w)+\omega t\big)\Big) \\
= \;& g(u,w)\Big(|v(u)||v(w)|\cos\big(\theta^v(u)-\theta^v(w)\big) - |v(u)|^2\Big) \\
& + b(u,w)|v(u)||v(w)|\sin\big(\theta^v(u)-\theta^v(w)\big)
\end{aligned}
\tag{B.5a}
$$

$$
\begin{aligned}
q(u,w) = \;& g(u,w)\Big(\mathcal{R}e(v(w))\,\mathcal{I}m(v(u)) - \mathcal{R}e(v(u))\,\mathcal{I}m(v(w))\Big) \\
& + b(u,w)\Big(\mathcal{R}e(v(u))^2 + \mathcal{I}m(v(u))^2 - \mathcal{R}e(v(u))\,\mathcal{R}e(v(w)) - \mathcal{I}m(v(u))\,\mathcal{I}m(v(w))\Big) \\
= \;& g(u,w)\Big(|v(u)||v(w)|\cos\big(\theta^v(w)+\omega t\big)\sin\big(\theta^v(u)+\omega t\big) \\
& \quad - |v(u)||v(w)|\cos\big(\theta^v(u)+\omega t\big)\sin\big(\theta^v(w)+\omega t\big)\Big) \\
& + b(u,w)\Big(|v(u)|^2 \underbrace{\big(\cos^2(\theta^v(u)+\omega t) + \sin^2(\theta^v(u)+\omega t)\big)}_{=1} \\
& \quad - |v(u)||v(w)|\cos\big(\theta^v(u)+\omega t\big)\cos\big(\theta^v(w)+\omega t\big) \\
& \quad - |v(u)||v(w)|\sin\big(\theta^v(u)+\omega t\big)\sin\big(\theta^v(w)+\omega t\big)\Big) \\
= \;& g(u,w)|v(u)||v(w)|\sin\big(\theta^v(u)-\theta^v(w)\big) \\
& - b(u,w)\Big(|v(u)||v(w)|\cos\big(\theta^v(u)-\theta^v(w)\big) - |v(u)|^2\Big)
\end{aligned}
\tag{B.5b}
$$

$$
|\underline{v}(u)| \le |v(u)| \le |\overline{v}(u)|, \tag{B.5c}
$$

$$
\underline{\Delta\theta^v}(u,w) \le \theta^v(u) - \theta^v(w) \le \overline{\Delta\theta^v}(u,w). \tag{B.5d}
$$

B.5.2 Rectangular PQV Formulation

The real part in Equation B.6b and the reactive part in Equation B.6c are come from Equation B.3c.

$$\left.\begin{aligned} &p(u,w) + \mathbf{j}\cdot q(u,w) \\ &v(u)\cdot i(u,w)^{\star} \\ &v(u)\cdot (v(w)^{\star}\cdot y(u,w)^{\star}) \end{aligned}\right\} = s(u,w) \tag{B.6a}$$

$$g(u,w)\begin{pmatrix} \mathcal{R}e(v(u))\,\mathcal{R}e(v(w)) \\ +\mathcal{I}m(v(u))\,\mathcal{I}m(v(w)) \\ -\mathcal{R}e(v(u))^2 - \mathcal{I}m(v(u))^2 \end{pmatrix} - b(u,w)\begin{pmatrix} \mathcal{R}e(v(u))\,\mathcal{I}m(v(w)) \\ -\mathcal{R}e(v(w))\,\mathcal{I}m(v(u)) \end{pmatrix} = p(u,w) \tag{B.6b}$$

$$-g(u,w)\begin{pmatrix} \mathcal{R}e(v(u))\,\mathcal{I}m(v(w)) \\ -\mathcal{R}e(v(w))\,\mathcal{I}m(v(u)) \end{pmatrix} - b(u,w)\begin{pmatrix} \mathcal{R}e(v(u))\,\mathcal{R}e(v(w)) \\ +\mathcal{I}m(v(u))\,\mathcal{I}m(v(w)) \\ -\mathcal{R}e(v(u))^2 - \mathcal{I}m(v(u))^2 \end{pmatrix} = q(u,w) \tag{B.6c}$$

$$|p(u,w)| \le \overline{p}(u,w) \tag{B.6d}$$

$$|q(u,w)| \le \overline{q}(u,w) \tag{B.6e}$$

$$|s(u,w)| \le \overline{s}(u,w) \tag{B.6f}$$

$$\mathcal{R}e(v(u))^2 + \mathcal{I}m(v(u))^2 \le \overline{v}(u)^2 \tag{B.6g}$$

$$\underline{v}(u)^2 \le \mathcal{R}e(v(u))^2 + \mathcal{I}m(v(u))^2 \tag{B.6h}$$

$$\underline{\Delta\theta^{v}}(u,w) \le \arctan\left(\frac{\mathcal{R}e(v(u))}{\mathcal{I}m(v(u))}\right) - \arctan\left(\frac{\mathcal{R}e(v(w))}{\mathcal{I}m(v(w))}\right) \le \overline{\Delta\theta^{v}}(u,w), \tag{B.6i}$$

B.5.3 Polar IV Formulation

The Equation B.7 comes from Equations 3.22 and 3.23.

$$
\begin{aligned}
i(u) = \; & g(u,0)|v(u)|\cos\big(\theta^v(u)\big) + \sum_{\{u,w\}\in\overrightarrow{E}} g(u,w)\big(|v(w)|\cos\big(\theta^v(w)\big) - |v(u)|\cos\big(\theta^v(u)\big)\big) \\
& - b(u,0)|v(u)|\sin\big(\theta^v(u)\big) - \sum_{\{u,w\}\in\overrightarrow{E}} b(u,w)\big(|v(w)|\sin\big(\theta^v(w)\big) - |v(u)|\sin\big(\theta^v(u)\big)\big) \\
& + \mathbf{j}\Big(g(u,0)|v(u)|\sin\big(\theta^v(u)\big) + \sum_{\{u,w\}\in\overrightarrow{E}} g(u,w)\big(|v(w)|\sin\big(\theta^v(w)\big) - |v(u)|\sin\big(\theta^v(u)\big)\big) \\
& + b(u,0)|v(u)|\cos\big(\theta^v(u)\big) + \sum_{\{u,w\}\in\overrightarrow{E}} b(u,w)\big(|v(w)|\cos\big(\theta^v(w)\big) - |v(u)|\cos\big(\theta^v(u)\big)\big)\Big),
\end{aligned}
\tag{B.7a}
$$

$$
\underbrace{|v(u)||i(u)|\cos\big(\theta^v(u)-\theta^i(u)\big)}_{=:p(u)} \le \overline{p}(u), \tag{B.7b}
$$

$$
\underline{p}(u) \le \underbrace{|v(u)||i(u)|\cos\big(\theta^v(u)-\theta^i(u)\big)}_{=:p(u)}, \tag{B.7c}
$$

$$
\underbrace{|v(u)||i(u)|\sin\big(\theta^v(u)-\theta^i(u)\big)}_{=:q(u)} \le \overline{q}(u), \tag{B.7d}
$$

$$
\underline{q}(u) \le \underbrace{|v(u)||i(u)|\sin\big(\theta^v(u)-\theta^i(u)\big)}_{=:q(u)}, \tag{B.7e}
$$

$$
|\underline{v}(u)| \le |v(u)| \le |\overline{v}(u)|, \tag{B.7f}
$$

$$
\underline{\Delta\theta^v}(u,w) \le \theta^v(u) - \theta^v(w) \le \overline{\Delta\theta^v}(u,w). \tag{B.7g}
$$

B.5.4 Rectangular IV Formulation

$$
\begin{aligned}
i(u) = \quad & g(u,0)\mathcal{R}e(v(u)) + \sum_{\{u,w\}\in\overrightarrow{E}} g(u,w)\big(\mathcal{R}e(v(w)) - \mathcal{R}e(v(u))\big) \\
& - b(u,0)\mathcal{I}m(v(u)) - \sum_{\{u,w\}\in\overrightarrow{E}} b(u,w)\big(\mathcal{I}m(v(w)) - \mathcal{I}m(v(u))\big) \\
& + \mathbf{j}\cdot\Big(g(u,0)\mathcal{I}m(v(u)) + \sum_{\{u,w\}\in\overrightarrow{E}} g(u,w)\big(\mathcal{I}m(v(w)) - \mathcal{I}m(v(u))\big) \\
& \quad + b(u,0)\mathcal{R}e(v(u)) + \sum_{\{u,w\}\in\overrightarrow{E}} b(u,w)\big(\mathcal{R}e(v(w)) - \mathcal{R}e(v(u))\big)\Big)
\end{aligned} \tag{B.8a}
$$

$$
\underbrace{\mathcal{R}e(v(u))\cdot\mathcal{R}e(i(u)) + \mathcal{I}m(v(u))\cdot\mathcal{I}m(i(u))}_{=:p(u)} \le \overline{p}(u) \tag{B.8b}
$$

$$
\underline{p}(u) \le \underbrace{\mathcal{R}e(v(u))\cdot\mathcal{R}e(i(u)) + \mathcal{I}m(v(u))\cdot\mathcal{I}m(i(u))}_{=p(u)} \tag{B.8c}
$$

$$
\underbrace{\mathcal{I}m(v(u))\cdot\mathcal{R}e(i(u)) - \mathcal{R}e(v(u))\cdot\mathcal{I}m(i(u))}_{=:q(u)} \le \overline{q}(u) \tag{B.8d}
$$

$$
\underline{q}(u) \le \underbrace{\mathcal{I}m(v(u))\cdot\mathcal{R}e(i(u)) - \mathcal{R}e(v(u))\cdot\mathcal{I}m(i(u))}_{=q(u)} \tag{B.8e}
$$

$$
\mathcal{R}e(v(u))^2 + \mathcal{I}m(v(u))^2 \le \overline{v}(u)^2 \tag{B.8f}
$$

$$
\underline{v}(u)^2 \le \mathcal{R}e(v(u))^2 + \mathcal{I}m(v(u))^2 \tag{B.8g}
$$

$$
|i(u,w)| \le \overline{i}(u,w) \tag{B.8h}
$$

$$
\underline{\Delta\theta^v}(u,w) \le \arctan\left(\frac{\mathcal{R}e(v(u))}{\mathcal{I}m(v(u))}\right) - \arctan\left(\frac{\mathcal{R}e(v(w))}{\mathcal{I}m(v(w))}\right) \le \overline{\Delta\theta^v}(u,w), \tag{B.8i}
$$

B.5.5 DC Assumption 3

$$q(u) = -|v(u)|^2 \left(b(u,u) + \sum_{w \in V \setminus \{u\}} b(u,w) \right) + \sum_{w \in V \setminus \{u\}} |v(u)||v(w)| \Big(b(u,w) \Big) \tag{B.9a}$$

$$= -|v(u)|^2 b(u,u) - \left(\sum_{w \in V \setminus \{u\}} |v(u)|^2 b(u,w) - |v(u)||v(w)| b(u,w) \right) \tag{B.9b}$$

$$= -|v(u)|^2 b(u,u) - \left(\sum_{w \in V \setminus \{u\}} |v(u)| b(u,w) \left(|v(u)| - |v(w)| \right) \right) \tag{B.9c}$$

$$\overset{(A3)}{=} -b(u,u) - \left(\sum_{w \in V \setminus \{u\}} b(u,w) \left(|v(u)| - |v(w)| \right) \right) \tag{B.9d}$$

C Discrete Changes to the Power Grid

This section is an extension of the Chapter 5 in which we consider discrete changes to the power grid topology with the focus on transmission switching. In Section 5.7, we evaluate two different algorithms and present for the DTP betweenness centralities two networks in Figure 5.13a&b. In this section, we extend this to other power grid sizes and structures such that we have a broader evaluation. Figure 5.13d illustrates the compressed representation.

In this section, we test the influence of switching edges one by one with different Dominating Theta Path (DTP) betweenness centralities and their influence on the maximum power flow (MPF). For each test case, we compute the DTP betweenness centrality for each edge and the MPF when only this edge is switched. The results of these simulations are shown in Figures C.1–C.3. We sort the edges from highest to lowest centrality. The centrality of the edges is shown as a dashed curve. The solid curve represents the value of the MPF if the edge is switched. We can see that for many edges switching them does not influence the value of the MPF. The edges where switching them decreases the value are often those with medium to low centrality values (see in particular `nesta_case14_ieee`, `nesta_case30_ieee` and `nesta_case300_ieee`). Switching edges with high centrality (relative to the other edges in the network) still keeps a large flow value. For a combination of all the results refer to Figure 5.13d.

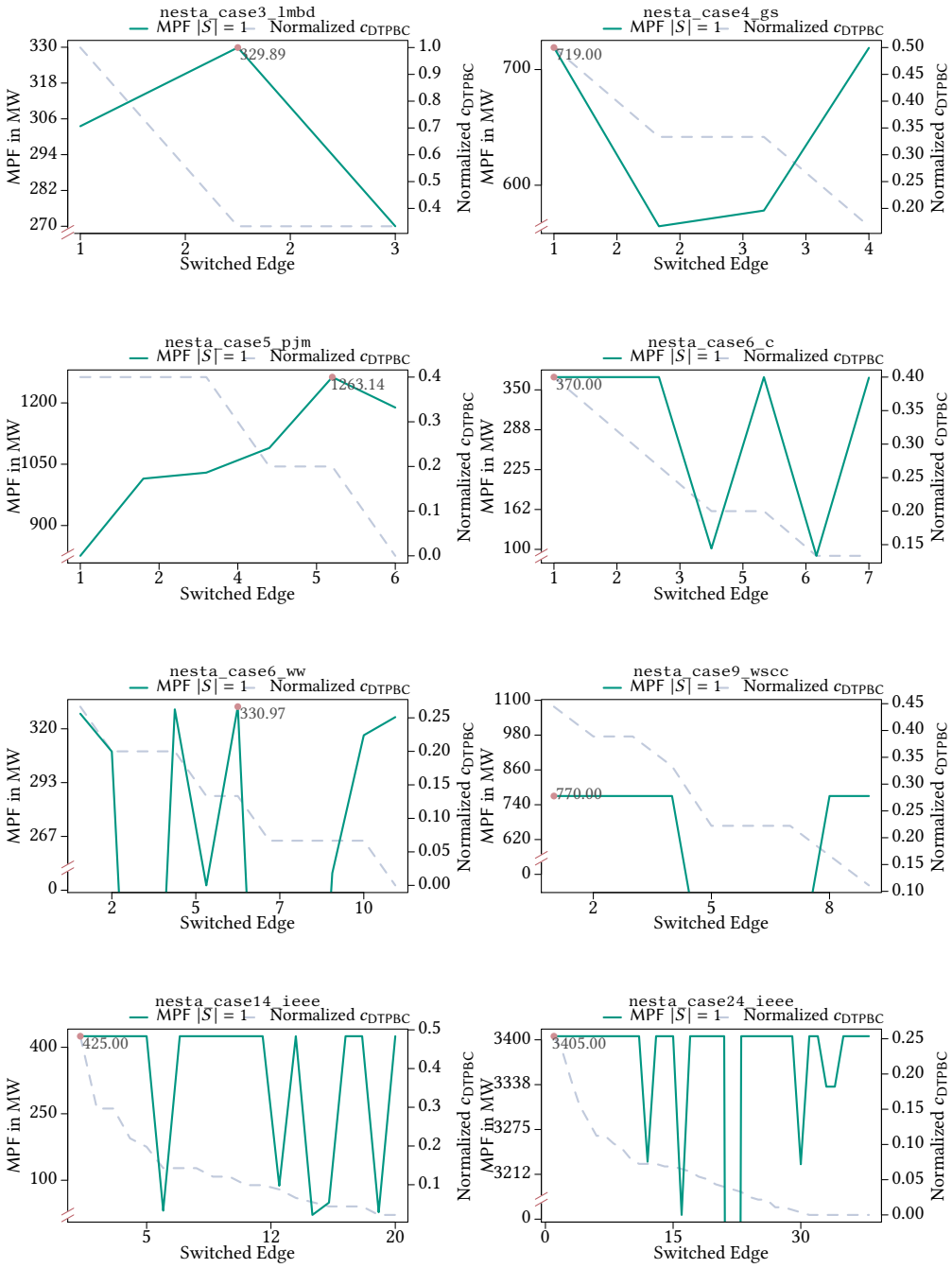

Figure C.1: Results of the simulations for the DTP betweenness centrality on `nesta_case3_lmbd` to `nesta_case24_ieee_rts`.

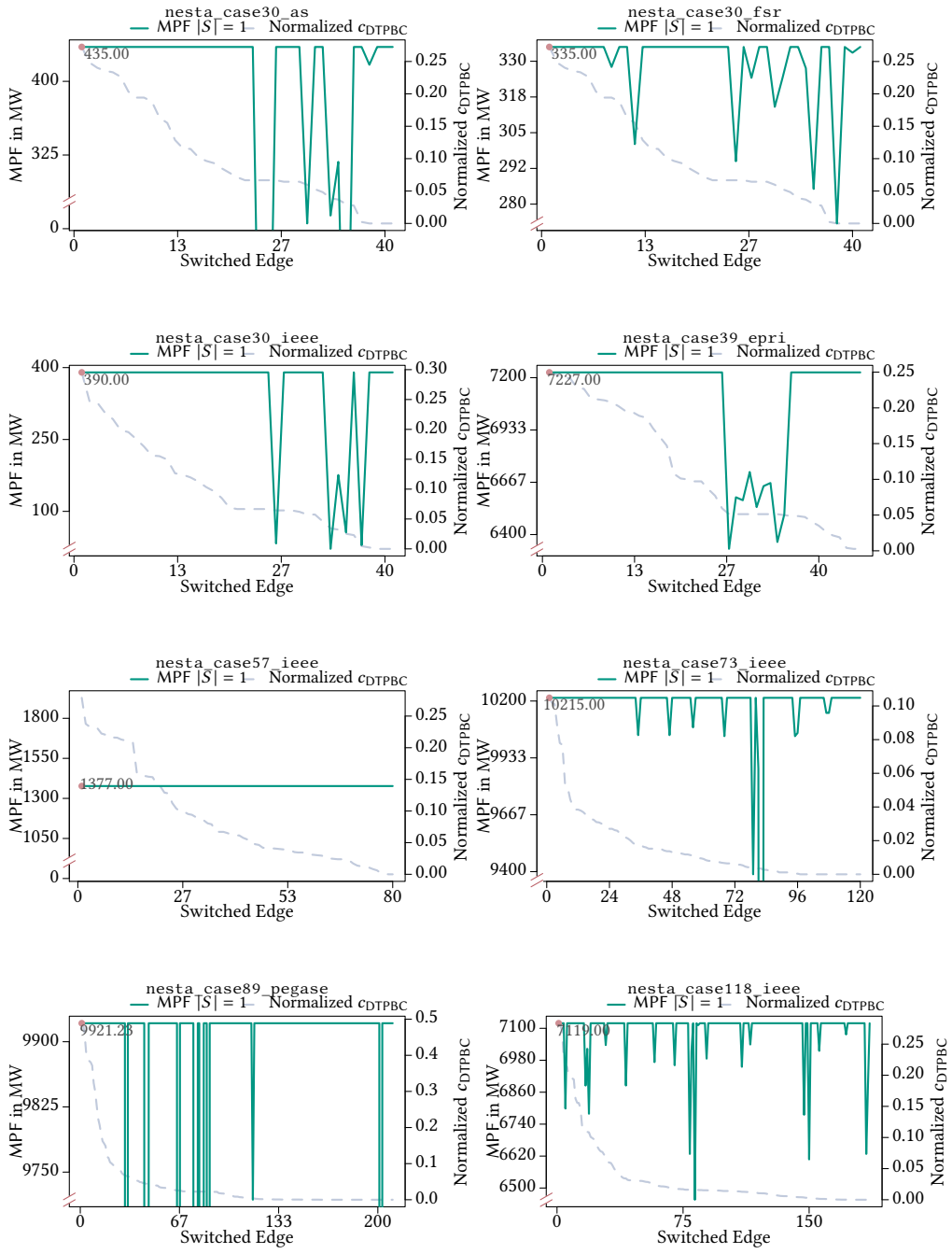

Figure C.2: Results of the simulations for the DTP betweenness centrality on cases `nesta_case30_as` to `nesta_case118_ieee`.

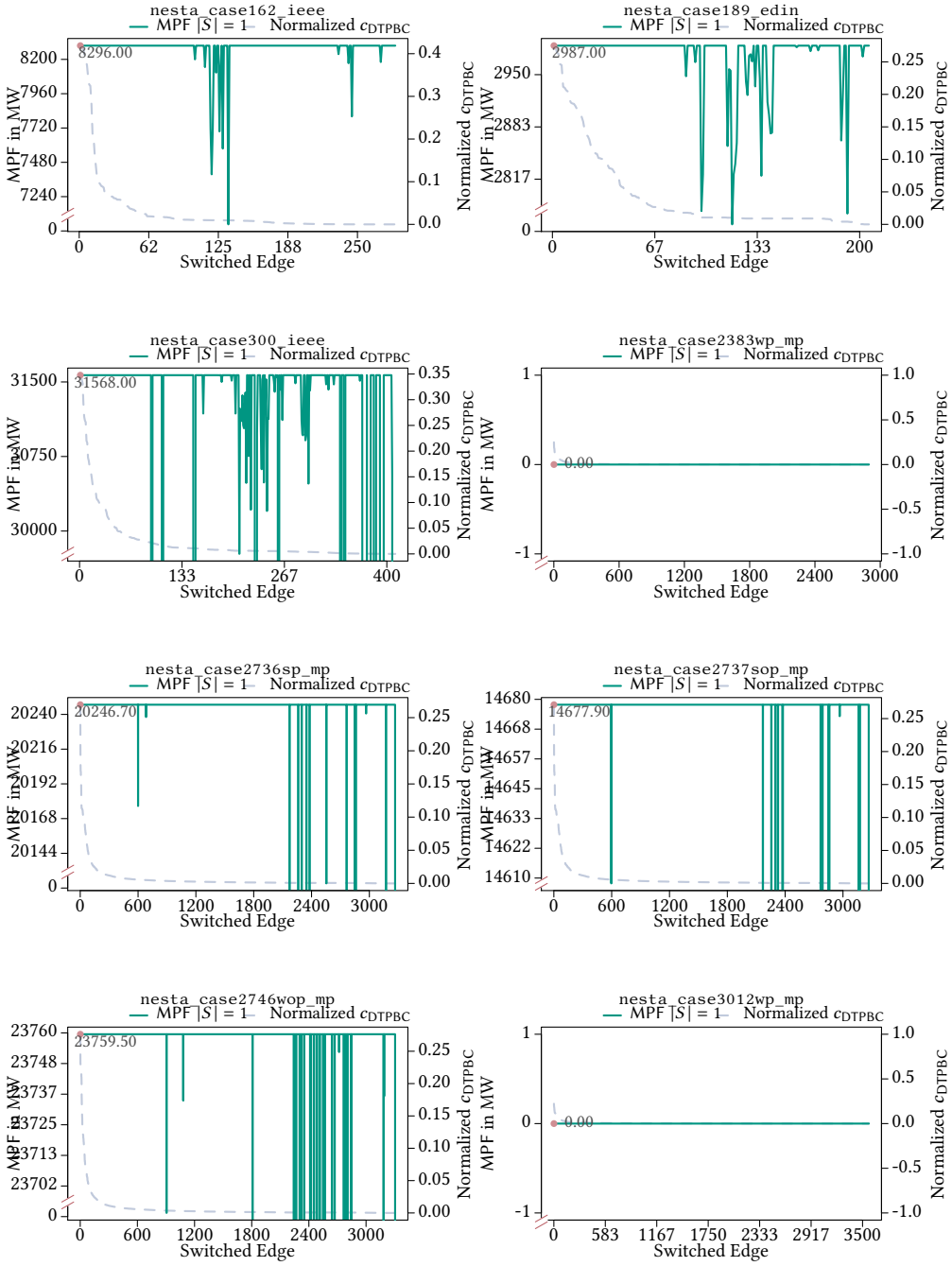

Figure C.3: Results of the simulations for the DTP betweenness centrality on cases `nesta_case162_ieee` to `nesta_case3012wp_mp`.

D Continuous Changes in the Power Grid

This section is an extension of the Chapter 6 in which we consider continuous changes to the power grid topology with the focus on the placement of Flexible AC Transmission Systems (FACTS). In Figure D.1, we investigate the trade-off between costs and losses of the multi-objective function (Equation 6.6) that we optimize in our hybrid model (Equation 6.12). In all our simulations, we see a Pareto front that shows for different $\lambda \in [0, 1]$ an optimal solution in Figure D.1.

If we concentrate on the placement problem, we can evaluate for different numbers of control vertices V_F the operation costs for different load increase factors. This is shown for different power grids in Figure D.2.

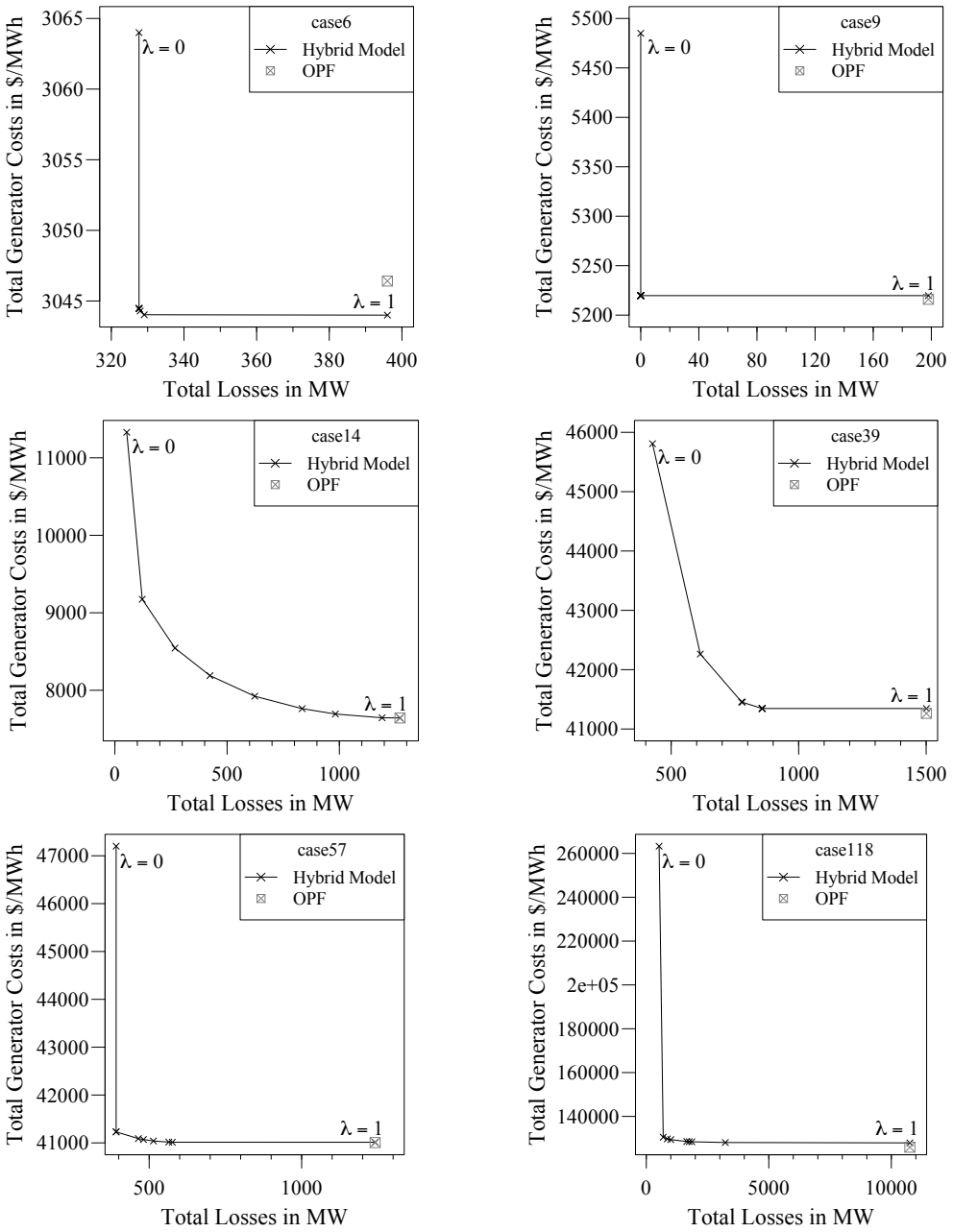

Figure D.1: Trade-off of generator costs and costs of the losses depending as λ varies from 0 to 1. The square cross marks the solution computed by OPF.

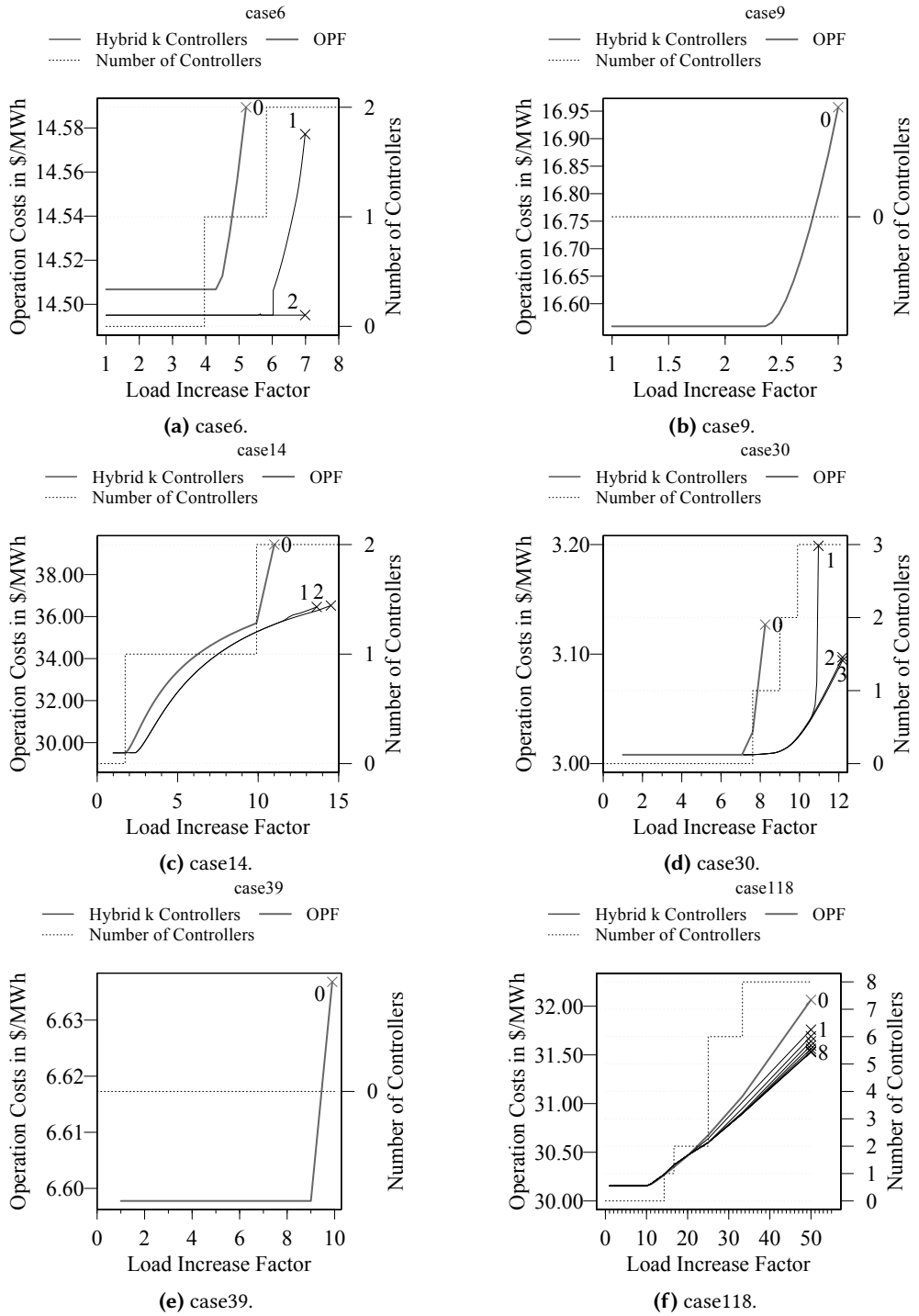

(a) case6. **(b)** case9. **(c)** case14. **(d)** case30. **(e)** case39. **(f)** case118.

Figure D.2: Operation costs of `case6` to `case118` for OPF and the hybrid model with their control buses with respect to the load factor ρ.

E Curriculum Vitæ

Name	Franziska Wegner
Place of Birth	Potsdam, Germany
Nationality	German

Education and Professional Experience

12/2019–07/2020	Research assistant at the Institute of Theoretical Informatics, Karlsruhe Institute of Technology (KIT)
04/2014–12/2019	PhD student at the Institute of Theoretical Informatics, Karlsruhe Institute of Technology (KIT) Advisors: Prof. Dr. Dorothea Wagner, Prof. Dr. Sylvie Thiébaux
01/2016–04/2016	Research stay at Australia's National Information and Communications Technology (NICTA), Canberra, Australia
10/2010–03/2014	Master of Science in Computer Science Karlsruhe Institute of Technology (KIT)
09/2007–04/2012	Employee at SAP SE Walldorf, Germany
10/2007–10/2010	Bachelor of Engineering in Information Technology University of Cooperative Education, Karlsruhe (SAP SE)

Teaching Experience

10/2019–03/2020	Seminar "Energy Informatics"
04/2019–07/2019	Lecture "Energy Informatics 2"
10/2018–03/2019	Seminar "Energy Informatics"

04/2018–07/2018	Lecture “Energy Informatics 2”
04/2018–07/2018	Seminar “Algorithms for NP-hard Problems”
10/2017–03/2018	Seminar “Energy Informatics”
04/2017–07/2017	Practical course “Visualization of Energy-Schedules”
04/2017–07/2017	Seminar “Classics in Theoretical Computer Science”
04/2017–07/2017	Lecture “Energy Informatics 2”
10/2016–03/2017	Seminar “Energy Informatics”
04/2016–07/2016	Seminar “Techniques in Algorithmic – Selected Topics in the Algorithmic Graph Theory”
10/2015–03/2016	Seminar “Modeling and Simulation of Smart Grids”
04/2015–07/2015	Practical course “Development of a Campus Route Planner”
04/2015–07/2015	Seminar “Methods and Algorithm for Evaluating and Optimizing Power Grids”
04/2015–07/2015	Seminar “The P unequal NP Hypothesis”
10/2014–03/2015	Seminar “Techniques in Algorithmic”
10/2014–03/2015	Lecture “Fundamentals of Theoretical Computer Science”
04/2014–07/2014	Practical course “Development of a Campus Route Planner”

Supervised Master’s Theses

07/2019–04/2020	Adrian Grupp, A Comparative Analysis of Switchings in Static and Dynamic Power Grids
11/2018–05/2019	Lena Winter, Transmission Network Expansion Planning for Curing Critical Edges
11/2017–05/2018	Chao Wang, Transmission Network Expansion Planning using the Railway Network
08/2017–04/2018	Larisa Duczek, Beobachtungen des Maximalen Flexiblen Drehstromübertragungssystem Flusses (Diploma thesis)
11/2016–06/2017	Carina Mieth, Observability of Multi-Carrier Energy Distribution Networks and Optimal Sensor Placement
12/2015–05/2016	Sebastian Lehmann, Simulated Annealing-Based Heuristics for Wind Farm Cabling Problems

Supervised Bachelor's Theses

11/2018–03/2019	Robert Mumper, Erweiterungsplanung in elektrischen Netzen mittels dynamischer Programmierung
07/2018–11/2018	Florian Krüger, A Block-Cut-Tree-based Switching Algorithm for Cacti
04/2018–08/2018	Niklas Fuhrberg, Wind Farm Cabling using Spectral Clustering
02/2017–06/2017	Hannah Wenk, Clusteringansätze von Windfarmen
01/2017–05/2017	Ivo Baar, Entwicklung eines genetischen Algorithmus zur effizienten Verkabelung von Windfarmen
01/2017–05/2017	Jakob Nedlin, Ant-based Algorithms for the Wind Farm Cable Layout Problem

F List of Publications

Journal Articles

[1] **Scalable Exact Visualization of Isocontours in Road Networks via Minimum-Link Paths**. *Journal of Computational Geometry* 9:1, pages 24–70, 2018. URL: http://jocg.org/index.php/jocg/article/view/313.
Cited on page 272. Joint work with Moritz Baum, Thomas Bläsius, Andreas Gemsa, and Ignaz Rutter.

[2] **Poster Abstract: Graph-theoretic Model for Observability in Multi-carrier Energy Distribution Networks**. *Computer Science - Research and Development*, 2017. URL: https://doi.org/10.1007/s00450-017-0366-3.
Cited on page 272. Joint work with Sören Hohmann, Heiko Maaß, Carina Mieth, Martin Pfeifer, and Dorothea Wagner.

Articles in Conference Proceedings

[3] **Scalable Exact Visualization of Isocontours in Road Networks via Minimum-Link Paths**. In *Proceedings of the 24th Annual European Symposium on Algorithms (ESA'16)*. Volume 57 of Leibniz International Proceedings in Informatics, pages 7:1–7:18. Schloss Dagstuhl - Leibniz-Zentrum für Informatik, 2016. URL: http://drops.dagstuhl.de/opus/frontdoor.php?source_opus=6349.
Cited on page 272. Joint work with Moritz Baum, Thomas Bläsius, Andreas Gemsa, and Ignaz Rutter.

[4] **Computing Minimum-Link Separating Polygons in Practice**. In *Proceedings of the 32nd European Workshop on Computational Geometry (EuroCG'16)*, 2016.
Cited on page 272. Joint work with Moritz Baum, Thomas Bläsius, Andreas Gemsa, and Ignaz Rutter.

[5] **The Maximum Transmission Switching Flow Problem**. In *Proceedings of the 9th ACM e-Energy International Conference on Future Energy Systems (ACM e-Energy'18)*, pages 340–360. ACM Press, 2018. URL: https://doi.org/10.1145/3208903.3208910. Joint work with Alban Grastien, Ignaz Rutter, Dorothea Wagner, and Matthias Wolf.

[6] **Towards Negative Cycle Canceling in Wind Farm Cable Layout Optimization**. In *Proceedings of the 7th DACH+ Conference on Energy Informatics*. Volume 1 (Suppl 1) of. Springer, 2018. URL: https://energyinformatics.springeropen.com/articles/10.1186/s42162-018-0030-6.
Cited on page 272. Joint work with Sascha Gritzbach, Torsten Ueckerdt, Dorothea Wagner, and Matthias Wolf.

[7] **Operating Power Grids with few Flow Control Buses**. In *Proceedings of the 6th ACM e-Energy International Conference on Future Energy Systems*, pages 289–294. ACM Press, 2015. URL: http://doi.acm.org/10.1145/2768510.2768521. Joint work with Thomas Leibfried, Tamara Mchedlidze, Nico Meyer-Hübner, Martin Nöllenburg, Ignaz Rutter, Peter Sanders, and Dorothea Wagner.

[8] **A Simulated-Annealing-Based Approach for Wind Farm Cabling**. In *Proceedings of the 8th ACM e-Energy International Conference on Future Energy Systems (ACM eEnergy'17)*, pages 203–215. ACM Press, 2017. URL: https://doi.org/10.1145/3077839.3077843. Joint work with Sebastian Lehmann, Ignaz Rutter, and Dorothea Wagner.

[9] **Towards Realistic Flow Control in Power Grid Operation**. In *Proceedings of the 4th D-A-CH Conference on Energy Informatics*. Volume 9424 of Lecture Notes in Computer Science, pages 192–199. Springer, 2015. URL: http://dx.doi.org/10.1007/978-3-319-25876-8_16. Joint work with Tamara Mchedlidze, Martin Nöllenburg, Ignaz Rutter, and Dorothea Wagner.

[10] **Analysis of Redispatch and Transmission Capacity Pricing on a Local Electricity Market Setup**. In *14th International Conference on the European Energy Market*, pages 1–6. IEEE, 2017. URL: http://doi.org/10.1109/EEM.2017.7981959.
Cited on page 272. Joint work with Philipp Staudt, Johannes Garttner, and Christof Weinhardt.

Technical Reports

[11] **Engineering Negative Cycle Canceling for Wind Farm Cabling**. 2019. arXiv: 1908.02129 [cs.DS].
Cited on page 272. Joint work with Sascha Gritzbach, Torsten Ueckerdt, Dorothea Wagner, Franziska Wegner, and Matthias Wolf.

The papers [Gri+19], [Bau+18], [Hoh+17], [Bau+16b], [Bau+16c], [Gri+18], and [SGW17] [Bau+16a] are omitted in this thesis because of missing thematically closeness and since the main author is someone else.

G Deutsche Zusammenfassung

Energienetze bilden das Rückgrat unserer Gesellschaft, die unter anderem unsere Nahrungskette und andere wichtige Infrastrukturen, wie die Wasser- und Wärmeversorgung, bestimmen. Um die grundlegenden menschlichen Bedürfnisse zu befriedigen, müssen wir ein nachhaltigeres und umweltfreundlicheres Verhalten im Allgemeinen und in Energienetzen im Speziellen an den Tag legen. In dieser Arbeit geht es um Energienetze, wobei wir uns auf Stromnetze spezialisieren und uns darauf fokussieren, wie wir die vorhandene Infrastruktur besser ausnutzen können. Wir merken an, dass die Ergebnisse aus dieser Arbeit auch auf andere Energienetze übertragen werden können [Gro+19] und bestimmte auftretende Phänomene legen es nahe, dass sich einige Ergebnisse eventuell auch auf Verkehrsnetze übertragen lassen. Diese Arbeit besteht aus vier inhaltlichen Teilen. Der erste Teil beschäftigt sich mit der Funktionsweise und Struktur von elektrischen Flüssen. Der zweite und dritte inhaltliche Teil der Arbeit beschäftigt sich jeweils mit der effizienten Ausnutzung der vorhandenen Energienetzinfrastruktur. Dabei verstehen wir hier unter effizienter Ausnutzung entweder die Maximierung der Gesamterzeugung und die damit verbundene Erweiterung des Betriebspunktes oder die Minimierung der Erzeugungskosten verstehen.

Das elektrische Netz besteht aus drei Spannungsebenen, die wir als Hoch-, Mittel-, und Niederspannungsebene bezeichnen. Das traditionelle elektrische Netz ist auf eine zentrale Energieversorgung ausgelegt, bei der die Erzeuger sich in der Hochspannungsebene befinden. Der elektrische Fluss im klassischen Sinne fließt von der Hoch- in die Mittel- und Niederspannungsebene. Die industriellen Verbraucher befinden sich zumeist auf der Mittelspannungsebene, während sich die Haushalte und kleineren Industrien in der Niederspannungsebene befinden. Durch nachhaltige Erzeuger, die ihre Energie aus erneuerbaren Energien wie beispielsweise Wind gewinnen, findet nun ein Paradigmenwechsel im elektrischen Netz statt. Diese nachhaltigen Erzeuger befinden sich zumeist im Nieder- und Mittelspannungsnetz und der elektrische Fluss könnte nun bidirektional fließen. Dieser Paradigmenwechsel kann zu Engpäßen und anderen Problemen führen, da das elektrische Netz für ein solches Szenario nicht konzipiert ist.

Eine Hauptaufgabe dieser Arbeit war die Identifizierung von Problemstellungen in elektrischen Netzen. Die extrahierten Problemstellungen haben wir dann in graphentheoretische Modelle übersetzt und Algorithmen entwickelt, die oftmals Gütegarantien besitzen. Wir haben uns dabei zunächst auf die Modellierung von elektrischen Netzen und das Verhalten von Flüssen in diesen Netzen mit Hilfe von Graphentheorie konzentriert. Zur Modellierung des elektrischen Flusses nutzen wir eine linearisierte

Modellierung, die mehrere vereinfachende Annahmen trifft. Diese linearisierte Modellierung ist für Hochspannungsnetze im Allgemeinen eine gute Annäherung und macht das Entscheidungsproblem für elektrische Flüsse, das heißt, ob ein gültiger elektrischer Fluss für eine bestimmte Konfiguration des Netzes und für einen bestimmten Verbrauch und eine bestimmte Erzeugung existiert, in Polynomialzeit lösbar.

Leistungsfluss. Fokusiert man sich auf das vereinfachte Zulässigkeitsproblem von elektrischen Flüssen und den Maximalen Leistungsflüssen, so existieren verschiedene mathematische Formulierungen, die den Leistungsfluss beschreiben. Auf allgemeinen Graphen ist es oftmals der Fall, dass graphentheoretischen Flüsse keine zulässigen Leistungsflüsse darstellen. Im Gegensatz zu graphentheoretischen Flüssen balancieren sich Leistungsflüsse. Wir diskutieren diese Eigenschaft aus graphentheoretischer Sicht. Die verschiedenen mathematischen Formulierungen geben uns strukturelle Einblicke in das Leistungsflussproblem. Sie zeigen uns die Dualität der zwei Kirchhoffschen Regeln. Diese nutzen wir um einen algorithmischen Ansatz zur Berechnung von Leistungsflüssen zu formulieren, der zu einem Algorithmus für Leistungsflüsse auf planaren Graphen führen könnte. Die Einschränkung auf planare zweifachzusammenhängende Graphen ist vertretbar, da elektrische Netze im Allgemeinen planar sind [COC12, S. 13]. Zudem hilft uns diese Sichtweise, um Analogien zu anderen geometrischen Problemen herzustellen.

Kontinuierliche Änderungen. Da graphentheoretische Flüsse sich in vielen Fällen anders als elektrische Flüsse verhalten, haben wir versucht, das Stromnetz mittels Kontrolleinheiten so auszustatten, dass der elektrische Fluss den gleichen Wert hat wie der graphentheoretische Fluss. Um dieses Ziel zu erreichen, platzieren wir die Kontrolleinheiten entweder an den Knoten oder an den Kanten. Durch eine Suszeptanz-Skalierung, die durch die Kontrolleinheiten ermöglicht wird, ist es nun prinzipiell möglich jeden graphentheoretischen Fluss elektrisch zulässig zu machen. Dabei konnten wir zeigen, dass das gezielte Platzieren von Kontrolleinheiten die Kosten der Erzeugung von elektrischer Leistung durch Generatoren im elektrischen Netz senken kann und den Betriebspunkt des Netzes in vielen Fällen auch erweitert. Platziert man Kontrolleinheiten so, dass der verbleibende Teil (d. h. das Netz ohne die Kontrolleinheiten) ein Baum oder Kaktus unter geeigneter Begrenzung der Kapazitäten ist, so ist es möglich, jeden graphentheoretischen Fluss als elektrisch zulässigen Fluss mit gleichwertigen Kosten zu realisieren. Die Kostensenkung und die Erweiterung des Betriebspunktes konnten wir experimentell auf IEEE-Benchmark-Daten bestätigen.

Diskrete Änderungen. Die oben beschriebenen Kontrolleinheiten sind eine idealisierte, aktuell nicht realisierbare Steuereinheit, da sie den elektrischen Fluss im gesamten Leistungsspektrum einstellen können. Damit ist vor allem gemeint, dass sie den elektrischen Fluss auf einer Leitung von „Die Leitung ist abgeschaltet." bis zur maximalen Kapazität stufenlos einstellen können. Diese Idealisierung ist auch ein großer Kritikpunkt an der Modellierung. Aus diesem Grund haben wir versucht, unser

Modell realistischer zu gestalten. Wir haben zwei mögliche Modellierungen identifiziert. In der ersten Modellierung können Leitungen ein- und ausgeschaltet werden. Dieser Prozess wird als Switching bezeichnet und kann in realen Netzen mittels Circuit Breakers (dt. Leistungsschaltern) realisiert werden. Die zweite Modellierung kommt der Kontrolleinheiten-Modellierung sehr nahe und beschäftigt sich mit der Platzierung von Kontrolleinheiten, die die Suszeptanz innerhalb eines gewissen Intervalls einstellen können. Diese wirkt im ersten Moment wie eine Verallgemeinerung der Schaltungsflussmodellierung. Nutzt man jedoch eine realistischere Modellierung der Kontrolleinheiten, so ist das Einstellen der Suszeptanz durch ein Intervall begrenzt, das das Ausschalten einer Leitung nicht mit beinhaltet. Sowohl ein optimales (im Sinne der Minimierung der Gesamterzeugungskosten oder der Maximierung des Durchsatzes) Platzieren von Switches als auch ein optimales Platzieren von Kontrolleinheiten ist im Allgemeinen NP-schwer [LGH14]. Diese beiden Probleme ergänzen sich dahingehend, dass man den maximalen graphentheoretischen Fluss, mit den zuvor genannten Platzierungen annähern kann.

Für Switching konnten wir zeigen, dass das Problem bereits schwer ist, wenn der Graph serien-parallel ist und das Netzwerk nur einen Erzeuger und einen Verbraucher besitzt [Gra+18]. Wir haben sowohl für den Maximalen Übertragungsschaltungsfluss (engl. Maximum Transmission Switching Flow; kurz MTSF) als auch für den optimalen Übertragungsschaltungsfluss (engl. Optimal Switching Flow; kurz OSF) erste algorithmische Ansätze vorgeschlagen und gezeigt, dass sie auf bestimmten graphentheoretischen Strukturen exakt sind, und dass auf anderen graphentheoretischen Strukturen Gütegarantien möglich sind [Gra+18]. Die Algorithmen haben wir dann auf allgemeinen Netzen evaluiert. Simulationen führen zu guten Ergebnissen auf den NESTA-Benchmark-Daten.

Erweiterungsplanung auf der Grünen Wiese. Eine vom Rest der Arbeit eher losgelöste Fragestellung war die Verkabelung von Windturbinen. Unter Verwendung einer Metaheuristik haben wir gute Ergebnisse im Vergleich zu einem „Mixed Integer Linear Program“ (MILP; dt. gemischt-ganzzahliges lineares Programm) erzielt, das wir nach einer Stunde abgebrochen haben. Die Modellierung der Problemstellung und die Evaluation des Algorithmus haben wir auf der ACM e-Energy 2017 veröffentlicht [Leh+17].

Schlusswort. Abschließend kann man sagen, dass mit dieser Arbeit allgemeine, tiefliegende Aussagen über elektrische Netze getroffen wurden, unter der Berücksichtigung struktureller Eigenschaften unterschiedlicher Netzklassen. Diese Arbeit zeigt wie das Netz ausgestaltet sein muss, um bestimmte Eigenschaften garantieren zu können und zeigt verschiedene Lösungsansätze mit oft beweisbaren Gütegarantien auf.